

**EFFECT OF ARTIFICIAL GAUGE FIELD ON
ULTRA COLD ATOMS WITH LONG-RANGE
INTERACTION AND SUPERSOLIDITY IN
LATTICE AND CONTINUUM SYSTEMS**

RASHI SACHDEVA



**DEPARTMENT OF PHYSICS
INDIAN INSTITUTE OF TECHNOLOGY
DELHI**

EFFECT OF ARTIFICIAL GAUGE FIELD ON ULTRA COLD ATOMS WITH LONG-RANGE INTERACTION AND SUPERSOLIDITY IN LATTICE AND CONTINUUM SYSTEMS

by

RASHI SACHDEVA

Department of Physics

Submitted

in fulfillment for the requirements of the degree of

DOCTOR OF PHILOSOPHY

to the



Indian Institute of Technology Delhi

August 2013

Dedicated to my grandmother...

Certificate

This is to certify that the thesis entitled **Effect of artificial gauge field on ultra cold atoms with long-range interaction and Supersolidity in lattice and continuum systems**, being submitted by **Rashi Sachdeva** to the Department of Physics, Indian Institute of Technology, Delhi for the award of Degree of Doctor of Philosophy, is a bonafide work carried by her under my supervision and guidance. The results obtained in this thesis have not been submitted to any university or institute for award the of any degree or Diploma.

Dr. Sankalpa Ghosh
Department of Physics
Indian Institute of Technology
New Delhi, 110016, INDIA

Date:

Acknowledgements

I would firstly like to express my gratitude for my supervisor, Dr. Sankalpa Ghosh, who gave me the opportunity to work on such an interesting research problem. His uncompromising approach to research has made a deep impression on me. I would like to thank him for invaluable guidance and constructive suggestions that enabled me to complete my work successfully.

I am grateful to Dr. Varsha Banerjee from the Physics Department, IIT Delhi and Prof. Charusita Chakravarty from Chemistry Department, IIT Delhi for serving as SRC members of my thesis. Their criticisms and valuable suggestions have helped me a lot to improve over myself.

I also thank Prof. R. K. Mittal from Department of Applied Mechanics, IIT Delhi and Prof. Sanjay Puri from School of Physical Sciences, JNU for their admirable help during the third problem of this thesis work.

I am also thankful to all the departmental staff at the Physics Department, IIT Delhi, for being helpful all the times.

I would also like to thank Max Planck Institute for Physics of Komplexer Systems, Dresden, Germany for giving me an opportunity to work with the group of Dr. T. Pohl during summers 2011. I enjoyed my short stay at MPIPKS and learnt many new things which hopefully will be very helpful for my research career.

I also owe a special gratitude to my labmates, Jasleen and Neetu, who have been wonderful friends and helped me any time I needed help or advice. I also would like to mention thanks to Nishant, who was a undergraduate student, with whom I enjoyed to work and discuss. I wish him the best for his future endeavours. I would like to thank my friends Bhavna and Neha for being such caring and wonderful friends cum roommates, Dipti who is more kind of elder sister to me, for her encouragement and love, Shweta, Chandra and Roli for all the good times I had with them during my stay at IIT Delhi. I will miss you all but hope to keep in touch with you. Kapil and Bhawna, who have been my friends since primary class, needs a special mention for always been there with me. Without any complain they listen to all my PhD related stories, though I know they hardly understand anything.

I also would like to thank my parents for *everything*. Their support and encouragement at every step is something without which I could not have come this way long. A special mention to my younger sister Anu, who always supported me morally at times when I needed it most. I feel lucky to have you as my sister, who is more like a best friend

to me. I also thank them for their kind understanding on the little time I spent with them during my course of study. I also thank my late grandmother for providing me the inspiration and support for pursuing PhD. Rather than describing your contribution to my life, I simply dedicate this thesis to you.

I owe special thanks to my fiancé Aditya, for his unconditional support and love throughout the years. His understanding and patience kept me going when life seemed difficult. *Thank you* is a small word to express my gratitude for you.

Finally, I acknowledge the financial support by CSIR, India during the course of my PhD at IIT Delhi and MPIPKS, Dresden, Germany for the period of my short stay there.

Abstract

Ultracold atomic condensates have emerged as fascinating systems for performing quantum simulation of physical systems which are otherwise difficult to study. In this thesis we study the quantum simulation of *Supersolid* phase using ultracold atomic condensates with long range interactions in presence of artificial gauge field. Due to tunability of the interaction and the interesting properties of these condensates in gauge fields, we explore the possibility of simulating Supersolid phase in such controllable system.

We first examine the ground state properties of ultracold atomic condensates with long range interactions loaded in optical lattice, in presence of gauge field. We study the system using extended Bose Hubbard model with nearest-neighbor interaction which describe minimally the effect of long-range interaction on ultracold atoms in deep optical lattices. The rotation of such optical lattices subjects such neutral cold atoms to the effect of an artificial magnetic field. We show that the modification of the phase boundaries of the Density Wave and Mott Insulator phases due to this rotation are shown to be related to the edge spectrum of spinorial and scalar Harper equations. We calculated the checkerboard vortex structure in a supersolid phase near the phase boundary and highlight its distinct structure compared to vortex in a superfluid.

We further go on to study the effect of an artificial gauge field on extended Bose Hubbard model by using strong-coupling perturbation theory. Using this technique, we determine analytically the effect of the artificial gauge field on the Density Wave-Supersolid (DW-SS) and the Mott Insulator Superfluid (MI-SF) transition boundary. We also calculate the momentum distribution at these two transition boundaries and show that such a momentum distribution, which can be observed in time-of-flight measurements, reveals the symmetry of the gauge potential through the formation of a magnetic Brillouin zone and clearly carry the distinguishing signatures between the DW-SS and MI-SF boundary.

Finally to complete our study of supersolid phase, we performed the study of such ultracold atomic condensates with long range interactions in presence of gauge field in the continuum limit. We construct a Gross-Pitaevskii hydrodynamic theory for rotating supersolid and treat the supersolid within the framework of well known two fluid approximation. Under fast rotation limit the superfluid part of the system forms a vortex lattice which co-exists with the supersolid lattice. We analyze the dispersion relations of such collective excitations within this hydrodynamic approach and calculate the distinct modes due to co-existence of two lattices in the system.

Contents

Certificate	ii
Acknowledgements	iii
Abstract	v
List of Figures	vii
1 Introduction	1
1.1 Bose Einstein Condensation	1
1.2 Research progress in ultra cold atomic condensates	4
1.3 Ultracold atomic gases as <i>quantum simulators</i>	9
1.4 <i>Quantum simulation</i> of Supersolid phase	12
1.4.1 History of Supersolid phase	12
1.4.2 Ultracold atomic condensates as <i>quantum simulators</i> for Super- solid phase	14
1.5 <i>Artificial</i> gauge fields for cold atoms	16
1.6 Motivation of the thesis	18
1.6.1 Outline of the thesis	20
2 Extended Bose Hubbard Model in presence of artificial gauge field: Mean field approach	24
2.1 Derivation of Hamiltonian	25
2.1.1 Extended Bose Hubbard Hamiltonian for bosons in an optical lat- tice potential	25
2.1.2 Application of <i>artificial</i> gauge field on cold atomic system	29
2.1.2.1 Transformation to rotating frame coordinates	30
2.1.3 Extended Bose Hubbard Hamiltonian in rotating frame coordinates	34
2.2 Extended Bose Hubbard model in presence of magnetic field	38
2.2.1 Phase diagram of the Extended Bose-Hubbard Hamiltonian in mean field approximation	40
2.2.2 Phase boundary for the non rotating case	43
2.2.3 Rotated case	47
2.2.4 Harper equation and Hofstadter Butterfly spectrum	52

2.3	Results and discussion	56
2.3.1	Modification of phase boundaries of DW and MI phases	56
2.3.2	Superfluid density profile for vortex in a supersolid near the DW-SS boundary	57
2.4	Possibilities of experimental detection	59
2.5	Summary of the chapter	62
3	DW-SS and MI-SF transition in presence of an artificial gauge field : a strong coupling perturbation approach	63
3.1	Introduction	66
3.2	Extended Bose Hubbard Model in presence of magnetic field	66
3.2.1	Formalism	67
3.2.2	Wave functions at zeroth order in t	68
3.3	Analytic expressions for the modification of phase boundaries	73
3.3.1	Ground state energy calculations for DW and MI phase	73
3.3.2	Calculation of energy of DW state with an extra particle or hole	75
3.3.3	Calculation of energy of MI state with an extra particle or hole	77
3.3.4	Determination of the DW-SS and MI-SF boundary from the strong coupling expansion	79
3.4	Extrapolation of the phase boundaries via Scaling theory	80
3.5	A brief overview of experimental methods and relation to momentum distribution	87
3.6	Calculation of Momentum distribution	88
3.6.1	Wave function expansion for the DW insulating phase	89
3.6.2	Momentum distribution as a function of gauge field	94
3.6.3	Effect of the presence of gauge field on the momentum distribution	96
3.7	Results and Discussions: <i>Apparent</i> Gauge dependence of momentum distribution function	97
3.7.1	<i>Apparent</i> gauge dependence of the momentum distribution	100
3.8	Quasi-angular momentum distribution	102
3.9	Summary of results of this chapter	105
4	Hydrodynamic theory for rotating supersolids	108
4.1	The Gross Pitaevskii equation	108
4.1.1	Hydrodynamic theory	111
4.1.2	Hydrodynamic equations for a rotating superfluid	113
4.1.3	Components of the elastic modulus tensor	119
4.1.4	Collective modes in a vortex lattice for rotating ultracold atomic superfluids	120
4.1.5	Experimental measurement of Tkachenko waves	124
4.2	The Gross Pitaevskii like model of Supersolid	125
4.2.1	Calculation of Bogoliubov dispersion relation	126
4.3	Hydrodynamic theory for rotating supersolids	130
4.3.1	Homogenization technique for long wave effective Lagrangian	133
4.4	Hydrodynamic equations of motion for rotating supersolid	145
4.5	Dispersion calculations	149
4.5.1	Checking with various existing limits: Non rotating Supersolid, Rotating superfluid and Non-rotating superfluid	157

4.6	Roots of the Dispersion Relation for Rotating Supersolid	161
4.6.1	Possibility of experimental verification	164
4.7	Summary of the work done in this Chapter	165
5	Conclusions	167
5.1	Summary	167
5.2	Future scope	171
A	Elliptical Polarization of Tkachenko waves	173
	References	175

List of Figures

1.1	Basic two-channel model for a Feshbach resonance. The phenomenon occurs when two atoms colliding at energy E in the entrance channel resonantly couple to a molecular bound state with energy E_c supported by the closed channel potential. The idea of the figure taken from ref. [29].	7
1.2	Observation of Bose-Einstein condensation by absorption imaging. The sharp peak is the Bose-Einstein condensate, characterised by its slow expansion observed after time of flight. The left picture shows an expanding cloud cooled to just above the transition point; middle: just after the condensate appeared; right: much below the critical temperature left an almost pure condensate. Picture is taken for data from ref. [6] with due permission from the author.	8
1.3	Schematic diagram of BEC-BCS crossover. Different colors of atoms represents the two spin types of fermionic atoms. In the BEC regime, two spin atoms form deep-bound molecules (composite bosons), while in the BCS regime, the fermions are loosely bound and paired in the momentum space. In the middle region the effective scattering length diverges, indicating a strong interaction between atoms	11
2.1	Single particle density profiles for lattice depth $V_0 = 10E_R$ described using Wannier functions. It shows density profile for $V_0 = 10E_R$, a depth at which the system is in the tight-binding regime where the Wannier functions extend up to nearest neighboring sites, where $E_R = \frac{\pi^2 \hbar^2}{2md^2}$ is the lattice recoil energy with d as the lattice spacing. The Wannier function extend up to nearest neighboring sites and no further.	29
2.2	Schematic diagram for a particle tunneling around a plaquette in a square lattice. Here, dark (pink) regions correspond to lattice sites and the light (yellow) regions correspond to the maxima in lattice potential. The particle picks up a phase of $2\pi\nu$ when it returns to its original position as marked by the solid (red) circle.	37
2.3	(a) Alternating particle number in Density Wave phase (b) Superfluid order parameter in Supersolid phase on the sites of A (red) and B(green) sublattices.	39
2.4	(a) Phase diagram for the eBHM for $2V=0.4$. Note that t , μ and V are measured in units of U .	47
2.5	Landau level energy spectra for free electrons in two dimensional in the presence of magnetic field. The energy spectrum is given by $E = \hbar\omega_c(n + \frac{1}{2})$ with $\omega_c = \frac{eB}{m}$.	53
2.6	Hofstadter butterfly: the energy (ε) spectrum for equation (2.93) or (2.94) for various $\nu\{0, 1\}$.	55

- 2.7 (Left) Hofstadter butterfly: the energy (ε) spectrum for the equation (2.90) for various $\nu\{0,1\}$. The upper edge (marked red) gives the boundary of the density wave and the Mott Insulator lobe as explained in the text. (Right) The first DW and MI lobe as a function of t, μ, ν in mean field approximation where t and μ are in the unit of U . V has been taken as 0.2 in the unit of U 57
- 2.8 Cross section of the phase diagram in Fig. (2.6) that shows the modification of the first two density wave lobe and the first Mott lobe at various values of circulation quanta ν . In all these plots V has been taken as 0.2 in the unit of U . The SS phase which appears after the DW phase followed by appearance of SF phase is also shown approximately. Please note that the position of the SS and SF phases shown is only approximate and is not calculated within the theory. 58
- 2.9 (a) Checkerboard vortices at the density wave ($|2,1,2,1,\dots\rangle$) phase boundary ($\tilde{t} = \tilde{t}_c$) corresponding to the highest eigenvalue (the edge) of the hofstadter butterfly spectrum for $\nu = \frac{1}{16 \times 16}$. The direction of the arrow gives φ_{i_A, i_B} where as the color axis gives the superfluid density. The superfluid density is normalized by the maximum superfluid density at the boundary. The x and y coordinates are given in units of optical lattice spacing and are the same in all the plots. (b) corresponding DW order parameter 59
- 2.10 (a) More complicated vortex structure corresponding to the higher value of \tilde{t} corresponding to a lower eigenvalue ((254(16 \times 16 - 2)th band)(b) corresponding DW order parameter. The direction of the arrow gives φ_{i_A, i_B} where as the color axis gives the superfluid density. The superfluid density is normalized by the maximum superfluid density at the boundary. The x and y coordinates are given in units of optical lattice spacing and are the same in all the plots. 60
- 2.11 Bragg spectroscopy set up. The momentum transfer is determined by the angle between the Bragg beams θ and the frequency $\Delta\omega = \omega_2 - \omega_1$ determines the energy transfer. 61
- 3.1 Single particle and hole excitations over pure DW phase. The picture shows that an extra particle or hole can go to any of the lattice site, resulting in degeneracy. Hence, to calculate particle or hole excited states and energies, degenerate perturbation theory is needed. 72
- 3.2 Phase diagram for the eBHM in presence of artificial magnetic field for $Vd=0.2$ obtained after scaling analysis. As seen, the effect of increasing magnetic field is to increase the stability of the DW and MI lobes. Please note that the position of the SS and SF phases shown is only approximate and is not calculated within the theory. 83
- 3.3 Comparison of the strong coupling (dotted line), scaling (dash dot line) and the mean field results (solid line) for flux $\nu = 0.09$ and $Vd = 0.2$. Please note that the position of the SS and SF phases shown is only approximate and is not calculated within the theory. 85
- 3.4 Possibilities for the first order intermediate (excited) state for the DW phase in a 2x2 lattice. Figure (a) corresponds to the ground state wave function in the limit $t = 0$ 91
- 3.5 Second order intermediate states for $|m\rangle = |n_A^{(1)} + 1, n_B^{(2)} - 1, n_A^{(3)}, n_B^{(4)}\rangle$ (the first diagram) 92

3.6	Momentum distribution at the (a) MI-SF and (b) DW-SS phase boundary in Landau gauge potential for $\nu = \frac{1}{4}$, plotted in the reduced Brillouin zone $-\pi \leq k_x \leq \pi$ and $-\pi/4 \leq k_y \leq \pi/4$	98
3.7	Momentum distribution for the (a) MI and (b) DW phase in symmetric gauge potential for $\nu = 1/2$, plotted in the range $-\pi/4 \leq k_x \leq \pi/4$ and $-\pi/4 \leq k_y \leq \pi/4$	100
3.8	Extra small peaks in the DW momentum distribution $n(\mathbf{k})$ symmetric gauge potential. The arrows show the location of the extra peaks at intermediate positions	101
3.9	Quasi angular momentum distribution of the DW phase for (a) $m=0$,(b) $m=1$, plotted over a range $-4\pi \leq k_x, k_y \leq 4\pi$	105
3.10	The cross sectional plots for $m=0$ and $m=1$ quasi angular momentum state for MI (a),(c) and DW (b),(d) phases. The DW phase shows distinctive peaks compared to MI phase	106
4.1	Inertial and Tkachenko mode frequencies vs wave vector, in units of Ω/c_s for a rotating superfluid system. Both the mode frequencies are in units of Ω	122
4.2	Model interaction potential (Step-like)	127
4.3	Plot of dispersion relation $\epsilon(q)$ in three dimensions for increasing values of interaction strength, $\Lambda = 10, 25, 65, 92$. Roton instability where the minima in the energy spectrum touches the q axis, is seen to occur after a critical value of the interaction strength, indicating the possible formation of a periodic ground state	128
4.4	Ground state of the GPE obtained numerically for one and two dimensions, using imaginary time propagation technique. The ground state shows a periodic modulation in density after critical value of interaction strengths. It is to note that the system favors the formation of a hexagonal lattice in two dimensions.	129
4.5	Dispersion roots for non-rotating supersolid, ω as a function of wave vector q . It is to note that the parameters for the the elastic wave c_k velocity, superfluid velocity c_s are taken from quantum monte carlo calculations done in [198] with superfluid fraction $f_{ss} = 0.3$	158
4.6	Dispersion roots for a rotating superfluid, ω in units of Ω as a function of wave vector q in units of Ω/c_s	160
4.7	Dispersion roots for rotating supersolid. Inertial(ω_1), coupled mode(ω_2) and shear mode (ω_3) frequencies as a function of wave vector q . The wave vector is in units of Ω/c_{sm} and the mode frequencies are in units of Ω . The value of vortex lattice velocity c_{vl} and c_{vs} have been taken from [182] and the elastic wave c_k velocity, superfluid velocity c_s are taken from quantum monte carlo calculations done in [198] with superfluid fraction $f_{ss} = 0.3$	163
4.8	Schematic diagram to show the symmetric (in phase) and antisymmetric (out of phase) oscillations of the two coupled lattices. The direction of the arrows shows the in-phase or out of phase oscillations of the lattices. .	164

Chapter 1

Introduction

1.1 Bose Einstein Condensation

In 1924 S. N. Bose [1] examined the nature of photons and was able to rederive Planck's law for black-body radiation assuming indistinguishability of the light quanta of photons. His work was subsequently extended by A. Einstein [2] in 1925, to an ideal gas of bosons, dealing with statistical properties and predicted a *new state of matter*. He predicted a phase transition of a gas of non-interacting particles with integer spin, to a phase where the lowest energy quantum mechanical state is macroscopically occupied [1, 2], forming a Bose-Einstein condensate (BEC) below a critical temperature. The occupation of a single quantum state by macroscopic number of particles in BEC is entirely due to quantum statistical effects. The occurrence of this peculiar phenomenon is explained as follows.

The statistical properties of massless photons, proposed by Bose [1] was extended by Einstein [2] for non-interacting massive bosons who arrived at the following distribution function for the i th state of the trapping potential

$$f(\epsilon_i) = \frac{1}{e^{(\epsilon_i - \mu)/k_B T} - 1} \quad (1.1)$$

which is termed as the Bose-Einstein distribution. Here, ϵ_i is the energy of the i th state, k_B is the Boltzmann's constant and T is the temperature. The conservation of the number of particles is taken into account by the chemical potential μ .

Consider a collection of N indistinguishable, non-interacting particles, trapped in some potential. As the temperature of this system is lowered, the particles start moving to lower quantum states of the trap potential. If the particles are fermions (half-integer spin), there cannot be more than two particles staying in the same state by the Pauli

exclusion principle. At $T = 0$ therefore all the N lowest quantum states will be occupied by precisely one particle, and nothing further can happen. However, bosons (particles with integer spin) do not have such constraint, and any arbitrary number of particles can occupy the same quantum state. Therefore, as the temperature is lowered, more and more particles are able to fall into the ground state of the trap and the population of this state becomes macroscopic.

When the temperature T is lowered, then chemical potential μ must increase in order to keep the number of particles $N = \sum_i f_0(\epsilon_i)$ fixed. However, to avoid the negative occupation numbers, $\mu < \epsilon_0$ must also hold. Therefore, for an arbitrary excited state ($i > 0$), the occupation number cannot exceed $(e^{(\epsilon_i - \epsilon_0)/k_B T} - 1)^{-1}$ and hence this imposes an upper bound of the total number of particles in the excited state. Thus, when the system is cooled below a critical temperature T_c , the N particles can no longer be accommodated in the excited states. The form of $f(\epsilon_i)$ ensures that below a critical temperature the population of excited states gets saturated and hence the remaining particles must reside in the ground state of the system. This leads to a macroscopic occupation of the ground state which is called as Bose Einstein condensation.

It is to note that Einstein's original prediction of Bose condensation was for an ideal non-interacting gas of bosons with little relevance to real physical systems. For an ideal gas the many body wave function of N bosons is simply the product of identical single particle ground state wave function. This single particle wave function is termed as macroscopic or condensate wave function. However, there are always interactions between atoms in any physical system, and one needs to go beyond the ideal gas formalism. In an interacting system, the ground state many body wave function should also account for the correlations among the particles. The microscopic theory of interacting bosons in the context of BEC was formulated first time in 1947 by N.N. Bogoliubov [3] and further, Penrose and Onsager [4] formally defined BEC in interacting systems and showed that the macroscopic nature of wave function retains its validity in this case too.

A general criterion for BEC was formulated by Penrose and Onsager [4] for interacting bosons, which is of fundamental importance for the understanding of macroscopic quantum phenomena. It states that the existence of a condensate refers to a non-vanishing value of the single particle density matrix

$$\rho(\mathbf{r}, \mathbf{r}') = \langle \hat{\psi}^\dagger(\mathbf{r}) \hat{\psi}(\mathbf{r}') \rangle \quad (1.2)$$

Their peculiar property of BEC is termed as Off diagonal long range order (ODLRO). This feature states that a Bose condensed system is characterised by finite long range correlations in the condensate and hence the condensate is phase coherent at large

distances. Subsequently, it was shown that both superconductivity [5] and superfluidity are quantum phases characterized by the existence of ODLRO.

We now present a simplified quantum mechanical description for the achievement of Bose condensed gas. In quantum mechanics we know that atoms are represented by wave packets with a spatial extension given by the de Broglie wavelength

$$\lambda_{dB} = \sqrt{\frac{2\pi\hbar^2}{mk_BT}} \quad (1.3)$$

with m as the particle mass and h as the Planck's constant. For high temperatures, the de Broglie wavelength becomes very small and the particles can be regarded as classical point masses, whereas for low temperatures the particles behave much more like waves. When BEC occurs the particles wavepackets overlap, or in other words, the de Broglie wavelength becomes equal to the mean atomic separation. Using n to denote the density of the atoms, we thus obtain

$$n\lambda_{dB}^3 \approx 1 \quad (1.4)$$

Using the definition of λ_{dB} from equation (1.3) in (1.4) one gets an estimate for the transition temperature T_c at which BEC occurs

$$T_c = \frac{2\pi\hbar^2 n^{2/3}}{mk_B} \quad (1.5)$$

To satisfy the condition (1.4) and achieve BEC, the experimentalists could either lower the temperature or increase the particle density. However, at low temperatures gases tend to liquify or solidify, and hence the gas actually needs to be very dilute instead. Typically, particle densities of $10^{13} - 10^{15} \text{ cm}^{-3}$ are needed to achieve BEC. At such low densities, three-body collisions are rare, and the rate at which atoms clump together and form liquids or solids is so slow that metastable BEC states can be achieved with lifetimes of seconds or even minutes, long enough for experiments to be conducted.

Bose Einstein condensate is a unique system in which quantum mechanical phenomena manifest themselves at a macroscopic scale. In 1995 the field of BEC took a huge leap when BEC was achieved experimentally for the first time in a dilute weakly-interacting gas of trapped ^{87}Rb atoms [6] and ^{23}Na atoms [7]. In contrast to liquid helium [8], where the strong interactions between particles leads to a substantial depletion of the BEC, the relatively weak two-particle interaction in dilute alkali atoms allows these systems to be used as a much better theoretical and experimental avenue for studying coherent matter wave phenomenon on a macroscopic scale.

Theoretically, the weakly interacting regime has the advantage that all the atoms can be described by a single macroscopic wave function. In 1961 an important equation was

derived for the treatment of weakly interacting dilute Bose condensed gases - the Gross Pitaevskii equation (GPE) [9], which considers the mean field of the quantum system.

$$i\hbar \frac{\partial \psi}{\partial t} = \left[-\frac{\hbar^2}{2m} \nabla^2 + V_{ext} + g|\psi(\mathbf{r}, t)|^2 \right] \psi(\mathbf{r}, t) \quad (1.6)$$

where $\psi(\mathbf{r}, t)$ is the wave function of the condensate and g is the contact interaction. The GPE assumes that all the atoms are in the condensate and completely neglects the quantum fluctuations around the ground state. To further go beyond the simple mean field theory, Bogoliubov [3] proposed a description where the small quantum fluctuations are treated as perturbations. The effect of fluctuations results in the small depletion of the condensate mode since other excited states different from the condensate ground state gets populated. Since in most of the experiments with dilute gases the condensate depletion fraction is quite small, the GPE [9] together with Bogoliubov analysis [3] have been in general very successful in predicting and describing the experimental observations [6, 7].

With the first experimental realization of BEC, both theoretical and experimental progress in this field has grown at an enormous rate. We highlight the history of the experimental realisation and research progress in ultra cold atomic gases over several years in the following section.

1.2 Research progress in ultra cold atomic condensates

Even though the discovery of macroscopic quantum phenomena like superconductivity [5] or superfluidity are related to the occurrence of Bose Einstein Condensation, it remained an elusive goal for experimentalists for many years to achieve BEC as envisaged by Einstein. This was because reaching the incredibly low temperatures for condensation of atomic systems was a great challenge. The reason lies in the experimental difficulties to cool down the atoms to temperatures in the required nK regime and catch and hold them in a trap.

It was only after 70 years of Einstein's prediction, that the first experimental realization of BEC was observed in dilute gases of Rubidium atoms [6] and Sodium atoms [7], and was honored with the Nobel Prize in 2001 [10]. This was possible due to the development of effective laser cooling and trapping techniques over the preceding decades, which were essential to observe this novel quantum phase at ultracold temperatures (~ 100 nK). This was also honored with the Nobel Prize in 1997 [11]. These experimental achievements provided novel systems for studying BEC, superfluidity, and allow one to experimentally achieve many other phenomena that demonstrate quantum physics on macroscopic scale.

Bose Einstein condensates have now been achieved for most of the alkali species atoms in numerous experimental groups typically with ^{87}Rb [6], ^{23}Na [7], Li [12], ^{85}Rb [13], ^{41}K [14], and ^{133}Cs [15] as well as in ^1H [16] and meta-stable ^4He [17, 18] in external traps (harmonic confinement).

In the beginning of BEC experiments the condensing atoms were alkali metals. In such dilute alkali gases the interaction is described quite well by the Lennard-Jones potential. In the theory of pseudo-potentials, the two-particle interactions in dilute alkali gases are theoretically using the short-range pseudo potential [19]

$$U_\delta(\mathbf{r} - \mathbf{r}') = \frac{4\pi\hbar^2 a}{m} \delta(\mathbf{r} - \mathbf{r}') \quad (1.7)$$

This pseudo potential is called contact- or delta-potential. Here, parameter a is the s-wave scattering length known from classical scattering theory. For alkali atoms, higher orbital waves like p , d or f waves are suppressed at low energy due to the centrifugal barrier in such extremely cooled systems. Thus, the atoms in alkali BEC interact through the isotropic, short range s wave interactions.

In addition to achievement of BEC with alkali species, experimental progress has also allowed to achieve BEC of atoms with long range interaction, realized for the first time with ^{52}Cr atoms [20], which have dipolar interactions among them. Chromium was recommendable due to its electronic structure $1s^2 2s^2 2p^6 3s^2 3p^6 3d^5 4s^1$, which following Hund's rule leads to a large magnetic dipole moment of six Bohr magnetons. So, in addition to equation (1.7), the atoms interact additionally via a magnetic dipole-dipole potential

$$U_{dd}(\mathbf{r}) = \frac{\mu_0}{4\pi} \frac{\mathbf{m}_1 \cdot \mathbf{m}_2 - 3(\mathbf{m}_1 \cdot \hat{\mathbf{r}})(\mathbf{m}_2 \cdot \hat{\mathbf{r}})}{r^3} \quad (1.8)$$

which, in comparison to equation (1.7), is not isotropic and depends on the specific angle between the dipoles and their distance vector. A further significant difference between contact and dipole interaction is their particular range. While the pseudo potential acts only on contact of two atoms, the dipole-dipole interaction falls off as $1/r^3$ and thus acts over long distances.

Long range interactions provide a rich theoretical laboratory for statistical physics, and therefore Bose-Einstein condensates with dipolar interactions could become a key system to investigate them. There has been subsequent progress to achieve BEC with controllable long range interactions. This has lead to the achievement of BEC of lanthanide bosonic Erbium atoms [21], quantum degenerate gas of fermionic dysprosium [22], and heteronuclear polar molecules [23]. Controllable long range interaction among ultra cold atoms nowadays can also be induced by making use of radiative coupling between electrical dipoles induced by off-resonant laser light which introduces a modified long range

interaction among dressed atoms [24–26]. Very recent progress in ultracold atomic gases is the observation of strong and controllable long-range interactions between Rydberg atoms [27] which provide a wide range of possibilities to tailor interactions in a ultracold gases [28].

One of the remarkable features of the ultracold atomic BEC is their high controllability. It makes this system a better choice for realizing a large number of quantum phenomenon where a macroscopic quantum order exists, in a highly controllable environment. Since this is going to be one of the main subject matter of this thesis, we shall explain this fact in more detail below.

Feshbach Resonance: An important experimental tool for ultra cold gases is the adjustability of the interaction between atoms achieved by means of Feshbach resonances [29]. This is the simplest, and so far most commonly used technique which allows for arbitrary tuning of atomic scattering lengths and hence the interaction strength between atoms, by varying an external magnetic field. Moreover, the nature of the interactions (sign of the scattering length) can also be turned from repulsive to attractive or vice versa by varying the applied magnetic field. We briefly describe it below.

We start by considering two potential curves $V_{bg}(\mathbf{R})$ and $V_c(\mathbf{R})$, as shown in Fig. 1.1 following [29]. For large internuclear distances \mathbf{R} , the background potential $V_{bg}(\mathbf{R})$ asymptotically connects to two free atoms in the ultracold gas. For a collision process with small energy E , this potential represents the energetically open channel or an entrance channel. The other potential $V_c(\mathbf{R})$ represents the closed channel. It is important too as it can support bound molecular states near the threshold of the open channel.

A Feshbach resonance occurs when the bound molecular state in the closed channel energetically approaches the scattering state in the open channel. Consequently even weak coupling can lead to strong mixing between the two channels. The energy difference is controllable via a magnetic field when the corresponding magnetic moments are different. This tuning is termed as magnetically tuned Feshbach resonance. The magnetic tuning method is the common way to achieve resonant coupling. A simple expression representing the magnetically tuned Feshbach resonance [30] is given by

$$a(B) = a_{bg} \left(1 - \frac{\Delta}{B - B_0} \right) \quad (1.9)$$

Here, a_{bg} is the background scattering length associated with $V_{bg}(\mathbf{R})$ which represents the off resonant value. The parameter B_0 denotes the resonance position, where the scattering length diverges and the parameter Δ is the resonance width [29].

Alternatively, there are ways where resonant coupling can be achieved by optical methods [31], leading to optical Feshbach resonances which are promising for cases where magnetically tunable resonances are absent. Thus, with such precision control over interaction strengths in ultracold gases, they promise to be an ideal toolbox to study quantum many body phenomena.

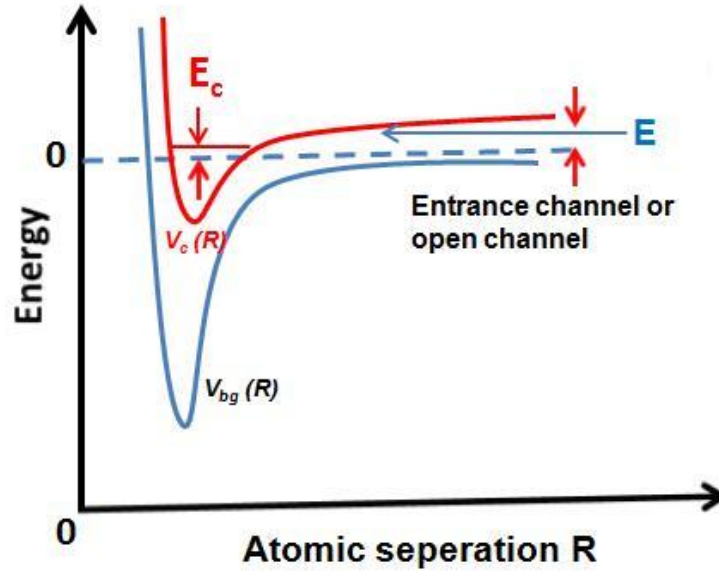


FIGURE 1.1: Basic two-channel model for a Feshbach resonance. The phenomenon occurs when two atoms colliding at energy E in the entrance channel resonantly couple to a molecular bound state with energy E_c supported by the closed channel potential. The idea of the figure taken from ref. [29].

Optical Lattices: Another way of tuning the interaction strength is by loading the atoms into tightly confining optical lattice potentials whose depth can be easily controlled [32, 33]. Optical lattices are periodic potentials created by counter-propagating laser beams which produce a standing light field. Cold atoms interacting with a spatially modulated optical potential resemble in many respects electrons in ion-lattice potential of a solid crystals. However, optical lattices have several advantages with respect to prototype solid state systems. They can be made to be largely free from defects. Moreover, optical lattices are highly controllable by changing the laser field properties. For example the lattice depth can be changed by modifying the laser intensity and the lattice geometry can be modified by changing the laser configuration. The interaction strengths between the atoms can be changed by changing the lattice depth of the optical lattice potential. The effective interaction strength is given by interaction matrix element between the Wannier orbits whose shape depends on the laser intensity. This allows to tune the effective interaction strength between atoms in optical lattices by changing intensity of the laser light. Moreover, in contrast to solids, where the lattice spacings are generally of order of Angstrom units, the lattice constants in optical lattices are typically three (or

more) order of magnitude larger. Thus, the combination of macroscopic matter waves like BECs and periodic potentials (optical lattices) offers the possibility to investigate the basic properties of condensed matter system with a much better external control.

Probing Techniques : The probing techniques in these systems allow a direct observation of the BEC in experiments. For instance, the velocity distribution of atoms taken by means of time of flight expansion method has clearly shown the appearance of a condensate below the transition temperature [6, 7]. In Fig. 1.2 the velocity distribution profile shows the experimental realization of BEC.

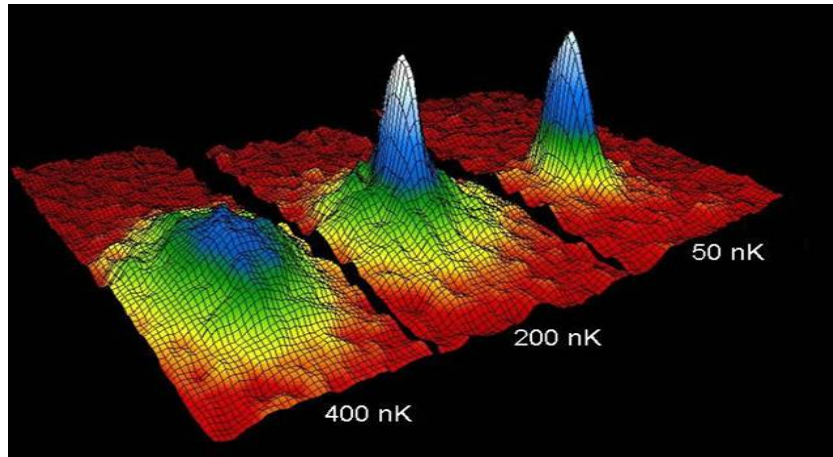


FIGURE 1.2: Observation of Bose-Einstein condensation by absorption imaging. The sharp peak is the Bose-Einstein condensate, characterised by its slow expansion observed after time of flight. The left picture shows an expanding cloud cooled to just above the transition point; middle: just after the condensate appeared; right: much below the critical temperature left an almost pure condensate. Picture is taken for data from ref. [6] with due permission from the author.

Furthermore, a lot of quantitative information can be extracted from simple spatial images of atomic cloud about the nature of the macroscopic quantum states, which is not possible in prototype condensed matter experiments. A sequence of in-situ observation has shown collective excitations of a condensate [34], which implies that one gets a detailed description of quantum mechanical ground state of the many body system and low energy excitations, in a clean and controlled manner.

These are the key features which make ultra cold atomic systems a powerful laboratory for studying a wide range of quantum many body problems. The great attraction that lead to the remarkable growth of this field arises from the fascinating properties of this system. Due to such controllable properties, ultracold atomic systems finds application to be used as efficient *quantum simulators*, which is the subject matter of discussion of next section.

1.3 Ultracold atomic gases as *quantum simulators*

Ultracold atomic systems can act as very efficient *quantum simulators* and, can implement Richard Feynmann's idea of *quantum simulation* [35]. This implies the simulation of properties of one quantum system by means of controlling and observing the properties of other quantum system. The purpose of a quantum simulation is to use a well understood and controllable physical system to simulate the various properties of another quantum system which otherwise is difficult or sometimes even impossible to investigate experimentally. Quantum simulation using cold atomic condensate thus promise to revolutionize scientific research by allowing us to simulate otherwise intractable physical systems. We explain in detail two remarkable examples of *quantum simulation* using cold atoms.

Quantum Simulation of Mott insulator - superfluid transition using cold atomic condensates: One of the well established examples of *quantum simulation* is the observation of quantum phase transition from the superfluid to a Mott insulator phase using cold atomic condensates in optical lattices [33]. This phase transition was originally proposed to occur in context of solid ^4He adsorbed in porous media and in granular superconductors [36] and described using Bose Hubbard Model. But due to incredibly complex nature of real solid state systems, presence of disorder and other such effects, it is quite difficult for experimentalists to test and prove such theoretical results in real solid state systems. Because of these reasons, such quantum phase transition is quite difficult to cleanly observe in the proposed solid state systems.

However, after the successful discovery of BEC in laboratory in 1995, Jaksch et.al [37] in 1998 proposed that such a phase transition could be feasible to observe with ultracold atoms in optical lattices. They theoretically showed that ultracold atomic condensates loaded in an optical lattice realizes exactly a Bose Hubbard Hamiltonian described in [36].

$$\hat{H} = -t \sum_{\langle i,j \rangle} \hat{a}_i^\dagger \hat{a}_j + \frac{U}{2} \sum_i \hat{n}_i (\hat{n}_i - 1) + \sum_i \epsilon_i \hat{n}_i \quad (1.10)$$

Here, t is the hopping parameter, U is the onsite interaction among atoms, ϵ_i is the zero-point energy. The tight binding condition can be experimentally controlled because of the unprecedented control of optical lattice parameters. Four years after this proposal, in 2002 such quantum phase transition from a superfluid to Mott insulator state was experimentally achieved [33] in laboratory using cold atoms in optical lattices. When the kinetic energy of the atoms is much larger the atom-atom interaction energy, i.e. for a sufficiently weak lattice potential, the system favors a superfluid many-body ground state. The condensate fraction is large and there is long-range phase coherence in the

system due to macroscopic occupation of a single quantum state. However when the lattice height is raised, the energetically preferable single-particle states are localized about each site, such that the many-body ground state is a Mott insulator. Experimentally, this phase transition has been observed by taking absorption images of the matter wave interference pattern [33] in time of flight.

Realization of such quantum phase transition is one of the many examples where ultracold atomic gases have proved their efficiency to be used as *quantum simulators*.

Thus, as already described in detail in section 1.2, combination of BEC with optical lattice potential [32, 33] provides an opportunity for exploring a quantum system analogous to electrons in solid state crystals with unprecedented control over the lattice and particles. This gives us a well established example of quantum simulation using ultracold atomic condensates.

Quantum Simulation of BEC-BCS crossover: Another example of *quantum simulation* using cold atomic condensates is the observation of BEC-BCS crossover obtained with the help of Feshbach resonance technique [29]. This subject describes the system of collection of interacting Fermi atoms being cooled to quantum degeneracy, where a macroscopic fraction of them can occupy the same quantum state. As already explained in section 1.1, that due to the Pauli exclusion principle, a single quantum state cannot be macroscopically occupied by individual fermions. However, if the fermionic atoms form pairs they can then be considered as composite bosons, making such a two-body bound state a diatomic molecule. Below a critical temperature, it can be expected that these two-body molecules condense like bosons when they are cooled below a critical temperature. This regime is called as the BEC side of the BEC-BCS crossover physics (the left panel of Fig. 1.3).

The other limiting case is that when fermions are only weakly attracting, which corresponds to a situation studied in the context of superconductivity [38]. In superconductivity, electrons form pairs called as Cooper pairs, in the presence of a weak inter-attraction mediated by crystal vibrations or phonons. According to the BCS theory, the favored ground state is that in which fermions form pairs in momentum space and condense below the critical temperature. Their two-body wavefunctions extend in space and significantly overlap with each other. This regime is thus called the BCS side (the right panel of Fig. 1.3).

The intermediate region between the BEC and BCS regime is defined when the two tightly bound fermions on the BEC side start to dissociate, or the overlap of the two-body wavefunctions on the BCS side diminishes (the middle panel of Fig. 1.3). In this region, called the unitary region [39], the crossover physics of the Fermi systems should

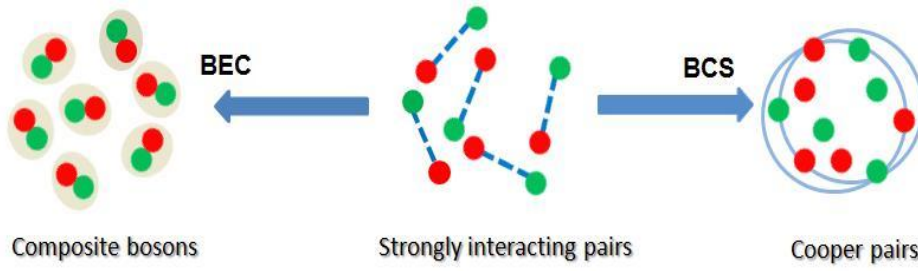


FIGURE 1.3: Schematic diagram of BEC-BCS crossover. Different colors of atoms represents the two spin types of fermionic atoms. In the BEC regime, two spin atoms form deep-bound molecules (composite bosons), while in the BCS regime, the fermions are loosely bound and paired in the momentum space. In the middle region the effective scattering length diverges, indicating a strong interaction between atoms

show unique properties, neither entirely bosonic nor fermionic in nature; interesting behaviors are expected and explored. With the help of Feshbach resonances, as already mentioned in detail in section 1.2 that the interaction between atoms can be tuned to change from attractive to repulsive. The existence of two separate states, a fermionic and a bound bosonic one, can be seen from the emergence of characteristic superfluid vortices [40]. This transition between the bosonic and fermionic state by simply tuning the scattering length in ultracold atomic systems simulates the so called BEC-BCS crossover [39], which was for long only a theoretical proposal [41, 42].

The technique of Feshbach resonances has become by now an important laboratory tool to prepare, control, and probe ultracold gases. This is another example where ultra cold gases act as *quantum simulator* for observation of BEC-BCS crossover in degenerate fermionic system [39], which otherwise was not realized experimentally.

These successful achievement opens up perspectives for a much broader range of quantum simulations using cold atomic condensates with much better external control. Several physical systems have been proposed and simulated using cold atomic condensates. Some examples of which are spin models [43], many-body systems with Rydberg atoms [44], simulation of the Tonks-Girardeau regime with BEC in 1D optical lattices [45], observation of Anderson Localization using BEC in random potentials [46] and many more.

One of such particular quantum simulation of interest is the simulation of properties of exotic supersolid phase in ultra cold atomic condensates which is the subject matter of the proposed thesis and is explained in detail in the following section.

1.4 *Quantum simulation* of Supersolid phase

Before getting into quantum simulation of supersolid phase in ultracold atomic system and its detection, we shall provide a historical perspective of the earlier theoretical and experimental work on the realization of supersolid phase.

1.4.1 History of Supersolid phase

The phenomenon of supersolidity is as interesting and fundamental as the phenomenon of superconductivity and superfluidity, and refers to a quantum many body state of interacting particles where off-diagonal long range order (ODLRO) co-exists with diagonal long range order [4]. It implies that a supersolid shows the properties of a superfluid and a solid simultaneously. However, it was concluded by Penrose and Onsager [4] in 1956 in their seminal paper that ODLRO cannot coexist with in a crystalline solid, and hence no such supersolid phase can exist. Their argument was based on a variational model of a crystal of atoms which are pinned at equilibrium lattice positions, and hence prevent the macroscopic quantum mechanical exchange of indistinguishable particles, thereby removing all effects of quantum statistics including BEC. This argument though recapitulated even many years later [47] has no formal proof for the non-existence of supersolid.

After the argument by Penrose and Onsager(1956), Gross [48, 49] showed that a superfluid system described by the nonlinear classical field equation has the possibility to exhibit a density wave modulation. This finding was formally the first theory of the supersolid phase but it was essentially overlooked, due to incomplete understanding of the conditions of the validity of calculation by Gross. Further, Yang [5] in 1962 proposed that the atoms in a crystal of helium possess a high degree of quantum delocalization and exchanges of adjacent atoms might be significant in this case. Successively, Leggett [50] in 1970 extended Yang's argument to suggest an experiment in which the superfluid response of a ^4He crystal could be measured.

A different context for the occurrence of supersolid was proposed by Andreev and Lifshitz [51] in 1969 and Chester [52] in 1970. They described supersolidity arising due to the high mobility of point defects such as vacancies or interstitials that may be present even in the ground state of some quantum many-body systems such as ^4He at low temperature. They proposed that it was likely that a gas of such repulsively interacting point defects ought to undergo BEC, and turn superfluid, at low temperatures. Recently, it was pointed out by Prokof'ev and Svistunov [53] in 2005 that the zero-point defects supersolid scenario is the only one possible in perfect continuous-space crystals. However, many apparently

contradictory findings have raised doubts on the applicability of this model to search the supersolid phase of matter.

The remarkable property of superfluidity observed in He-4 by P.L. Kapitza [54] and the solidification of Helium being achieved by Keesom [55], together with Yang's argument [5], made He-4 a suitable candidate to look into for supersolid behaviour. Leggett [50] particularly suggested way back in 1970 that the observation of Non Classical Rotational Inertia (NCRI) in solid He-4 could be one of the ways to confirm the existence of superfluid behavior in solid. NCRI refers to an observable drop in the moment of inertia of a solid below a certain temperature due to the formation of superfluid fraction which does not follow the rigid body rotation of an ordinary solid, and hence does not contribute to the inertia value.

In 2004, the first successful yet questionable test for the existence of supersolid phase was reported by Kim and Chan [56]. They observed a downward shift in the period of a torsional oscillator filled with solid ^4He , at temperatures below 250 mK [56, 57]. The findings of this experiment have been explained in terms of decoupling of the superfluid fraction within the solid helium at low temperatures, and appears to be acceptable. However, there are other experimental observations which remain unexplained within the present context. This includes the increase in shear modulus for solid helium with a similar temperature dependence as that of NCRI [58–60], which cannot explain mechanically the drop in NCRI. Moreover, there is no evidence of superfluid in solid helium when it is subjected to localized pressure gradient [61–63] under the conditions of NCRI.

It has also been proposed that supersolidity does not exist in perfect crystals [64] and that defects such as dislocations in single crystals, grain boundaries in polycrystals are necessary. Balibar [65] interpreted the observation of flow in *He* as arising due to the formation of grain boundaries in crystals. In contrast, Anderson, Brinkman and Huse [66] have presented a theory based on the idea that solid helium is 'incommensurate'. Anderson [67] proposes that supersolidity can be an intrinsic property of ideal crystals that is only enhanced by disorder. These are among some of the issues whose interpretation remains partly unexplained and hence, controversial. These outcomes require a robust and unified theoretical and experimental approach for the case of solid He-4, which is not yet achieved.

Very recently, the controversy with solid ^4He appears to be eventually resolved by Kim and Chan [68] themselves, with the conclusion that solid ^4He does not support the direct and clear observation of supersolid phenomenon. The question of existence of supersolidity is still intact and thus one needs to look into other physical systems that may allow a relatively easy and clear identification of this novel phase.

The search for the supersolid phase of matter has thus now extended beyond solid helium, in many new directions. One of the exciting direction could be spatially confined dilute ultracold atoms interacting via a pair potential. The remarkable progress in cold atom physics has made it feasible to investigate such exotic phases of matter, in a clean and controlled experimental many-particle system. Moreover, as explained in detail in section 1.3, cold atomic systems allows one to tailor the inter particle potential which can stabilise the supersolid phase and hence, confirm its existence rigorously. Thus, ultracold atomic condensates are promising candidates for the *quantum simulation* of the supersolid phase of matter, whose existence is otherwise a matter of debate.

Here we shall describe briefly relevant ultracold atomic system which may be considered for realization of supersolid phase.

1.4.2 Ultracold atomic condensates as *quantum simulators* for Supersolid phase

As already explained in detail in section 1.3, due to the unprecedented tunability of the interaction potentials between atoms under well defined and highly controllable conditions, ultracold atomic condensates have emerged as prominent candidates to study the supersolid phase. It has been pointed out by several theoretical works that certain type of long range interaction potentials [24, 48, 69, 70] stabilize the supersolid phase in BEC and since the interactions are tunable in these systems, they are excellent systems to study supersolidity and its properties. Prominent candidates in the domain of ultra cold atomic system with long range interaction are ultra cold gases with strong dipolar interactions, realized with atoms like ^{52}Cr [20], ultra cold lanthanide bosonic Erbium atoms [21], quantum degenerate gas of fermionic dysprosium [22], and heteronuclear polar molecules [23]. We discuss the progress and possibility of supersolid phase in two such cases below.

Dipolar quantum gases : Ultracold quantum gases with alkali atoms are usually dominated by isotropic (*s*-wave) contact interactions. On the other hand, dipolar quantum gases possess dipole-dipole interaction (DDI) between permanent dipole moments which play a significant or even dominant role in determining the system properties. Recently, there has been much progress in bringing longer-ranged interactions into the system by using dipolar atoms or molecules [71]. Long range interactions provide a rich theoretical laboratory for statistical physics, and therefore Bose-Einstein condensates with dipolar interactions could become a key system to investigate them in. Peculiar effects of long-range interactions such as new quantum phase transitions have been found theoretically in dipolar BECs [72]. It is expected that due to long range nature of dipolar interactions,

the dipolar gases support the existence of supersolid phase. It has been predicted that in 2D lattices the presence of finite range interactions (where the interactions are generally cut off at the nearest or next-nearest neighbor) gives rise to novel quantum phases, like the density wave (checkerboard), namely an insulating phase with modulated density, and the supersolid phase [73].

On the other hand, numerical studies of the ground-state phase diagram of a two-dimensional homogeneous system of dipolar bosons have yielded evidence of a superfluid-to-crystal quantum phase transition [74] and not exactly superfluid to supersolid phase transition. These implications make the existence and stability of supersolid phase in such purely dipolar systems a matter of debate [75].

Rydberg atom condensates : One of the promising candidates which support the formation of supersolid phase are the ultracold atomic condensates with long range interactions between atoms in Rydberg states [24]. Combination of high-lying Rydberg states with cold atomic gases provides a promising approach to achieve the supersolid phase. This is because the strong long-range van der Waals interactions between Rydberg atoms cause strongly correlated, many-body quantum states to emerge directly as Rydberg atoms are excited in dense clouds of cold atoms. This is related with a physical mechanism called *Rydberg Blockade* [76, 77] which occurs when the excitation of an atom to a Rydberg state does not occur, if another already excited atom is less than the so-called blockade radius away, which has been demonstrated in experiments using two independent atoms [78]. Recent theoretical work has studied the excitation dynamics and the many-body phase diagram of large Rydberg atom in chains and lattices, and demonstrated their utility for quantum simulation of exotic many-body Hamiltonians [79].

The idea of quantum simulation using Rydberg atoms, for instance, has led to the prediction of long-range ordered, crystalline Rydberg atom structures [80], whose properties and stability are being investigated by several groups. This was also proposed as a way to engineer novel type of interaction potentials between ultra cold atoms that lead to the formation of supersolid phase. Specifically, an interaction of the type which flattens and essentially remains constant below a characteristic cut-off [24] has been shown to support the supersolid phase in Rydberg excited cold atomic condensates.

$$V_{ryd} = \frac{\tilde{C}_6}{r_{ij}^6 + R_c^6} \quad (1.11)$$

For atomic pairs at large distance, this potential is vdW type with an effective coefficient

$$\tilde{C}_6 = \left(\frac{\Omega}{2\Delta} \right)^4 C_6 \quad (1.12)$$

whereas it approaches a constant value below a critical distance $R_c = (C_6/2\hbar|\Delta|)^{1/6}$.

Prospects of obtaining ultracold atomic supersolid became brighter with the recent experiments where roton like mode softening [81], which indicates the instability towards the formation of uniform superfluid, has been demonstrated through cavity mediated long-range interaction in ultra cold atomic BEC [82]. These type of long range interaction are thus realizable in assemblies of cold atoms, making cold atomic gases an entirely new, likely more direct pathway for the *quantum simulation* of supersolid phase.

Given this exciting theoretical development in identifying the correct type of long-range interaction that can lead to the formation of supersolid phase and associated experimental progress in achieving the relevant system, it is crucial to understand the nature of such supersolidity in ultra cold atomic system and differentiate it from the relatively well understood ordinary superfluidity in such system which forms the motivation of the work done in this thesis.

As mentioned earlier, supersolid is defined as a quantum system which exhibits crystalline structure and superfluid properties simultaneously. It is known that one of the most distinct features of superfluidity is the quantization of circulation and formation of vortices in such systems due to the existence of a macroscopic wave function for the system. Superfluid forms vortices as a response to application of an effective gauge (magnetic) field. To differentiate the supersolid phase from the superfluid in ultracold atomic system, one of the ways is to probe their response in presence of effective gauge field and point out the distinguishing features between them. Before going into details of this motivation, in the next section we describe the effective gauge fields for such neutral ultra cold atomic system and its effect on cold atomic condensates.

1.5 *Artificial* gauge fields for cold atoms

The generation of artificial gauge fields for quantum gases has intrigued much interest since the first realization of BEC. Unlike the charged systems which respond to a magnetic field, one needs to rely on methods that applies a magnetic field on such neutral systems in an artificial manner. The conceptually convenient way is by uniformly rotating the cloud of atoms, which mimicks the Lorentz force experienced by a charged particle in a magnetic field. Due to the existence of macroscopic wave function for the system, BEC shows the quantization of circulation and formation of vortices under rotation. The spectacular generation of a vortex lattice in a BEC by rotation [34], which in addition to proving its superfluidity, provides a direct analogue of the Abrikosov lattice in a type-II superconductor under a magnetic field [83].

There are many proposals put forward and hence implemented to generate gauge fields without a large scale rotation [84]. This is because of the constraint on the rotation frequency $\Omega < \omega$ (trap frequency) which does not allow application of very high effective magnetic fields (of the order $\Omega \sim \omega$) by rotating the system. On the experimental front, such proposals have been successfully implemented by means of Raman techniques [85, 86], which generates relatively very high effective magnetic fields with high stability of the system compared to rotating potentials. The details of the application of magnetic field either by rotation or by light induced gauge potentials is provided in chapter 2 of this thesis.

This experimental progress has opened up study of wide range of new features in the physics of quantized vortices and vortex arrays, allowing access to parameter regimes unlike those accessible in the helium superfluids or type-II superconductors. Moreover this has lead to novel properties of the ground states in presence of gauge (magnetic) fields, including the possibility of exotic strongly correlated phases.

Examples of which include the realization of Fractional Quantum Hall effect [87] in ultracold atomic systems. The fractional quantum Hall phases realized by two-dimensional electron gases in very large magnetic fields are among the most intriguing states of matter [88]. In such systems, electrons 'bind' to magnetic vortices, forming strongly correlated phases with striking properties, such as exotic excitations ('anyons') which obey fractional statistics [89]. Experimental evidences [90] strongly support the existence of fractionally charged excitations in these systems, but evidence for their statistics is less conclusive [91]. Due to the similarity with the electron system, the physics of the FQHE should emerge for a two-dimensional (2D) condensate in the regime of very high magnetic fields, which is now feasible by using light induced gauge potentials [85, 86].

With ultracold atoms in optical lattices, the application of gauge field mimicks the trivial problem of Bloch electrons in a magnetic field. In context of the Bose Hubbard model in presence of a uniform magnetic field, the system shows the breaking of degeneracy of Landau levels and the formation of Hofstadter Butterfly energy spectrum [92] in the strongly correlated regime. This has been explained in chapter 2 of the thesis.

With the background of ultracold atoms, optical lattices, supersolid phase and *artificial* gauge fields, in the next section we present the motivation of the work done in this thesis.

1.6 Motivation of the thesis

As mentioned in detail in earlier sections, supersolid is a quantum phase which exhibits crystalline and superfluid properties simultaneously. One of the ways to characterize superfluidity is by the quantization of circulation and formation of vortices. This happens due to the existence of a macroscopic wave function for the system. Superfluid forms vortices as a response to application of an effective gauge (magnetic) field. This effective gauge field can be generated either by rotation [93–96] or by engineering the phase of the condensate using certain type of laser-atom interaction [85, 86, 97] which couples their internal states with raman lasers. The formation of quantized vortices and their collective oscillations has been experimentally observed [34] and studied extensively in case of superfluid of ultracold atomic condensates [98, 99].

Motivated by theoretical and experimental success in the observation of vortices and their collective motion, we theoretically explore the possibility for the detection of supersolid phase in ultracold atomic condensates, by probing their response to rotation or application of equivalent gauge fields. To confirm the existence of supersolid, one needs to look into the signatures for solid like behavior coexisting with superfluidity simultaneously. In this thesis, we performed calculations for such supersolid phase both for the lattice and continuum systems under the effect of such artificial gauge field.

The thesis highlights the interesting features exhibited by supersolid phase in artificial gauge potentials. After this brief introduction to the problem considered in the thesis, we describe below the detailed description of the system and specifically mention the properties we investigate in the proposed thesis.

We start our study of the supersolid phase in the context of ultracold atoms with general long range interactions in the presence of optical lattice potentials. As mentioned, lattice potentials can act as a bridge where one can simulate the periodically modulated condensed matter systems on a macroscopic scale and in clean environment, with extreme control over parameters. For atoms interacting via contact interaction, a quantum phase transition [100] from a superfluid (SF) to a Mott insulator (MI) has been predicted and observed [33]. In the simplest case, these systems can be theoretically described by the Bose-Hubbard model (BHM), which has two parameters: hopping parameter t and on-site interaction U [37]. A natural extension of the BHM comes from including above mentioned long-range interactions between atoms which is called as extended Bose Hubbard model (eBHM). Under tight binding approximation, the long range interaction term in the eBHM can be written as sum of contribution from the onsite interaction, nearest neighbor interaction, the next nearest neighbor interactions between atoms and so on [101, 102].

As mentioned before, recent experiments in observing BEC of ultracold atoms with long range interactions and polar molecules have deepened interest in such extended Bose-Hubbard models [101, 102]. Long-range interactions play a crucial role in the collective behavior of the system, leading to the appearance of states with different types of long-range order, like various insulating states as well as supersolids. In the deep optical lattice situation, one considers minimal eBHM with only the onsite and nearest neighbor interactions, and the new phases which appear are the Density Wave (DW) and supersolid (SS) phases [103] alongwith the MI and SF phases. These phases have different characterising properties and behavior as compared to their MI and SF counterparts.

Chapter 2 and 3 describe the detailed study of the effect of an artificial gauge field on the SS phase and its signatures at the DW transition boundary, lying deeply inside the strongly interacting regime. The summary of work done in these chapters is given in section 1.6.1.

As we decrease the height of the lattice potential, we move away from the strongly interacting regime to the weakly interacting regime, where the Hubbard model description can be replaced by the weakly interacting Gross-Pitaevskii mean field formalism [19]. In the absence of optical lattice, the continuum limit of studying supersolid phase and its signatures in an artificial gauge field are much more convincing as compared to the lattice counterparts. The reason is that the induced periodicity of the underlying lattice is partly responsible for supersolidity.

An important method of investigation of such continuum supersolids is to study the collective modes of the system and detect the various sound modes which are the reflection of system's elastic properties. The study of vortex dynamics in rotating superfluids is quite remarkable both theoretically and experimentally and served as an important test for superfluidity [34, 98, 104]. The theoretical approach based on macroscopic Gross-Pitaevskii based hydrodynamics was found capable of describing the oscillation modes of a regular vortex lattice in ultracold atomic superfluids [98, 104], which was subsequently verified experimentally by Coddington et al. [34]. They were able to detect the Tkachenko modes, which are transverse sound modes in the vortex lattice.

Motivated by this success in observation of collective vortex lattice oscillation in ultracold atomic rotating superfluid, in Chapter 4 of the thesis we constructed a Gross-Pitaevskii hydrodynamic theory for rotating supersolid in the weakly interacting regime, where a vortex lattice co-exist with supersolid lattice. The purpose of our study is to understand the nature of the collective excitations of such vortex lattice as much as possible within an analytical framework and point out its difference with the corresponding situation

in a superfluid. Rotating supersolids when subjected to small perturbations reveal interesting features that result due to the interplay of two embedded lattice structures, the supersolid lattice and the vortex lattice, and provide signatures in the sound modes to detect it in comparison to rotating superfluids. The appearance of such modes in the excitation spectrum differentiate the system from rotating superfluids and can be a signature for supersolid behavior. This may provide a convincing way of verifying supersolidity in continuum systems.

In the next sub section 1.6.1, we provide the chapter wise description of the work done in this thesis.

1.6.1 Outline of the thesis

In the following chapters, we present a detailed theoretical study of the properties of supersolid phase in *artificial* gauge fields, including both the strongly interacting and weakly interacting regime. The outline of the thesis is as below :

Chapter 2 provides the calculations of modification of the DW-SS phase boundary as a function of increasing strength of *artificial* gauge field and the structure of vortex profiles in the supersolid phase near the DW-SS phase boundary using mean field Gutzwiller variational formalism [105]. We perform analytical calculations using mean field Gutzwiller variational formalism to study the effect of artificial gauge field on cold atomic condensates with long range interactions loaded in optical lattices in the framework of extended BHM so that it can be contrasted against similar studies done using Bose Hubbard model [106, 107]. In this chapter, we report the modification of the DW and MI phase boundary by using a reduced-basis ansatz for the Gutzwiller variational wave function, within the framework of mean-field approximation. The minimization of the energy functional very close to the DW phase boundary shows that the superfluid order parameter satisfies a spinorial Harper equation [105]. Consequently, the phase boundary can be determined from the edge of a Hofstadter butterfly (HB) spectrum [92].

In the resulting vortices, the spatial profile of the superfluid density shows a checkerboard-like two sublattice modulation with a relative phase winding between the superfluid order parameter defined on each of these sublattices. Thus, from the spectrum of the Harper equation (equation for electron in a periodic potential in presence of a magnetic field), we have analytically demonstrated how the superfluid and crystal order coexist in the vortex profile of a supersolid around a DW vortex core [105]. This can be used to identify the supersolid phase in cold-atom experiments. We also discuss their possible ways of experimental detection, which includes the Time of Flight (TOF) imaging technique

to get the sublattice modulation of the superfluid density and to get the detailed vortex structure, one can use the Bragg scattering technique, which is sensitive to the spatial phase distribution of the initial state and the direction of rotation.

In **Chapter 3** we adopt the strong coupling perturbation theory [108] to calculate the effect of artificial gauge field on the phase diagram and the experimental signatures of the vortex structures in a supersolid phase [109]. We also show that, in the presence of an artificial magnetic field, the TOF image actually depends on the means to produce such an effective magnetic field, and hence one can notice that the momentum distribution depends on the type of the gauge potential, and hence, not gauge invariant. We explain this apparent gauge dependence of momentum distribution as a direct result of the realization of a specific vector potential and not the field, in the typical experimental setups.

In part 3A of the chapter, we look into the modification of the DW and MI phase boundaries as a function of magnetic field in the framework of strong coupling perturbation approach. This is basically a many-body perturbation expansion in terms of hopping parameter t/U , and can have higher order corrections in t/U , which gives us a quantitative insight of the critical points. As expected, we found that the shapes of the insulating lobes depend on the dimensionality of the system and, also on the application of artificial gauge field. Mean-field theory always gives a concave shape to the MI and DW lobes because the dimensionality only enters as a prefactor in the expressions, while the strong-coupling expansion easily distinguishes the shape of insulating lobes in different dimensions, both in the absence and presence of the artificial magnetic field. The determination of DW-SS and MI-SF transition boundaries as a function of gauge field, using strong-coupling perturbation theory, is one of the important results of this work [109].

We carried out an extrapolation of phase boundaries using chemical potential exploration technique to go beyond the finite order strong coupling expansion scheme. The system shows the increasing stability of the insulating phase (i.e. the DW and MI phases grow in size as the strength of the magnetic field is increased from zero to finite values). This can be explained due to the localization effect of magnetic field on the moving bosons, thus favoring the insulating phases to occupy a larger area in the phase diagram.

In part 3B of the chapter, we calculate some possible experimental signatures for vortex structures in a SS obtained in chapter 2. Using the strong coupling perturbation theory, we determine the momentum distribution profile in presence of artificial gauge field, which gives us distinguishing features to detect a rotating SS. The standard experimental way to probe the properties of an ultracold atomic condensate is through TOF absorption imaging of the freely expanding atoms released from the trap. The same method is used

to probe the condensate loaded in optical lattices as well. The quantity that is measured experimentally in such TOF expansions is the momentum distribution of the ultracold atomic ensembles in the long time limit. Since, we perform our calculations at the phase boundary, so the results for the momentum distribution at the DW and MI phase boundary, in the presence of a symmetric gauge potential provides information about the vortex signature in a SS (at the DW-SS phase boundary) and the vortex in a SF (at the MI-SF phase boundary) [109]. Our calculations demonstrates that the rotating SS reflects some extra peaks in the momentum distribution in addition to the peaks observed in a rotating ordinary SF. This occurrence of extra peaks in the momentum distribution for a rotating SS is another important result of this work [109].

To analyze this issue further, we compared the momentum distribution in a symmetric gauge to the momentum distribution corresponding to the many-body states having definite quasi-angular momentum in a symmetric gauge potential. This quasi-angular momentum is analogous to the Bloch momentum for a rotationally invariant system in presence of lattice. Thus, we re-evaluate the momentum distribution, but for a given fixed quasi-angular momentum and found that the results at the DW-SS phase boundary can be distinguished from the MI-SF phase boundary by noting the appearance of small extra peaks in the former [109]. The fact that a zero quasi-angular momentum state can be distinguished from a nonzero one by looking at the corresponding momentum distribution allows the experimentalists to verify that vorticity has entered the system through the TOF measurement.

Chapter 4 of the proposed thesis is devoted to the study of rotating supersolid in continuum systems [110]. As already mentioned about the necessity of the continuum model, we develop the hydrodynamic theory for rotating Supersolids in such continuum systems. More specifically, we construct a Gross-Pitaevskii based hydrodynamic theory [104] for rotating supersolid in the regime where a vortex lattice co-exists with the supersolid [110]. The purpose of our study is to understand the nature of the collective excitations of such vortex lattice as much as possible within an analytical framework and point out its difference with the corresponding situation in a superfluid.

The lattice part of the supersolid is described as the normal component within the well known two-fluid approximation. Within this framework, we derive the set of hydrodynamic equations for rotating supersolid. This is valid under the general conditions of applicability of hydrodynamic theory, in particular the perturbations under consideration are long wave (practically much longer than the lattice size). We also point out typical cold atomic systems where such theory may be applicable. Using these equations, we calculate and analyze the dispersion relations for such collective excitations of vortex lattice in a supersolid within this hydrodynamic approach [110] and compare them

against the results for a fast rotating superfluid that was studied theoretically and experimentally. We also check and describe the solutions of such hydrodynamic equations under various limits, like for a rotating superfluid and for non-rotating supersolid. We shall also briefly discuss how such hydrodynamic equations gets modified where mutual friction between the supersolid lattice and the vortex lattice is taken into account. We calculate the excitations for the vortex lattice in supersolid and found that it distinctly depends on the quantized nature of circulation in a supersolid and provide unambiguous signature of the existence of macroscopic quantum order [110].

Chapter 5 of the thesis will be the concluding chapter, summarizing the outcome of the thesis with a brief outline about the future possible scope of the work.

Chapter 2

Extended Bose Hubbard Model in presence of artificial gauge field: Mean field approach

This chapter is based on the publication *R. Sachdeva, S. Johri and Sankalpa Ghosh, 'Cold atoms in rotating optical lattice with nearest neighbor interaction', Physical Review A, 82, 063617 (2010) [105]*

Remarkable progress has been made in the study of strongly interacting atomic regime, realized experimentally with the help of cold atoms in optical lattices. The study of interacting bosons in a lattice was originally proposed by M.P.A. Fisher et.al in 1989 [36]. In their landmark paper, they proposed the Hubbard Hamiltonian for the bosonic atoms in a periodic potential and predicted the Mott Insulator(MI)-superfluid (SF) quantum phase transition for bosonic systems. In 1998, Jaksch et.al [37] proposed that this description for interacting bosons in lattice could be extended to cold bosonic atoms in an optical lattice and it was further experimentally established in 2002 by Greiner et.al [33]. They observed MI-SF transition with ultracold atomic condensates with short range interactions. This experimental success has proved the usefulness of optical lattice for studying strongly correlated systems using cold atomic condensates and opened up a new direction for this field of study.

A further step in this direction is the study of ultracold atoms with long range interactions placed in optical lattice potential. They are described by an extended version of Bose Hubbard (BHM) model [111] where in addition to onsite interactions, one needs to take into account the interactions between atoms at different lattice sites [112]. The interest in this model stems from the appearance of new phases, namely the Density

Wave (DW) phase and the Supersolid (SS) phase, apart from the MI and SF phase. As explained in detail in chapter 1, there are quite a number of promising candidates of such ultra cold atomic system with long range interaction, that could be suitable for observing the new phases.

Before going into further discussion we provide a systematic derivation of the Hamiltonian for the extended Bose Hubbard Model (eBHM) that describes ultracold atomic condensates with long range interaction in optical lattice under tight binding approximation. In this context, we also introduce *artificial* gauge field for such neutral ultracold atoms and differences for true gauge field that represent electromagnetic field for charged particle.

2.1 Derivation of Hamiltonian

We begin with the derivation of extended Bose Hubbard Hamiltonian. Accordingly, this section is thus divided into three parts. The first part introduces the general extended Bose Hubbard Hamiltonian used to study bosons with long range interactions in a stationary periodic potential under the tight binding approximation. The second part presents the effect of rotation on the system and provides a detailed explanation for showing its equivalence with application of *artificial* gauge field. The third part describes the derivation of modified extended Bose Hubbard Hamiltonian to include the effect of *artificial* gauge field on the system, done using a symmetric gauge transformation.

2.1.1 Extended Bose Hubbard Hamiltonian for bosons in an optical lattice potential

An optical lattice is created by making coherent laser beams propagating in opposite directions interfere with each other. It results in the formation of standing wave with a periodic alternate pattern of dark and bright regions [19]. The basic mechanism involves the interaction of the electric field with the dipole moment of the atom which leads to an effective potential proportional to the intensity of the laser field. To describe the interaction between the atom and the electric field, within the dipole approximation the Hamiltonian can be written as

$$H_{dip} = -\mathbf{d} \cdot \mathbf{E}(\mathbf{r}, t) \quad (2.1)$$

where \mathbf{d} is the electric dipole moment of the atom and $\mathbf{E}(\mathbf{r}, t)$ is the electric field. For two identical laser beams counter- propagating along the x-direction polarized in the ϵ

direction, with electric fields $\mathbf{E}_{\pm}(x, t) = \epsilon E_0 e^{i(\pm kx - \omega_L t)}$, the standing light field is given by

$$\mathbf{E}(x, t) = \mathbf{E}_+(x, t) + \mathbf{E}_-(x, t) = 2\epsilon E_0 \cos(kx) e^{-i\omega_L t} \rightarrow 2\epsilon E_0 \cos(kx) \cos(\omega_L t) \quad (2.2)$$

where $k = \omega_L/c$ is the magnitude of the wave vector of the laser light. Due to the AC Stark effect, an electric dipole moment is induced in the ultracold atoms and hence their energy is modified.

$$\Delta E_g(x) = -\frac{1}{2}\alpha \langle E^2(x, t) \rangle \quad (2.3)$$

with α as the atomic polarizability. With only the term in α with the smallest energy denominator [19]

$$\alpha \approx -\frac{|\langle e | \mathbf{d} \cdot \epsilon | g \rangle|^2}{\hbar \delta} \quad (2.4)$$

where $|g\rangle$ is the ground state, $|e\rangle$ is the single excited state and δ is the detuning. The time average of the squared electric field can be calculated from equation (2.2) from which the optical lattice potential can be written as

$$V_L(x) \equiv \Delta E_g(x) = V_0 \sin^2(kx) \quad (2.5)$$

where the lattice height $V_0 = -\alpha E_0^2$ is proportional to the laser intensity. The atoms are pulled towards either the bright or the dark regions depending on the frequency of light and are thus trapped in localized region in space. For 2D optical lattices, the effective potential energy experienced by the atoms is given by

$$V_L(\mathbf{r}) = V_0 (\sin^2(k_x x) + \sin^2(k_y y)) \quad (2.6)$$

where d is the lattice spacing and V_0 is proportional to the laser power intensity. We write the Hamiltonian for a single particle in this lattice potential

$$H_0(\mathbf{r}) = -\frac{\hbar^2}{2m} \nabla^2 + V_L(\mathbf{r}) \quad (2.7)$$

where m is the mass of single particle. The corresponding Schrödinger equation is

$$H_0(\mathbf{r}) \phi_{\mathbf{q}}^l(\mathbf{r}) = E_{\mathbf{q}}^l \phi_{\mathbf{q}}^l(\mathbf{r}) \quad (2.8)$$

and the eigen solutions are $E_{\mathbf{q}}^l$ which are Bloch functions [113]. Here, l is the band index and \mathbf{q} is the quasi momentum associated with eigen functions. It is known that, for any band l the Bloch functions can be combined to yield a set of orthonormal Wannier basis

functions [114]. This is done by using discrete fourier transform as

$$W_S^l(\mathbf{r} - \mathbf{r}_i) = \frac{1}{\sqrt{N}} \sum_{\mathbf{q}} e^{-i\mathbf{q}\cdot\mathbf{r}_i} \phi_{\mathbf{q}}^l(\mathbf{r}) \quad (2.9)$$

where \mathbf{r}_i denotes the center of i th site and N is the total number of sites. This gives site localized Wannier wavefunctions. For small interaction energies, the particles can be considered to be confined in the lowest Wannier orbitals because the energy separation between the lowest and first excited band is quite large as compared to interaction energy. We work in this regime and now onwards drop the band index l .

Extending the single particle picture to many particles, we consider bosonic atoms with long range repulsive interactions. We then use the following second quantized Hamiltonian

$$\hat{H}_0 = \int d\mathbf{r} \hat{\psi}^\dagger(\mathbf{r}) \left[H_0(\mathbf{r}) + \int d\mathbf{r}' V(|\mathbf{r} - \mathbf{r}'|) \hat{\psi}(\mathbf{r}') \hat{\psi}(\mathbf{r}) \right] \hat{\psi}(\mathbf{r}) \quad (2.10)$$

Here, $V(|\mathbf{r} - \mathbf{r}'|)$ is the non-local long range interaction between atoms at different sites of lattice. $\hat{\psi}(\mathbf{r})$ is the bosonic field operator and it obeys the commutation relation $[\hat{\psi}(\mathbf{r}), \hat{\psi}^\dagger(\mathbf{r}')] = \delta(\mathbf{r} - \mathbf{r}')$. The bosonic field operator $\hat{\psi}(\mathbf{r})$ can be expanded in terms of the Wannier basis, $W_S(\mathbf{r} - \mathbf{r}_i)$ and the site-specific annihilation operators as

$$\hat{\psi}(\mathbf{r}) = \sum_{i=1}^N \hat{a}_i W_S(\mathbf{r} - \mathbf{r}_i) \quad (2.11)$$

We work in the tight binding regime, where the Wannier function are completely site localized which implies that only the tunneling between sites which are nearest neighbors will be considered. This is because in the tight binding regime, the Wannier functions roughly assumes the form of a highly localized gaussian in the lowest Bloch band (s band) (as shown in Fig. 2.1), only tunneling between sites which are nearest neighbors will be finite. The tunneling between sites which are not nearest neighbors can be neglected. However, the interaction between particles on the neighboring sites will be taken into account due to long range of interactions. Under this approximation, we substitute $\hat{\psi}(\mathbf{r})$ and $\hat{\psi}^\dagger(\mathbf{r})$ into equation (2.10), which yields the general extended Bose Hubbard Hamiltonian [101] given as

$$\begin{aligned} \hat{H}_0 = & -t \sum_{\langle i,j \rangle} \hat{a}_i^\dagger \hat{a}_j + \frac{U}{2} \sum_i \hat{n}_i (\hat{n}_i - 1) + \sum_i \epsilon_i \hat{n}_i + \frac{1}{2} V_{\sigma_1} \sum_{\langle i,j \rangle} \hat{n}_i \hat{n}_j \\ & + \frac{1}{2} V_{\sigma_2} \sum_{\ll i,j \gg} \hat{n}_i \hat{n}_j + \dots \end{aligned} \quad (2.12)$$

where i and j are the site indices, $\langle i, j \rangle$ indicates that the sum is over nearest neighbor, $\ll i, j \gg$ indicates the sum over next nearest neighbors and so on. \hat{n}_i is

the number operator for site i . The parameters t and ϵ_i are integrals describing the hopping(tunneling) and onsite zero-point energy respectively, given by

$$t = \int_{\langle i,j \rangle} d\mathbf{r} W_S^*(\mathbf{r} - \mathbf{r}_i) H_0(\mathbf{r}) W_S(\mathbf{r} - \mathbf{r}_j) \quad (2.13)$$

$$\epsilon_i = \int d\mathbf{r} W_S^*(\mathbf{r} - \mathbf{r}_i) H_0(\mathbf{r}) W_S^*(\mathbf{r} - \mathbf{r}_i) \quad (2.14)$$

The tunneling parameter t is independent of choice of $\langle i, j \rangle$, where $\langle \rangle$ implies nearest neighbors. The inter particle interactions are characterized by the parameter

$$V_\sigma = \int |W_S^*(\mathbf{r} - \mathbf{r}_i)|^2 V(|\mathbf{r} - \mathbf{r}'|) |W_S(\mathbf{r} - \mathbf{r}_j)|^2 d\mathbf{r} d\mathbf{r}' \quad (2.15)$$

where $|\mathbf{r} - \mathbf{r}'| = 4\pi\sigma/|\mathbf{k}|$. U determines the on-site interactions, V_{σ_1} the nearest-neighbor interactions, V_{σ_2} the interactions between the next-nearest neighbors, etc. In this way, the summations in equation (2.12) can be carried out over appropriate pairs of sites, giving rise to terms with nearest neighbor, next nearest neighbor and so on. This gives the general form of extended Bose Hubbard Hamiltonian.

It is to note that, to study this system one of the convenient unit is the recoil energy given by

$$E_R = \frac{\pi^2 \hbar^2}{2md^2} \quad (2.16)$$

The energies measured in Fig. 2.1 for the single particle density profiles in tight binding regime are in units of recoil energy E_R . However, in our subsequent calculations, the energies are scaled in units of onsite interaction strength U . Again, as seen from the density profile in Fig. 2.1, the density falls off very rapidly and hence, the long range interaction is cut-off only till nearest neighbor interactions. The other interaction terms beyond the nearest neighbor are too small to be taken into account. Thus, in this thesis we take into account the interaction between particles sitting on the same site and on the nearest neighboring sites. So, the extended Bose Hubbard Hamiltonian with onsite and nearest neighbor interaction is given as below

$$\hat{H}_0 = -t \sum_{\langle i,j \rangle} \hat{a}_i^\dagger \hat{a}_j + \frac{U}{2} \sum_i \hat{n}_i(\hat{n}_i - 1) + \sum_i \epsilon_i \hat{n}_i + V \sum_{\langle i,j \rangle} \hat{n}_i \hat{n}_j \quad (2.17)$$

with t as the hopping parameter, U as the onsite interaction, ϵ_i as the zero-point energy and V as the nearest neighbor interaction strength. Here and throughout the thesis, we denote the nearest neighbor interaction strength V_{σ_1} in equation (2.12) by V . Now we shall describe the effect of *artificial* gauge (magnetic) field on such ultracold atoms.

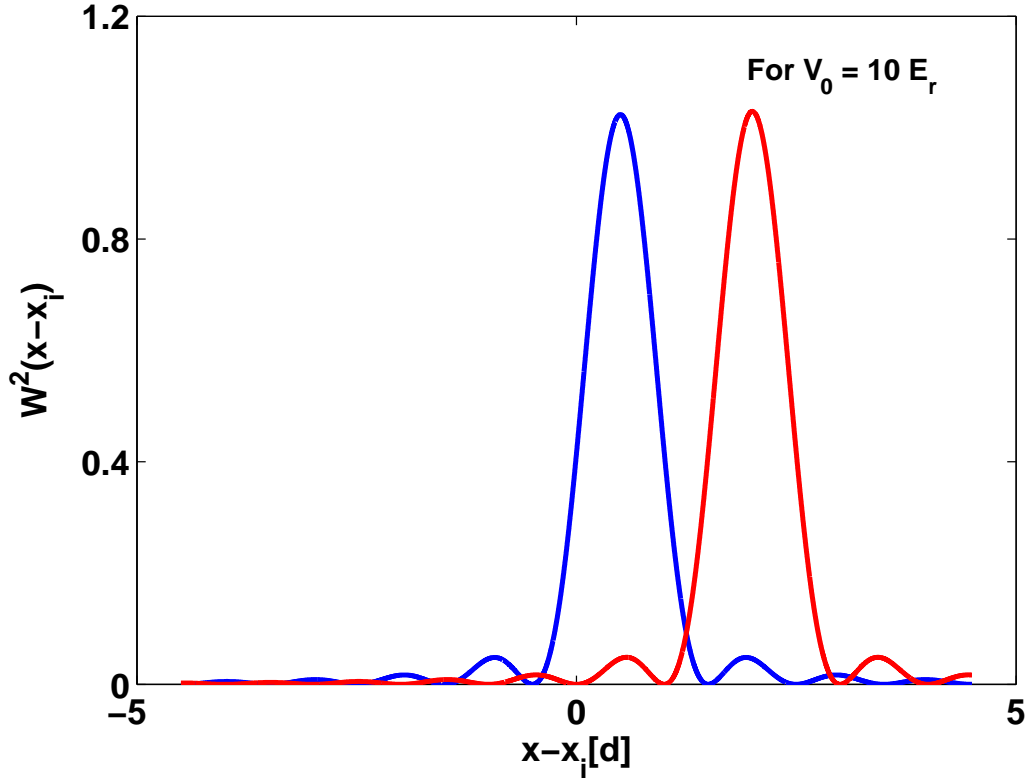


FIGURE 2.1: Single particle density profiles for lattice depth $V_0 = 10E_R$ described using Wannier functions. It shows density profile for $V_0 = 10E_R$, a depth at which the system is in the tight-binding regime where the Wannier functions extend up to nearest neighboring sites, where $E_R = \frac{\pi^2 \hbar^2}{2md^2}$ is the lattice recoil energy with d as the lattice spacing. The Wannier function extend up to nearest neighboring sites and no further.

2.1.2 Application of *artificial* gauge field on cold atomic system

Rotation: One of the conventional ways to apply an effective magnetic field to the neutral cold atomic system is to rotate the trap plus lattice potential. Combination of effective magnetic fields and optical lattices also increases the stability of the experimental systems. It was realized experimentally [95, 96] for trapped cold atoms with and without optical lattice. The first experiments with rotating lattices used masks [95] to produce parallel beams, whose subsequent interference formed the optical lattice potential. Mechanical rotation of the mask caused the interference pattern to rotate, and hence imparts an effective magnetic field on the system. More recently [96] the mask has been replaced with an acousto-optic modulator which allows for considerably deeper lattices and lower temperatures.

However an obvious outcome of rotation represents a complicated time dependence in rotating potentials. This makes the theoretical study of the system quite difficult resulting in subtlety in understanding the fundamentals of the related phenomena. It can

be avoided by switching to a coordinate system rotating with same angular velocity as the potential. It is explained as below [115, 116].

Let us consider a cylindrically symmetric Hamiltonian H_0 in the laboratory frame and a stirring potential $V(X, Y)$ is applied to the system. The coordinates (X, Y) in the rotating frame are related to the coordinates (x, y) in the laboratory frame by

$$\begin{aligned} X &= x \cos(\Omega t) + y \sin(\Omega t) \\ Y &= -x \sin(\Omega t) + y \cos(\Omega t) \end{aligned} \quad (2.18)$$

In experimental system, when the stirring potential is acting on the fluid, the only frame where the Hamiltonian is time-independent is the frame rotating with the stirrer. It is in this frame only where one can apply the principles of equilibrium statistical physics. Hence, the Hamiltonian in the rotating frame is $H = H_0 - \Omega L_z$.

This implies that we perform our calculations in the rotating frame and thus, we rewrite the Hamiltonian in rotating frame coordinates. To show the transformation, as an example we take the case of classical free particle following [117].

2.1.2.1 Transformation to rotating frame coordinates

Consider a particle rotating about the z axis with an angular velocity ω in the stationary frame. We denote the position vector of the particle by $\mathbf{r}(\equiv \mathbf{r}_0)$ and the velocity in the stationary frame by $\mathbf{v}_0 = \omega \times \mathbf{r}$. The angular momentum in the stationary frame is given by $L_0 = m(\mathbf{r} \times \mathbf{v}_0) = \mathbf{r} \times \mathbf{p}_0$. In the stationary frame, the Lagrangian is given by

$$L = \frac{1}{2} m v_0^2 = H_0 \quad (2.19)$$

with H_0 as the Hamiltonian in the stationary coordinate system.

If we examine the particle in a frame of reference rotating with an angular velocity Ω with respect to the stationary frame. The velocity of the particle in the rotating frame is

$$\mathbf{v} = \mathbf{v}_0 - \Omega \times \mathbf{r} = (\omega - \Omega) \times \mathbf{r} \quad (2.20)$$

The principle of least action is frame independent, thus the Lagrangian in rotating frame coordinates is

$$\begin{aligned} L &= L_0 = \frac{1}{2} m v_0^2 = \frac{1}{2} m (\mathbf{v} + \Omega \times \mathbf{r})^2 \\ &= \frac{1}{2} m v^2 + m \mathbf{v} \cdot (\Omega \times \mathbf{r}) + \frac{1}{2} m (\Omega \times \mathbf{r})^2 \end{aligned} \quad (2.21)$$

The conjugate momentum is given by

$$dL = m\mathbf{v} \cdot d\mathbf{v} + m(\boldsymbol{\Omega} \times \mathbf{r}) \cdot d\mathbf{v} + m\mathbf{v} \cdot (\boldsymbol{\Omega} \times d\mathbf{r}) + m(\boldsymbol{\Omega} \times d\mathbf{r}) \cdot (\boldsymbol{\Omega} \times \mathbf{r}) \quad (2.22)$$

$$\mathbf{p} = \frac{\partial L}{\partial \mathbf{v}} = m\mathbf{v} + m(\boldsymbol{\Omega} \times \mathbf{r}) = m\mathbf{v}_0 = \mathbf{p}_0 \quad (2.23)$$

It is to note that the angular momentum in the rotating frame which is constructed using the conjugate momentum \mathbf{p} is the same as the angular momentum operator in the stationary frame

$$\mathbf{L} = \mathbf{r} \times \mathbf{p} = \mathbf{r} \times \mathbf{p}_0 = \mathbf{L}_0 \quad (2.24)$$

The Hamiltonian in the rotating frame is thus

$$\begin{aligned} H &= \mathbf{p} \cdot \mathbf{v} - L = mv^2 + m\mathbf{v} \cdot (\boldsymbol{\Omega} \times \mathbf{r}) - \frac{1}{2}mv^2 - m\mathbf{v} \cdot (\boldsymbol{\Omega} \times \mathbf{r}) - \frac{1}{2}m(\boldsymbol{\Omega} \times \mathbf{r})^2 \\ &= \frac{1}{2}mv^2 - \frac{1}{2}m(\boldsymbol{\Omega} \times \mathbf{r})^2 \\ &= \frac{1}{2}m(\mathbf{v}_0 - \boldsymbol{\Omega} \times \mathbf{r})^2 - \frac{1}{2}m(\boldsymbol{\Omega} \times \mathbf{r})^2 \\ &= \frac{1}{2}mv_0^2 - \boldsymbol{\Omega} \cdot (\mathbf{r} \times \mathbf{p}_0) = \frac{p_0^2}{2m} - \boldsymbol{\Omega} \cdot \mathbf{L} \\ &= H_0 - \boldsymbol{\Omega} \cdot \mathbf{L}_0 \end{aligned} \quad (2.25)$$

This coordinate transformation renders the Hamiltonian time independent and hence facilitates the calculation of the ground state in the laboratory frame. This example is for a single classical particle, the analogy can be extended to other systems with many particles as long as the system is undergoing uniform rotation [117].

The Hamiltonian for bosons in a rotating optical lattice [93, 95, 96] is thus given by,

$$H_{rot} = -\frac{\hbar^2}{2m}\nabla^2 + \frac{1}{2}m\omega^2(x^2 + y^2) + V_L(\mathbf{r}) - \frac{\hbar\boldsymbol{\Omega}}{i}(x\partial_y - y\partial_x)$$

This can be re-written as

$$\begin{aligned} H_{rot} &= \frac{1}{2m} \left(\frac{\hbar}{i}\nabla - m(\boldsymbol{\Omega} \times \mathbf{r}) \right)^2 + \frac{1}{2}m(\omega^2 - \Omega^2)(x^2 + y^2) + V_L(\mathbf{r}) \\ &= \frac{1}{2m}(\mathbf{p} - m\mathbf{A})^2 + \frac{1}{2}m(\omega^2 - \Omega^2)(x^2 + y^2) + V_L(\mathbf{r}) \end{aligned} \quad (2.26)$$

with $\mathbf{A} = \boldsymbol{\Omega} \times \mathbf{r}$. It may be seen that the kinetic energy part of the Hamiltonian can be written in a form which is similar to the one that describes a charged particle in magnetic field in a symmetric gauge with $\mathbf{A} = B(-y, x, 0)$. Thus rotation of this cold atomic system is equivalent to application of an *artificial* magnetic field with symmetric gauge vector potential.

As seen from equation (2.26), in case of rotating potential, the effect of rotation is partitioned into two parts. The role of the first part is to modify the kinetic energy term, producing an effective magnetic field, whereas the other part weakens the trapping potential of the system. The effect of rotation (which is equivalent to symmetric gauge vector potential) in the term $\frac{1}{2}m(\omega^2 - \Omega^2)(x^2 + y^2)$ in equation (2.26) implies that the centrifugal potential weakens the role of trapping potential. In order to stabilize the system for rotating potentials, the constraint on the rotation frequency is $\Omega < \omega$ and thus not very high enough effective magnetic fields (of the order $\Omega \sim \omega$) can be applied by rotating the system.

One can get rid of such constraint by engineering vector potentials by means of Raman lasers as in [86]. In such system, there is no such weakening of trap potential and hence relatively very high effective magnetic fields can be applied to the system with high stability of the system compared to rotating potentials. This has been explained in detail below.

Application of *artificial* gauge field using laser induced potentials:

In addition to the conventional method like rotation to apply an effective magnetic field to the neutral cold atomic system as described in (2.1.2.1), there are more efficient ways which uses laser coupling to realize such magnetic field on the system. There have been many proposals [118–121] for creating high enough effective magnetic fields without rotation, which include optical coupling between internal atomic states, where the atoms are dressed in a spatially dependent manner. Here, the light induced gauge potentials generate an effective magnetic field as a consequence of changing into a spatially varying basis of internal states. This was firstly experimentally reported [85, 86] in 2009 where a spatially varying Hamiltonian for ultra cold atoms was created by dressing them in an optical field which couples different spin states of the atoms.

The technique involves two counter propagating Raman laser beams which couple internal spin states with linear momenta which differ by two times of the photon momentum. This coupling gives rise to spatial gradient of the phase difference between the spin components of the dressed state. Eventually, this spatially varying state leads to non-zero vector potential when the coupling is detuned from the Raman resonance. Thus, the actual physical system of cold neutral bosonic atoms interacts with laser induced potential, and uses the concept of laser assisted tunneling [97]. It allows one to control the phase of the tunneling matrix elements and realize *artificial* gauge potentials. We explain in detail how a vector potential $\mathbf{A} = A_x \hat{x}$ is engineered in practice, which produces an effective magnetic field for ultracold atoms.

In the NIST set up [86], to engineer a vector potential $\mathbf{A} = A_x \hat{x}$, the condensate is illuminated with pair of counter propagating Raman laser beams along \hat{x} . These beams couple internal states $|m_F, k_x\rangle$ which differ in internal angular momentum by $\hbar(\Delta m_F = \pm 1)$ and in linear momentum $\hbar k_x$ by $2\hbar k_r$, with $\hbar k_r$ as the single photon recoil momentum. Since the momentum transfer is only along \hat{x} direction, the Hamiltonian associated with motion along \hat{x} direction is given by

$$H_x^* = \frac{\hbar^2}{2m^*} \left(k_x - \frac{q^* A_x}{\hbar} \right)^2 \quad (2.27)$$

where A_x is the engineered vector potential which depends on the externally controlled Zeeman shift of the atom with q^* as the *artificial* charge of the atom and m^* is the effective mass along \hat{x} direction. The complete single atom Hamiltonian is

$$H = H_x^* + \frac{\hbar^2}{2m} (k_y^2 + k_z^2) + V(\mathbf{r}) \otimes \mathbf{1} \quad (2.28)$$

where $\mathbf{1}$ is the 3×3 unit matrix acting on the spins. In above expression, H_x^* when expanded in the state basis of the family of three states coupled by the Raman field, is given by

$$\begin{pmatrix} \frac{\hbar}{2m} (\tilde{k}_x + 2k_r)^2 - \delta & \Omega_R/2 & 0 \\ \Omega_R/2 & \frac{\hbar}{2m} \tilde{k}_x^2 - \epsilon & \Omega_R/2 \\ 0 & \Omega_R/2 & \frac{\hbar}{2m} (\tilde{k}_x - 2k_r)^2 - \delta \end{pmatrix} \quad (2.29)$$

Here $\delta = (\Delta\omega_L - \omega_z)$ is the detuning from Raman resonance, Ω_R is the resonant Raman Rabi frequency, and ϵ accounts for a small quadratic Zeeman shift. \tilde{k}_x is the wave vector for the quasi momentum. For each \tilde{k}_x , diagonalizing H_x^* gives three energy eigenvalues $E_j(\tilde{k}_x) (j = 1, 2, 3)$, which is the effective dispersion relation depending on experimental parameters, δ , Ω_R , and ϵ . The number of energy minima (from one to three) and their positions \tilde{k}_{min} are thus experimentally tunable. Around each \tilde{k}_{min} , the dispersion can be expanded as

$$E(\tilde{k}_x) \simeq \frac{\hbar^2}{2m^*} (\tilde{k}_x - \tilde{k}_{min})^2 \quad (2.30)$$

where m^* is the effective mass. In this expansion, we identify \tilde{k}_{min} with the light-induced vector gauge potential, in analogy to the Hamiltonian for a particle of charge q in the usual magnetic vector potential \mathbf{A} : $(\mathbf{p} - e\mathbf{A})^2/2m$.

Thus, the kinetic energy part again resembles the one for charged particle in magnetic field, but with vector potential in Landau gauge, $\mathbf{A} = B(0, x, 0)$. The artificial gauge field defined for this problem however, could be the same as the one in previous. Therefore, one can see that in principle, the actual physical interaction is represented by the *artificial* gauge potential and not by the *artificial* gauge field. The corresponding Hamiltonian is written in a way so that it resembles that of a particle in a gauge field for a

specific choice of the gauge potential. Unlike the real gauge field, for example one used in standard electromagnetic theory, this artificial gauge field does not have any independent dynamics or alternatively it does not obey any Maxwell's like equation. This is why such a gauge field is *artificial* and all observable quantities are not necessarily gauge invariant. The gauge dependence of the momentum distribution profile which is an experimentally observable quantity is calculated using strong coupling perturbation theory and is described in detail in chapter 3.

In the next subsection, we derive the eBHM in rotating frame coordinates to get rid of the time-dependence of rotating potentials in the laboratory frame of coordinates.

2.1.3 Extended Bose Hubbard Hamiltonian in rotating frame coordinates

As mentioned in previous subsection 2.1.2, the effect of rotation is equivalent to a application of *artificial* gauge field resulting from a symmetric gauge potential. To avoid the complicated time dependence in rotating potentials, we switch to a coordinate system rotating with same angular velocity as the potential. Thus, we rewrite the Hamiltonian for eBHM with rotating optical lattice in the reference frame co-rotating with same angular velocity Ω about the z -axis as

$$\hat{H} = \hat{H}_0 - \int d\mathbf{r} \hat{\psi}^\dagger(\mathbf{r}) \Omega L_z \hat{\psi}(\mathbf{r}) \quad (2.31)$$

which can be written more explicitly as

$$\begin{aligned} \hat{H} = & \int d\mathbf{r} \hat{\psi}^\dagger(\mathbf{r}) \left[-\frac{\hbar^2}{2m} \nabla^2 + V_L(\mathbf{r}) + V_{trap}(\mathbf{r}) + \frac{g}{2} \hat{\psi}^\dagger(\mathbf{r}) \hat{\psi}(\mathbf{r}) \right. \\ & \left. + \int d\mathbf{r}' V(|\mathbf{r} - \mathbf{r}'|) \hat{\psi}(\mathbf{r}') \hat{\psi}(\mathbf{r}) - \Omega L_z \right] \hat{\psi}(\mathbf{r}) \end{aligned} \quad (2.32)$$

Here, $V_L(\mathbf{r})$ is the lattice potential given by equation (2.6) and $V_{trap}(\mathbf{r})$ is the trapping potential given by $V_{trap}(\mathbf{r}) = m\omega^2 r^2/2$ with $r = |\mathbf{r}|$. Equation (2.32) can be written in the following form as

$$\begin{aligned} \hat{H} = & \int d\mathbf{r} \hat{\psi}^\dagger(\mathbf{r}) \left[\frac{1}{2m} \left(\frac{\hbar}{i} \partial_x + m\Omega y \right)^2 + \left(\frac{\hbar}{i} \partial_y - m\Omega x \right)^2 \right] + V_L(\mathbf{r}) + \frac{1}{2} m(\omega^2 - \Omega^2) r^2 \\ & + \frac{g}{2} \hat{\psi}^\dagger(\mathbf{r}) \hat{\psi}(\mathbf{r}) + \int d\mathbf{r}' V(|\mathbf{r} - \mathbf{r}'|) \hat{\psi}(\mathbf{r}') \hat{\psi}(\mathbf{r}) \\ = & \int d\mathbf{r} \hat{\psi}^\dagger(\mathbf{r}) \left[\frac{\hbar^2}{2m} + V_L(\mathbf{r}) + \frac{1}{2} m(\omega^2 - \Omega^2) r^2 + \frac{g}{2} \hat{\psi}^\dagger(\mathbf{r}) \hat{\psi}(\mathbf{r}) \right. \\ & \left. + \int d\mathbf{r}' V(|\mathbf{r} - \mathbf{r}'|) \hat{\psi}(\mathbf{r}') \hat{\psi}(\mathbf{r}) \right] \hat{\psi}(\mathbf{r}) \end{aligned} \quad (2.33)$$

Here, the covariant momentum is given by

$$\mathbf{\Pi}(\mathbf{r}) = -i\hbar\nabla + m\mathbf{A}(\mathbf{r}) \quad (2.34)$$

and the effective magnetic vector potential due to rotation which is equivalent to symmetric gauge is

$$\mathbf{A}(\mathbf{r}) = \mathbf{r} \times \boldsymbol{\Omega} \quad (2.35)$$

As mentioned in section 2.1.1, the field operator can be expanded in terms of Wannier functions $W_S^l(\mathbf{r} - \mathbf{r}_i)$ and annihilation operator \hat{a}_i for the stationary lattice problem [37]. At very low rotational frequency, the the lowest Bloch band and the first excited energy band are well separated, and hence the particle dynamics is effectively described by considering only the lowest Bloch band $l = 0$. It takes into account Wannier orbitals only from the lowest band which is an excellent approximation for small Ω and deep lattice.

To take into account relatively higher rotational frequencies or equivalently, moderate magnetic field strengths, a better suited basis is given by the modified Wannier functions [122]. This is because at higher rotational frequencies, the rotational term get mixed up with the higher bands to a considerable extent. This results mainly in the modification of the phase structure within the sites. So, instead of choosing the usual Wannier basis functions for the expansion of field operators, we consider a modified Wannier basis [122] which is given by

$$W_R(\mathbf{r} - \mathbf{r}_i) = \exp\left(-i\frac{m}{\hbar} \int_{\mathbf{r}_i}^{\mathbf{r}} \mathbf{A}(\mathbf{r}') d\mathbf{r}'\right) W_S(\mathbf{r} - \mathbf{r}_i) \quad (2.36)$$

The choice of modified Wannier basis captures the phase gradient within the sites which is proportional to the rotational frequency Ω . The modified Wannier basis $W_R(\mathbf{r} - \mathbf{r}_i)$ is connected to the usual Wannier basis functions $W_S(\mathbf{r} - \mathbf{r}_i)$ by the transformation [122]

$$\mathbf{\Pi}W_R(\mathbf{r} - \mathbf{r}_i) = \exp\left(-i\frac{m}{\hbar} \int_{\mathbf{r}_i}^{\mathbf{r}} \mathbf{A}(\mathbf{r}') d\mathbf{r}'\right) \frac{\hbar}{i} \nabla W_S(\mathbf{r} - \mathbf{r}_i) \quad (2.37)$$

We restrict our calculations to the rotational frequencies ($\Omega \sim \omega$) where the relation (2.37) is applicable and takes into account the modification of phase within the sites. Using this modified Wannier basis $W_R(\mathbf{r} - \mathbf{r}_i)$, the field operator can now be expressed as

$$\hat{\psi}(\mathbf{r}) = \sum_{i=1}^N \hat{a}_i W_R(\mathbf{r} - \mathbf{r}_i) \quad (2.38)$$

with \hat{a}_i as the site-specific annihilation operator. Substituting this expansion of field operator (2.38) into equation (2.33) under the tight binding approximation, we get

$$\begin{aligned} \hat{H} = & - \sum_{\langle i,j \rangle} \left(t + \frac{m(\Omega^2 - \omega^2)}{2} A_1 \right) (\hat{a}_i^\dagger \hat{a}_j e^{-i\varphi_{ij}} + \hat{a}_i \hat{a}_j^\dagger e^{i\varphi_{ij}}) \\ & + \sum_i \left(\epsilon_i - \frac{m(\Omega^2 - \omega^2)}{2} (r_i^2 + A_2) \right) \hat{n}_i + \frac{U}{2} \sum_i \hat{n}_i (\hat{n}_i - 1) + V \sum_{\langle i,j \rangle} \hat{n}_i \hat{n}_j \end{aligned} \quad (2.39)$$

Here again $\langle i, j \rangle$ indicates that the sum is over nearest neighbor sites and $\hat{n}_i = \hat{a}_i^\dagger \hat{a}_i$ is the number operator, which gives the number of particles at any site i . It is to note that we have kept only the nearest neighbor interaction term, which is the minimal version of eBHM. There can be other successive terms too, which are too small to be taken into account. The parameters t and ϵ are defined as in equations (2.13) and (2.14) respectively. The modification to the hopping and onsite energies due to rotation are proportional to $(\Omega^2 - \omega^2)$ and the parameters A_1 and A_2 are given as

$$A_1 = \int dx W_S^*(x - x_i)(x - x_i)^2 W_S(x - x_j) \quad (2.40)$$

$$A_2 = 2 \int dx W_S^*(x - x_i)(x - x_i)^2 W_S(x - x_i) \quad (2.41)$$

The phase in the hopping term is given in terms of vector potential as

$$\phi_{ij} = \int_{r_j}^{r_i} \mathbf{A}(\mathbf{r}') \cdot d\mathbf{r}' \quad (2.42)$$

with the effective vector potential

$$\mathbf{A}^S(\mathbf{r}) = (m/\hbar)(\mathbf{r} \times \boldsymbol{\Omega}) = \pi\nu(x\hat{y} - y\hat{x})$$

in the symmetric gauge. The resulting artificial magnetic field is $2\Omega\hat{z}$ with Ω is the frequency of rotation in the xy -plane. As mentioned before, a similar expression can be obtained by using the Landau gauge where the vector potential is

$$\mathbf{A}^L(\mathbf{r}) = 2\pi\nu x\hat{y}$$

which is more suitable for the experimental set-up in ref. [86]. In the symmetric gauge, the particle picks up along all sides of the plaquette while in the Landau gauge, the particle picks up phase only along either the x direction or y direction. The quantity

$$\nu = \frac{2\Omega}{\frac{h}{m}} = -\frac{1}{2\pi} \oint d\mathbf{r} \cdot \nabla \varphi_{i,j}$$

gives the number of circulation quanta through a unit cell in the square lattice and is gauge invariant which is discussed as follows [123].

This quantity ν represents an important topological feature of the system. If we consider an arrow whose directional angles are given by $\varphi_{ij}(x, y)$ of the wave function, then as we go around the boundary the arrow rotates p times and thus gives a topological constraint to the wave function. For $\nu = \frac{p}{q}$ (p and q are co-prime) as the boson hops around a unit cell in the square lattice it acquires a non trivial phase factor $\exp(-2\pi i\nu)$. To achieve a winding which is integer multiple of the 2π , the boson should therefore hop around q such unit cell leading to the formation of magnetic unit cell [124]. This in turn implies

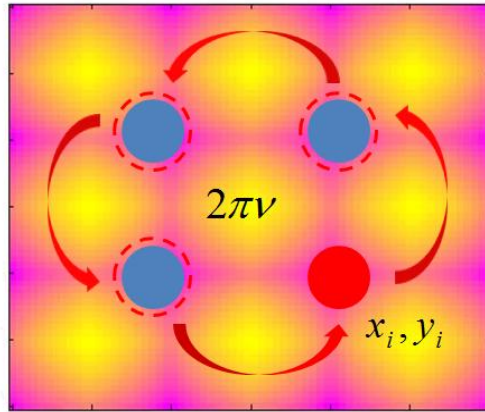


FIGURE 2.2: Schematic diagram for a particle tunneling around a plaquette in a square lattice. Here, dark (pink) regions correspond to lattice sites and the light (yellow) regions correspond to the maxima in lattice potential. The particle picks up a phase of $2\pi\nu$ when it returns to its original position as marked by the solid (red) circle.

that if we denote the phase of the bosonic wave function by the direction of an arrow then as one goes around such magnetic unit cell, the arrow will rotate p times and the magnetic field imposes the wave function to have $-p$ vorticity in a magnetic unit cell. The same thing will happen even if we start from some other lattice than the square lattice as long as the number of flux quanta goes through the unit cell will remain ν . This is a topological constraint because the total vorticity in the magnetic unit cell does not depend on the local features such as the type of the lattice potential [123].

When the angular velocity Ω is equal to the frequency ω of the harmonic trap i.e the effect of an overall trap potential can be neglected assuming that it is sufficiently shallow and

gets neutralized by the centrifugal force. The Hamiltonian (2.39) in this limit becomes

$$\hat{H} = - \sum_{\langle i,j \rangle} t(\hat{a}_i^\dagger \hat{a}_j e^{-i\varphi_{ij}} + \hat{a}_i \hat{a}_j^\dagger e^{i\varphi_{ij}}) + \sum_i \epsilon_i \hat{n}_i + \frac{U}{2} \sum_i \hat{n}_i(\hat{n}_i - 1) + V \sum_{\langle i,j \rangle} \hat{n}_i \hat{n}_j \quad (2.43)$$

As seen from equation (2.14), ϵ_i is the energy offset at lattice site i due to the external potential. We deal with the grand-canonical ensemble, by introducing the chemical potential μ which fixes the average occupation. Thus, we write the full Hamiltonian,

$$\hat{H}_{full} = \hat{H} - \mu \sum_i \hat{n}_i$$

From now on we drop the subscripts from \hat{H} and, unless otherwise stated, always work with the full Hamiltonian. The chemical potential term follows directly from the argument leading to ϵ_i . Since both parameters multiply the number operator, it is convenient to define a local chemical potential for each site,

$$\mu_i = \mu - \epsilon_i$$

For a trapped system, by applying the local density approximation (LDA) [125], the local density at site i in the trapped case is given by the density of a homogeneous system with a chemical potential

$$\mu_i = \mu - \epsilon_i - V_{trap} r_i^2$$

Here μ refers to the chemical potential at the center of the lattice where the trap potential is zero. This results in formation of plateaus in the density profile of the system which is effectively due to the trap potential. However, we restrict our study to spatially uniform system. Thus, the spatially uniform eBHM in presence of *artificial* gauge field is described by the full Hamiltonian

$$\hat{H} = -t \sum_{\langle i,j \rangle} (\hat{a}_i^\dagger \hat{a}_j \exp(i\varphi_{ij}) + h.c.) + \frac{1}{2} \sum_i \hat{n}_i(\hat{n}_i - 1) + V \sum_{\langle i,j \rangle} \hat{n}_i \hat{n}_j - \mu \sum_i \hat{n}_i \quad (2.44)$$

2.2 Extended Bose Hubbard model in presence of magnetic field

In this section we study the effect of rotation on such eBHM that includes nearest neighbor interaction (NNI) apart from the on-site interaction. The addition of the

NNI to the Bose-Hubbard Hamiltonian has pronounced effect on the phases since the corresponding phase diagram [103, 126, 127] contains the DW and SS phases apart from the MI and SF phases. The DW and MI phases lack coherence as the SF order parameter vanishes. Both have fixed number of particles at a given site. But DW has alternating particle numbers on successive sites (Fig. 2.3(a)) where as in the MI phase they are uniform. In the intriguing SS phase the superfluid order parameter and the crystal order co-exist and the superfluid density gets spatially modulated.

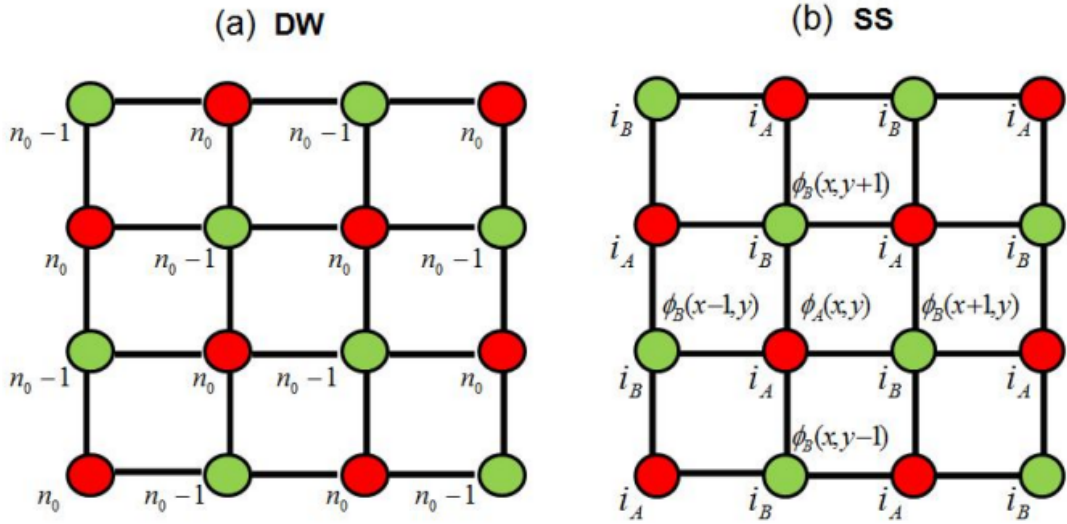


FIGURE 2.3: (a) Alternating particle number in Density Wave phase (b) Superfluid order parameter in Supersolid phase on the sites of A (red) and B (green) sublattices.

As already mentioned, SS is defined as a quantum system which exhibits crystalline structure and superfluid properties simultaneously. One of the most distinct features of superfluidity is the quantization of circulation and formation of vortices in such systems due to the existence of a macroscopic wave function for the system [19]. Superfluid forms vortices as a response to application of an effective gauge (magnetic) field. Motivated by theoretical and experimental success in the observation of vortices for the rotating ultracold atomic superfluid system [93–96], we explore the possibility to detect supersolid phase in ultracold atomic condensates, by probing their response to rotation or application of equivalent gauge fields. An unambiguous way of identifying the SS phase is to study the modulation of the superfluid order in the vortices created in such phase which will be different from the vortices created in a uniformly rotated superfluid. To understand such vortex profiles one thus needs to study the effect of such gauge field on the phases of EBH model which was introduced through equation (2.44) in section 2.1.3.

In the subsequent parts of this chapter, we describe the modification of the DW-SS phase boundary and the novel vortex profiles in SS phase near such phase boundary due to such gauge field [105]. We calculate the modification of the DW phase boundary in the mean field approximation by using a reduced basis ansatz for the Gutzwiller variational wavefunction. The minimization of the energy functional very close to the DW phase boundary shows that the superfluid order parameter satisfies a spinorial Harper equation [128]. Consequently the phase boundary can be determined from the edge of a Hofstadter butterfly (HB) spectrum [92]. In the resulting vortices, the spatial profile of the superfluid density shows a checkerboard like two sublattice modulation with a relative phase winding between the superfluid order parameter defined on each of these sublattices [105]. We also discuss possible ways to experimentally detect such vortex profiles in SS.

2.2.1 Phase diagram of the Extended Bose-Hubbard Hamiltonian in mean field approximation

As already introduced in equation (2.44), the extended Bose Hubbard Hamiltonian with onsite interaction and NNI is given as

$$\hat{H} = -t \sum_{\langle i,j \rangle} (\hat{a}_i^\dagger \hat{a}_j \exp(i\varphi_{ij}) + h.c.) + \frac{1}{2} \sum_i \hat{n}_i(\hat{n}_i - 1) + V \sum_{\langle i,j \rangle} \hat{n}_i \hat{n}_j - \mu \sum_i \hat{n}_i \quad (2.45)$$

For simplicity we work in the grand-canonical ensemble by introducing the chemical potential μ which fixes the average occupation. Here, we have rescaled the Hamiltonian by the onsite interaction strength U and thus, all parameters are measured in units of U . The first term gives us the nearest neighbor hopping where the hopping matrix elements are non zero only for nearest neighbors with $\varphi_{ij} = \int_{r_j}^{r_i} d\mathbf{r} \cdot \mathbf{A}(\mathbf{r})$ and $\mathbf{A}(\mathbf{r})$ is the vector potential corresponding to the artificial gauge field. $\langle \rangle$ implies that site index i, j on the two dimensional square lattice are the nearest neighbors and \hat{a}_i^\dagger , \hat{a}_i and \hat{n}_i are the boson creation, annihilation and number operators respectively. V is the strength of nearest neighbor interaction that minimally captures the effect of long range interaction, μ is the chemical potential. As already explained in previous sub section 2.1.3, the effect of overall trap potential is neutralized by the centrifugal force in the bulk of the system and hence is neglected in above expression.

Gutzwiller approach : The basis of our mean field approximation is the Gutzwiller (GW) approach, based on an ansatz for the many-body ground state that factorizes the many body wave function into single lattice-site wavefunctions. It was originally proposed by Gutzwiller for strongly correlated fermionic systems [129]. However when

generalized for the bosonic systems [130],

$$\Psi_g = \prod_i \gamma(n_i) |G\rangle \quad (2.46)$$

where $\prod_i \gamma(n_i)$ is a factor which suppresses the amplitudes of states with large potential energies and $|G\rangle$ is the non interacting ground state. For bosonic system, the non interacting ground state can be occupied macroscopically i.e

$$|G\rangle = (\hat{a}_{k=0}^\dagger)^N |0\rangle \quad (2.47)$$

In the grand canonical ensemble, it can be written as a coherent state of definite phase as

$$|G\rangle = \exp[\sqrt{\lambda} \hat{a}_{k=0}^\dagger] |0\rangle = \prod_i \exp[\sqrt{\lambda} a_i^\dagger] |0\rangle \quad (2.48)$$

Since the bosonic operators on different sites commute with each other,

$$[\Psi^\dagger(\mathbf{r}), \Psi(\mathbf{r}')] = \delta_{\mathbf{r},\mathbf{r}'} \quad (2.49)$$

both the non-interacting ground state (2.48) and the variational wave function (2.46) can be written as a product of single site wave functions. This permits an exact treatment of GW function for bosons [130].

The Gutzwiller approach is a self-consistent mean-field method which corresponds to the approximation in which the hopping term is decoupled as [131, 132]

$$\begin{aligned} \hat{a}_i^\dagger \hat{a}_j &= \langle \hat{a}_i^\dagger \rangle \hat{a}_j + \hat{a}_i^\dagger \langle \hat{a}_j \rangle - \langle \hat{a}_i^\dagger \rangle \langle \hat{a}_j \rangle \\ &= \phi_i \hat{a}_j + \hat{a}_i^\dagger \phi_j - \phi_i \phi_j \end{aligned} \quad (2.50)$$

The average value $\langle \hat{a}_i \rangle = \phi_i$ represents the order parameter that accounts for the transition from insulating phase to SF/SS phase. It is equal to zero on the insulator side of the transition when the ground state of the system has a definite particle number on every site of the lattice, and has a nonzero value for the SF or SS state when there are large quantum fluctuations of the atom number in the optical lattice i.e

$$\hat{n} = \langle \hat{n} \rangle + \delta \hat{n}$$

The Gutzwiller product ansatz [129] for the present case of ultracold bosonic atoms in optical lattice is given by

$$|\Psi\rangle = \prod_i \sum_n f_n^i |n_i\rangle$$

Under this approximation the eigenstates of Hamiltonian can be expanded in terms of Fock states and then this Hamiltonian matrix is diagonalised under Fock basis truncated until a given number of particle to obtain the eigenvalues. Here, the variational parameters f_n^i are the amplitudes for the Fock state $|n_i\rangle$ with n particles at site i , the sum is over all possible occupation numbers, and the product is over all sites. Using the GW ansatz to obtain an approximate variational solution for the eBHM corresponds, however, to restricting the Hilbert space to the subset of product states.

But, due to the factorized form of the wave function and restriction of Hilbert space, the GW approximation recapitulated so far is unable to incorporate any type of intersite correlations. The calculation of inter site correlations is important for determination of experimentally measurable observables, such as momentum distribution which is proportional to the fourier transform of atom-atom correlation function [133]. To get such momentum distribution profiles for the eBHM phases in presence of artificial gauge fields, in the next chapter 3 we have done calculations using strong coupling expansion technique which is comparatively more accurate and reliable method to capture the short range correlations between different lattice sites.

We perform our calculations at the boundary of the insulating phases (DW and MI) where we truncate the fock space basis such that only the neighboring Fock states become occupied, where also the GW wave function is fairly valid. Thus, the ground state of the Hamiltonian (2.45) can be found by calculating the expectation value $\langle\Psi|\hat{H}|\Psi\rangle$ in the mean field approximation.

As shown in Fig. 2.4, for $t = 0$ and $Vd < 1/2$, we have transitions between DW($n_0/2$) to MI(n_0) at $\mu = (n_0 - 1) + 2Vdn_0$ and then to DW($n_0/2 + 1$) at $\mu = n_0 + 2Vdn_0$ and hence can be obtained analytically. Whereas, for $Vd > 1/2$, the MI lobes vanish and the new DW phases such as DW(1) with particle modulation $|\cdots, 2, 0, \cdots\rangle$ appear [127]. At $t = 0$, the DW(1/2) transforms to DW(1) when $\mu > U$, which in turn transforms to DW(3/2) when $\mu > 2U$.

We restrict to the two dimensional lattice ($d = 2$) such that $0 < V < \frac{1}{4}$ for which at $t = 0$, the system goes through an alternating sequence of DW phase with n_0 and $n_0 - 1$ particles at successive sites, followed by a MI phase with n_0 particles per site with $n_0 = 1, 2, 3, \cdots$ (Fig. 2.4). As t increases a SS phase appears before the DW states makes transition to a uniform superfluid phase.

Before performing the detailed calculations and analysis for the rotating eBHM, in the next sub-section we analytically determine the phase boundary for the DW and MI phases for the non-rotating case to demonstrate our method.

2.2.2 Phase boundary for the non rotating case

The phase boundary of the DW and MI phase can be determined analytically by obtaining the energy of the particle-hole type excitations using a reduced basis variational ansatz for the Gutzwiller wave function near the phase boundary. The DW phase consists of two sublattices A and B having fixed n_0 and $n_0 - 1$ particles per site (Fig. 2.3(a)). Thus it is convenient to decompose

$$|\Psi\rangle = (|\Psi^A\rangle)(|\Psi^B\rangle) \quad (2.51)$$

Here

$$|\Psi^A\rangle = \prod_{i_A=1}^{N/2} |\psi^{i_A}\rangle$$

with

$$|\psi^{i_A}\rangle = \sum_n f_n^{i_A} |n_{i_A}\rangle$$

with $f_n^{i_A} = \delta_{n,n_0}$. Similarly

$$|\Psi^B\rangle = \prod_{i_B=1}^{N/2} |\psi^{i_B}\rangle$$

with

$$|\psi^{i_B}\rangle = \sum_m f_m^{i_B} |m_{i_B}\rangle$$

with $f_m^{i_B} = \delta_{m,n_0-1}$. For brevity, we write n_A as n and m_B as m in the subsequent expressions. For the non rotating case of $\Omega = 0$, very close to the DW phase boundary only the neighboring Fock states are populated [106, 107]. Thus for all i and j

$$|\psi^{i_A}\rangle = f_{n-1}^{i_A} |n-1\rangle + f_n^{i_A} |n\rangle + f_{n+1}^{i_A} |n+1\rangle, n = n_0 \quad (2.52)$$

$$|\psi^{i_B}\rangle = f_{m-1}^{i_B} |m-1\rangle + f_m^{i_B} |m\rangle + f_{m+1}^{i_B} |m+1\rangle, m = n_0 - 1 \quad (2.53)$$

We set the variational amplitudes

$$(f_{n-1}^{i_A}, f_n^{i_A}, f_{n+1}^{i_A}) = (\epsilon_{1A}, \sqrt{1 - \epsilon_{1A}^2 - \epsilon_{2A}^2}, \epsilon_{2A}) \quad (2.54)$$

and

$$(f_{m-1}^{i_B}, f_m^{i_B}, f_{m+1}^{i_B}) = (\epsilon_{1B}, \sqrt{1 - \epsilon_{1B}^2 - \epsilon_{2B}^2}, \epsilon_{2B}) \quad (2.55)$$

with variational parameters $\epsilon_{1A,1B}, \epsilon_{2A,2B}$ all $\ll 1$ and ensure the normalization condition of states $|\psi^{i_A}\rangle, |\psi^{i_B}\rangle$. The expectation value of the Hamiltonian using the decomposed

wave function (2.51) can be written as

$$\begin{aligned}
 \langle \Psi | \hat{H} | \Psi \rangle &= -t \sum_{\langle i,j \rangle} (\langle \hat{a}_i^\dagger \rangle \langle \hat{a}_j \rangle + \langle h.c. \rangle) + \sum_{i=1}^{N/2} \left[\frac{1}{2} \langle \hat{n}_i^2 \rangle - \left(\mu + \frac{1}{2} \right) \langle \hat{n}_i \rangle \right] \\
 &+ \sum_{j=1}^{N/2} \left[\frac{1}{2} \langle \hat{n}_j^2 \rangle - \left(\mu + \frac{1}{2} \right) \langle \hat{n}_j \rangle \right] + V \sum_{\langle i,j \rangle} \langle \hat{n}_i \rangle \langle \hat{n}_j \rangle
 \end{aligned} \quad (2.56)$$

We calculate the quantities $\langle \hat{a}_i^\dagger \rangle \langle \hat{a}_j \rangle$, $\langle \hat{n}_i \rangle \langle \hat{n}_j \rangle$, $\langle \hat{n}_i \rangle$ and $\langle \hat{n}_i^2 \rangle$ using the reduced basis ansatz from equations (2.52) and (2.53) as below,

$$\begin{aligned}
 \langle \hat{a}_i^\dagger \rangle &= \sum_n \sqrt{n} f_{n-1} f_n^* \\
 &= \sqrt{n} f_{n-1} f_n + \sqrt{n+1} f_n f_{n+1}
 \end{aligned}$$

and,

$$\begin{aligned}
 \langle \hat{a}_j \rangle &= \sum_m \sqrt{m} f_{m-1}^* f_m \\
 &= \sqrt{m} f_{m-1} f_m + \sqrt{m+1} f_m f_{m+1}
 \end{aligned}$$

which using (2.54) and (2.55) implies

$$\begin{aligned}
 \langle \hat{a}_i^\dagger \rangle \langle \hat{a}_j \rangle &\simeq \sqrt{nm} \epsilon_{1A} \epsilon_{1B} + \sqrt{n(m+1)} \epsilon_{1A} \epsilon_{2B} \\
 &+ \sqrt{m(n+1)} \epsilon_{2A} \epsilon_{1B} + \sqrt{(n+1)(m+1)} \epsilon_{2A} \epsilon_{2B}
 \end{aligned} \quad (2.57)$$

Similarly, we calculate

$$\begin{aligned}
 \langle \hat{n}_i \rangle &= \sum_n n |f_n|^2 \\
 &= n + (\epsilon_{2A}^2 - \epsilon_{1A}^2)
 \end{aligned} \quad (2.58)$$

$$\langle \hat{n}_j \rangle = m + (\epsilon_{2B}^2 - \epsilon_{1B}^2) \quad (2.59)$$

which implies

$$\langle \hat{n}_i \rangle \langle \hat{n}_j \rangle \simeq nm + n(\epsilon_{2B}^2 - \epsilon_{1B}^2) + m(\epsilon_{2A}^2 - \epsilon_{1A}^2) \quad (2.60)$$

Using equations (2.57)- (2.60) into equation (2.56), we get

$$\frac{\langle \hat{H} \rangle}{N} = f(\epsilon_{1A}, \epsilon_{2A}, \epsilon_{1B}, \epsilon_{2B})$$

with

$$\begin{aligned}
 f(\epsilon_{1A}, \epsilon_{2A}, \epsilon_{1B}, \epsilon_{2B}) = & \frac{1}{2} \left[\frac{1}{2} n^2 - \left(\mu + \frac{1}{2} \right) n + \frac{1}{2} m^2 - \left(\mu + \frac{1}{2} \right) m + 4Vnm \right] \\
 & + \frac{1}{2} [(n - \mu + 4Vm)\epsilon_{2A}^2 + (-n + 1 + \mu - 4Vm)\epsilon_{1A}^2] \\
 & + \frac{1}{2} [(m - \mu + 4Vn)\epsilon_{2B}^2 + (-m + 1 + \mu - 4Vn)\epsilon_{1B}^2] \\
 & - 4t[\sqrt{nm}\epsilon_{1A}\epsilon_{1B} + \sqrt{n(m+1)}\epsilon_{1A}\epsilon_{2B} \\
 & + \sqrt{m(n+1)}\epsilon_{2A}\epsilon_{1B} + \sqrt{(n+1)(m+1)}\epsilon_{2A}\epsilon_{2B}] \quad (2.61)
 \end{aligned}$$

Minimizing $f(\epsilon_{1A}, \epsilon_{2A}, \epsilon_{1B}, \epsilon_{2B})$ with respect to the parameters ϵ_{1A} , ϵ_{1B} , ϵ_{2A} and ϵ_{2B} , we get the following four equations,

$$[(n-1) - \mu + 4Vm]\epsilon_{1A} + 4t\sqrt{nm}\epsilon_{1B} + 4t\sqrt{n(m+1)}\epsilon_{2B} = 0 \quad (2.62)$$

$$[n - \mu + 4Vm]\epsilon_{2A} - 4t[\sqrt{m(n+1)}\epsilon_{1B} - 4t\sqrt{(n+1)(m+1)}\epsilon_{2B}] = 0 \quad (2.63)$$

$$[(m-1) - \mu + 4Vn]\epsilon_{1B} + 4t\sqrt{nm}\epsilon_{1A} + 4t\sqrt{m(n+1)}\epsilon_{2A} = 0 \quad (2.64)$$

$$[m - \mu + 4Vn]\epsilon_{2B} - 4t\sqrt{n(m+1)}\epsilon_{1A} - 4t\sqrt{(n+1)(m+1)}\epsilon_{2A} = 0 \quad (2.65)$$

Their non trivial solution demands

$$\det \begin{vmatrix} (n-1) - \mu + 4Vm & 0 & 4t\sqrt{nm} & 4t\sqrt{n(m+1)} \\ 0 & (n - \mu + 4Vm) & -4t\sqrt{m(n+1)} & -4t\sqrt{(m+1)(n+1)} \\ 4t\sqrt{nm} & 4t\sqrt{m(n+1)} & (m-1) - \mu + 4Vn & 0 \\ -4t\sqrt{n(m+1)} & -4t\sqrt{(n+1)(m+1)} & 0 & (m - \mu + 4Vn) \end{vmatrix} = 0 \quad (2.66)$$

A particle (p) or hole (h) like excitation from either site of A and B are respectively given by

$$\epsilon_p^A = n + 4Vm, \epsilon_h^A = -[(n-1) + 4Vm]$$

$$\epsilon_p^B = m + 4Vn, \epsilon_h^B = -[(m-1) + 4Vn]$$

Defining $\tilde{\epsilon}_{p,h}^{A,B} = \epsilon_{p,h}^{A,B} \pm \mu$ equation (2.66) gives the relation [103]

$$\tilde{\epsilon}_p^A \tilde{\epsilon}_p^B \tilde{\epsilon}_h^A \tilde{\epsilon}_h^B - (4t)^2 [(n+1)\tilde{\epsilon}_h^A + n\tilde{\epsilon}_p^A] [(m+1)\tilde{\epsilon}_h^B + m\tilde{\epsilon}_p^B] = 0 \quad (2.67)$$

The above equation determines the minima of the particle hole like excitations in the limit $\mathbf{k} \rightarrow 0$ where \mathbf{k} is the wave vector of such particle-hole like excitations. It will determine the chemical potential μ at each t for a given strength V of the nearest neighbor interaction and will give the phase boundary between the DW-SS and MI-SF phase. To understand the significance of this equation in a better way we compare it

with the similar results obtained within the framework of other mean field approaches such as time dependent Gutzwiller mean field theory [103].

In the time dependent Gutzwiller mean field theory, the minimal perturbation around a perfect DW state is also considered in the Fock space basis. In the time dependent theory, the excitation spectrum of the system is calculated by dynamical Gutzwiller approach with the variational parameters f_n^i being time dependent. Minimization of the effective action $\langle \psi | i \frac{\partial}{\partial t} - \hat{H} + \mu \hat{N} | \psi \rangle$ gives the equation of motion for f_n^i [103]

$$i \frac{\partial f_n^i}{\partial \tau} = \left[\frac{U}{2} n(n-1) - \mu n + V n \rho^{(i)} \right] f_n^i - t(\phi_i^* \sqrt{n+1} f_{n+1}^i + \phi_i^* \sqrt{n} f_{n-1}^i) \quad (2.68)$$

where $\rho^{(i)} = \sum_{\delta, n} n |f_n^{i+\delta}|^2$ and τ is the time. The small amplitude fluctuations $\delta f_n^i(t)$ around the ground state give the excitation spectrum. The DW state can have four low-lying excitations corresponding to particle and hole excitations in each of the A (with n_A particles per site) and B (with n_B particles per site) sublattices. When a particle or hole like excitation is created over a perfect DW or MI state, they do not remain localized at a site, but moves around the lattice to create a Bloch wave to minimize their energy. The kinetic energy of such a Bloch wave is given by

$$\epsilon(\mathbf{k}) = 2t(\cos k_x + \cos k_y)$$

where k_x, k_y are the components of the Bloch wave vector. The excitation spectrum of such particle-hole like excitations with finite wave vector obtained within the time dependent Gutzwiller mean field theory is given as below

$$\tilde{\epsilon}_p^A \tilde{\epsilon}_p^B \tilde{\epsilon}_h^A \tilde{\epsilon}_h^B - \epsilon(\mathbf{k})^2 [(n+1)\tilde{\epsilon}_h^A + n\tilde{\epsilon}_p^A] [(m+1)\tilde{\epsilon}_h^B + m\tilde{\epsilon}_p^B] = 0 \quad (2.69)$$

where $\mathbf{k} = (k_x, k_y)$. From the dispersion spectrum, one can obtain the nature of excitations of different phases. The excitation spectra is gapped for the insulating phases (MI or DW) since a finite amount of energy is required for particle or hole excitation in such incompressible phase. On the other hand, the excitation spectra becomes gapless for SF or SS compressible phases. Hence the system shows a transition when the excitation spectrum changes from becoming gapped to gapless and thus the phase boundary can be determined [103].

The analytical form of the phase boundaries can be retrieved by taking the zero wave vector limit, namely $k_x \rightarrow 0, k_y \rightarrow 0, \epsilon(\mathbf{k}) = 0$ and $\omega = 0$ in the dispersion equation (2.69) obtained using the time dependent Gutzwiller theory [103]. It expectedly reproduces our result equation (2.67). We again emphasize that all the above displayed relations are for two dimensional square lattice, but can be generalized in other dimensions.

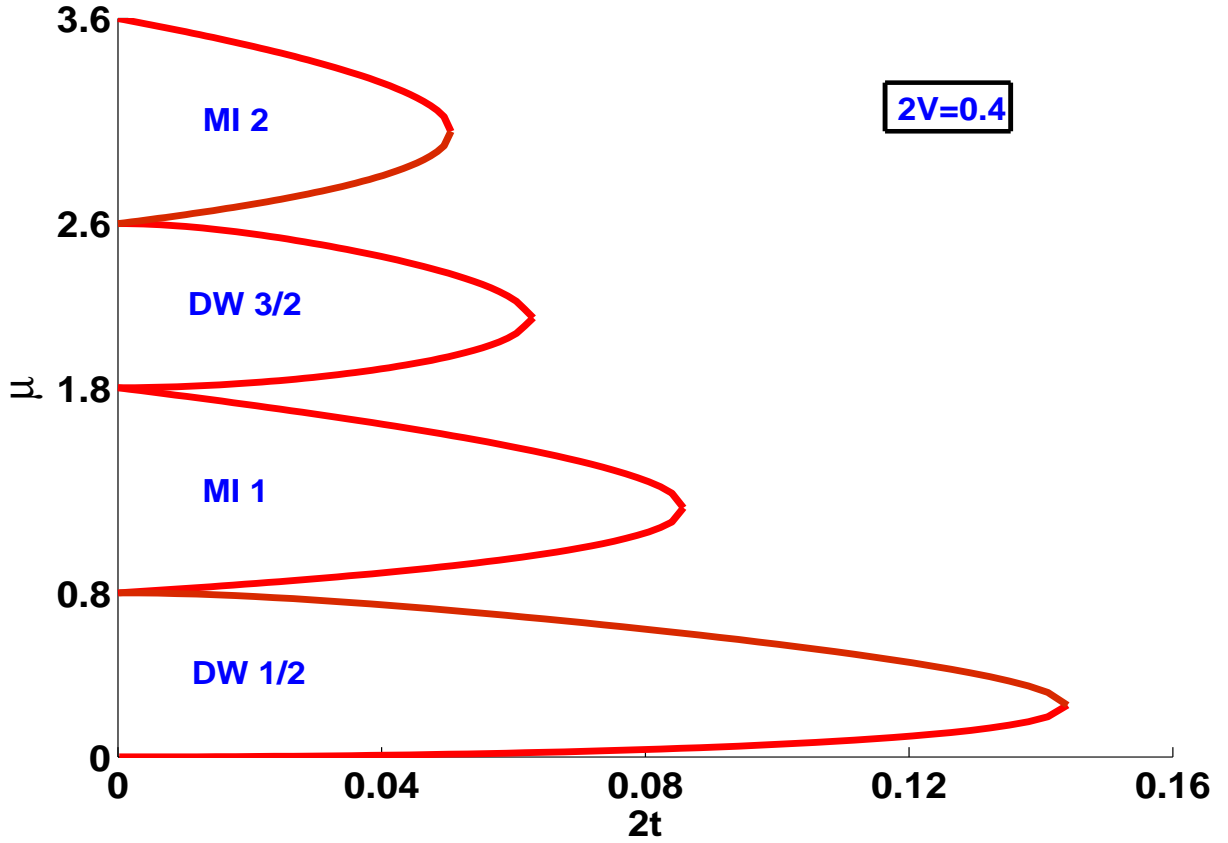


FIGURE 2.4: (a) Phase diagram for the eBHM for $2V=0.4$. Note that t , μ and V are measured in units of U .

In the next subsection we shall extend the above treatment for the rotating case and will show that the limiting particle-hole excitation spectrum that determines such phase boundary in presence of the finite rotation (or magnetic field) is actually the edge of a Hofstadter butterfly (HB) energy spectrum.

2.2.3 Rotated case

For the rotated case, the Hamiltonian is given by equation (2.45)

$$\hat{H} = -t \sum_{\langle i,j \rangle} (\hat{a}_i^\dagger \hat{a}_j \exp(i\varphi_{ij}) + h.c.) + \frac{1}{2} \sum_i \hat{n}_i(\hat{n}_i - 1) + V \sum_{\langle i,j \rangle} \hat{n}_i \hat{n}_j - \mu \sum_i \hat{n}_i \quad (2.70)$$

The expectation value of this equation (2.70) using the DW wave function (2.51) can be calculated as

$$\begin{aligned}
 \langle \Psi | \hat{H} | \Psi \rangle &= -t \sum_{\langle i_A, i_B \rangle} (\langle \hat{a}_{i_A}^\dagger \rangle \langle \hat{a}_{i_B} \rangle \exp(i\varphi_{i_A i_B}) + \langle h.c. \rangle) + \frac{1}{2} \sum_{i=1}^{i=N} (\langle \hat{n}_i^2 \rangle - \langle \hat{n}_i \rangle) - \mu \sum_{i=1}^{i=N} \langle \hat{n}_i \rangle \\
 &\quad + \sum_{\langle i_A, i_B \rangle} \langle \hat{n}_{i_A} \rangle \langle \hat{n}_{i_B} \rangle \\
 &= -2t \text{Re} \sum_{\langle i_A, i_B \rangle} [e^{i\varphi_{i_A i_B}} \phi_A^{i_A*} \phi_B^{i_B}] + \frac{1}{2} \left[\sum_{i_A=1}^{i_A=N/2} \sum_{n_A} (n_A^2 - n_A) |f_{n_A}^{i_A}|^2 \right] \\
 &\quad - \mu \sum_{i_A=1}^{i_A=N/2} \sum_{n_A} n_A |f_{n_A}^{i_A}|^2 + \frac{1}{2} \left[\sum_{i_B=1}^{i_B=N/2} \sum_{m_B} (m_B^2 - m_B) |f_{m_B}^{i_B}|^2 \right] \\
 &\quad - \mu \sum_{i_B=1}^{i_B=N/2} \sum_{m_B} m_B |f_{m_B}^{i_B}|^2 + V \sum_{\langle i_A, i_B \rangle} \left(\sum_{n_A} n_A |f_{n_A}^{i_A}|^2 \right) \left(\sum_{m_B} m_B |f_{m_B}^{i_B}|^2 \right)
 \end{aligned} \tag{2.71}$$

The first, second, fourth and sixth term gives the mean kinetic, on site energy for sublattice A and B and nearest neighbor interaction energy respectively. The superfluid order parameter on two sublattices (Fig. 2.3 (b)) are given by

$$\phi_A^{i_A}, \phi_B^{i_B} = \langle \hat{a}_{i_A} \rangle, \langle \hat{a}_{i_B} \rangle$$

whereas the DW order parameter is given by

$$\phi_{DW} = (-1)^i \left[\langle n_i \rangle - \frac{1}{N} \langle \sum_i n_i \rangle \right]$$

on any site i on either sublattices.

Near the DW phase boundary we again assume that only the neighboring Fock states become occupied. This approximation is valid very close to the phase boundary because in the vicinity of the insulating DW or MI phase, number fluctuations are small. In this regime, the effective Hamiltonian truncated into the subspace of lowest local number states is able to capture the essential correlations around the transition [134]. The corresponding variational parameters $(f_{n_A-1}^{i_A}, f_{n_A}^{i_A}, f_{n_A+1}^{i_A})$ for i_A sites are

$$(f_{n_A-1}^{i_A}, f_{n_A}^{i_A}, f_{n_A+1}^{i_A}) = [\lambda_1^{i_A} \Delta \phi_A^{i_A*}, \sqrt{1 - |\Delta \phi_A^{i_A}|^2 (|\lambda_1^{i_A}|^2 + |\lambda_2^{i_A}|^2)}, \lambda_2^{i_A} \Delta \phi_A^{i_A}] \tag{2.72}$$

and, for i_B sites we write

$$(f_{m_B-1}^{i_B}, f_{m_B}^{i_B}, f_{m_B+1}^{i_B}) = [\delta_1^{i_B} \Delta \phi_B^{i_B*}, \sqrt{1 - |\Delta \phi_B^{i_B}|^2 (|\delta_1^{i_B}|^2 + |\delta_2^{i_B}|^2)}, \delta_2^{i_B} \Delta \phi_B^{i_B}] \tag{2.73}$$

The superfluid order parameters on the two sublattices are respectively given by

$$\phi_A^{iA} = \sum_{n_A} \sqrt{n_A + 1} f_{n_A}^{iA*} f_{n_A+1}^{iA}$$

$$\phi_B^{iB} = \sum_{m_B} \sqrt{m_B + 1} f_{m_B}^{iB*} f_{m_B+1}^{iB}$$

From the definition of superfluid order parameter ϕ_A^{iA}, ϕ_B^{iB} it can be shown

$$\phi_A^{iA} = \Delta\phi_A^{iA} + O((\Delta\phi_A^{iA})^3)$$

with

$$\lambda_2^{iA} = \frac{1}{\sqrt{n_A + 1}} (1 - \sqrt{n_A} \lambda_1^{iA}) \quad (2.74)$$

and similarly

$$\phi_B^{iB} = \Delta\phi_B^{iB} + O((\Delta\phi_B^{iB})^3)$$

with

$$\delta_2^{iB} = \frac{1}{\sqrt{m_B + 1}} (1 - \sqrt{m_B} \delta_1^{iB}) \quad (2.75)$$

Thus if we neglect third and higher order corrections, $\Delta\phi_{A,B}$ can be replaced by the superfluid order parameter $\phi_{A,B}$ on the two sublattices. We also calculate $\langle \hat{n}_A \rangle$, $\langle \hat{m}_B \rangle$, $\langle \hat{n}_A^2 \rangle$ and $\langle \hat{m}_B^2 \rangle$ as below,

$$\begin{aligned} \langle \hat{n}_A \rangle &= \sum_{n_A} n_A |f_{n_A}^{iA}|^2 \\ &= n_A + |\Delta\phi_A^{iA}|^2 (|\lambda_2^{iA}|^2 - |\lambda_1^{iA}|^2) \end{aligned} \quad (2.76)$$

$$\begin{aligned} \langle \hat{m}_B \rangle &= \sum_{m_B} m_B |f_{m_B}^{iB}|^2 \\ &= m_B + |\Delta\phi_B^{iB}|^2 (|\delta_2^{iB}|^2 - |\delta_1^{iB}|^2) \end{aligned} \quad (2.77)$$

$$\langle \hat{n}_A^2 \rangle = n_A^2 + 2n_A (|\lambda_2^{iA}|^2 - |\lambda_1^{iA}|^2) |\Delta\phi_A^{iA}|^2 + (|\lambda_2^{iA}|^2 + |\lambda_1^{iA}|^2) |\Delta\phi_A^{iA}|^2 \quad (2.78)$$

$$\langle \hat{m}_B^2 \rangle = m_B^2 + 2m_B (|\delta_2^{iB}|^2 - |\delta_1^{iB}|^2) |\Delta\phi_B^{iB}|^2 + (|\delta_2^{iB}|^2 + |\delta_1^{iB}|^2) |\Delta\phi_B^{iB}|^2 \quad (2.79)$$

Using equations (2.74) and (2.75), we calculate

$$|\lambda_2^{iA}|^2 - |\lambda_1^{iA}|^2 = \frac{1}{n_A + 1} (1 - 2\sqrt{n_A} |\lambda_1^{iA}|^2 - |\lambda_1^{iA}|^2) \quad (2.80)$$

$$|\lambda_2^{i_A}|^2 + |\lambda_1^{i_A}|^2 = \frac{1}{n_A + 1} (1 - 2\sqrt{n_A}|\lambda_1^{i_A}|^2 + 2n_A|\lambda_1^{i_A}|^2 + |\lambda_1^{i_A}|^2) \quad (2.81)$$

and

$$|\delta_2^{i_B}|^2 - |\delta_1^{i_B}|^2 = \frac{1}{m_B + 1} (1 - 2\sqrt{m_B}|\delta_1^{i_B}|^2 - |\delta_1^{i_B}|^2) \quad (2.82)$$

$$|\delta_2^{i_B}|^2 + |\delta_1^{i_B}|^2 = \frac{1}{m_B + 1} (1 - 2\sqrt{m_B}|\delta_1^{i_B}|^2 + 2m_B|\delta_1^{i_B}|^2 + |\delta_1^{i_B}|^2) \quad (2.83)$$

In all further description again for brevity n_A and m_B will be written as n and m . Substituting these replacements and the expressions for variational parameters in equation (2.71), we obtain

$$\begin{aligned} \langle \Psi | \hat{H} | \Psi \rangle &= -2t \text{Re} \sum_{\langle i_A, i_B \rangle} [e^{i\varphi_{i_A i_B}} \phi_A^{i_A*} \phi_B^{i_B}] \\ &+ \sum_{i_A} \left[\frac{(n - \mu + 4Vm)}{n + 1} \left[1 - 2\sqrt{n}|\lambda_1^{i_A}| - |\lambda_1^{i_A}|^2 \right] + |\lambda_1^{i_A}|^2 \right] |\phi_A^{i_A}|^2 \\ &+ \sum_{i_B} \left[\frac{(m - \mu + 4Vn)}{m + 1} \left[1 - 2\sqrt{m}|\delta_1^{i_B}| - |\delta_1^{i_B}|^2 \right] + |\delta_1^{i_B}|^2 \right] |\phi_B^{i_B}|^2 + E_G \end{aligned} \quad (2.84)$$

with E_G is the energy of the pure density wave state, given by

$$E_G = \sum_{i_A=1}^{N/2} \frac{1}{2} n(n-1) + \sum_{i_B=1}^{N/2} \frac{1}{2} m(m-1) - \mu \sum_{i_A=1}^{N/2} n - \mu \sum_{i_B=1}^{N/2} m + \sum_{\langle i_A, i_B \rangle} Vnm$$

To obtain the ground state energy, $\langle \Psi | \hat{H} | \Psi \rangle$ is extremized with respect to $\lambda_1^{i_A}$ and $\delta_1^{i_B}$ i.e.

$$\frac{\partial \langle \hat{H} \rangle}{\partial \lambda_1^{i_A}} = 0, \frac{\partial \langle \hat{H} \rangle}{\partial \delta_1^{i_B}} = 0$$

yielding

$$\lambda_1^{i_A} = \sqrt{n} \frac{n - \mu + 4Vm}{1 + \mu - 4Vm}$$

$$\delta_1^{i_B} = \sqrt{m} \frac{m - \mu + 4Vn}{1 + \mu - 4Vn}$$

Here the second order derivative is positive which implies the minimization of the energy. Substituting the above expressions in $\langle \Psi | \hat{H} | \Psi \rangle$, and setting

$$\tilde{\phi}_A^{i_A} = \sqrt{\epsilon_1} \phi_A^{i_A}; \tilde{\phi}_B^{i_B} = \sqrt{\epsilon_2} \phi_B^{i_B}; \tilde{t} = \frac{t}{\sqrt{\epsilon_1 \epsilon_2}}$$

where

$$\epsilon_1 = \frac{(n - \mu + 4Vm)}{n + 1} \left[1 - n \frac{n - \mu + 4Vm}{1 + \mu - 4Vm} \right]; \epsilon_2 = \frac{(m - \mu + 4Vn)}{m + 1} \left[1 - m \frac{m - \mu + 4Vn}{1 + \mu - 4Vn} \right] \quad (2.85)$$

gives us the energy functional \mathcal{E} near the DW phase boundary as

$$\mathcal{E} = -\tilde{t} \sum_{\langle i_A, i_B \rangle} \tilde{\phi}_A^{i_A*} \tilde{\phi}_B^{i_B} + \sum_{i_A} |\tilde{\phi}_A^{i_A}|^2 + \sum_{i_B} |\tilde{\phi}_B^{i_B}|^2 + E_G \quad (2.86)$$

It can also be written as

$$\mathcal{E} = -\tilde{t} \sum_{\langle i_A, i_B \rangle} \begin{bmatrix} \tilde{\phi}_A^{i_A*} & \tilde{\phi}_B^{i_B*} \end{bmatrix} (\hat{\mathbf{n}} \cdot \boldsymbol{\sigma}) \begin{bmatrix} \tilde{\phi}_A^{i_A} & \tilde{\phi}_B^{i_B} \end{bmatrix}^T + \sum_{i_A} |\tilde{\phi}_A^{i_A}|^2 + \sum_{i_B} |\tilde{\phi}_B^{i_B}|^2 + E_G \quad (2.87)$$

The unit vector

$$\hat{\mathbf{n}} = \cos \varphi_{i_A i_B} \hat{x} + \sin \varphi_{i_A i_B} \hat{y}$$

and

$$\boldsymbol{\sigma} = \sigma_x \hat{x} + \sigma_y \hat{y}$$

where $\sigma_{x,y}$ are the Pauli matrices. As already explained, the reduced basis ansatz assumes very low superfluid density ($\phi_{A,B} \ll 1$). Thus \mathcal{E} contain terms only linear in the superfluid density. This is unlike the Gross-Pitaevskii energy functional [19]

$$\mathcal{E}(\psi) = \int d\mathbf{r} \left[\frac{\hbar^2}{2m} |\nabla \psi(\mathbf{r})|^2 + V(\mathbf{r}) |\psi(\mathbf{r})|^2 + \frac{1}{2} U_0 |\psi(\mathbf{r})|^4 \right] \quad (2.88)$$

which contains terms quadratic in the superfluid density and is valid deep inside the superfluid regime.

Minimization of the above energy functional with respect to $\tilde{\phi}_A^{i_A*}, \tilde{\phi}_B^{i_B*}$ gives equations for the superfluid order parameter that can be written as a spinorial Harper equation,

$$\sum_{\langle i_A, i_B \rangle} (\hat{\mathbf{n}} \cdot \boldsymbol{\sigma}) \begin{bmatrix} \tilde{\phi}_A^{i_A} & \tilde{\phi}_B^{i_B} \end{bmatrix}^T = \frac{1}{\tilde{t}} \begin{bmatrix} \tilde{\phi}_A^{i_A} & \tilde{\phi}_B^{i_B} \end{bmatrix}^T \quad (2.89)$$

Its solution can be written as

$$\tilde{\phi}(x, y) \otimes \left[\exp(-i \frac{\varphi_{A i_B}}{2}) \quad \exp(i \frac{\varphi_{A i_B}}{2}) \right]^T$$

where $\tilde{\phi}(x, y)$ satisfies the following symmetric gauge Harper equation [128]

$$\tilde{\phi}(x+1, y)e^{i\pi\nu y} + \tilde{\phi}(x-1, y)e^{-i\pi\nu y} + \tilde{\phi}(x, y+1)e^{-i\pi\nu x} + \tilde{\phi}(x, y-1)e^{i\pi\nu x} = \frac{1}{t}\tilde{\phi}(x, y) \quad (2.90)$$

$\frac{1}{t}$ in the right hand side of the equation (2.90) can be mapped on the eigenvalues ε of HB [92] spectrum plotted in Fig. 2.6. Before discussing our results we shall provide a brief description to Harper equation and Hofstadter butterfly.

2.2.4 Harper equation and Hofstadter Butterfly spectrum

In the previous subsection, the Harper equation is obtained from the modified extended Bose Hubbard Hamiltonian, effectively showing the analogy between bosons in a rotating optical lattice and electrons in a magnetic field. It is known that a free electron which is subjected to a magnetic field performs a circular motion with a frequency given by the cyclotron frequency. Quantum mechanically, its eigen states are the well-known Landau levels - evenly spaced cyclotron energies that linearly increase with magnetic field (Fig. 2.5). The combination of a periodic potential along with the magnetic field creates a rather interesting problem, for which exist a specialized solution named as Hofstadter's Butterfly [92]. As can be clearly seen from Fig. 2.6, the spectrum of an electron in a periodic potential and a strong magnetic field bears little resemblance of Landau levels (Fig. 2.5) and reveals a complex fractal spectrum instead. It shows that in the high magnetic field limit, the weak periodic potential lifts the high degeneracy of the Landau levels which split into a complex mini band structure.

For a magnetic flux $\nu = p/q$, this Landau level splits into p magnetic mini bands. This is due to the commensurability effect of the magnetic fields. It means that whenever the magnetic flux through the unit cell is a rational multiple of the flux quantum h/e , the periodic potential alongwith the magnetic field act as an effective periodic potential with a periodicity that is a multiple of the unit cell dimension. It is responsible for the highly aesthetic, self similar structure of energy bands and gaps. As mentioned, the magnetic field must be strong to reveal this effect. Strong in this context means that the cyclotron energy must be comparable to the strength of the periodic potential.

Alternatively, this problem can also be seen as free electrons in a periodic potential with single particle spectra of Bloch bands subjected to a magnetic field. In theory, the self-similar energy spectrum can be obtained from either of the methods. Though both the methods are complementary to each other, but they are mathematically equivalent and are the limiting cases, where either the influence of the magnetic field on the strong lattice potential in the tight-binding approximation is considered or the influence of the

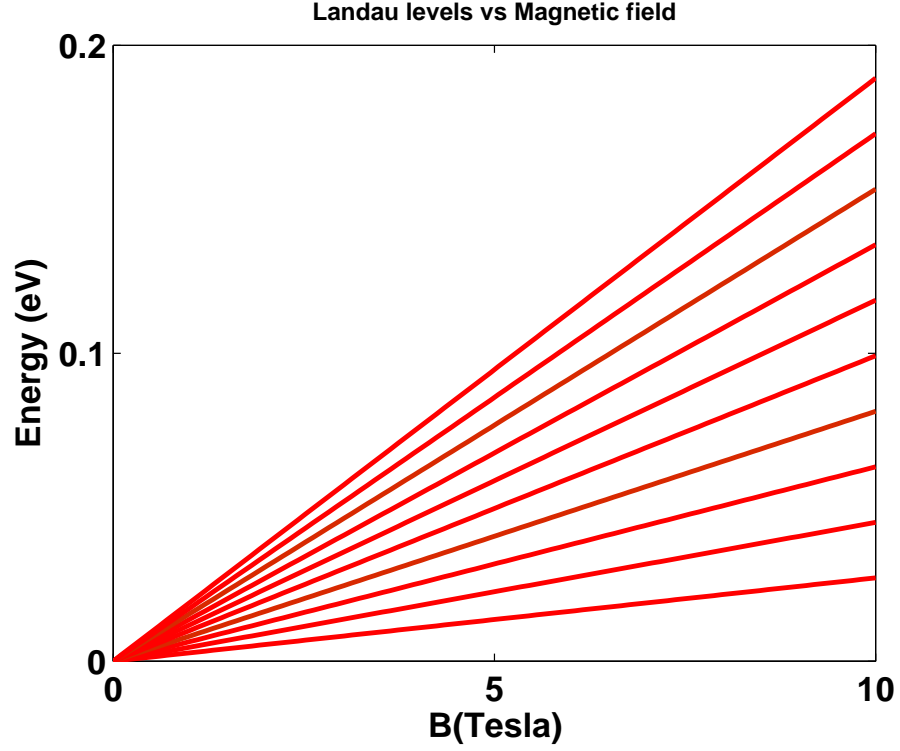


FIGURE 2.5: Landau level energy spectra for free electrons in two dimensional in the presence of magnetic field. The energy spectrum is given by $E = \hbar\omega_c(n + \frac{1}{2})$ with $\omega_c = \frac{eB}{m}$.

modulation potential on the Landau levels in two-dimensional electron system may be considered as a small perturbation. In both cases, the energy spectrum is obtained by solving the Harper equation [128]. We here show the derivation by the alternate method where the energy bands associated with Bloch waves are subjected to magnetic field.

The Harper equation was originally used to obtain the single particle energy spectra for electrons in a periodic potential (Bloch electrons) in the presence of gauge field [128]. The description for the Bloch electrons in a magnetic field was suggested by Peierls by substituting the crystal momentum $\hbar\mathbf{k}$ in a tight binding band by the kinetic momentum $(\mathbf{p} - \frac{e\mathbf{A}}{c})$ and is known as *Peierls substitution* [135].

We start with a single tight binding band for a two-dimensional square lattice with lattice constant a with the following dispersion as

$$E(\mathbf{k}) = 2E_0(\cos(k_x a) + \cos(k_y a)), \mathbf{k} = (k_x, k_y)$$

Applying *Peierls substitution*, $\mathbf{k} \rightarrow \frac{1}{\hbar}(\mathbf{p} - \frac{e\mathbf{A}}{c})$, we obtain a tight binding Hamiltonian H_{tb} whose spectrum depends on the magnetic field. For the Landau gauge $\mathbf{A}^L(\mathbf{r}) =$

$\mathbf{B}(0, x, 0)$, H_{tb} takes the form

$$H_{tb} = E_0 \left(e^{\frac{i}{\hbar} p_x a} + e^{-\frac{i}{\hbar} p_x a} + e^{\frac{i}{\hbar} (p_y - \frac{eB}{c} x) a} + e^{-\frac{i}{\hbar} (p_y - \frac{eB}{c} x) a} \right) \quad (2.91)$$

The exponential factors with the momentum operators p_x , p_y are the translational operators, thus the eigenvalue equation $H_{tb}\phi(x, y) = E\phi(x, y)$ can be written as

$$E_0 \left(\phi(x+a, y) + \phi(x-a, y) + e^{-i\frac{xa}{\hbar c/eB}} \phi(x, y+a) + e^{i\frac{xa}{\hbar c/eB}} \phi(x, y-a) \right) = E\phi(x, y)$$

We make use of translational invariance along y direction in Landau gauge by replacing $x = ma$, $y = na$ and $\phi(x, y) = e^{i\sigma n} \phi_m$ which gives the following Harper equation

$$\phi_{m+1} + \phi_{m-1} + 2\cos(2\pi m\nu - \sigma) = \epsilon \phi_m \quad (2.92)$$

where $\epsilon = E/E_0$ and $\nu = Ba^2/\phi_0$ is the number of flux quanta through the unit cell of the square lattice.

In the present case for bosons in a rotating optical lattice, we get a similar Harper equation (2.89) in coupled form for two sublattices, by minimization of the energy functional for eBHM in presence of *artificial* gauge field. In the Landau gauge $\mathbf{A}^L(\mathbf{r}) = \mathbf{B}(0, x, 0)$, following [136] we denote the co-ordinate of a site i on the square lattice by pair of integers $\{x, y\}$ in the unit of the lattice spacing a . For Landau gauge potential therefore the phase of the hopping parameter $\varphi_{ij} = 0$ if the link along x direction ($i \rightarrow j = \{x, y\} \rightarrow \{x+1, y\}$) and $\phi_{ij} = 2\pi n\nu$ if the link is along the y direction such ($i \rightarrow j = \{x, y\} \rightarrow \{x, y+1\}$). In terms of these notations the eigenvalue equation on the lattice can be written as

$$\tilde{\phi}(x+1, y) + \tilde{\phi}(x-1, y) + e^{2\pi i\nu x} \tilde{\phi}(x, y+1) + e^{-2\pi i\nu x} \tilde{\phi}(x, y-1) = \frac{1}{t} \tilde{\phi}(x, y) \quad (2.93)$$

The lattice wavefunctions that appears in equation (2.93) can be obtained by operating $\tilde{\phi}(x, y)$ by magnetic translation operator. Such operators are given as $T_{\mathbf{R}} = \exp(\frac{i}{\hbar} \mathbf{R} \cdot [\mathbf{p} + \frac{\hbar}{m} \mathbf{A}(\mathbf{r})])$ [124] where R is the lattice translational vector and it is known that the operators along the x and y axis do not commute since $\hat{T}_{a\hat{x}} \hat{T}_{a\hat{y}} \hat{T}_{a\hat{x}}^{-1} \hat{T}_{a\hat{y}}^{-1} = \exp(2\pi i\nu)$. For $\nu = \frac{p}{q}$, the required commutator is given by $[T_{qa\hat{x}}, T_{a\hat{y}}] = 0$. To ensure that the wave function remain single valued at a given lattice point as a unit cell is traversed, the enlarged unit cell known as magnetic unit cell, therefore, has $1 \times q$ sites as compared to the unit cell in the absence of such magnetic field. Correspondingly the Brillouin Zone (BZ) is reduced with

$$-\pi \leq k_x \leq \pi, -\pi/q \leq k_y \leq \pi/q$$

and is called the magnetic Brillouin zone (MBZ).

Similarly, for symmetric gauge potential, the Harper equation assumes the following form

$$\tilde{\phi}(x+1, y)e^{i\pi\nu y} + \tilde{\phi}(x-1, y)e^{-i\pi\nu y} + \tilde{\phi}(x, y+1)e^{-i\pi\nu x} + \tilde{\phi}(x, y-1)e^{i\pi\nu x} = \frac{1}{t}\tilde{\phi}(x, y) \quad (2.94)$$

When one uses a symmetric gauge potential $\mathbf{A}^S(\mathbf{r}) = \mathbf{B}(-y, x, 0)$, the commuting magnetic translation operators are $\hat{T}_{2qa\hat{x}}$ and $\hat{T}_{2qa\hat{y}}$. Following the preceeding discussion it can be shown that the magnetic unit cell should be $2q \times 2q$ of the unit cell in the absence of the magnetic field. The factor 2 comes because the phase accumulated when one goes around an unit cell in the square lattice is $\pi i\nu$ in presence of the gauge potential. Accordingly, the MBZ will be defined as

$$\left(-\frac{\pi}{2q} \leq k_x \leq \frac{\pi}{2q}, -\frac{\pi}{2q} \leq k_y \leq \frac{\pi}{2q}\right)$$

The solution of Harper equation in either of the gauge choices yield the energy spectrum as a function of increasing magnetic flux as shown in Fig. 2.6. This energy spectrum of

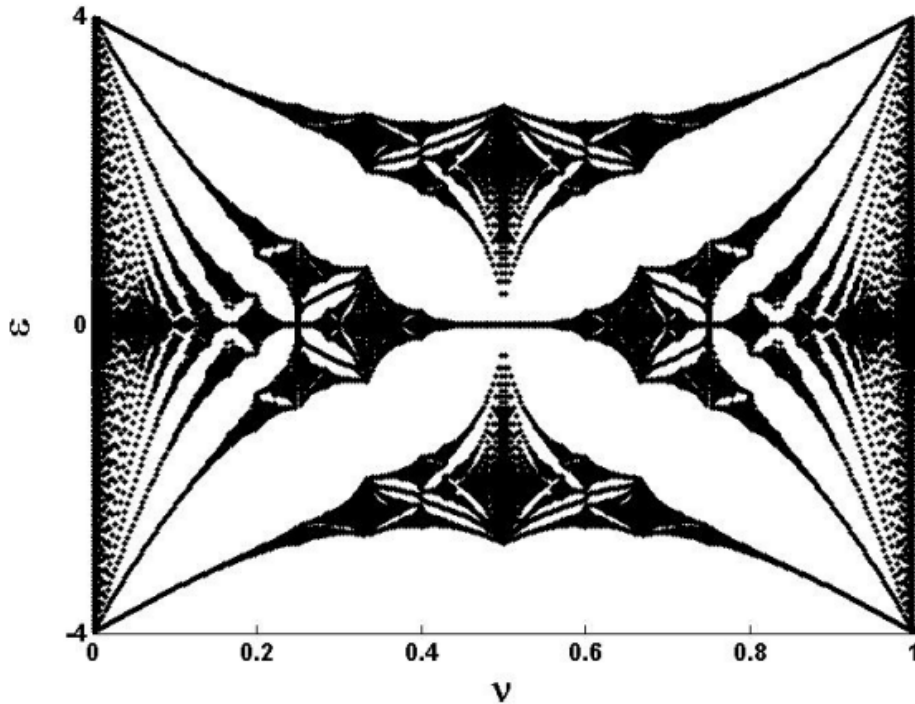


FIGURE 2.6: Hofstadter butterfly: the energy (ε) spectrum for equation (2.93) or (2.94) for various $\nu \in [0, 1]$.

the Harper equation as a function of increasing magnetic flux is termed as Hofstadter Butterfly spectrum [92]. The most striking feature of this spectrum is the fractal or self similarity of the structure of energy bands and gaps, which implies that if we take

a suitable portion of this spectrum, we can obtain the full spectrum again [92]. Its graph is periodic in ν with period 1 so that the pattern repeats for each additional flux quantum per unit cell and the unit interval $(0, 1)$ exhibits reflection symmetry in the lines $\epsilon = 0$ and $\nu = \frac{1}{2}$ as seen from Fig. 2.6. When looking at the spectrum as evolving from a single Landau level due to weak periodic potential, this Landau level splits into p magnetic bands for flux $\nu = p/q$.

2.3 Results and discussion

2.3.1 Modification of phase boundaries of DW and MI phases

An important feature of the HB spectrum obtained in previous section is that the edge of the HB spectrum (marked red in Fig. 2.7(a)) is related to the highest eigenvalue of the equation (2.90) as function of $\nu \in [0, 1]$. This corresponds to the minimum value of \tilde{t}

$$\tilde{t} = \tilde{t}_c = \frac{t_c}{\sqrt{\epsilon_1 \epsilon_2}}$$

with non vanishing SF order parameter $\tilde{\phi}$ for each given value of μ , and, hence the boundary of the DW phase at that particular ν (marked red in Fig. 2.7(b)). Same observation holds true for MI boundary at the MI-SF transition in a rotating optical lattice [106, 107]. Setting $m = n$ in the preceeding analysis the MI-SF transition in rotated lattice can be studied for eBHM. The phase boundary of the ordinary BHM under rotation or magnetic field can be retrieved by setting $V = 0$ and also putting $n = m$ in the preceding analysis. The results obtained in this way matches with those in reference [106, 107] for BHM in presence of such artificial magnetic field. However the superfluid order parameter of the excitations at the boundary of the DW phase are different from those near the MI boundary as we shall see in Fig. 2.9. The modification of DW as well as MI phase boundaries are plotted in Fig. 2.7 as a function of increasing magnetic flux, which clearly follows the edge eigen-value spectrum of HB. The cross sectional plot in Fig. 2.8 shows the modification of DW and MI phase boundaries as a function of increasing magnetic flux ν . As compared to the modification of the phase boundary of a MI phase in ordinary BH model here also the phase boundary of the DW phase extends as the strength of the gauge field ν is enhanced. This is due to the stronger localization of the bosonic states by the increasing strength of the gauge field.

However it is important to note that the Fig. 2.8 only provides analytically the phase boundary of DW as well as MI phases and does not provide the phases themselves over the entire $t - \mu$ plane for various ν unlike in the references [103, 126, 127]. The boundary separating the SS and SF phases from the DW and MI phases cannot be determined

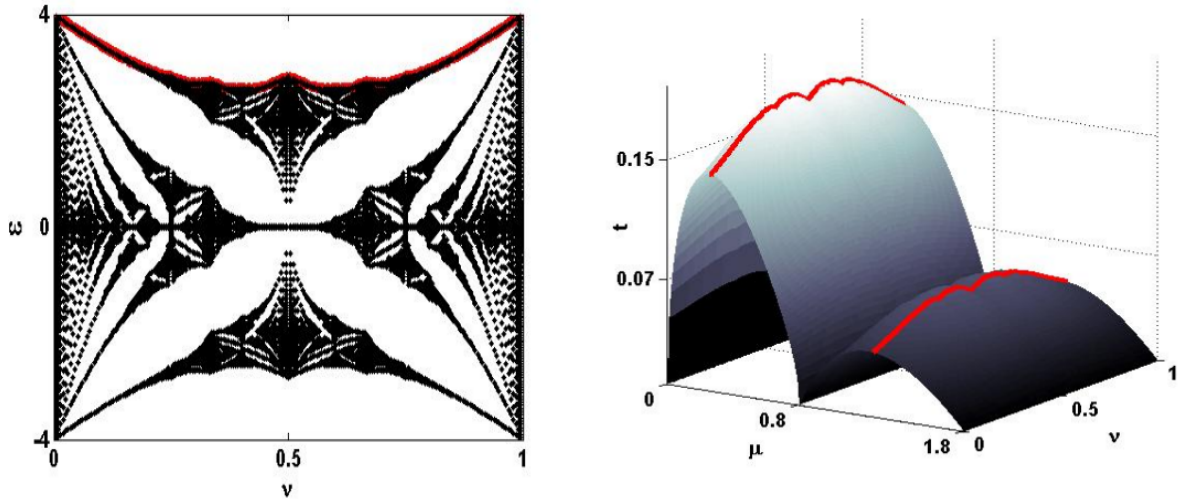


FIGURE 2.7: (Left) Hofstadter butterfly: the energy (ε) spectrum for the equation (2.90) for various $\nu \in \{0, 1\}$. The upper edge (marked red) gives the boundary of the density wave and the Mott Insulator lobe as explained in the text. (Right) The first DW and MI lobe as a function of t, μ, ν in mean field approximation where t and μ are in the unit of U . V has been taken as 0.2 in the unit of U

within the Gutzwiller mean field analytical calculations performed. So, the approximate positions of these phases is shown in Fig. 2.8. But, in mean field approximation it can be obtained numerically by using the full Gutzwiller wavefunction as was done in [103] with no magnetic flux.

2.3.2 Superfluid density profile for vortex in a supersolid near the DW-SS boundary

In addition to the modification of the phase boundaries of the insulating lobes, we can also calculate the effect of artificial gauge field on the superfluid density profile near the DW and MI phases. It is known that the SS phase starts appearing near the phase boundary of DW phase and hence the effect of rotation on such phase will result in the formation of vortex structures in SS phase. We calculated the resulting vortex profiles and found that the spatial profile of the superfluid density shows a checkerboard-like two sublattice modulation with a relative phase winding between the superfluid order parameter defined on each of these sublattices.

At $\tilde{t} = \tilde{t}_c$ and $\nu = \frac{1}{L^2}$ each magnetic unit cell that consists of $L \times L$ lattice sites, contains one single vortex of unit winding. The strong sublattice modulation of the superfluid density around the vortex core is calculated shown in Fig. 2.9(a) for $L = 16$. It shows the formation of a single vortex in a rotating supersolid and clearly show the structural difference of vortex in supersolid as compared to vortex in a superfluid. The DW order parameter given in Fig. 2.9(b) becomes 1 at the vortex core and co exists alongside the

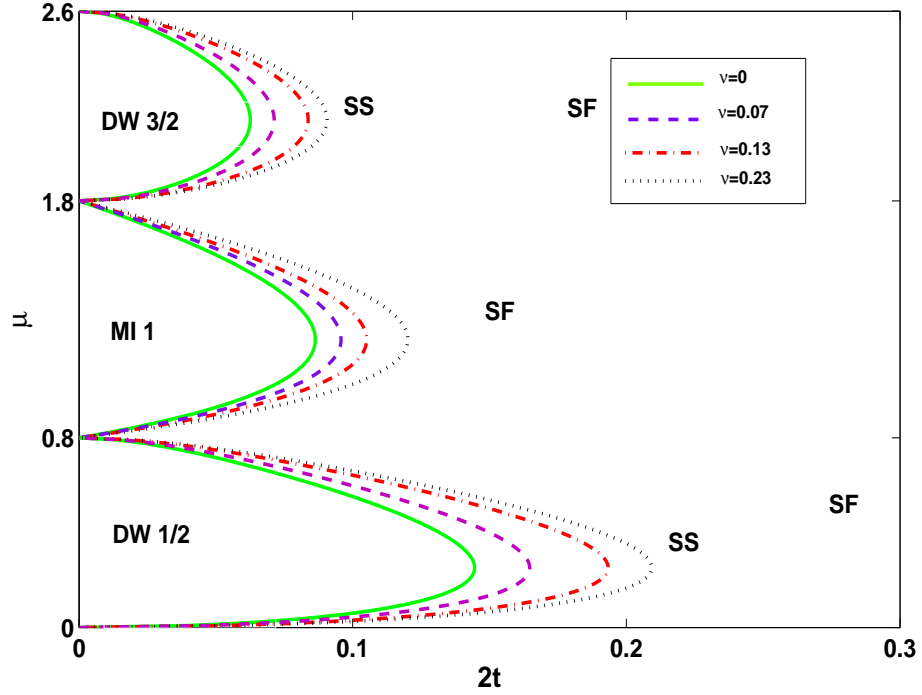


FIGURE 2.8: Cross section of the phase diagram in Fig. (2.6) that shows the modification of the first two density wave lobe and the first Mott lobe at various values of circulation quanta ν . In all these plots V has been taken as 0.2 in the unit of U . The SS phase which appears after the DW phase followed by appearance of SF phase is also shown approximately. Please note that the position of the SS and SF phases shown is only approximate and is not calculated within the theory.

superfluid order in the bulk. From the spectrum of the Harper equation, we have thus analytically demonstrated how the superfluid and crystal order coexist in the vortex profile of a SS around a DW vortex core.

We know that in a HB problem, for $\nu = \frac{p}{q}$, a given degenerate Landau level is broken into q bands for p fluxes through a given magnetic unit cell. In our present case we have taken $\nu = \frac{1}{256}$. The highest of these energy levels correspond to the critical value of $\tilde{t} = \tilde{t}_c$ at the phase boundary. Thus one may think that the eigenfunction for the lower energy levels that correspond to higher values of \tilde{t} can be related with the superfluid phases away from the phase boundary of the DW state inside the supersolid regime. However this simplistic argument is not correct since the entire derivation presented above is only within the reduced basis ansatz, which is valid only at $\tilde{t} \sim \tilde{t}_c$. Nevertheless we also plot the eigenfunction corresponding to a band which is very close to the highest band in Fig. 2.10. This approximately depicts the superfluid order parameter in a rotated SS phase for $\tilde{t} > \tilde{t}_c$, but still very close to the DW phase boundary. This state, corresponding to the lower band of the same spectrum contains multiple vortices in a given magnetic unit cell and the winding number of these vortices could also be integers > 1 . Such

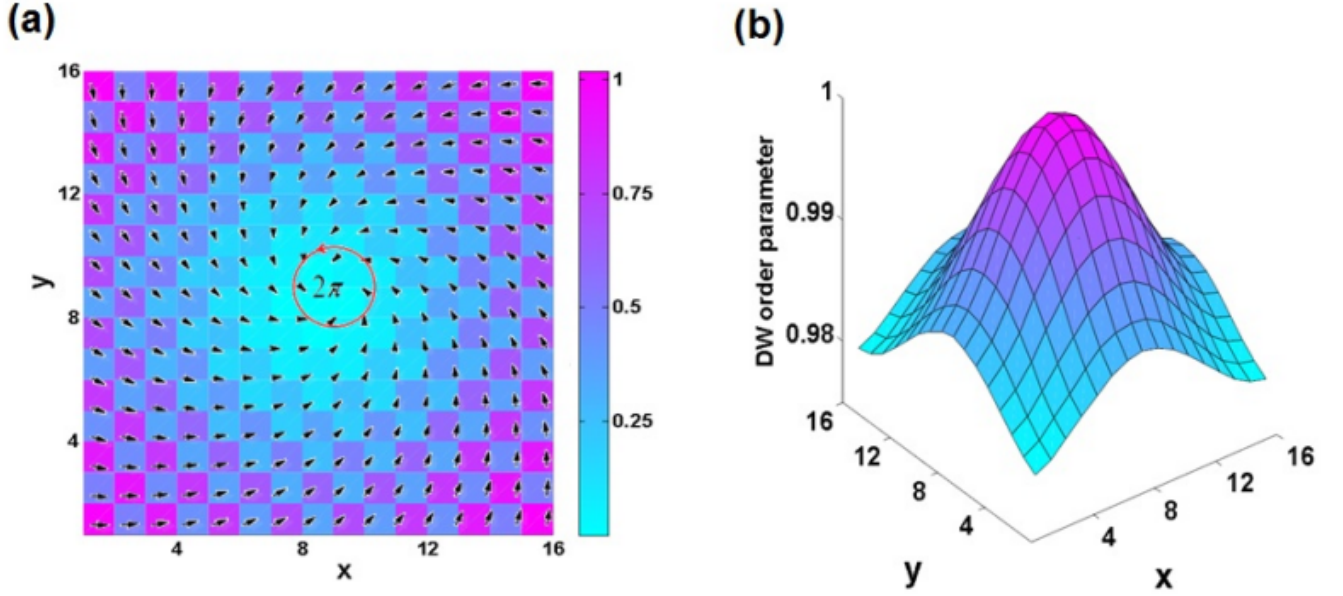


FIGURE 2.9: (a) Checkerboard vortices at the density wave ($|2, 1, 2, 1, \dots\rangle$) phase boundary ($\tilde{t} = \tilde{t}_c$) corresponding to the highest eigenvalue (the edge) of the hofstadter butterfly spectrum for $\nu = \frac{1}{16 \times 16}$. The direction of the arrow gives φ_{i_A, i_B} where as the color axis gives the superfluid density. The superfluid density is normalized by the maximum superfluid density at the boundary. The x and y coordinates are given in units of optical lattice spacing and are the same in all the plots. (b) corresponding DW order parameter

a vortex structure is plotted in Fig. 2.9. For calculating vortex structure at higher \tilde{t} that corresponds to deep inside the SS phase, one needs to go beyond the reduced basis ansatz and include the non linear terms due to SF interaction.

2.4 Possibilities of experimental detection

Experimental detection of the SS vortices near the phase boundary seems to be practically possible with the presently available techniques. The characterising feature of SS phase is the sublattice modulation of the superfluid density and can be detected through the time of flight measurement and studying the resulting interference pattern. Time-of-flight expansion gives access to the momentum distribution and correlations via detection of the average density and noise. The periodicity in the superfluid density in the SS phase will give rise to additional peaks at finite momenta values in the reduced magnetic BZ, in addition to the zero momentum peak already observed for superfluid phase [33]. The signatures of the gauge potential will appear in the reciprocal space in

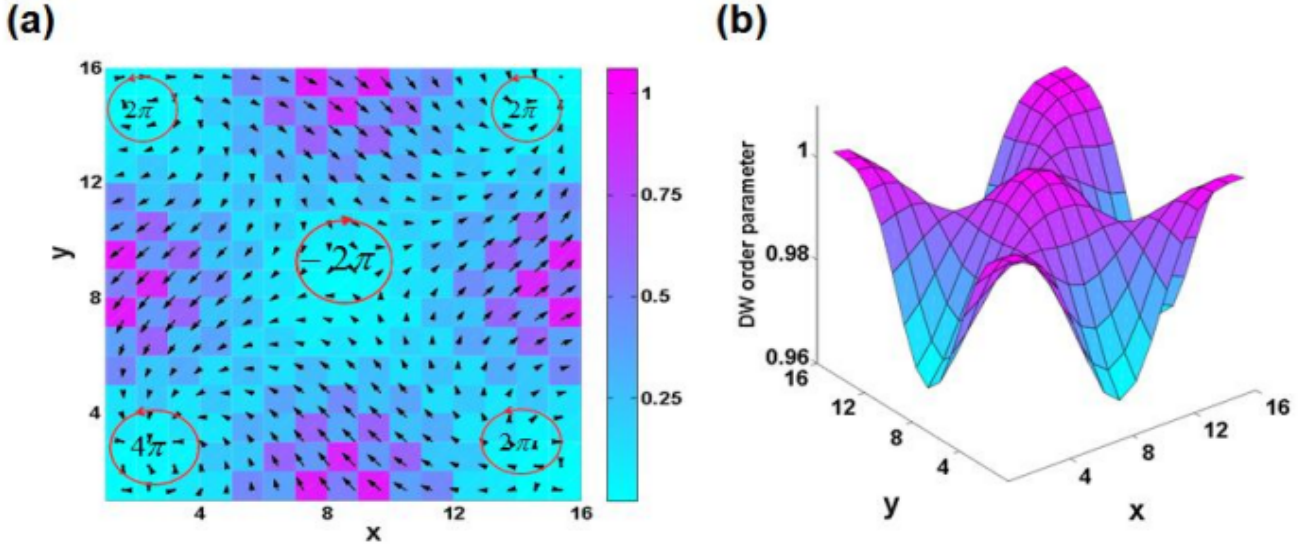


FIGURE 2.10: (a) More complicated vortex structure corresponding to the higher value of \tilde{t} corresponding to a lower eigenvalue ((254(16 × 16 − 2)th band)(b) corresponding DW order parameter. The direction of the arrow gives φ_{i_A, i_B} where as the color axis gives the superfluid density. The superfluid density is normalized by the maximum superfluid density at the boundary. The x and y coordinates are given in units of optical lattice spacing and are the same in all the plots.

the form of reduction of the BZ and further the signature for vortex in SS can be probed using standard time of flight imaging by detecting peaks at finite momenta values in addition to the peak at zero momentum.

We shall describe this in more detail in the next chapter 3, where we calculate the momentum distribution and quasi-momentum distribution for SS phase in presence of *artificial* gauge field using the strong coupling perturbation technique.

To measure the detailed vortex structure in a magnetic unit cell one can also use the Bragg scattering technique [137–140] which is sensitive to the spatial phase distribution of the initial state [141]. In the Bragg scattering technique, two momentum states of the same ground state are connected by a stimulated two-photon process. It can be thought of as a Raman process where two momentum states are coupled as opposed to the internal states of the atoms. This stimulated two photon process is referred to as Bragg spectroscopy in analogy to Raman spectroscopy. It is explained as below.

When an atomic beam passes through a periodic optical potential formed by a standing light wave, and interacts with it for a sufficiently long time, it can Bragg diffract in a

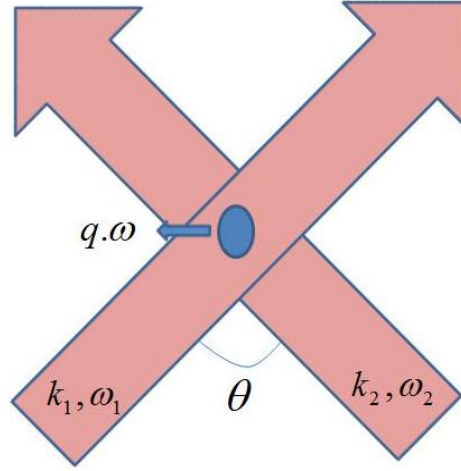


FIGURE 2.11: Bragg spectroscopy set up. The momentum transfer is determined by the angle between the Bragg beams θ and the frequency $\Delta\omega = \omega_2 - \omega_1$ determines the energy transfer.

manner similar to the Bragg diffraction of X-rays from a thick crystal. In each case the incident beam must satisfy a condition on the angle of incidence. In contrast to the Bragg diffraction of an atomic beam [142], the interaction time is determined not by the passage of the atoms through a standing wave, but by the duration of a laser pulse. The condition on the angle of incidence becomes a condition on the frequency difference between the two beams comprising the standing wave, or equivalently, the velocity of the moving standing wave [137, 138]. The momentum transfer \mathbf{q} and energy transfer $\hbar\omega$ are given by

$$|\mathbf{q}| = 2N\hbar k \sin\left(\frac{\theta}{2}\right)$$

and,

$$\omega = N\Delta\omega$$

where θ is the angle between the two laser beams with wave vector k and frequency difference $\Delta\omega$ (Fig. 2.11).

Thus, Bragg diffraction under these conditions can also be thought conveniently as a stimulated Raman transition between two momentum states. This process can be used to probe density fluctuations of the system and thus to measure directly the dynamic structure factor $S(\mathbf{q}, \omega)$ [137, 138]. The dynamic structure factor is the Fourier transform of the density-density correlation function between atoms at various sites and is given by [143]

$$S(\mathbf{q}, \omega) = \frac{1}{Z} \sum_{mn} e^{-\beta E_m} |\langle m | \rho_{\mathbf{q}} | n \rangle|^2 \delta(E - E_m - E_n) \quad (2.95)$$

where \mathbf{q} is the wave vector of the momentum, E is the energy transfer to the system from the probe, E_n is the eigen value of the state $|n\rangle$, $\rho_{\mathbf{q}} = \sum_j e^{i\mathbf{q}\cdot\mathbf{r}_j}/\hbar$ is the fourier transform of the single particle density operator and Z is the canonical partition function. From the density fluctuations and hence the dynamic structure factor obtained using Bragg scattering technique, one can look into the signatures of the vortex structure in supersolid compared to that of a superfluid.

Thus, Bragg scattering is a stimulated process which greatly enhances resolution and sensitivity to the direction of rotation [144] and could be an efficient way for a robust signature of the vortex state in a SS.

2.5 Summary of the chapter

To summarize, in this chapter we report the modification of the DW and MI phase boundary by using a reduced-basis ansatz for the Gutzwiller variational wave function, within the framework of mean-field approximation. The minimization of the energy functional very close to the DW phase boundary shows that the super fluid order parameter satisfies a spinorial Harper equation. Consequently, the phase boundary can be determined from the edge of a HB spectrum [105].

In the resulting vortices, the spatial profile of the superfluid density shows a checkerboard-like two sublattice modulation with a relative phase winding between the superfluid order parameter defined on each of these sublattices. Thus, from the spectrum of the Harper equation (in analogy with equation for electron in a periodic potential in presence of a magnetic field), we have analytically demonstrated how the superfluid and crystal order coexist in the vortex profile of a supersolid around a DW vortex core [105]. This can be used to identify the supersolid phase in cold-atom experiments. We also discuss their possible ways of experimental detection, which includes the Time of flight imaging technique to get the sublattice modulation of the superfluid density and to get the detailed vortex structure, one can use the Bragg scattering technique, which is sensitive to the spatial phase distribution of the initial state and the direction of rotation and thus can provide signature of the vortex state in a SS.

Chapter 3

DW-SS and MI-SF transition in presence of an artificial gauge field : a strong coupling perturbation approach

This chapter is based on the publication *R. Sachdeva and Sankalpa Ghosh, 'Density Wave Supersolid and Mott Insulator Superfluid transition in the presence of an artificial gauge field: a Strong Coupling perturbation approach', Physical Review A, 85, 013624 (2012) [109]*

The effect of *artificial* gauge field on the MI-SF transition in BHM has been studied extensively in recent times both within mean field approximation [106, 107, 122, 145–148] and also by going beyond mean field description [149–152]. In comparison, the DW-SS transition in eBHM in presence of a finite flux due to such gauge field [105] as well as in presence of a staggered flux [153] is still in very early stage and was carried out only in mean field framework.

The results for eBHM obtained using mean field approach in Chapter 2 gave us important information namely the modification of the phase boundaries of the insulating phases as a function of magnetic flux, and the structure of vortex in a SS. But one of the drawbacks of mean field theory is that it is linear in the hopping parameter t , and hence the accuracy of the critical transition points is somewhat limited. Also, we can not extract information about the dimension dependence of the lobes of phase diagram with in the mean field theory. Other methods which are frequently used to study such systems face some issues, namely Quantum Monte Carlo (QMC) which is extremely successful

without gauge field [154] suffers with a sign problem in presence of gauge fields, and thus cannot be implemented; Density Matrix Renormalization Group (DMRG) [155] is restricted to work mostly in one dimension and cannot take into account the vortex formation for which $d = 2$ is the minimum spatial dimension.

So, to overcome most of the limitations in above listed methods, we use strong coupling perturbation theory [108] which is one of the strong and reliable technique to study such systems in strongly correlated regimes. Strong coupling perturbation theory has no dimension restriction like DMRG [155] and thus gives the correct dependence on the dimensionality of the spatial lattice. Applying perturbation theory improves the Gutzwiller correlation function. It reproduces the correct slope for the off-diagonal decay and thus, the perturbative approach represents a qualitative improvement on the Gutzwiller result. Also, this technique works equally well in presence of gauge fields.

Since QMC is difficult to implement in presence of gauge field, and DMRG is $1d$ specific, strong coupling perturbation theory is arguably one of the most accurate way to evaluate the phase diagram and the present work accomplishes this partly. Thus, in two dimensions, and in presence of artificial gauge fields, strong coupling perturbation theory emerge as one of the most reliable technique to study the effect of artificial gauge field on such system. We will describe it in details in the chapter.

Keeping in mind the detailed nature of calculations, we have divided this chapter of the thesis into two sub-parts, namely 3A and 3B.

Chapter 3A

3.1 Introduction

In this part of the chapter, we use the strong coupling perturbation formalism to determine the phase diagram of the system in presence of gauge field. The strong coupling perturbation expansion which we adopt here to study the eBHM model treats the hopping as perturbation [108, 156, 157] and we perform the energy and wave function expansion for the insulating and particle hole excited phases as a function of hopping parameter.

The part 3A of this chapter is organized as follows. In section 3.2, we present the model Hamiltonian and the formalism of our calculations within the framework of strong coupling perturbation theory. In section 3.3, we develop the strong coupling perturbation theory in the hopping parameter and derive the analytical expressions for the phase boundaries between the incompressible (DW and MI) phases and compressible (SS and SF) phases, in presence of artificial gauge field. We found that the shapes of the insulating lobes depend on the dimensionality of the system and, also on the application of artificial gauge field, unlike the mean field results. Further we carried out an extrapolation of phase boundaries using chemical potential exploration technique to extrapolate our expansion into a functional form appropriate for MI and DW phases in section 3.4.

3.2 Extended Bose Hubbard Model in presence of magnetic field

We take the same eBHM Hamiltonian (equation (2.44)) with nearest neighbor interaction which was treated in variational mean field approximation in the previous chapter 2.

$$H = -t \sum_{i,j} (\hat{a}_i^\dagger \hat{a}_j e^{-i\varphi_{ij}} + h.c) + \frac{1}{2} \sum_i \hat{n}_i (\hat{n}_i - 1) - \mu \sum_i \hat{n}_i + V \sum_{i,j} \hat{n}_i \hat{n}_j \quad (3.1)$$

Though all the quantities in the above Hamiltonian are already described in detail in chapter 2, for convenience we briefly mention them again here.

The Hamiltonian in above equation (3.1) is rescaled by U and thus, all parameters are measured in units of U . The first term gives us the nearest neighbor hopping where

$$\varphi_{ij} = \int_{r_j}^{r_i} d\mathbf{r} \cdot \mathbf{A}(\mathbf{r})$$

where $\mathbf{A}(\mathbf{r})$ is the vector potential corresponding to the artificial gauge field. Again, \hat{a}_i^\dagger , \hat{a}_i and \hat{n}_i are the boson creation, annihilation and number operators respectively, and V

is the strength of nearest neighbor interaction that minimally captures the effect of long range interaction, μ is the chemical potential. The effect of an overall trap potential is neglected assuming that it is sufficiently shallow and is neutralized by the effect of centrifugal force particularly at the central region of the condensate.

We are particularly interested in the limit when $Vd < 1/2$, where d is the dimension of the system which is 2 in the present case. In this limit, the alternating sites of the lattice in the DW phase contains n_0 and $n_0 - 1$ particles and such a phase is called $n_0 - \frac{1}{2}$ DW phase. In the rest of the chapter, for the the alternative sites of DW phase having population n_A and n_B , we set $n_A = n_0$ and $n_B = n_0 - 1$ to obtain the corresponding results for $n_0 - \frac{1}{2}$ DW phase. However the theory is generalizable to other type of DW phases as well in a straightforward manner.

3.2.1 Formalism

Within the framework of the strong coupling perturbative expansion we calculate the ground-state energy $E_{DW}(n_A, n_B)$ of the DW phase with n_A and n_B bosons on alternating lattice sites, and $E_{MI}(n_A = n_B = n_0)$ of the MI phase with n_0 bosons on each lattice site, respectively. Then we calculate the energies of the DW particle-hole excitations and MI particle-hole excitations (states with an extra particle or hole), $E_{DW}^{par}(n_A, n_B)$, $E_{DW}^{hol}(n_A, n_B)$, and $E_{MI}^{par}(n_0)$, $E_{MI}^{hol}(n_0)$, respectively. The unperturbed system corresponds to the case $t \rightarrow 0$ where t refers to the scaled hopping amplitude. Using the Rayleigh-Schroedinger perturbative expansion [158], the ground state energy of DW and MI phases as well the energy of particle hole like excitations over these ground state is calculated in various orders of t .

Both the DW and MI states are gapped since the energy to create a single particle-hole excitations is finite. With increasing t this excitation gap starts decreasing (Fig. 2.4). At the critical hopping parameter $t = t_c$ the energy to create a particle-hole pair vanishes and DW phase becomes degenerate with its particle and hole excited state. This gives the value of t at which DW-SS transition takes place. Thus, the phase boundary between DW and SS phase is determined by :

$$E_{DW}(n_A, n_B) = E_{DW}^{par/hol}(n_A, n_B) \quad (3.2)$$

Similarly, the phase boundary between MI phase and SF phase is determined as :

$$E_{MI}(n_0) = E_{MI}^{par/hol}(n_0) \quad (3.3)$$

These conditions determine the particle and hole branches of both the insulating lobes (DW and MI), giving us μ^{par} and μ^{hol} as functions of t, V, n_A, n_B (for DW phase) or t, V, n_0 (for MI phase).

3.2.2 Wave functions at zeroth order in t

In this section we shall define the ground state wave functions for the DW and MI phases after setting the scaled hopping amplitude $t = 0$ for Hamiltonian defined in (3.1). In this limit these wavefunctions are determined by the competition between interaction energies alone and can be found out exactly. The wave functions for the particle and hole excited states above these ground states will also be mentioned both for DW and MI phase and we shall particularly emphasize the degeneracy associated with such excited states in the $t \rightarrow 0$ limit.

For the DW state, we divide the lattice into sublattices A and B , where each site in sublattice A contains n_A particles and each site in sublattice B contains n_B particles. For $t = 0$, DW wave function can be written as

$$|\Psi_{DW}^{(0)}\rangle = \prod_{i \in A, j \in B}^{M/2} \frac{(\hat{a}_i^\dagger)^{n_A}}{\sqrt{n_A!}} \frac{(\hat{a}_j^\dagger)^{n_B}}{\sqrt{n_B!}} |0\rangle \quad (3.4)$$

where M is the total number of lattice sites, and $|0\rangle$ is the state with no particle. Here $\hat{a}_{i,j}^\dagger$ refer to boson creation operator on A and B sublattices, respectively. Since we are interested in calculating the wave function as well as energy of such a state for finite t , as a perturbative expansion in the parameter t , the wavefunction defined in (3.4) is also the wavefunction at the zeroth order of this perturbative expansion.

Unlike the ground state wave function defined in (3.4), the wave functions for the DW states with an extra particle or hole for $t = 0$ is degenerate. This is because when an extra particle or hole is added to the system, it can go to any of the M lattice sites. In the present case, the alternating sites belong to A and B sublattice and contain $n_A = n_0$ and $n_B = n_0 - 1$ number of particles. Therefore a particle state over the DW ground state will consist of one particle added to any of site in sublattice B , which contains less number of particle in the ground state. All such states as well their linear combination are degenerate for $t = 0$. Since the total number of sites in B sublattice is $\frac{M}{2}$, therefore the dimension of this degenerate subspace of the one particle excitation is also $\frac{M}{2}$. For the single hole type of excitation over the DW ground state similarly the hole can be created in any site that belongs to sublattice A , containing higher number of particle in the ground state. Therefore the dimension of the degenerate subspace of single hole like excitation is also $\frac{M}{2}$. Because of this degeneracy, to find out the states and energies of

particle and hole like excitation for finite t as perturbative expansion in t , we need to use the degenerate perturbation theory.

To use degenerate perturbation theory to find out the wave function as well as the energy for particle or hole like excited state, we need to diagonalize the perturbed part of the Hamiltonian in this degenerate subspace. To do this we write H given in equation (3.1) as

$$H = H_0 + H_P \quad (3.5)$$

The unperturbed part is

$$H_0 = \frac{1}{2} \sum_i \hat{n}_i(\hat{n}_i - 1) - \mu \sum_i \hat{n}_i + V \sum_{i,j} \hat{n}_i \hat{n}_j \quad (3.6)$$

and the perturbed part, which is the kinetic energy (hopping) term.

$$\begin{aligned} H_P &= - \sum_{i,j} t e^{-\varphi_{ij}} \hat{a}_i^\dagger \hat{a}_j \\ &= - \sum_{i,j} t_{ij} \hat{a}_i^\dagger \hat{a}_j \end{aligned} \quad (3.7)$$

where $t_{ij} = t e^{-\varphi_{ij}}$. It is to note that H_P is actually the Harper Hamiltonian [128], whose energy eigen value spectrum is the Hofstadter Butterfly [92]. This has been explained in detail in section 2.2.4 in chapter 2.

When we diagonalize H_P in the degenerate subspace of either particle or hole like excitation over the DW ground state, we shall find that the degeneracy is only lifted when we include the second order (next nearest neighbor) hopping processes. This is because, each site in sublattice $A(B)$ has only the sites of sublattice $B(A)$ as its neighbor. Thus all the matrix element related by the first order hopping is 0 and we need to go upto the second order to lift the degeneracy.

Here we briefly mention the methodology.

To find out the particle and hole excited state which will break the degeneracy when the perturbation is included, we write it as a linear superposition of the degenerate basis states, namely

$$|\Psi_{DW}^{par(0)}\rangle = \frac{1}{\sqrt{n_B + 1}} \sum_{j \in B}^{M/2} f_j^{DWB} \hat{a}_j^\dagger |\Psi_{DW}^{(0)}\rangle \quad (3.8)$$

$$|\Psi_{DW}^{hol(0)}\rangle = \frac{1}{\sqrt{n_A}} \sum_{i \in A}^{M/2} f_i^{DWA} \hat{a}_i |\Psi_{DW}^{(0)}\rangle \quad (3.9)$$

The correct choice for f_j and f_i will be obtained by diagonalizing the second order perturbation due to the hopping matrix $-t_{ij}$ and identifying the corresponding minimum eigenvalue. Therefore f_j^{DWB} will be the eigenvector of $\sum_i t_{ji}t_{ij'}$ with the minimum eigenvalue ($\epsilon^2 t^2$) such that

$$\sum_{i,j'} t_{ji}t_{ij'} f_{j'}^{DWB} = \epsilon^2 t^2 f_j^{DWB} \quad (3.10)$$

and f_i^{DWA} will be the eigenvector of $\sum_j t_{ij}t_{ji'}$ with the minimum eigenvalue ($\epsilon^2 t^2$) such that

$$\sum_{j,i'} t_{ij}t_{ji'} f_{i'}^{DWA} = \epsilon^2 t^2 f_i^{DWA} \quad (3.11)$$

This is derived as shown below.

We already know that

$$\sum_{k'} t_{kk'} f_{k'} = \epsilon t f_k \quad (3.12)$$

This can be written in the matrix form as below:

$$\begin{bmatrix} t_{11} & t_{12} & t_{13} & \dots & t_{1M} \\ t_{21} & t_{22} & t_{23} & \dots & t_{2M} \\ \vdots & \vdots & \vdots & & \vdots \\ t_{M1} & t_{M2} & t_{M3} & \dots & t_{MM} \end{bmatrix} \begin{bmatrix} f_1 \\ f_2 \\ \vdots \\ f_M \end{bmatrix} = \epsilon t \begin{bmatrix} f_1 \\ f_2 \\ \vdots \\ f_M \end{bmatrix} \quad (3.13)$$

where M is the number of lattice sites.

We can separately write the equations for different k components of above relation (3.12) or (3.13) as

$$t_{11}f_1 + t_{12}f_2 + \dots + t_{1M}f_M = \epsilon t f_1 \quad (3.14)$$

$$t_{21}f_1 + t_{22}f_2 + \dots + t_{2M}f_M = \epsilon t f_2 \quad (3.15)$$

$$\vdots$$

$$t_{M1}f_1 + t_{M2}f_2 + \dots + t_{MM}f_M = \epsilon t f_M \quad (3.16)$$

Now, for the DW phase we have the following eigen value equation given by (3.10) or (3.11)

$$\sum_{i,j'} t_{ji}t_{ij'} f_{j'} = \epsilon^2 t^2 \quad (3.17)$$

To derive this equation, we start with the left hand side as

$$\sum_{ij'} t_{ji}t_{ij'} f_{j'} = \sum_{j'} \left(\sum_i t_{ji}t_{ij'} \right) f_{j'} = \sum_{j'} T_{jj'} f_{j'}$$

Here,

$$\begin{aligned} T_{jj'} &= \sum_i t_{ji} t_{ij'} \\ &= (t_{j1} t_{1j'} + t_{j2} t_{2j'} + t_{j3} t_{3j'} + \dots + t_{jM} t_{Mj'}) \end{aligned} \quad (3.18)$$

Now, we finally calculate

$$\begin{aligned} \sum_{j'} T_{jj'} f_{j'} &= \sum_{j'} [t_{j1} t_{1j'} + t_{j2} t_{2j'} + t_{j3} t_{3j'} + \dots + t_{jM} t_{Mj'}] f_{j'} \\ &= [t_{j1} (t_{11} f_1 + t_{12} f_2 + \dots + t_{1M} f_M) \\ &\quad + t_{j2} (t_{21} f_1 + t_{22} f_2 + \dots + t_{2M} f_M) \\ &\quad + t_{j3} (t_{31} f_1 + t_{32} f_2 + \dots + t_{3M} f_M) \\ &\quad + \dots + t_{jM} (t_{M1} f_1 + t_{M2} f_2 + \dots + t_{MM} f_M)] \\ &= [t_{j1} (\epsilon t) f_1 + t_{j2} (\epsilon t) f_2 + \dots + t_{jM} (\epsilon t) f_M] \end{aligned} \quad (3.19)$$

$$\begin{aligned} &= (\epsilon t) [t_{j1} f_1 + t_{j2} f_2 + \dots + t_{jM} f_M] \\ &= (\epsilon t) (\epsilon t) f_j \end{aligned} \quad (3.20)$$

$$= \epsilon^2 t^2 f_j \quad (3.21)$$

We have used equation (3.14)-(3.16) in steps (3.19) and (3.20) to get the right hand side of above equation (3.17). Thus, it is proved that

$$\sum_{ij'} t_{ji} t_{ij'} f_{j'} = \epsilon^2 t^2 \quad (3.22)$$

The normalization condition also requires that

$$\sum_{j \in B}^{M/2} |f_j^{DWB}|^2 = 1$$

$$\sum_{i \in A}^{M/2} |f_i^{DWA}|^2 = 1$$

Similarly for the MI phase, the non degenerate ground state wave function for $t = 0$ is given by:

$$|\Psi_{MI}^{(0)}\rangle = \prod_{k=1}^M \frac{(\hat{a}_k^\dagger)^{n_0}}{\sqrt{n_0!}} |0\rangle \quad (3.23)$$

where the index k refers to all the lattice sites. Here also, for $t = 0$ the single particle or hole like excited states over this non-degenerate ground state is degenerate and dimension of the degenerate subspace is M , the total number of lattice sites. Since all sites

are equivalent, this degeneracy is lifted in the first order correction of the degenerate perturbation theory, namely when the nearest neighbor hopping is included, unlike the previous case in DW phase, where to lift the degeneracy one needs to include the next nearest neighbor hopping.

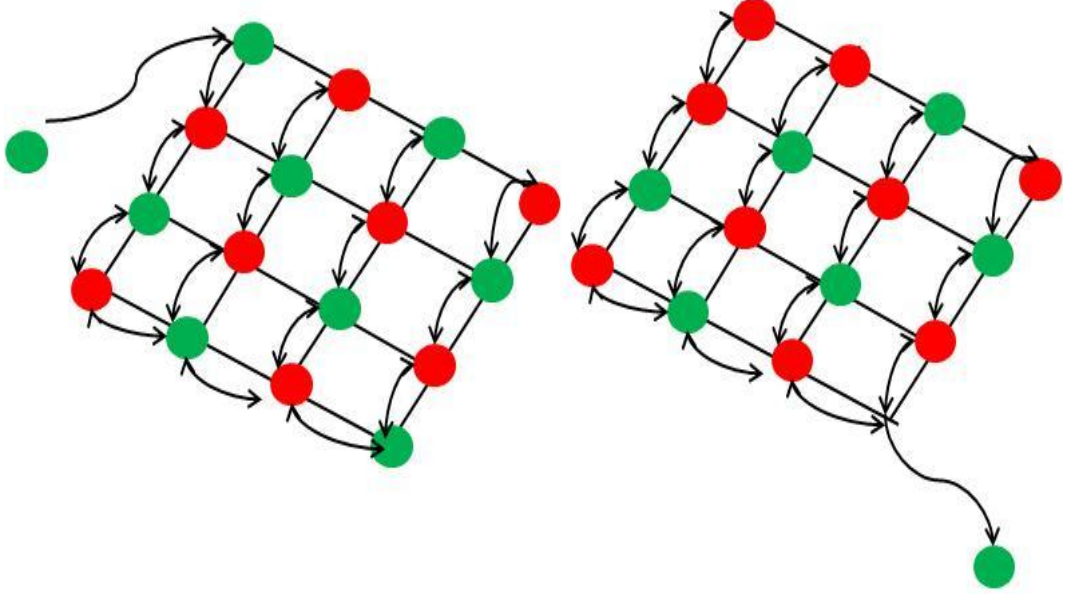


FIGURE 3.1: Single particle and hole excitations over pure DW phase. The picture shows that an extra particle or hole can go to any of the lattice site, resulting in degeneracy. Hence, to calculate particle or hole excited states and energies, degenerate perturbation theory is needed.

The single particle and hole excited state (Fig. 3.1) wave functions that will break the degeneracy for finite t is written as

$$|\Psi_{MI}^{par(0)}\rangle = \frac{1}{\sqrt{n_0 + 1}} \sum_{k=1}^M f_k^{MI} \hat{a}_k^\dagger |\Psi_{MI}^{(0)}\rangle \quad (3.24)$$

$$|\Psi_{MI}^{hol(0)}\rangle = \frac{1}{\sqrt{n_0}} \sum_{k=1}^M f_k^{MI} \hat{a}_k |\Psi_{MI}^{(0)}\rangle \quad (3.25)$$

The correct choice of f_k will be obtained by diagonalizing the first order perturbation due to hopping and locating the minimum eigenvalue state. Thus f_k^{MI} is the eigenvector of the hopping matrix $-t_{kk'}$ with the minimum eigenvalue ϵt which can be written in matrix form as in equation (3.13).

It may be noted that H_P (equation (3.7)) is same as the Harper Hamiltonian whose eigenvalue spectrum is given by the Hofstadter butterfly. This has been already explained in detail in section 2.2.4. Formally, finding the solution that corresponds to the minimal eigenvalue of the hopping matrix $-t_{ij}$ is identical to finding the band minimum in the Hofstadter problem and to locate their corresponding eigenstates in either of the gauge

potentials [92, 128]. The hopping term in H_P has a complex phase φ_{ij} which basically changes the eigen value of the hopping matrix, which is a function of magnetic field. The effect of magnetic field appears in the form of magnetic flux $2\pi\nu$ enclosed by a plaquette when a particle or hole travels around the plaquette. Also, it changes the minimal energy of extra particle or hole which moves in the insulating phase background. This minimal eigen value is independent of gauge choice, however its location in the BZ is dependent on the type of gauge potential. This feature appears in the physical observables such as momentum distribution function and is shown in detail in part 3B of this chapter.

In the following section, we shall provide the analytical expression of the perturbatively calculated energy of the ground state and the particle-hole excitation energy at finite t and evaluate the phase boundary of the DW-SS transition and the MI-SF transition from this result.

3.3 Analytic expressions for the modification of phase boundaries

Using many body version of the Rayleigh-Schroedinger perturbation theory [158], the ground state energy of the insulating phases (DW or MI) as well as the energies of the particle or hole like excitation can be expressed as a power series in the scaled hopping amplitude t

$$E(t) = t^0 E_n^{(0)} + t^1 E_n^{(1)} + t^2 E_n^{(2)} + t^3 E_n^{(3)} + \dots \quad (3.26)$$

where $E_n^{(0)}$ is the energy in the limit $t = 0$, and $tE_n^{(1)}$, $t^2 E_n^{(2)}$ and $t^3 E_n^{(3)}$ are the first order, second order and third order corrections to energy. In the following, we present the perturbative results upto the third order in t and the details of the calculations is provided below.

3.3.1 Ground state energy calculations for DW and MI phase

Here we provide the detail expressions of $E_n^{(0)}, E_n^{(1)}, E_n^{(2)}, E_n^{(3)}$ for calculating the ground state energy for DW phase with n_A and n_B particles on alternating sites. The various terms appearing at the various orders of the perturbation theory are calculated by considering all the first and second order hopping processes respectively, as shown in Fig. 3.4 and Fig. 3.5 for the simplest case of a 2×2 square lattice unit cell. To get the correct dependence of the energy and wave function expansion on the number of lattice sites M , we start the calculations with the simplest 2×2 lattice, and generalise the calculations for any number of lattice sites. For a finite square lattice of M sites, the

expressions are obtained by taking into account the fact that the hopping of the atom at the left edge of the lattice is restricted to only along the right side in addition to up and down directions. Similarly, the calculations for the atoms on the other edges of the square lattice are done by restricting hopping to only within the finite lattice, which effectively implies hard wall boundary conditions for the hopping parameter. The calculations are done for the energy expression for the ground state, and for the particle-hole excited states too. The zeroth order term is given by

$$\begin{aligned}
 E_{DW}^{(0)} &= \langle \Psi_{DW}^{(0)} | H_0 | \Psi_{DW}^{(0)} \rangle \\
 &= \prod_{i \in A, j \in B}^{M/2} \langle 0 | \frac{(\hat{a}_i)^{n_A}}{\sqrt{n_A!}} \frac{(\hat{a}_j)^{n_B}}{\sqrt{n_B!}} \left| \frac{1}{2} \sum_i \hat{n}_i(\hat{n}_i - 1) - \mu \sum_i \hat{n}_i + V \sum_{i,j} \hat{n}_i \hat{n}_j \right| \\
 &\quad \prod_{i \in A, j \in B}^{M/2} \frac{(\hat{a}_i^\dagger)^{n_A}}{\sqrt{n_A!}} \frac{(\hat{a}_j^\dagger)^{n_B}}{\sqrt{n_B!}} | 0 \rangle \\
 &= M \left(\frac{n_A(n_A - 1) + n_B(n_B - 1)}{4} - \mu \frac{n_A + n_B}{2} + zV \frac{n_A n_B}{2} \right) \quad (3.27)
 \end{aligned}$$

The first order correction is given as

$$E_{DW}^{(1)} = \langle \Psi_{DW}^{(0)} | H_P | \Psi_{DW}^{(0)} \rangle = 0 \quad (3.28)$$

This is because

$$\langle n_A - 1 | n_A \rangle_i = \langle n_B - 1 | n_B \rangle_j = 0 \quad (3.29)$$

where i and j can be any site. For the same reason, all odd order correction like $E_n^{(3)}$ also vanishes.

The second order correction, which is also the first non-vanishing correction is given by

$$\begin{aligned}
 E_{DW}^{(2)} &= \sum_{m \neq n} \frac{|\langle \Psi_{DW}(m_A, m_B) | H_P | \Psi_{DW}^{(0)}(n_A, n_B) \rangle|^2}{(E_{n_A, B} - E_{m_A, B})} \\
 &= \left[\frac{n_A(n_B + 1)}{(n_A - n_B - 1) + (zn_B - zn_A + 1)V} + \frac{n_B(n_A + 1)}{(n_B - n_A - 1) + (zn_A - zn_B + 1)V} \right] \\
 &\quad \times \frac{Mzt^2}{2} \quad (3.30)
 \end{aligned}$$

Substituting the above expressions in the right hand side of equation (3.26) one gets the ground state energy of the DW state upto the third order as

$$\begin{aligned} \frac{E_{DW}^{ins}(n_A, n_B)}{M} = & \frac{n_A(n_A - 1) + n_B(n_B - 1)}{4} + zV \frac{n_A n_B}{2} - \mu \frac{n_A + n_B}{2} \\ & + \left[\frac{n_A(n_B + 1)}{(n_A - n_B - 1) + (zn_B - zn_A + 1)V} \right. \\ & \left. + \frac{n_B(n_A + 1)}{(n_B - n_A - 1) + (zn_A - zn_B + 1)V} \right] \frac{zt^2}{2} + O(t^4) \end{aligned} \quad (3.31)$$

Setting $n_A = n_0$ and $n_B = n_0 - 1$ in the above equation we get the expression

$$\begin{aligned} \frac{E_{DW}^{ins}}{M} = & \left[\frac{1}{2}(n_0 - 1)^2 + zV \frac{n_0(n_0 - 1)}{2} - \mu \frac{2n_0 - 1}{2} \right] - z \left[\frac{n_0^2}{V(z - 1)} + \frac{n_0^2 - 1}{2 - V(z + 1)} \right] \frac{t^2}{2} \\ & + O(t^4) \end{aligned} \quad (3.32)$$

In the above expressions $z = 2d$ is the co-ordination number of given lattice site, which in the case of a square lattice is 4.

Also, we can get the corresponding corrections for the ground state in MI phase by substituting in the above expressions for the DW state $n_A = n_B = n_0$. The ground state energy of the MI phase is given below and is obtained from the expression (3.31) by putting $n_A = n_B = n_0$.

$$\frac{E_{MI}^{ins}}{M} = \frac{1}{2}n_0(n_0 - 1) - \mu n_0 + zV \frac{n_0^2}{2} - zt^2 \frac{n_0(n_0 + 1)}{(1 - V)} + O(t^4) \quad (3.33)$$

In the next subsection, we calculate the energies of the DW states with an extra particle or hole, using equations (3.8) and (3.9) in the framework of degenerate perturbation theory.

3.3.2 Calculation of energy of DW state with an extra particle or hole

The explicitly written wave function of the DW phase with an extra particle is

$$|\Psi_{DW}^{par(0)}\rangle = \sum_{j \in B, j=1}^{M/2} f_j^{DW(B)} |n_A^{(1)}, n_A^{(3)} \dots n_A^{(M/2)}; n_B^{(2)} \dots n_B^{(j-1)}, n_B^{(j)} + 1 \dots n_B^{(M)}\rangle \quad (3.34)$$

where $f_j^{DW(B)}$ is the eigenvector of $\sum_i t_{ji} t_{ij'}$ with the minimum eigenvalue $(\epsilon^2 t^2) f_j^{DW(B)}$, as shown in equation (3.22)

$$\sum_{ij'} t_{ji} t_{ij'} f_{j'}^{DW(B)} = \epsilon^2 t^2 f_j^{DW(B)}$$

The zeroth order energy of the DW phase is

$$\begin{aligned} E_{DW}^{par(0)} &= \langle \Psi_{DW}^{par(0)} | H_0 | \Psi_{DW}^{par(0)} \rangle \\ &= E_{DW}^{(0)} + n_B + zVn_A - \mu \end{aligned} \quad (3.35)$$

where $E_{DW}^{(0)}$ is given by equation (3.27). The first-order correction in energy is

$$E_{DW}^{par(1)} = \langle \Psi_{DW}^{par(0)} | H_P | \Psi_{DW}^{par(0)} \rangle = 0 \quad (3.36)$$

Here again all the odd order terms vanishes by the same reason as given by equation (3.29).

The second order correction to the energy of DW phase with an extra particle is calculated and given as

$$\begin{aligned} E_{DW}^{par(2)} &= \sum_{m \neq n} \frac{|\langle \Psi_{DW}^{par}(m_A, m_B) | H_P | \Psi_{DW}^{par(0)}(n_A, n_B) \rangle|^2}{(E_{n_A, B} - E_{m_A, B})} \\ &= E_{DW}^{(2)} + \frac{(n_A + 1)(n_B + 1)\epsilon^2 t^2}{(n_B - n_A) + (zn_A - zn_B)V} - \frac{n_A(n_B + 1)\epsilon^2 t^2}{(n_A - n_B - 1) + (zn_B - zn_A + 1)V} \\ &\quad - \frac{n_B(n_A + 1)\epsilon^2 t^2}{(n_B - n_A - 1) + (zn_A - zn_B + 1)V} + \frac{n_A(n_B + 2)zt^2}{(n_A - n_B - 2) + (zn_B - zn_A + 2)V} \\ &\quad + \frac{n_B(n_A + 1)(\epsilon^2 - z)t^2}{(n_B - n_A - 1) + (zn_A - zn_B)V} + \frac{2n_A(n_B + 1)(\epsilon^2 - z)t^2}{(n_A - n_B - 1) + (zn_B - zn_A + 2)V} \end{aligned} \quad (3.37)$$

Thus, adding equations (3.35)-(3.37) gives us the energy of DW state with an extra particle upto the third order. For DW state with $n_A = n_0$ and $n_B = n_0 - 1$ particles on alternating sites, we get the following expression for the particle excited DW state

$$\begin{aligned} E_{DW}^{par} &= E_{DW}^{ins} + (n_0 - 1) + zVn_0 - \mu + t^2 \left[-\frac{n_0(n_0 + 1)\epsilon^2}{1 - zV} + \frac{n_0^2 \epsilon^2}{(z - 1)V} + \frac{(n_0^2 - 1)\epsilon^2}{2 - (z + 1)V} \right. \\ &\quad \left. - \frac{n_0(n_0 + 1)z}{1 + (z - 2)V} - \frac{(n_0^2 - 1)(\epsilon^2 - z)}{2 - zV} - \frac{2n_0^2(\epsilon^2 - z)}{(z - 2)V} \right] + O(t^4) \end{aligned} \quad (3.38)$$

where E_{ins}^{DW} is given by equation (3.31). In the same way, the energy of the DW phase with an extra hole can be calculated and is given as

$$\begin{aligned}
 E_{DW}^{hol}(n_A, n_B) = & E_{DW}^{ins}(n_A, n_B) - (n_A - 1) - zVn_B + \mu + \frac{n_A n_B \epsilon^2 t^2}{(n_B - n_A) + (zn_A - zn_B)V} \\
 & - \frac{n_A(n_B + 1)\epsilon^2 t^2}{(n_A - n_B - 1) + (zn_B - zn_A + 1)V} \\
 & + \frac{n_B(n_A + 1)(\epsilon^2 - z)t^2}{(n_B - n_A - 1) + (zn_A - zn_B)V} \\
 & - \frac{n_B(n_A + 1)\epsilon^2 t^2}{(n_B - n_A - 1) + (zn_A - zn_B + 1)V} \\
 & + \frac{(n_A - 1)(n_B + 1)zt^2}{(n_A - n_B - 2) + (zn_B - zn_A + 2)V} \\
 & + \frac{2n_A(n_B + 1)(\epsilon^2 - z)t^2}{(n_A - n_B - 1) + (zn_B - zn_A + 2)V} + O(t^4)
 \end{aligned} \tag{3.39}$$

Thus, for the hole excited DW state with $n_A = n_0$ and $n_B = n_0 - 1$, the expression for the energy turns out to be

$$\begin{aligned}
 E_{DW}^{hol} = & E_{DW}^{ins} - (1 + zV)(n_0 - 1) + \mu + t^2 \left[-\frac{n_0(n_0 - 1)\epsilon^2}{1 - zV} + \frac{n_0^2 \epsilon^2}{(z - 1)V} + \frac{(n_0^2 - 1)\epsilon^2}{2 - (z + 1)V} \right. \\
 & \left. - \frac{n_0(n_0 - 1)z}{1 + (z - 2)V} - \frac{(n_0^2 - 1)(\epsilon^2 - z)}{2 - zV} - \frac{2n_0^2(\epsilon^2 - z)}{(z - 2)V} \right] + O(t^4)
 \end{aligned} \tag{3.40}$$

3.3.3 Calculation of energy of MI state with an extra particle or hole

The expression for energy of the MI single particle or hole excitation calculated over ground state as perturbative expansion in the scaled hopping parameter t upto third order is calculated in a similar manner. Unlike the case of DW phase (section 3.3.2), for the MI phase, the perturbative correction to the energy for finite t appears in the first order term itself and the second and third order corrections calculated below in equation (3.45) and (3.46) are comparatively much smaller in magnitude. However we still kept the calculation upto the same order so that the entire phase diagram which comprises of DW as well as MI phase is given within the same order of the perturbation theory.

The MI phase with an extra particle has the following wave function,

$$|\Psi_{MI}^{par(0)}\rangle = \sum_{j=1}^M f_j^{MI} |n_0^{(1)}, n_0^{(2)} \dots n_0^{(j)} + 1, \dots n_0^{(M)}\rangle$$

where the coefficient f_j are to be determined from the lowest eigenvalue

$$- \sum_{j'} t_{jj'} f_{j'}^{MI} = \epsilon t f_j^{MI}$$

The zeroth order correction to the energy of MI phase with an extra particle is now given as

$$\begin{aligned} E_{MI}^{par(0)} &= \langle \Psi_{MI}^{par(0)} | H_0 | \Psi_{MI}^{par(0)} \rangle \\ &= E_{MI}^{(0)} + n_0 + zVn_0 - \mu \end{aligned} \quad (3.41)$$

The first order correction to the energy of this state is

$$E_{MI}^{par(1)} = \langle \Psi_{MI}^{par(0)} | H_P | \Psi_{MI}^{par(0)} \rangle = (n_0 + 1)\epsilon t \quad (3.42)$$

The second order energy correction for the extra particle MI phase is as calculated below

$$\begin{aligned} E_{MI}^{par(2)} &= \sum_{m \neq n} \frac{|\langle \Psi_{MI}^{par}(m_0) | H_P | \Psi_{MI}^{par(0)}(n_0) \rangle|^2}{(E_n^0 - E_m^0)} \\ &= E_{MI}^{(2)} + n_0(n_0 + 1) \left[(z - \epsilon^2) + \frac{2(z - \epsilon^2)}{(1 - 2V)} + \frac{2\epsilon^2}{(1 - V)} \right] t^2 - \frac{n_0(n_0 + 2)zt^2}{2(1 - V)} \end{aligned} \quad (3.43)$$

Next is the third order correction, which is finite for the case of MI phase unlike the DW phase,

$$\begin{aligned} E_{MI}^{par(3)} &= \sum_{k \neq n} \sum_{m \neq n} \frac{\langle \Psi_{MI}^{par(0)}(n_0) | H_P | \Psi_{MI}^{par}(m_0) \rangle \langle \Psi_{MI}^{par}(m_0) | H_P | \Psi_{MI}^{par}(k_0) \rangle \langle \Psi_{MI}^{par}(k_0) | H_P | \Psi_{MI}^{par}(n_0) \rangle}{(E_m^0 - E_n^0)(E_k^0 - E_n^0)} \\ &\quad - \langle \Psi_{MI}^{par(0)}(n_0) | H_P | \Psi_{MI}^{par(0)}(n_0) \rangle \sum_{m \neq n} \frac{|\langle \Psi_{MI}^{par(0)}(n_0) | H_P | \Psi_{MI}^{par}(m_0) \rangle|^2}{(E_m^0 - E_n^0)^2} \\ &= n_0(n_0 + 1)n_0 \left[(z - 2)\epsilon + \frac{(\epsilon^2 - 3z + 3)\epsilon}{(1 - V)^2} \right] t^3 \\ &\quad + n_0(n_0 + 1)(n_0 + 1) \left[(z - \epsilon^2)\epsilon - \frac{(2\epsilon^2 - 6z + 6)\epsilon}{(1 - V)^2} + \frac{2\epsilon(z - \epsilon^2)}{(1 - 2V)^2} \right. \\ &\quad \left. + \frac{2\epsilon(\epsilon^2 - 3z + 3)}{(1 - V)} + \frac{4(z - 2)\epsilon}{(1 - 2V)} \right] t^3 + n_0(n_0 + 1)(n_0 + 1) \frac{4\epsilon(\epsilon^2 - 3z + 3)}{(1 - V)(1 - 2V)} t^3 \\ &\quad - n_0(n_0 + 1)(n_0 + 2) \left[\frac{\epsilon(z - 1)}{(1 - V)} - \frac{z\epsilon}{4(1 - V)^2} \right] t^3 \end{aligned} \quad (3.44)$$

Adding equations (3.41)-(3.44) gives the energy expression for MI phase with an extra particle given as

$$\begin{aligned}
 E_{MI}^{par} = & E_{MI}^{ins} + n_0 + zVn_0 - \mu \\
 & + t(n_0 + 1)\epsilon + n_0 t^2 \left\{ (n_0 + 1) \left[(z - \epsilon^2) + \frac{2(z - \epsilon^2)}{1 - 2V} + \frac{2\epsilon^2}{1 - V} \right] \right. \\
 & \left. - (n_0 + 2) \frac{z}{2(1 - V)} \right\} + n_0(n_0 + 1)t^3 \left[(z - 2)\epsilon + \frac{(\epsilon^2 - 3z + 3)\epsilon}{(1 - V)^2} \right] \\
 & + (n_0 + 1) \left[(z - \epsilon^2)\epsilon - \frac{(2\epsilon^2 - 6z + 6)\epsilon}{(1 - V)^2} + \frac{2(z - \epsilon^2)\epsilon}{(1 - 2V)^2} + \frac{2\epsilon(\epsilon^2 - 3z + 3)}{1 - V} \right. \\
 & \left. + \frac{4(z - 2)\epsilon}{1 - 2V} + \frac{4\epsilon(\epsilon^2 - 3z + 3)}{(1 - V)(1 - 2V)} \right] + (n_0 + 2) \left[\frac{\epsilon(z - 1)}{1 - V} - \frac{z\epsilon}{4(1 - V)^2} \right] + O(t^4)
 \end{aligned} \tag{3.45}$$

where E_{MI}^{ins} is given by equation (3.33). This expression recovers the known result of onsite Bose Hubbard model [156] when $V = 0$ and $\epsilon = z$. The energy expression for MI phase with extra hole is calculated in a similar manner and is given as

$$\begin{aligned}
 E_{MI}^{hol} = & E_{MI}^{ins} - (n_0 - 1) - zVn_0 + \mu \\
 & + tn_0\epsilon + (n_0 + 1)t^2 \left\{ n_0 \left[(z - \epsilon^2) + \frac{2(z - \epsilon^2)}{1 - 2V} + \frac{2\epsilon^2}{1 - V} \right] \right. \\
 & \left. - (n_0 + 1)(n_0 - 1) \frac{z}{2(1 - V)} \right\} + n_0(n_0 + 1)t^3 \left[(n_0 + 1) \left[(z - 2)\epsilon \right. \right. \\
 & \left. + \frac{(\epsilon^2 - 3z + 3)\epsilon}{(1 - V)^2} \right] + n_0 \left[(z - \epsilon^2)\epsilon - \frac{(2\epsilon^2 - 6z + 6)\epsilon}{(1 - V)^2} + \frac{2(z - \epsilon^2)\epsilon}{(1 - 2V)^2} \right. \\
 & \left. + \frac{2\epsilon(\epsilon^2 - 3z + 3)}{1 - V} + \frac{4(z - 2)\epsilon}{1 - 2V} + \frac{4\epsilon(\epsilon^2 - 3z + 3)}{(1 - V)(1 - 2V)} \right] \\
 & + (n_0 - 1) \left[\frac{\epsilon(z - 1)}{1 - V} - \frac{z\epsilon}{4(1 - V)^2} \right] + O(t^4)
 \end{aligned} \tag{3.46}$$

In the following section, using the above expressions of energy of the ground state and their corresponding particle hole excitation, we shall determine the MI-SF and DW-SS phase boundary using the relations (3.2) and (3.3).

3.3.4 Determination of the DW-SS and MI-SF boundary from the strong coupling expansion

The minimum eigen value ϵ used in calculation of energy expressions, involves the diagonalization of the hopping matrix, where the hopping matrix is gauge dependent. The location of the minimum eigen value ϵ depends on the choice of the gauge potential, while the eigen value itself is not. We consider a rational flux $\nu = p/q$ through the

square lattice and calculate the minimum eigen values of the hopping matrix $-t_{ij}$ following [136]. The shape of the insulating lobes for the Mott phase is different from the DW phase, as observed in Fig. 3.2 in two dimensions. This is because, the Mott states with an extra particle or hole, have corrections to first order in t , while the DW states have corrections to second order in t . So, as $t \rightarrow 0$, the slope of the Mott state will be finite, while it will vanish for the DW lobes. Hence, the shapes of the two insulating lobes are always different.

Moreover, the shapes of the insulating lobes depend on the dimensionality of the system and also depends on the applied *artificial* magnetic field [149]. The mean field theories always give a concave shape to the MI and DW lobes [105] as the dimensionality only enters as a prefactor in the expression for μ as a function of t as can be seen from equation (2.85), while the strong coupling expansion easily distinguishes the shape of insulating lobes in different dimensions and also, in presence of artificial magnetic field. The determination of these transition boundary as a function of the gauge field, using strong coupling perturbation theory is one of the main results of this work.

The strong coupling expansion performed here has limited accuracy because the expansion is truncated upto third order. For this reason, an extrapolation of this third order expansion to infinite order in t is required to determine more accurate phase diagrams and the critical transition points. Since the transition at the boundary in this model belongs to the universality class of $(2+1)$ dimensional XY model [36], the critical exponents can also be found out through an expansion of the chemical potential and hence, an extrapolation of phase boundary can be done. This was done in [156, 157] and we also describe it in the next subsection.

3.4 Extrapolation of the phase boundaries via Scaling theory

The accuracy of the phase boundary obtained from the strong coupling expansion is limited by the fact that the expansion is cut-off at a finite order in the scaled hopping amplitude t . An extrapolation technique is used to extend these results beyond finite order in t to yield a more accurate phase boundary.

Several earlier works [149, 156, 157, 159] implemented extrapolation techniques using different methods for Bose Hubbard models with and without a gauge field. In the vicinity of the phase transition, using scaling arguments it is known that around the critical point, most physical quantities (which we denote here by X) scale according to

the general rule [36] given by

$$XL^{\xi/\nu} = F(|\mu - \mu_c|)L^{1/\nu} \quad (3.47)$$

where F is a universal scaling function, $\mu - \mu_c$ is the shifted control parameter (μ being the control parameter and μ_c its critical value), ν is the correlation length critical exponent, and ξ is the critical exponent belonging to the observable X . The values of these exponents are determined by the universality class the transition belongs to. The concept of universality classes of critical behavior was first clearly put forth by Kadanoff [160].

For bosons placed in optical lattice, it is known that at the tip of the DW and MI lobe the scaling behavior lies in the universality class of a $(d + 1)$ dimensional classical XY model. Such an extrapolation technique is based on the observation that critical hopping parameter at which the MI-SF and DW-SS transition takes place, has the scaling behavior of the $(d + 1)$ dimensional XY model [36, 156, 157] and hence, the lobes have Kosterlitz Thouless shape for $d = 1$ and power law shape for $d > 1$. Fitting of the chemical potential or the particle/hole excitation energy to its scaling form given by the corresponding XY model, thus obtained a critical hopping parameter whose accuracy is not limited by the finite orderness of the perturbation expansion.

Thus for the case of the eBHM in the presence of an artificial gauge field we employ the chemical potential extrapolation technique following [156, 157] to go beyond the finite order strong-coupling scheme. This way of doing the scaling based extrapolation using the known critical behavior of the $(d + 1)$ dimensional XY model is valid for BHM or eBHM in the absence of gauge field. Here we are assuming that, for not too strong gauge field, a similar extrapolation can be done.

In the subsequent discussion, we employ this extrapolation technique to yield the improved phase boundary and compare this with the one obtained from bare strong coupling expansion as well as the one obtained from the mean field treatment [105]. However unlike the references [156, 157] we shall limit our discussion only for $d = 2$ and will not generalize it for higher dimension. The reason of this restriction will be explained in the later part of this section.

The extrapolation technique is done in the following manner. The chemical potential that determines the boundary of the insulating lobes (MI/DW) are fitted to the form

$$\begin{aligned} \mu_{ins}^p &= A_{ins}(x) + B_{ins}(x)(x_{ins}^c - x)^{z\nu} \\ \mu_{ins}^h &= A_{ins}(x) - B_{ins}(x)(x_{ins}^c - x)^{z\nu} \end{aligned} \quad (3.48)$$

where the critical exponent $z\nu \approx 2/3$ is known from the critical behavior of $(2 + 1)$ dimensional XY model [36, 156]. Here x_{ins}^c is the critical point which determines the location of tip of the insulating (MI and DW) lobes. The coefficient A and B are regular function of $x = td$ and thus can be expanded as

$$\begin{aligned} A_{ins}(x) &= a_{ins} + b_{ins}x + c_{ins}x^2 + d_{ins}x^3 + \dots \\ B_{ins}(x) &= \alpha_{ins} + \beta_{ins}x + \gamma_{ins}x^2 + \delta_{ins}x^3 + \dots \end{aligned}$$

The coefficients $a_{ins}, b_{ins}, c_{ins}, d_{ins}$ and $\alpha_{ins}, \beta_{ins}, \gamma_{ins}, \delta_{ins}$ can be extracted by matching the above form with the strong coupling results. These results are given upto the second order for DW lobe and upto the third order for MI lobe in equations (3.38)-(3.40), (3.45)-(3.46), such that

$$\begin{aligned} A_{ins}(x) &= \frac{\mu_{ins}^p + \mu_{ins}^h}{2} \\ B_{ins}(x)(x_{ins}^c - x)^{\frac{2}{3}} &= \frac{\mu_{ins}^p - \mu_{ins}^h}{2} \end{aligned}$$

From this relation the extrapolated values for chemical potential as a function of td can be found which determined DW and MI lobe respectively and thus the phase-boundaries can be redrawn using these scaling results.

Fig. 3.2 represents the phase diagram of the first four insulating lobes for the eBHM in two dimension (square lattice) in presence of artificial magnetic field, obtained under scaling hypothesis using chemical potential extrapolation technique. It shows the increasing stability of the insulating phase i.e the DW and MI phases grows in size as the strength of magnetic field is increased from zero to finite values. This is due to the localizing effect of magnetic field on the moving bosons, thus favoring the insulating phases to occupy a larger area in the phase diagram. As discussed in [108], the correct shape of the DW and MI lobes should be dimension dependent. Since our strong coupling calculations are restricted to finite order and for $d = 2$, it is pertinent to ask does the dimension dependence already appears at the order where we have terminated the perturbation expansion. To extract the dimension dependence of the strong coupling results we rewrite the expression of chemical potential for DW-SS phase boundary

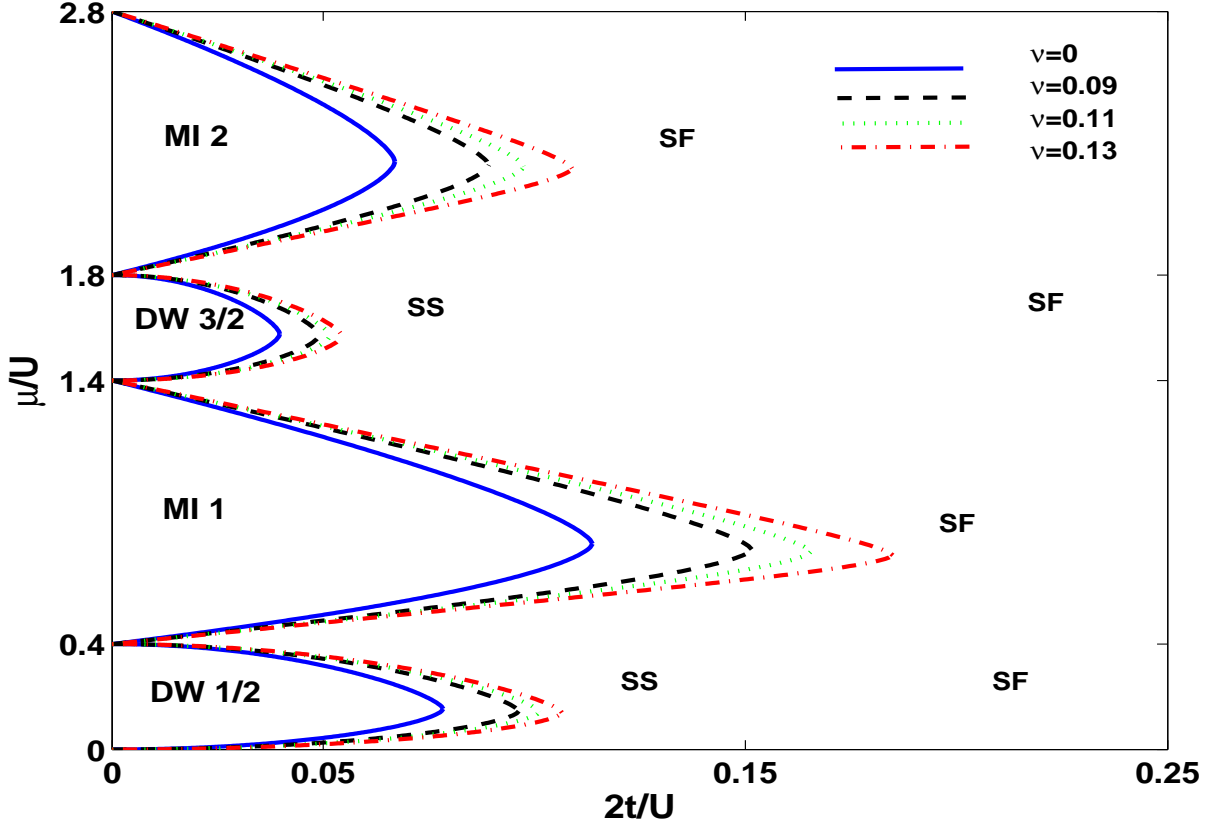


FIGURE 3.2: Phase diagram for the eBHM in presence of artificial magnetic field for $Vd=0.2$ obtained after scaling analysis. As seen, the effect of increasing magnetic field is to increase the stability of the DW and MI lobes. Please note that the position of the SS and SF phases shown is only approximate and is not calculated within the theory.

(equation (3.38)) upto the second order, in the following form.

$$\begin{aligned}
 \mu_{DW}^{par}(B) &= (n_0 - 1) + 2Vdn_0 - \frac{4n_0(n_0 + 1)(td)^2g^2}{1 - 2Vd} + \frac{4n_0^2(td)^2g^2}{Vd(2 - \frac{1}{d})} + \frac{4(n_0^2 - 1)(td)^2g^2}{2 - Vd(2 + \frac{1}{d})} \\
 &\quad - \frac{2(n_0^2 - 1)(td)^2g^2}{1 - Vd} - \frac{4n_0^2(td)^2g^2}{Vd(1 - \frac{1}{d})} - \frac{2n_0(n_0 + 1)}{1 + 2Vd(1 - \frac{1}{d})} + \frac{(n_0^2 - 1)}{1 - Vd} + \frac{2n_0^2}{Vd - 1} \\
 &= (n_0 - 1) + 2V'n_0 + x^2 \left[-\frac{4n_0(n_0 + 1)g^2}{1 - 2V'} + \frac{4n_0^2g^2}{2V' - V} + \frac{4(n_0^2 - 1)g^2}{2 - (2V' + V)} \right. \\
 &\quad \left. - \frac{2(n_0^2 - 1)g^2}{1 - V'} - \frac{4n_0^2g^2}{V' - 1} \right] + x^2 \left[-\frac{2n_0(n_0 + 1)}{1 + 2(V' - V)} + \frac{(n_0^2 - 1)}{1 - V'} + \frac{2n_0^2}{V' - 1} \right] d^{-1}
 \end{aligned}
 \tag{3.49}$$

Here, $x = td$ is a dimensionless constant in any dimension since the scaling behavior of t goes as $\frac{1}{d}$ [161] and for the same reason $V' = Vd$ is also a dimensionless constant. g is a constant which is dependent on the amount of artificial magnetic flux and it is equal to 1 in absence of such gauge field. The above expression is upto second order in t and

one can see that the $\frac{1}{d}$ type dimension dependence already appears in the this term and shows the presence of correction due to finite dimension.

The next significant order is fourth order correction which is proportional to t^4 . For the values of scaled hopping amplitude t that we use, these terms are insignificantly small and their analytical expressions are very large. Thus we do not explicitly mention them. The corresponding result for eBHM in the absence of such artificial gauge field was reported in [157], and is given by equation (3.50). As can be seen, the substitution $g = 1$ in expression (3.49) produce expression (3.50).

$$\begin{aligned} \mu_{DW}^{par} = & (n_0 - 1) + 2V'n_0 + x^2 \left[-\frac{4n_0(n_0 + 1)}{1 - 2V'} + \frac{4n_0^2}{2V' - V} + \frac{4(n_0^2 - 1)}{2 - (2V' + V)} - \frac{2(n_0^2 - 1)}{1 - V'} \right. \\ & \left. - \frac{4n_0^2}{V' - 1} \right] + x^2 \left[-\frac{2n_0(n_0 + 1)}{1 + 2(V' - V)} + \frac{(n_0^2 - 1)}{1 - V'} + \frac{2n_0^2}{V' - 1} \right] d^{-1} \end{aligned} \quad (3.50)$$

A similar analysis can also be performed for the Mott lobes to show their dimension dependence.

The above expansion suggests that one can write the expressions for μ_{DW}^{par} and μ_{DW}^{hol} as a function of dimensionless constant td and Vd which yields a dimension dependence of the form $\frac{1}{d^n}$. In the absence of gauge field, such a calculation can be generalized for an infinite dimensional BHM by setting these dimension dependent term in the limit $d \rightarrow \infty$, to 0 [161]. These results can then be compared to the mean field result in the same limit which is exact [36, 162].

We could not perform this trick here. Our calculations are specific for a two-dimensional system and the effect of gauge field enters as the minimum eigen value ϵ of the hopping matrix which gives a Hofstadter Butterfly (HB) spectrum. Thus a generalization of these results to higher dimension in the presence of gauge field requires the solution of HB problem for the corresponding dimension. This is a highly non-trivial problem. For the same reason a straightforward generalization of the mean field treatment of the 2d eBHM done in [105, 163] to the infinite dimensional case is also quite non-trivial. Because of these all the comparisons we have done is restricted to two dimensional problem. For our case of $d = 2$, we have compared the strong coupling perturbative expansion results, scaling results and mean field results. It is expected that the scaling analysis is most appropriate due to the universality of $(d + 1)$ dimensional XY model. For the first DW lobe $|1, 0, 1, 0, \dots\rangle$, with a flux $\nu = 0.09$, the mean field value of the critical hopping parameter $t_c = 0.08946$ [105] for two dimensions, the strong coupling perturbative results gives the value of $t_c = 0.114$ whereas the scaling analysis gives the value as $t_c = 0.09631$.

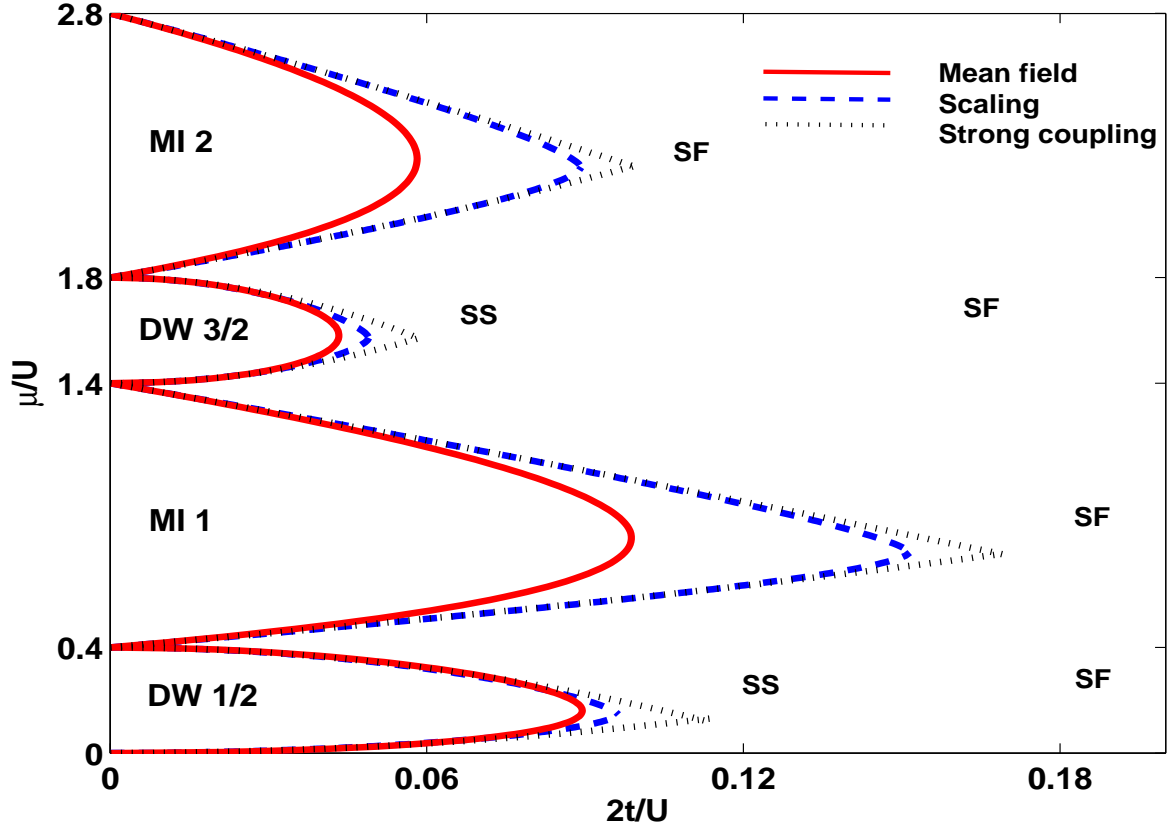


FIGURE 3.3: Comparison of the strong coupling (dotted line), scaling (dash dot line) and the mean field results (solid line) for flux $\nu = 0.09$ and $Vd = 0.2$. Please note that the position of the SS and SF phases shown is only approximate and is not calculated within the theory.

Fig. 3.3 shows the comparison between phase boundaries obtained from the strong coupling expansion results, the scaling results and the mean field results in two dimensions with flux $\nu = 0.09$. It is to note that the strong-coupling expansion overestimates the phase boundaries leading to unphysical pointed tips for all the Mott and DW lobes. This is because of the finite orderness of the perturbation expansion which cannot take into account the physics at the critical point correctly. The mean field results in $d = 2$ are compared with the scaling results which is comparatively more accurate. As already mentioned, the accuracy of mean field is higher in higher dimensions and it becomes exact in the limit $d \rightarrow \infty$ [162]. Therefore, we conclude that, the scaling results obtained after extrapolation of strong coupling expansion are comparatively more accurate and reliable.

Chapter 3B

3.5 A brief overview of experimental methods and relation to momentum distribution

As mentioned earlier, the standard experimental way of probing the properties of an ultra cold atomic condensate is through the Time of flight (TOF) absorption imaging of the freely expanding atoms released from the trap [164]. Same method is used for probing the condensate loaded in optical lattice as well. In a time-of-flight measurement, the trapping potential confining the atoms within the lattice is suddenly switched off, causing a rapid expansion. After a fixed period of time, the density profile of the cloud is determined in an indirect manner, by illuminating the atoms and measuring the transmitted intensity also known as absorption spectroscopy [33]. Since the interactions between the atoms during the expansion are sufficiently weak, the expansion is ballistic. So, the particle positions in the absorption image are strongly correlated with their velocity distribution which is given by their momentum distribution at the moment of release from the trap. Thus, the quantity that is measured experimentally in such TOF expansion is the momentum distribution of these ultra cold atomic ensembles.

In the absence of *artificial* magnetic field, the density profile after a fixed time-of-flight measures the original momentum distribution in the trap [33]. The same is true with a field, apart from the fact that TOF images depend on certain details of the experiment and, in particular, the means used to produce the effective *artificial* magnetic field. In the case of a rotating system, the momentum in the stationary (laboratory) frame is equal, up to a possible global rotation, to the symmetric gauge momentum in the rotating frame. Thus, as explained in detail in chapter 2 the Hamiltonian is time independent in the rotating frame of reference and the principles of equilibrium statistical physics are applicable in this frame only [115].

With *artificial* gauge field produced using Raman lasers as in the experiments by Lin et. al [85, 86], the Raman beams are suddenly switched off simultaneously with the trap. The expansion of an atomic cloud is determined by the momentum immediately after the gauge field is switched off, which is equal to the Landau gauge momentum before switch-off.

The strong coupling perturbation technique allows to calculate this very important physically observable with high accuracy, and can give us an insight of the effect of *artificial* magnetic field on ultracold atomic system with long range interactions. We perform our calculations at the phase boundary of the DW and MI lobes. The results obtained using this technique in the presence of a either of the gauge potential provides information about the characterising behavior of a SS (at the DW-SS phase boundary) as compared to a SF (at the MI-SF phase boundary) in presence of gauge field.

This part of the chapter is organized as follows. Section 3.6 includes the calculation of momentum distribution in presence of artificial gauge field obtained by using wave function for insulating phases calculated by strong coupling perturbation theory expansion. We shall particularly show that in the presence of an *artificial* magnetic field, the TOF image actually depends on the means to produce such effective magnetic field, and is thus gauge dependent. Subsequently in section 3.8 we calculate the quasi angular momentum distribution of the states in a symmetric gauge potential.

3.6 Calculation of Momentum distribution

The momentum distribution $n(\mathbf{k})$ measured in TOF experiments is mathematically calculated by taking the fourier transform of the one body density matrix [133] given by

$$\rho(\mathbf{r}, \mathbf{r}') = \langle \hat{\psi}^\dagger(\mathbf{r}) \hat{\psi}(\mathbf{r}') \rangle \quad (3.51)$$

The diagonal components ($\mathbf{r} = \mathbf{r}'$) of the one-body density matrix gives the diagonal density of the system, whereas for $\mathbf{r} \neq \mathbf{r}'$, it gives the correlation between atoms at different sites. Therefore,

$$n(\mathbf{k}) = \int d\mathbf{r} \int d\mathbf{r}' \rho(\mathbf{r}, \mathbf{r}') e^{i\mathbf{k} \cdot (\mathbf{r} - \mathbf{r}')} \quad (3.52)$$

where $\hat{\psi}^\dagger(\mathbf{r})$ and $\hat{\psi}(\mathbf{r})$ are the bosonic field operators at the position \mathbf{r} , respectively, and \mathbf{k} is the momentum.

The expectation value in equation (3.51) is taken in the many-body ground state and the corresponding wave function for the insulating DW and MI phases is determined using strong coupling perturbation theory as a power series in scaled hopping amplitude t (in units of U). To evaluate (3.52), we expand the field operators in the basis set of Wannier functions, such that

$$\hat{\psi}(\mathbf{r}) = \frac{1}{\sqrt{M}} \sum_l W(\mathbf{r} - \mathbf{R}_l) \hat{a}_l$$

where M is the total number of lattice sites, $W(\mathbf{r} - \mathbf{R}_l)$ is the Wannier function localized at site l with position R_l and \hat{a}_l is the boson annihilation operator. Consequently, the momentum distribution becomes

$$n(\mathbf{k}) = \frac{1}{M} \sum_{\mathbf{R}_l, \mathbf{R}_{l'}} W^*(\mathbf{k}_l) W(\mathbf{k}_{l'}) \langle \hat{a}_l^\dagger \hat{a}_{l'} \rangle e^{i\mathbf{k} \cdot (\mathbf{R}_l - \mathbf{R}_{l'})} \quad (3.53)$$

where $W(\mathbf{k}) = \int d\mathbf{r} W(\mathbf{r}) e^{i\mathbf{k}\cdot\mathbf{r}}$ is the fourier transform of the usual Wannier function $W(\mathbf{r})$. The summation indices $l \in \{A, B\}$ and $l' \in \{A, B\}$ includes the entire lattice. We can see that the momentum distribution is actually proportional to the fourier transform of the atom-atom correlation function, with proportionality factors as the Wannier functions of the trapped atoms.

3.6.1 Wave function expansion for the DW insulating phase

The wave functions for the insulating phases are calculated perturbatively using degenerate perturbation theory, upto second order in t which is the first significant order. The higher order correction can be neglected since $t \ll 1$. Upto second order, the wave function for the insulating state (MI/DW) can then be written as

$$|\psi_{ins}\rangle = |\Psi_{ins}^{(0)}\rangle + |\Psi_{ins}^{(1)}\rangle + |\Psi_{ins}^{(2)}\rangle + O(t^3) \quad (3.54)$$

Here, $|\Psi_{ins}^{(0)}\rangle = |\Psi_{MI/DW}^{(0)}\rangle$ defined in (3.4) and (3.23) and

$$|\Psi_{ins}^{(1)}\rangle = \sum_{m \neq |\Psi_{ins}^{(0)}\rangle} \frac{\langle m | H_P | \Psi_{ins}^{(0)} \rangle}{E_{0m}} |m\rangle \quad (3.55)$$

$$|\Psi_{ins}^{(2)}\rangle = \sum_{m, m' \neq |\Psi_{ins}^{(0)}\rangle} \frac{\langle m' | H_P | m \rangle \langle m | H_P | \Psi_{ins}^{(0)} \rangle}{E_{0m'} E_{0m}} |m'\rangle \quad (3.56)$$

In the expression for the first order correction (3.55), the matrix element of H_P (hopping matrix) is taken between the first-order intermediate (excited) state $|m\rangle$ and the zeroth-order state defined in (3.4) and (3.23), where as $|m'\rangle$ in the expression of the second order correction (3.56) is the second order intermediate (excited) state. Also, $E_{0m} = E_0 - E_m$ is the energy difference between the first order intermediate state $|m\rangle$ and zeroth order state $|\Psi_{ins}^{(0)}\rangle$ and $E_{0m'} = E_0 - E_{m'}$ is the energy difference between the second order intermediate state $|m'\rangle$ and zeroth order state $|\Psi_{ins}^{(0)}\rangle$.

Thus, when the wave functions are expanded upto second order in t (equation (3.54)), the momentum distribution in equation (3.53) can be written as

$$\begin{aligned} n(\mathbf{k}) &= \frac{|W(\mathbf{k})|^2}{M} \sum_{l, l'} \langle \Psi_{DW} | \hat{a}_l^\dagger \hat{a}_{l'} | \Psi_{DW} \rangle e^{-i\mathbf{k}\cdot(\mathbf{R}_l - \mathbf{R}_{l'})} \\ &= n(\mathbf{k})^{(0)} + n(\mathbf{k})^{(1)} + n(\mathbf{k})^{(2)} \end{aligned}$$

where

$$n(\mathbf{k})^{(0)} = \frac{|W(\mathbf{k})|^2}{M} \sum_{l,l'} \{ \langle \Psi_{DW}^{(0)} | \hat{a}_l^\dagger \hat{a}_{l'} | \Psi_{DW}^{(0)} \rangle \} e^{-i\mathbf{k} \cdot (\mathbf{R}_l - \mathbf{R}_{l'})} \quad (3.57)$$

$$n(\mathbf{k})^{(1)} = \frac{|W(\mathbf{k})|^2}{M} \sum_{l,l'} (\langle \Psi_{DW}^{(0)} | \hat{a}_l^\dagger \hat{a}_{l'} | \Psi_{DW}^{(1)} \rangle + \langle \Psi_{DW}^{(1)} | \hat{a}_l^\dagger \hat{a}_{l'} | \Psi_{DW}^{(0)} \rangle) e^{-i\mathbf{k} \cdot (\mathbf{R}_l - \mathbf{R}_{l'})} \quad (3.58)$$

$$n(\mathbf{k})^{(2)} = \frac{|W(\mathbf{k})|^2}{M} \sum_{l,l'} (\langle \Psi_{DW}^{(0)} | \hat{a}_l^\dagger \hat{a}_{l'} | \Psi_{DW}^{(2)} \rangle + \langle \Psi_{DW}^{(1)} | \hat{a}_l^\dagger \hat{a}_{l'} | \Psi_{DW}^{(1)} \rangle + \langle \Psi_{DW}^{(2)} | \hat{a}_l^\dagger \hat{a}_{l'} | \Psi_{DW}^{(0)} \rangle) e^{-i\mathbf{k} \cdot (\mathbf{R}_l - \mathbf{R}_{l'})} \quad (3.59)$$

Here we keep terms only upto second order and terms $\langle \Psi_{DW}^{(1)} | \hat{a}_l^\dagger \hat{a}_{l'} | \Psi_{DW}^{(2)} \rangle$, $\langle \Psi_{DW}^{(2)} | \hat{a}_l^\dagger \hat{a}_{l'} | \Psi_{DW}^{(1)} \rangle$, $\langle \Psi_{DW}^{(2)} | \hat{a}_l^\dagger \hat{a}_{l'} | \Psi_{DW}^{(2)} \rangle$ and higher order terms are neglected.

To elucidate the meaning of the above terms appearing at the various orders of the perturbation theory, we depict the first and second order hopping processes respectively in Fig. 3.4 and Fig. 3.5 for the simplest case of a 2×2 square lattice unit cell. In the diagram given in Fig. 3.4(a), we depict the ground state wave function for the DW state for $t = 0$ for this unit cell as

$$|\Psi_{DW}^{(0)}\rangle = |n_A^{(1)}, n_B^{(2)}, n_A^{(3)}, n_B^{(4)}\rangle \quad (3.60)$$

Here the superscript (i) correspond to the location of a given lattice site. All the subsequent diagrams in the same figure (Fig. 3.4(b)-(i)) depict all the possible $|m\rangle$ state defined in (3.55) which is connected to the DW ground state in Fig. 3.4(a) by a single hopping.

For example, the state depicted in Fig. 3.4 correspond to

$$|m\rangle = |n_A^{(1)} + 1, n_B^{(2)} - 1, n_A^{(3)}, n_B^{(4)}\rangle \quad (3.61)$$

The matrix element of H_P between this state and the ground state can be calculated as

$$\frac{\langle m | H_P | \Psi_{ins}^{(0)} \rangle}{E_{0m}} = \frac{-\sqrt{n_B(n_A + 1)} t_{12}}{-2 + (z + 1)V}$$

and contribute to the first order corrections in the expression (3.55). Similarly all the first order possibilities are taken into account and added for size of square lattice. Thus, using the diagrams given in Fig. 3.4, the 1st order correction to the ground state wave function of DW state for a unit cell in a 2×2 square lattice (for all possible $|m'\rangle$) can

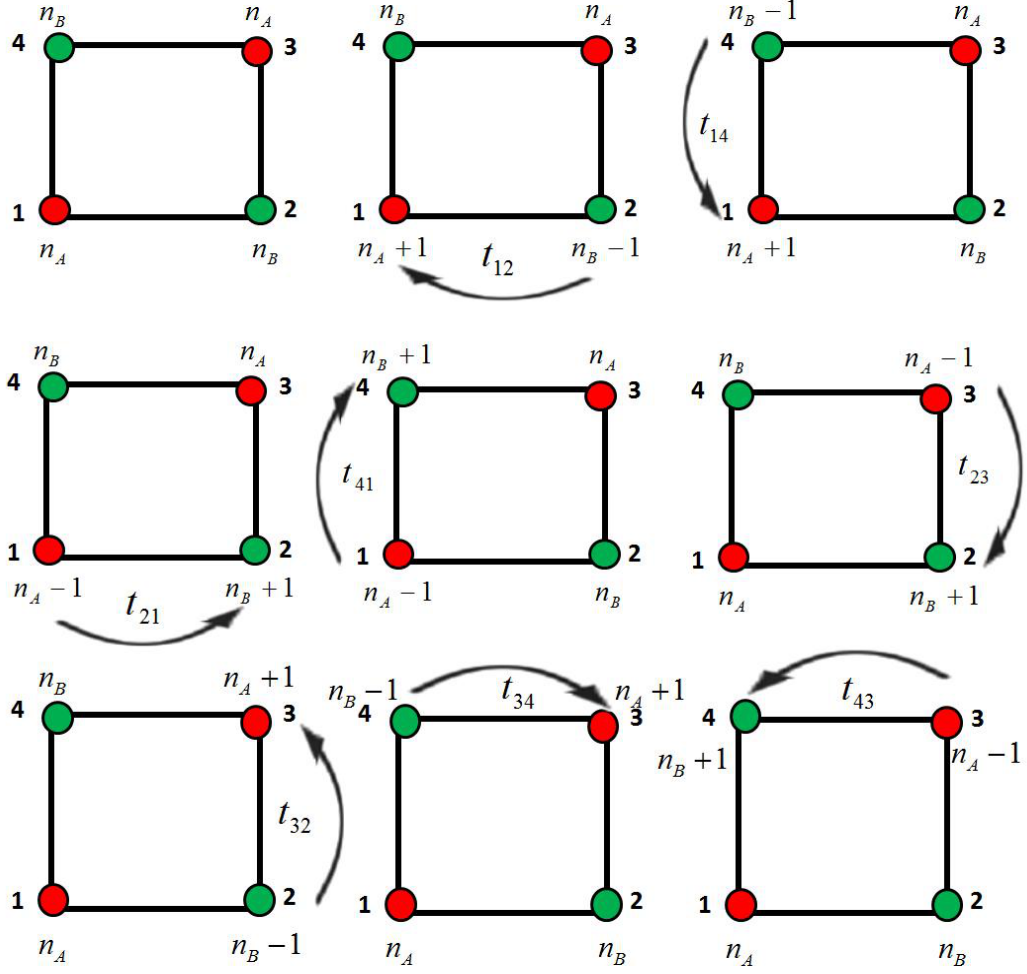


FIGURE 3.4: Possibilities for the first order intermediate (excited) state for the DW phase in a 2x2 lattice. Figure (a) corresponds to the ground state wave function in the limit $t = 0$

be explicitly written as

$$\begin{aligned}
 |\Psi_{DW}^{(1)}\rangle &= \sum_{m \neq |\Psi_{DW}^{(0)}\rangle} \frac{-\sum_{ll'} t_{ll'} \langle m | \hat{a}_l^\dagger \hat{a}_{l'} | 0 \rangle}{E_{0m}} |m\rangle \\
 &= -\frac{\sqrt{n_B(n_A+1)}}{E_1} [t_{12} |n_A^{(1)}+1, n_B^{(2)}-1, n_A^{(3)}, n_B^{(4)}\rangle \\
 &\quad + t_{14} |n_A^{(1)}+1, n_B^{(2)}, n_A^{(3)}, n_B^{(4)}-1\rangle + t_{32} |n_A^{(1)}, n_B^{(2)}-1, n_A^{(3)}+1, n_B^{(4)}\rangle \\
 &\quad + t_{34} |n_A^{(1)}, n_B^{(2)}, n_A^{(3)}+1, n_B^{(4)}-1\rangle] \\
 &\quad - \frac{\sqrt{n_A(n_B+1)}}{E_2} [t_{21} |n_A^{(1)}-1, n_B^{(2)}+1, n_A^{(3)}, n_B^{(4)}\rangle \\
 &\quad + t_{23} |n_A^{(1)}, n_B^{(2)}+1, n_A^{(3)}-1, n_B^{(4)}\rangle + t_{41} |n_A^{(1)}-1, n_B^{(2)}, n_A^{(3)}, n_B^{(4)}+1\rangle \\
 &\quad + t_{43} |n_A^{(1)}, n_B^{(2)}, n_A^{(3)}-1, n_B^{(4)}+1\rangle]
 \end{aligned} \tag{3.62}$$

where

$$E_1 = (n_B - n_A - 1) + (zn_A - zn_B + 1)V \quad (3.63)$$

$$E_2 = (n_A - n_B - 1) + (zn_B - zn_A + 1)V \quad (3.64)$$

Next, we calculate the second order correction to the wave function of the DW state (equation (3.56)). For every first order intermediate state $|m\rangle$, there will be number of possible second order intermediate states. For example, for the just discussed $|m\rangle = |n_A^{(1)} + 1, n_B^{(2)} - 1, n_A^{(3)}, n_B^{(4)}\rangle$ Fig. 3.4(b) which is connected to the ground state by single hopping, the corresponding possibilities for $|m'\rangle$ are shown in Fig. 3.5(a)-(g) which is seven in number.

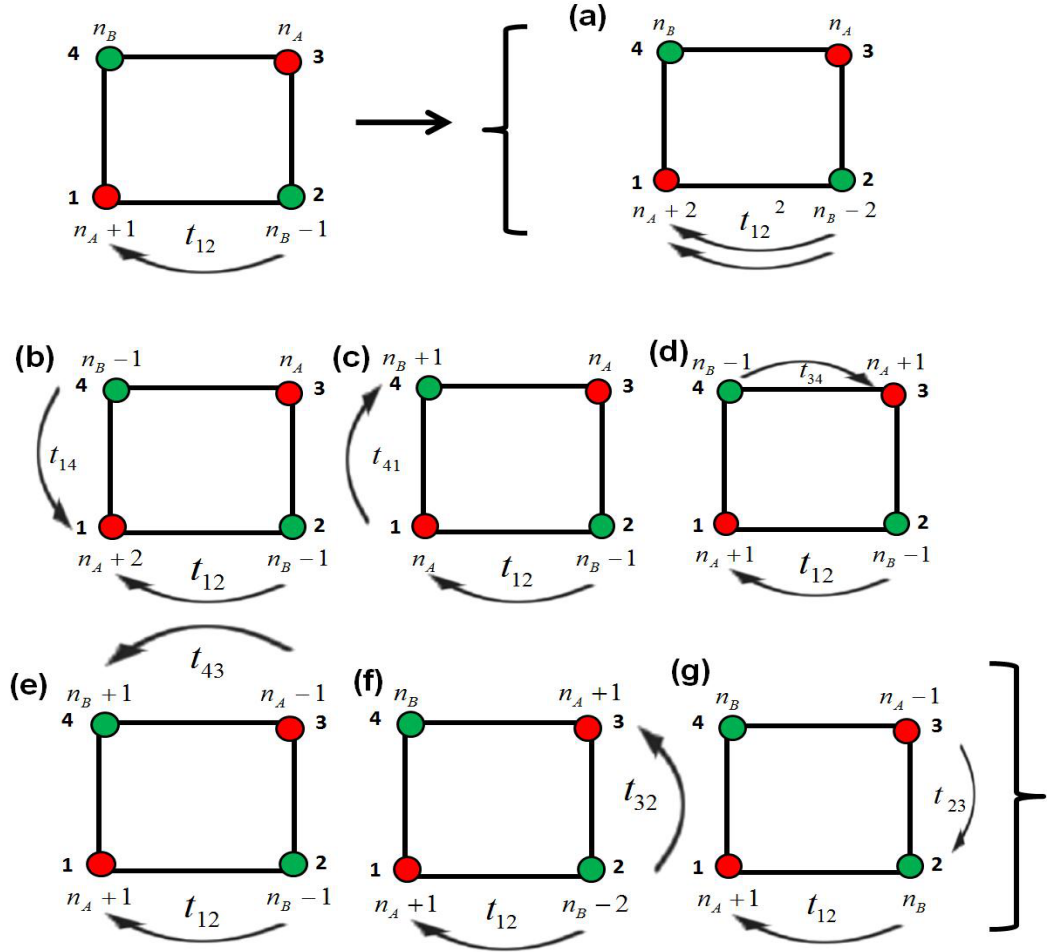


FIGURE 3.5: Second order intermediate states for $|m\rangle = |n_A^{(1)} + 1, n_B^{(2)} - 1, n_A^{(3)}, n_B^{(4)}\rangle$ (the first diagram)

For $|m\rangle = |n_A^{(1)} + 1, n_B^{(2)} + 1, n_A^{(3)}, n_B^{(4)}\rangle$

$$\frac{\langle m | H_P | 0 \rangle}{E_{0m}} = \frac{-\sqrt{n_B(n_A + 1)}t_{12}}{E_1} \quad (3.65)$$

The corresponding possibilities for $|m'\rangle$ for $|m\rangle = |n_A^{(1)} + 1, n_B^{(2)} - 1, n_A^{(3)}, n_B^{(4)}\rangle$ are represented in Fig. 3.5(a)-(g). For illustration let us choose

$$|m'\rangle = |n_A^{(1)} + 2, n_B^{(2)} - 2, n_A^{(3)}, n_B^{(4)}\rangle$$

Then

$$E_{0m'} = E_0 - E_{m'} = E_{01} = 2(n_A - n_B - 2) + (2zn_A - 2zn_B + 4)V$$

The contribution of this $|m'\rangle$ state to the second order correction to DW wave function is

$$|\Psi_{DW}^{(2)}\rangle_{a_1} = \frac{\sqrt{n_B(n_A + 1)(n_A + 2)(n_B - 1)}}{(E_1)(E_{01})} t_{12}^2 |n_A^{(1)} + 2, n_B^{(2)} - 2, n_A^{(3)}, n_B^{(4)}\rangle$$

Summing over these contributions, we get the second order correction to the wave function due to this $|m\rangle$ state which looks like

$$\begin{aligned} |\Psi_{DW}^{(2)}(|m\rangle)\rangle_a = & \frac{\sqrt{n_B(n_A + 1)(n_A + 2)(n_B - 1)}}{(E_1)(E_{01})} t_{12}^2 |n_A^{(1)} + 2, n_B^{(2)} - 2, n_A^{(3)}, n_B^{(4)}\rangle \\ & + \frac{n_B \sqrt{(n_A + 1)(n_A + 2)}}{(E_1)(E_{02})} t_{12} t_{14} |n_A^{(1)} + 2, n_B^{(2)} - 1, n_A^{(3)}, n_B^{(4)} - 1\rangle \\ & + \frac{(n_A + 1) \sqrt{n_B(n_B + 1)}}{(E_1)(E_{03})} t_{12} t_{41} |n_A^{(1)}, n_B^{(2)} - 1, n_A^{(3)}, n_B^{(4)} + 1\rangle \\ & + \frac{(n_A + 1) \sqrt{n_B(n_B - 1)}}{(E_1)(E_{04})} t_{12} t_{32} |n_A^{(1)} + 1, n_B^{(2)} - 2, n_A^{(3)} + 1, n_B^{(4)}\rangle \\ & + \frac{n_B \sqrt{n_A(n_A + 1)}}{(E_1)(E_{05})} t_{12} t_{23} |n_A^{(1)} + 1, n_B^{(2)}, n_A^{(3)} - 1, n_B^{(4)}\rangle \\ & + \frac{\sqrt{n_A n_B(n_A + 1)(n_B + 1)}}{(E_1)(E_{06})} t_{12} t_{43} |n_A^{(1)} + 1, n_B^{(2)} - 1, n_A^{(3)} - 1, n_B^{(4)} + 1\rangle \\ & + \frac{n_B(n_A + 1)}{(E_1)(E_{07})} t_{12} t_{34} |n_A^{(1)} + 1, n_B^{(2)} - 1, n_A^{(3)}, n_B^{(4)} - 1\rangle \end{aligned} \quad (3.66)$$

Following the same procedure for all other $|m\rangle$ states defined in Fig. 3.4 and adding all contributions, we get the total second order correction to wave-function for the DW phase. We mention here again that, for a finite square lattice of M sites, the expressions are obtained by taking into account the fact that the atoms on the edges of the square lattice are restricted to hop to only within the finite lattice and not beyond the edges, which effectively implies hard wall boundary conditions for the hopping parameter as also evident from Fig. 3.4.

3.6.2 Momentum distribution as a function of gauge field

With the help of expressions (3.62),(3.66) for perturbation corrections in previous section, the DW ground state wave function can be determined upto the second order in perturbation theory using the general expression (3.54) and subsequently normalized within the same order of perturbation theory. Thus, substituting the obtained wave-function in the expression (3.53) for momentum distribution yields the $n(\mathbf{k})^{(0)}$, $n(\mathbf{k})^{(1)}$ and $n(\mathbf{k})^{(2)}$ for the DW phase with n_A and n_B as

$$n(\mathbf{k})^{(0)} = |W(\mathbf{k})|^2 \left(\frac{n_A + n_B}{2} \right) \quad (3.67)$$

$$\begin{aligned} n(\mathbf{k})^{(1)} &= -\frac{n_B(n_A + 1)}{E_1} \frac{|W(\mathbf{k})|^2}{M/2} \sum_{l,l'} t_{ll'} e^{i\mathbf{k} \cdot (\mathbf{R}_l - \mathbf{R}_{l'})} \\ &\quad - \frac{n_A(n_B + 1)}{E_2} \frac{|W(\mathbf{k})|^2}{M/2} \sum_{l,l'} t_{ll'} e^{i\mathbf{k} \cdot (\mathbf{R}_l - \mathbf{R}_{l'})} \\ &= |W(\mathbf{k})|^2 \left[\frac{n_B(n_A + 1)}{E_1} + \frac{n_A(n_B + 1)}{E_2} \right] \epsilon(\mathbf{k}) \end{aligned} \quad (3.68)$$

$$\begin{aligned} n(\mathbf{k})^{(2)} &= \frac{|W(\mathbf{k})|^2}{M/2} \left[\frac{n_B(n_A + 1)}{2E_1^2} + \frac{n_A(n_B + 1)}{2E_2^2} - \frac{n_B(n_A + 1)}{E_1} - \frac{n_A(n_B + 1)}{E_2} \right] \\ &\quad \times (n_B + n_A + 1) \left(\sum_{l,l',l''} t_{ll'} t_{l'l''} e^{i\mathbf{k} \cdot (\mathbf{R}_l - \mathbf{R}_{l''})} \right) \\ &= |W(\mathbf{k})|^2 \left[\frac{n_B(n_A + 1)}{2E_1^2} + \frac{n_A(n_B + 1)}{2E_2^2} - \frac{n_B(n_A + 1)}{E_1} - \frac{n_A(n_B + 1)}{E_2} \right] \\ &\quad \times (n_B + n_A + 1) (\epsilon^2(\mathbf{k}) - 2dt^2) \end{aligned} \quad (3.69)$$

where

$$\epsilon^2(\mathbf{k}) - 2dt^2 = \frac{2}{M} \sum_{l,l',l''} t_{ll'} t_{l'l''} e^{i\mathbf{k} \cdot (\mathbf{R}_l - \mathbf{R}_{l''})} \quad (3.70)$$

and, E_1 and E_2 are given by equation (3.63) and (3.64) respectively. The expression (3.70) is obtained as shown below

$$\begin{aligned} \epsilon^2(\mathbf{k}) &= \frac{2}{M} \sum_{ll'l''} t_{ll'} t_{l'l''} e^{i\mathbf{k} \cdot (\mathbf{R}_l - \mathbf{R}_{l'})} e^{i\mathbf{k} \cdot (\mathbf{R}_{l'} - \mathbf{R}_{l''})} \\ &= \frac{2}{M} \sum_{ll'l''} t_{ll'} t_{l'l''} e^{i\mathbf{k} \cdot (\mathbf{R}_l - \mathbf{R}_{l''})} + \frac{2}{M} t^2 (2d) M \end{aligned}$$

This implies

$$\epsilon^2(\mathbf{k}) - 2dt^2 = \frac{2}{M} \sum_{l,l',l''} t_{ll'} t_{l'l''} e^{i\mathbf{k} \cdot (\mathbf{R}_l - \mathbf{R}_{l''})} \quad (3.71)$$

This is also evident from equation (3.22) where $\epsilon^2 t^2$ is the eigen value of \mathbf{t}^2 matrix. It is to note that the term $|W(\mathbf{k})|^2$ in the expression for momentum distribution (3.68-3.69) is dependent on the experimental details i.e the optical lattice parameters and the effective gauge potential, while the theoretical analysis gives the calculation of the correlation function $\langle \hat{a}_l^\dagger \hat{a}_{l'} \rangle$ [165]. Since, the Wannier function $W(\mathbf{k})$ is a non universal property of the lattice potential and has nothing to do with the eBHM model in presence of gauge field, in our subsequent calculations we set this to unity [166].

For DW phase we substituted $n_A = n_0$ and $n_B = n_0 - 1$ particles on alternating sites in the expression (3.67)-(3.69). This yields the momentum distribution in presence of gauge field as

$$\begin{aligned} n_{DW}(\mathbf{k}) = & \frac{2n_0 - 1}{2} - \left[\frac{n_0^2}{(z-1)V} + \frac{(n_0^2 - 1)}{2 - (z+1)V} \right] \epsilon(\mathbf{k}) \\ & + 2n_0 \left[\frac{n_0^2}{2V^2(z-1)^2} + \frac{(n_0^2 - 1)}{2(2 - (z+1)V)^2} + \frac{n_0^2}{(z-1)V} + \frac{(n_0^2 - 1)}{(2 - (z+1)V)} \right] \\ & \times (\epsilon^2(\mathbf{k}) - 2dt^2) + O(t^3) \end{aligned} \quad (3.72)$$

Similarly, for the MI phase with n_0 particles on each lattice site, the momentum distribution in presence of gauge field is

$$\begin{aligned} n_{Mott}(\mathbf{k}) = & n_0 - \frac{2n_0(n_0 + 1)}{1 - V} \epsilon(\mathbf{k}) + n_0(n_0 + 1)(2n_0 + 1)(\epsilon^2(\mathbf{k}) - 2dt^2) \frac{3 - 2V}{(1 - V)^2} \\ & + O(t^3) \end{aligned} \quad (3.73)$$

In either of the above expression of momentum distribution (3.72) and (3.73), the dispersion $\epsilon(\mathbf{k})$ is the minimum eigenvalue of the artificial magnetic flux dependent hopping matrix T or $-t_{ij}$ multiplied by a pre-factor $\frac{2}{M}$ for DW phase and $\frac{1}{M}$ for the MI phase where M is the total number of sites along a given direction. The matrix T in the lattice site basis is already shown in equation (3.13).

As described in equation (3.1), $t_{ij} = te^{i\varphi_{ij}}$ is the gauge dependent hopping amplitude from site i to site j and non-vanishing only if i and j are nearest neighbors. Through $\varphi_{ij} = \int_{r_j}^{r_i} d\mathbf{r} \cdot \mathbf{A}(\mathbf{r})$, this hopping amplitude explicitly depend on the gauge potential with $\mathbf{A}(\mathbf{r})$ as the vector potential. The calculation of eigen value $\epsilon(\mathbf{k})$ is explained in detail in next section.

3.6.3 Effect of the presence of gauge field on the momentum distribution

The effect of artificial gauge field on the MI-SF and DW-SS transition boundary have distinctive features which can be demonstrated by plotting the momentum distribution derived in (3.72) and (3.73) in the $k_x - k_y$ plane at these transition boundaries. Since the matrix T in (3.13) explicitly depends on the gauge potential, the momentum distribution reflects in itself the gauge potential structure, since the location of eigenvalues $\epsilon(\mathbf{k})$ is gauge dependent.

The calculation of eigen value of the hopping matrix and its dependence on the type of gauge potential has already been explained in detail in section 3.2.2. However for completeness of the discussion, we briefly mention some salient points here again.

We calculate the dispersion $\epsilon(\mathbf{k})$ for two types of artificial gauge fields on the system, the Landau gauge and the Symmetric gauge and evaluate the corresponding momentum distribution structure. The vector potential in Landau (L) and Symmetric (S) gauge are respectively given as

$$\mathbf{A}^L(\mathbf{r}) = \mathbf{B}(0, x, 0) = 2\pi\nu x\hat{y} \quad (3.74)$$

$$\mathbf{A}^S(\mathbf{r}) = \mathbf{B}(-y, x, 0) = \pi\nu(x\hat{y} - y\hat{x}) \quad (3.75)$$

where we consider that the flux through the unit cell $\nu = p/q$ is rational.

In the Landau gauge \mathbf{A}^L , following [136] we denote the co-ordinate of a site i on the square lattice by pair of integers $\{m, n\}$ in the unit of the lattice spacing a . In terms of these notations the eigenvalue equation $T\psi = \epsilon\psi$ on the lattice can be written as

$$-t[\psi_{n+1,m} + \psi_{n-1,m} + e^{2\pi i\nu n}\psi_{n,m+1} + e^{-2\pi i\nu n}\psi_{n,m-1}] = \epsilon\psi_{n,m} \quad (3.76)$$

The lattice wave functions that appears in equation (3.76) can be obtained by operating $\psi_{n,m}$ by magnetic translation operator. Such operators are given as [124]

$$T_{\mathbf{R}} = \exp\left(\frac{i}{\hbar}\mathbf{R} \cdot \left[\mathbf{p} + \frac{\hbar}{m}\mathbf{A}(\mathbf{r})\right]\right)$$

where \mathbf{R} is the lattice translational vector. The Brillouin Zone (BZ) is reduced in Landau gauge as

$$-\pi \leq k_x \leq \pi, -\pi/q \leq k_y \leq \pi/q$$

and is called the magnetic Brillouin zone (MBZ). As we shall see the momentum distribution $n(\mathbf{k})$ shows the formation of such MBZ.

Since $[T, \hat{p}_y] = 0$ in the Landau gauge, the wave function

$$\psi_{n,m}(k_x, k_y) = e^{ik_y m} e^{ik_x n} \phi_n(k_x, k_y)$$

where $k_{x,y}$ are the components of the Bloch wave vectors. Substituting this expression in the eigenvalue equation (3.76) one gets the following one dimensional eigenvalue equation

$$-t[e^{ik_x} \phi_{n+1} + e^{-ik_x} \phi_{n-1} + 2 \cos(k_y + 2\pi\nu n) \phi_n] = \epsilon \phi_n \quad (3.77)$$

The eigenvalues $\epsilon(\mathbf{k})$ now can be determined from the condition

$$\det \begin{bmatrix} M_1 & e^{-ik_x} & 0 & \dots & e^{ik_x} \\ e^{ik_x} & M_2 & \dots & \dots & \\ 0 & \vdots & \vdots & \vdots & 0 \\ \dots & \dots & & M_{q-1} & e^{-ik_x} \\ N_q & & 0 & e^{ik_x} & M_q \end{bmatrix} = 0 \quad (3.78)$$

with

$$M_n = 2\cos(k_y a + 2\pi n \phi) - \epsilon(\mathbf{k})$$

and, where $n = 0, 1, \dots, q-1$. The eigenvalue matrix is $q \times q$ dimensional because of the q times enhancement of the magnetic unit cell. And its minimum eigenvalue $\epsilon(\mathbf{k})$ is q fold degenerate, since

$$\epsilon(k_x, k_y) = \epsilon \left(k_x, k_y + \frac{2\pi\alpha}{q} \right)$$

where $\alpha = 0, \dots, (q-1)$. Each of this minimum will correspond to a peak in the momentum distribution which is calculated using (3.72) and (3.73). This has been plotted in Fig. 3.6(a) and (b) for MI and DW phase.

3.7 Results and Discussions: *Apparent* Gauge dependence of momentum distribution function

For a flux $\nu = p/q$, q peaks appear in the first Brillouin zone for the momentum distribution for both gauge choices, near the MI-SF boundary. However, the positions of the peaks in the Brillouin zone depends on the specific form of vector potential realized in the experiments. The number of peaks for a flux $\nu = p/q$ depends only on q and also, on the lattice geometry.

For Landau gauge potential, the peaks appear at $(2\pi\alpha/q, 0)$, while for the symmetric gauge choice, it appears at $(\pi\alpha/q, \pi\alpha/q)$. This is because, the magnitude of eigen

value is the same for two gauge choices but the location of the minimum eigen value in the Brillouin zone depends on the specific form of the vector potential for the reasons elaborated in the preceeding discussion. It is because of this, the manifestly gauge choice dependent form of the momentum distribution function that we use, is justifiable here. Thus, for this artificial gauge potential, this apparent gauge dependence does not violate any fundamental principle.

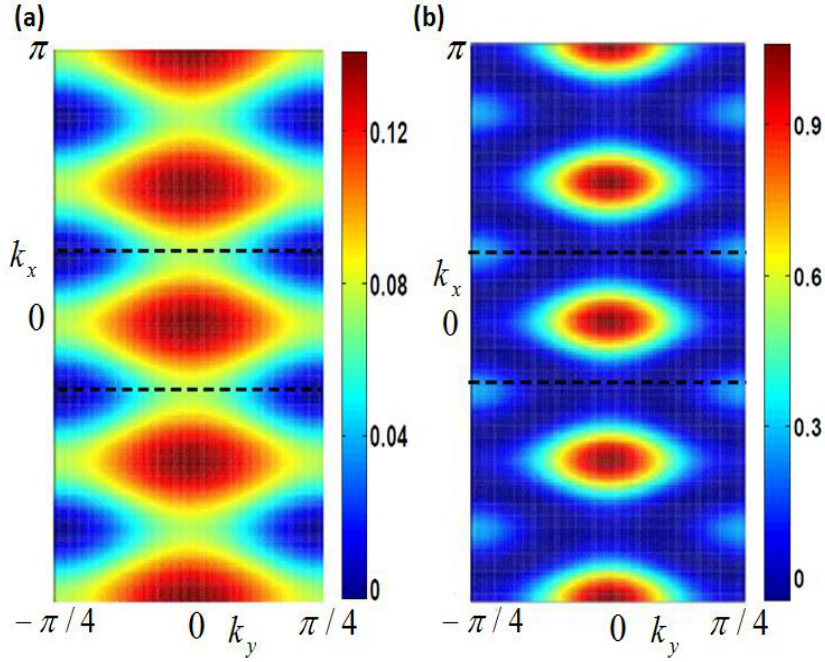


FIGURE 3.6: Momentum distribution at the (a) MI-SF and (b) DW-SS phase boundary in Landau gauge potential for $\nu = \frac{1}{4}$, plotted in the reduced Brillouin zone $-\pi \leq k_x \leq \pi$ and $-\pi/4 \leq k_y \leq \pi/4$

It is to note that the calculations are performed at the DW-SS and MI-SF transition boundaries, where the superfluidity, though small, is finite and hence the momentum distribution at the boundaries show the signatures of the SS and SF phases. Moreover, the pure MI and DW phases are insulating and incoherent phases, which results in a flat momentum distribution for these phases, indicating no correlations between atoms. We show here appearance of distinct peaks at the DW-SS and MI-SF boundary which is due to finite superfluidity at the transition boundaries.

In the Landau gauge potential, at the MI-SF phase boundary one gets q peaks in $n(\mathbf{k})$ at $(k_x, k_y) = (\frac{2\pi n}{q}, 0)$, with $n = 0, 1, \dots, q-1$. Accordingly, Fig. 3.6(a) shows the momentum distribution for $q = 4$ which has peaks at $(0, 0)$, $(\pm\pi/2, 0)$ and $(\pm\pi, 0)$.

At the DW-SS phase boundary, for $\nu = 1/q$ with $q = 4$, we again get peaks at $n(\mathbf{k})$ at $(0, 0)$, $(\pm\pi/2, 0)$ and $(\pm\pi, 0)$, but in addition, there also exists small peaks at the corners of the reduced BZ, as shown in Fig. 3.6(b).

The appearance of extra peaks at the BZ corners is a distinguishing feature at the DW-SS phase boundary from the MI-SF boundary. Since the DW phase consists of two interpenetrating sublattices A and B , even in the absence of any applied magnetic field, the BZ structure at the DW-SS phase boundary has double periodicity whereas the usual MI-SF phase boundary has a single periodicity. This results in appearance of small extra peaks in the momentum distribution at DW-SS phase boundary even in the absence of magnetic field [166]. Upon application of magnetic field, we observe small peaks in the momentum distribution at the BZ corners at the DW-SS phase boundary, which is again attributed to the reduced periodicity at the DW-SS phase boundary compared to MI-SF phase boundary (Fig. 3.6). The effect of the applied magnetic field can be seen through the enlargement of the unit cell in real space or equivalently reduction in the BZ in the fourier space [109]. The reduced Brillouin zone is a clear sign that the flux per plaquette is at (or sufficiently close to) a rational value and the additional peaks at these BZ corners is a clear distinction at the DW-SS phase boundary from the MI-SF phase boundary in presence of gauge field as can be seen from Fig. 3.6 [109].

When one uses a symmetric gauge potential given in (3.75), the commuting magnetic translation operators are $\hat{T}_{2qa\hat{x}}$ and $\hat{T}_{2qa\hat{y}}$. The corresponding discretized eigenvalue equation was discussed in detail in chapter 2. Following the preceding discussion it can be shown that the magnetic unit cell should be $2q \times 2q$ of the unit cell in the absence field. Accordingly, the MBZ will be defined as

$$\left(-\frac{\pi}{2q} \leq k_x \leq \frac{\pi}{2q}, -\frac{\pi}{2q} \leq k_y \leq \frac{\pi}{2q} \right)$$

This results in the formation of peaks in momentum distribution at $(\pm\pi n/q, \pm\pi n/q)$.

The momentum distribution at the MI-SF phase boundary in presence of symmetric gauge potential, for rational flux $\nu = 1/2$ is shown in Fig. 3.7(a). The peak in the momentum distribution is observed at the center $(0,0)$ and smaller peaks are seen at the corners in the range $(-\pi/4 \leq k_x \leq \pi/4, -\pi/4 \leq k_y \leq \pi/4)$ [109].

Same calculation at the DW-SS phase boundary, in a symmetric gauge potential, shows the existence small peaks at the BZ (doubly reduced) corners, in addition to the peak at $(0,0)$, as shown in Fig. 3.7(b).

The effect of application of symmetric gauge potential to the system is equivalent to rotating the system [105, 107] and thus, leads to formation of vortices in the system when the superfluid order parameter is finite. Since we perform our calculations at the phase boundary, the results for the momentum distribution of the DW and MI phases in presence of symmetric gauge potential, provides information about the signature of vortex in a SS (at the DW-SS phase boundary) and vortex in a SF (at the MI-SF

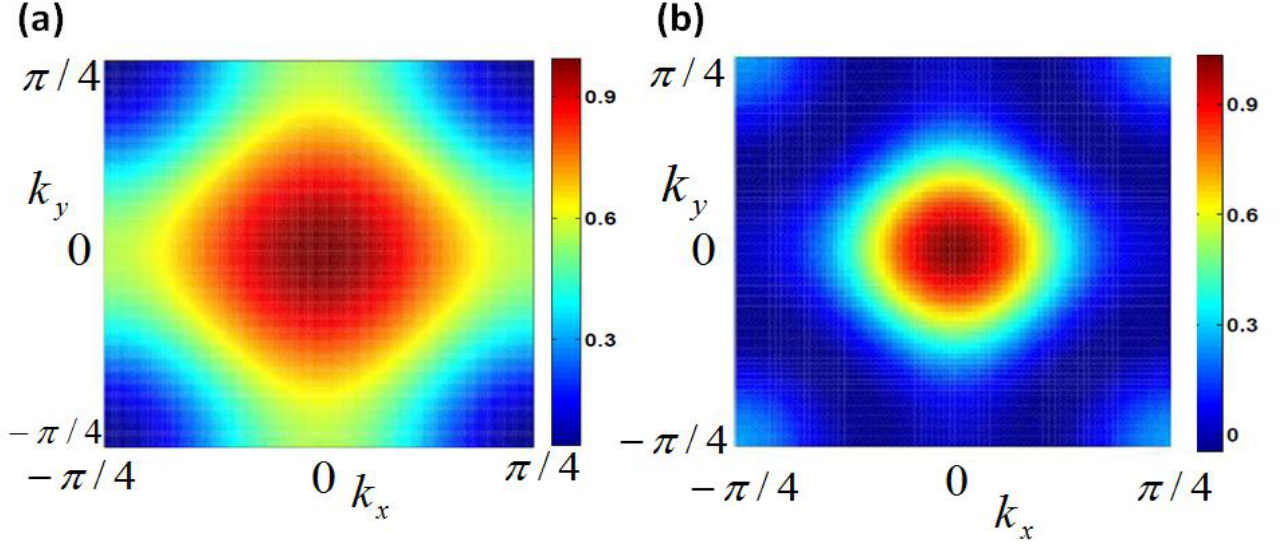


FIGURE 3.7: Momentum distribution for the (a) MI and (b) DW phase in symmetric gauge potential for $\nu = 1/2$, plotted in the range $-\pi/4 \leq k_x \leq \pi/4$ and $-\pi/4 \leq k_y \leq \pi/4$

phase boundary). Fig. 3.7 demonstrate rotating SS reflects some extra peaks in the momentum distribution in addition to the peaks observed in a rotating ordinary SF and the corresponding reduction in the BZ shows that there is a finite rational flux per plaquette [109].

These extra peaks are clearly demonstrated in Fig. (3.8 and is one of the central result of this work. Since momentum distribution can be measured using TOF absorption imaging technique, this provides a way to experimentally distinguish between the supersolid phase and superfluid phase by comparing the respective vortex profile. Our calculations demonstrates that the rotating SS reflects some extra peaks in the momentum distribution in addition to the peaks observed in a rotating ordinary SF together with the reduction of the size of the BZ depending on the amount of flux passed through the unit cell [109]. This occurrence of extra peaks in the momentum distribution for a rotating SS one of the important result of this work and has been illustrated in Fig. 3.8.

3.7.1 Apparent gauge dependence of the momentum distribution

From above set of results, we can see that the momentum distribution profiles depend on the type of gauge potential used to produce the *artificial* gauge field. This apparent gauge dependence of $n(\mathbf{k})$ is a direct result of the realization of specific vector potential and not the field, in the typical experimental set ups. This was also discussed in

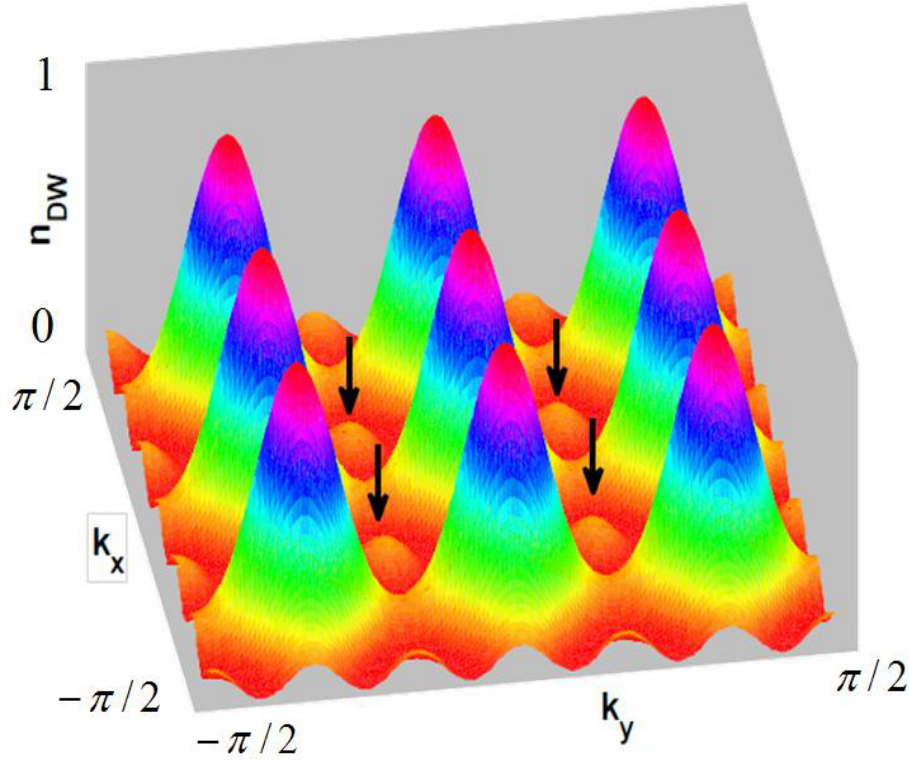


FIGURE 3.8: Extra small peaks in the DW momentum distribution $n(\mathbf{k})$ symmetric gauge potential. The arrows show the location of the extra peaks at intermediate positions

[152] using strong coupling RPA theory. They obtained the following expression for the momentum distribution of the MI phase in presence of synthetic gauge field.

$$n(k) = \sum_{\alpha=0 \dots q-1} \frac{E_q^{\alpha-}(k) + \delta\mu + Ux}{E_q^{\alpha+} - E_q^{\alpha-}} \quad (3.79)$$

where $\delta\mu = \mu - U(n_0 - 1/2)$, $x = n_0 + 1/2$ and

$$E_q^{\alpha\pm}(k) = \frac{1}{2}[-2\delta\mu + \epsilon_q^\alpha(k) \pm \sqrt{\epsilon_q^\alpha(k)^2 + 4\epsilon_q^\alpha(k)Ux + U^2}]$$

Comparing the above expression with our expression in equation (3.73), one can see that the momentum distribution actually depends on $\epsilon(k)$, which is a gauge independent quantity. However location of these eigenvalues in the \mathbf{k} plane is dependent on the form of the artificial gauge potential used.

As already explained in detail in section 2.1.2 in chapter 2, the actual physical interaction is represented by the artificial gauge potential and not by the artificial gauge field. This is why such a gauge field is actually *artificial* and the observable quantities such as

momentum distribution are not necessarily gauge invariant. The same point has been emphasized also in ref. [167] in context of Bose Hubbard Model with staggered flux.

To analyze this issue further in the next section, we compare the momentum distribution $n(\mathbf{k})$ in symmetric gauge to the momentum distribution corresponding to the many body states having definite quasi-angular momentum in a symmetric gauge potential. This quasi-angular momentum are analogues of the Bloch-momentum, for a rotationally invariant system and has been discussed in following section.

3.8 Quasi-angular momentum distribution

In this section, we present results for quasi angular momentum distribution for strongly-interacting bosons with long range interactions in rotating optical lattices. Quasi-angular momentum is analogous to quasi-momentum for periodic translationally invariant systems and has been previously used in the context of rotating ring lattices [168, 169] to label eigenstates.

Discrete rotational symmetry and quasi angular momentum

Quasi angular momentum is a quantum number for systems with a discrete rotational symmetry and can be a useful tool in investigating the symmetry properties of the ground state. The continuous rotational symmetry of the system is broken by the presence of the lattice resulting in discrete rotational symmetry, and thus the eigenvalues of the angular-momentum operator are therefore no longer good quantum numbers. Here, the concept of discrete translational symmetry and Bloch's theorem are mapped onto the system with discrete rotational symmetry to generate quasi-angular momentum states [170].

We can say that a moving N site linear lattice with periodic boundary conditions is analogous to a rotating N site ring lattice. The analogy can be made by writing the Hamiltonian of a moving, one-dimensional, sinusoidal N site lattice in the co-moving frame, given by

$$H(x) = -\frac{\hbar^2}{2m} \frac{\partial^2}{\partial x^2} + V_0 \cos^2(qx) - v \frac{\hbar}{i} \frac{\partial}{\partial x} \quad (3.80)$$

The wave number of the lattice is $q = \pi/d$, with d as the lattice spacing. The periodic boundary conditions for the wave function is $\psi(x + Nd) = \psi$.

On the other hand, the Hamiltonian of a rotating, sinusoidal N site ring lattice in the rotating frame is given by

$$H(\phi) = -\frac{\hbar^2}{2m} \frac{1}{R^2} \frac{\partial^2}{\partial \phi^2} + V_0 \cos^2\left(N \frac{\phi}{2}\right) - \Omega \frac{\hbar}{i} \frac{\partial}{\partial \phi} \quad (3.81)$$

with Ω as the rotation frequency, and R as the radius of the ring. The two Hamiltonians in equations (3.80) and (3.81), are mathematically identical if we perform a transformation $x = \phi Nd/2\pi$ and identify $Nd/2\pi$ with R and v/R with Ω .

We can see that the Hamiltonian given by equation (3.80) and (3.81) are identical implying that the properties of one-dimensional systems with a discrete translational invariance can be mapped over for ring systems with a discrete rotational invariance. The analogy can be carried further for two dimensional system with free-space solution in polar coordinates,

$$\psi_j(\phi, \rho) = e^{ij\phi} R_j(\rho) \quad (3.82)$$

Here $R_j(\rho)$ is the radial function and j is an integer. The presence of a potential breaks the rotational symmetry of the system and hence the eigenstates are linear combinations of these free-space solutions (3.82). If the potential has a discrete N fold rotational symmetry, its eigenstates can be expanded in the free space solutions given below

$$\psi_m(\rho, \phi) = \sum_{j=-\infty}^{\infty} a_j^{(m)} \frac{e^{i(Nj+m)\phi}}{\sqrt{N\pi}} R_j(\rho) \quad (3.83)$$

From above expression (3.83), we have

$$\psi_m\left(\phi - \frac{2\pi}{N}, \rho\right) = e^{-i2\pi m/N} \psi_m(\phi, \rho) \quad (3.84)$$

Thus, $\psi_m(\phi, \rho)$ is an eigen vector of the discrete rotation operator $R_{2\pi/N}$ with $e^{-i2\pi m/N}$ as the eigen value. $R_{2\pi/N}$ rotates the system by $\frac{2\pi}{N}$ and takes the place of the translational operator T_d . It is to note that the analogy is complete when the eigenstates are linear combinations of angular momentum eigenstates, where $\hbar m$ is called as the quasi-angular momentum of the state $\psi_m(\phi, \rho)$. For simplicity, we drop the factor of \hbar and call the value m as the quasi-angular momentum.

After explaining the physical meaning of quasi angular momentum, we perform our calculations to identify transitions between states of different symmetry for the ground state of a rotating system. However, it cannot be directly measured in experiments. A possible avenue for experimentally detecting these results is via the momentum distribution of the ground state is presented. So, for detecting quasi-angular momentum states, we look for a signature of quasi-angular momentum in the momentum distribution of a state.

In this sub section, we re evaluate the momentum distribution $n(\mathbf{k})$, but for a fixed quasi angular momentum and compare this with $n(\mathbf{k})$ demonstrated in Fig. 3.7.

To simplify calculation, we approximate the Wannier functions as delta functions to calculate the correlation function with a fixed value of angular momentum given to the system. The field operators can now be expanded as

$$\hat{\psi}(\mathbf{r}) = \frac{1}{\sqrt{M}} \sum_l e^{i2\pi m l/M} \delta(\mathbf{r} - \mathbf{r}_l) \hat{a}_l \quad (3.85)$$

where m is the quasi-angular momentum, M is the number of lattice sites, $\delta(\mathbf{r} - \mathbf{r}_l)$ is the delta function localized at site l with position \mathbf{r}_l and \hat{a}_l is the boson annihilation operator. Substituting this in the expression (3.52) yields

$$n(\mathbf{k}) = \frac{1}{M} \sum_{l,l'} e^{i2\pi m(l-l')/M} \delta^*(\mathbf{r} - \mathbf{r}_l) \delta(\mathbf{r} - \mathbf{r}_{l'}) \times \langle \psi_{ins} | \hat{a}_l^\dagger \hat{a}_{l'} | \psi_{ins} \rangle e^{i\mathbf{k} \cdot (\mathbf{r}_l - \mathbf{r}_{l'})} \quad (3.86)$$

As compared to the expression (3.53), in (3.86) the system now has a prefixed value of quasi angular momentum. Hence, we can associate a vortex phase with the system and determine the difference in symmetry of the ground state with different pre-fixed quasi angular momentum.

Using the wave function obtained by strong coupling expansion for the DW phase obtained in section 3.6.1 and substituting in equation (3.86), we can get the quasi momentum distribution [109]. For DW phase with n_0 and $n_0 - 1$ particles on alternating sites it is given by

$$\begin{aligned} n_{DW}(\mathbf{k}) &= \frac{1}{M} \sum_{l,l'} e^{i2\pi m(l-l')/M} \delta^*(\mathbf{r} - \mathbf{r}_l) \delta(\mathbf{r} - \mathbf{r}_{l'}) e^{i\mathbf{k} \cdot (\mathbf{r}_l - \mathbf{r}_{l'})} \times \\ &\quad \left(\frac{2n_0 - 1}{2} - \left[\frac{n_0^2}{V(z-1)} + \frac{(n_0^2 - 1)}{2 - V(z+1)} \right] t \right. \\ &\quad \left. + 2n_0 \left[\frac{n_0^2}{2V^2(z-1)^2} + \frac{(n_0^2 - 1)}{2(2 - V(z+1))^2} + \frac{n_0^2}{V(z-1)} + \frac{(n_0^2 - 1)}{2 - V(z+1)} \right] t^2 \right. \\ &\quad \left. + O(t^3) \right) \end{aligned}$$

Similar expression for $n(\mathbf{k})$ with a given quasi angular momentum for the MI phase can also be evaluated within strong coupling expansion.

We consider the most simple example of square lattice with four sites. Fig. 3.9(a) shows the momentum distribution for $m = 0$ for DW phase. It can be seen that the $m = 0$ state has a peak at $k = 2\pi n$, with n as an integer. However for higher quasi angular momentum state $m=1$, $n(\mathbf{k})$ vanishes at $k = 2\pi n$ in Fig. 3.9(b). Thus we see that the quasi momentum distribution changes the symmetry and position of peaks as vorticity enters into the system [109].

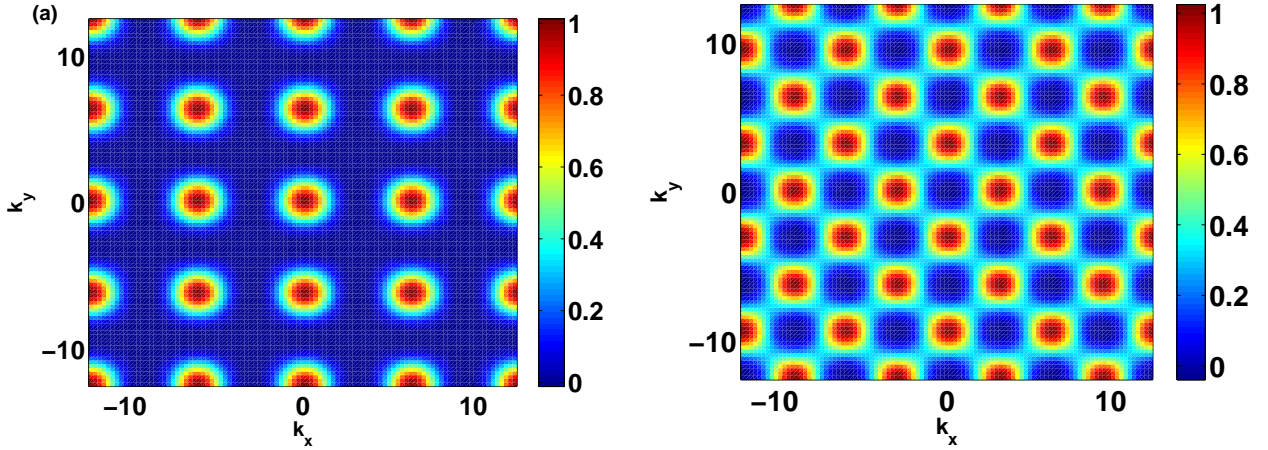


FIGURE 3.9: Quasi angular momentum distribution of the DW phase for (a) $m=0$, (b) $m=1$, plotted over a range $-4\pi \leq k_x, k_y \leq 4\pi$

Here, again the results at the DW-SS phase boundary can be distinguished from the MI-SF phase boundary by noting the appearance of small extra peaks in the former case. To demonstrate these small peaks clearly, we plot the cross sectional plots for the quasi momentum distribution state $m = 0$ and $m = 1$ for both DW phase and MI phase in Fig. 3.10 at the DW-SS boundary and MI-SF boundary [109]. It shows that there are additional peaks for DW phase at DW-SS phase boundary as compared to MI phase at MI-SF boundary, for any value of quasi momentum m . The reason is the reduced periodicity of the DW phase unlike the MI phase. It is important to note that there is a shift in peaks as the quasi momentum value changes from $m = 0$ to $m = 1$. This shift characterises that vorticity has entered the system and is thus a clear signature that a zero quasi angular momentum state can be distinguished from a non-zero one. It allows the experimenters to verify that vorticity has entered in the system through the TOF measurement by looking at the corresponding $n(\mathbf{k})$.

Thus, the quasi momentum distribution gives us clear measurable distinctions between states with different quasi momentum and also, the distinguishing features for the MI and DW phases with same quasi momentum. This confirms the results obtained for momentum distribution in section 3.7.

3.9 Summary of results of this chapter

To summarize, part 3A of the chapter presented a strong coupling expansion up to third order in hopping parameter to study the DW-SS and MI-SF phase transitions of the two-dimensional eBHM under the influence of an *artificial* magnetic field. We found

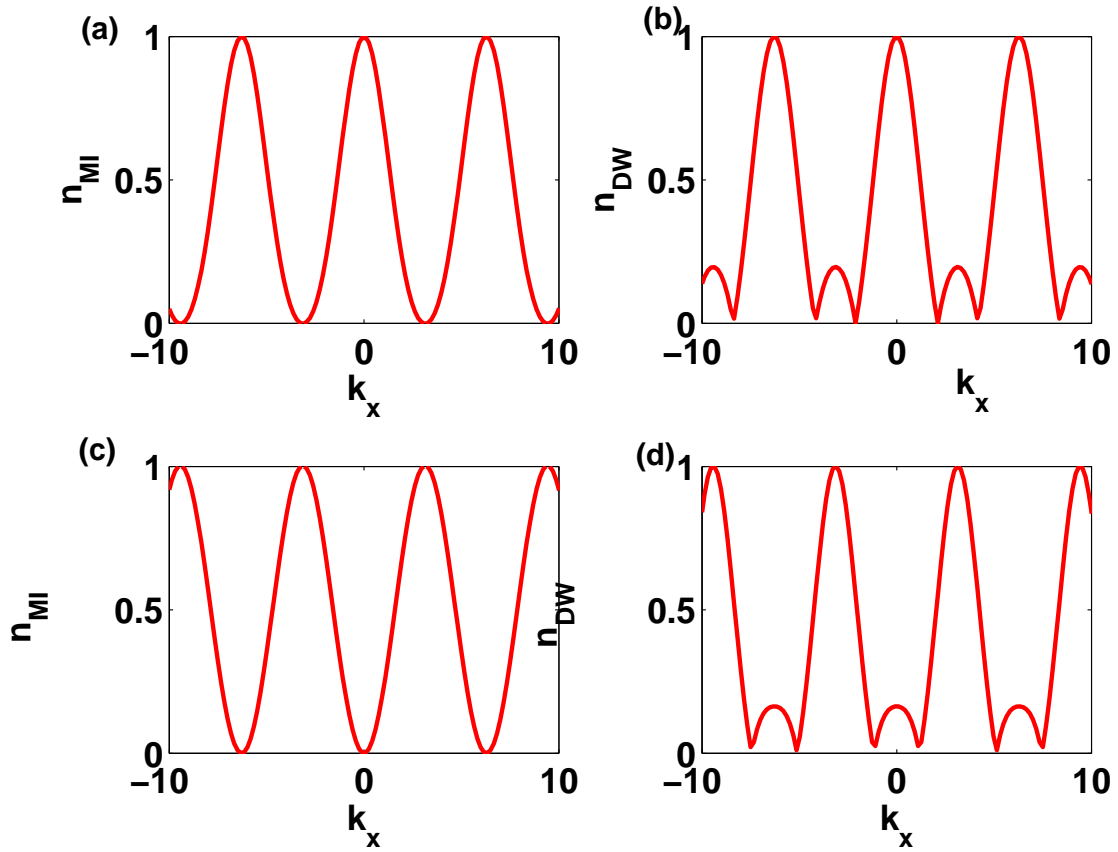


FIGURE 3.10: The cross sectional plots for $m=0$ and $m=1$ quasi angular momentum state for MI (a),(c) and DW (b),(d) phases. The DW phase shows distinctive peaks compared to MI phase

that the insulating phases (both DW and MI) enlarges with an increasing magnetic field [109]. This is explained by the localizing effect of the magnetic field on the moving bosons. The perturbative results can be extrapolated in a number of different ways and we performed a chemical potential extrapolation technique to determine the critical points of the phase transition in presence of small magnetic field strengths [109]. More work is needed to understand the change in character of the DW to SS and MI to SF phase transition at higher strengths of magnetic field. It would also be interesting to extend the scaling analysis of the eBHM to include its behavior in an external magnetic field.

In part 3B of the chapter, using the strong coupling perturbation calculations, we calculated the momentum distribution at the phase boundary which can be verified experimentally using the TOF imaging. The momentum distribution reflects the symmetry of the gauge potential. The momentum distribution shows distinctive feature at the DW-SS phase boundary as compared to the MI-SF phase boundary. Our calculations

demonstrates that the rotating SS reflects some extra peaks in the momentum distribution in addition to the peaks observed in a rotating ordinary SF. This occurrence of extra peaks in the momentum distribution for a rotating SS is another important result of this work [109].

We re-evaluate the momentum distribution, but for a given fixed quasi-angular momentum and found that the results at the DW-SS phase boundary can be distinguished from the MI-SF phase boundary by noting the appearance of small extra peaks in the former. This is also useful in experimentally detecting whether the system acquires vorticity because quasi-angular momentum is connected with the phase information and thus, the vorticity. Particularly, evaluating the momentum distribution for states with definite quasi-angular momentum at such phase boundary in a symmetric gauge, we clearly demonstrate how this can be used to probe the vortex profile of the SS phase at the DW-SS boundary due to the action of the gauge field.

There has been significant progress in cold atom experiments in identifying the enigmatic SS phase in ultra cold atomic systems [171–173] and our calculations will hopefully be useful for the identification of SS phase in optical lattices.

So far the calculations for the supersolid phase have been done when the ultracold atomic condensates with long range interactions are placed in an optical lattice. In the tight binding regime, this is well described by the Hubbard model description, and the calculations were performed very near to the transition boundaries [105, 109]. In this regime, the optical lattice might be partially responsible for the induced periodicity in the ultracold atomic supersolid. Thus, for more convincing study of supersolid we also perform the calculations without the presence of any optical lattice potential, to verify that the superfluid density modulations in the supersolid phase are entirely due to long range nature of interactions. As the depth of the lattice potential is reduced, we move away from the strongly interacting regime to the weakly interacting regime, where the Hubbard model description is replaced by the weakly interacting mean field Gross-Pitaevskii formalism [19]. In the absence of optical lattice, the continuum limit of studying supersolid phase and its signatures in an artificial gauge field will be much more convincing as compared to the lattice counterparts. This forms the basis for the work done in chapter 4.

Chapter 4

Hydrodynamic theory for rotating supersolids

Apart from the review of the work on rotating superfluids, this chapter contains new results based on *Rashi Sachdeva and Sankalpa Ghosh, Hydrodynamic theory for rotating supersolids*, arXiv:1308.1592[110]

4.1 The Gross Pitaevskii equation

As already mentioned in chapter 1, the theoretical formalism of trapped weakly interacting BEC was formulated by Gross and Pitaevskii [9]. This lead to the formulation of the Gross-Pitaevskii equation, which forms the basis and starting point of this chapter. Here we outline an overview and origin of this equation.

We consider a gas of N bosons at zero temperature. Within the framework of second quantization, the many-body problem with N interacting bosons can be described by the following Hamiltonian

$$\hat{H} = \int d\mathbf{r} \hat{\Psi}^\dagger(\mathbf{r}) \left[H_0(\mathbf{r}) + \int d\mathbf{r}' U(\mathbf{r} - \mathbf{r}') \hat{\Psi}(\mathbf{r}') \hat{\Psi}(\mathbf{r}) \right] \hat{\Psi}(\mathbf{r}) \quad (4.1)$$

Here, $U(\mathbf{r} - \mathbf{r}')$ is the effective two body interaction potential, and

$$H_0 = -\frac{\hbar^2}{2m} \nabla^2 + V_{ext} \quad (4.2)$$

and, $\hat{\Psi}(\mathbf{r})$ is the bosonic field operator satisfying the following commutation relations

$$[\hat{\Psi}(\mathbf{r}), \hat{\Psi}^\dagger(\mathbf{r}')] = \delta(\mathbf{r} - \mathbf{r}') \quad (4.3)$$

and,

$$[\hat{\Psi}(\mathbf{r}), \hat{\Psi}(\mathbf{r}')] = [\hat{\Psi}^\dagger(\mathbf{r}), \hat{\Psi}^\dagger(\mathbf{r}')] = 0 \quad (4.4)$$

We now use Heisenberg's relation

$$i\hbar \frac{\partial \hat{\Psi}}{\partial t} = [\hat{\Psi}, \hat{H}] \quad (4.5)$$

and the commutation relations (4.3) and (4.4) for bosonic field operators to get the following equation of motion

$$i\hbar \frac{\partial \hat{\Psi}(\mathbf{r}, t)}{\partial t} = H_0 \hat{\Psi}(\mathbf{r}, t) + \int d\mathbf{r}' \hat{\Psi}^\dagger(\mathbf{r}', t) U(\mathbf{r} - \mathbf{r}') \hat{\Psi}(\mathbf{r}', t) \hat{\Psi}(\mathbf{r}, t) \quad (4.6)$$

As already explained in chapter 1, BEC involves the macroscopic occupation of a single quantum state. Particularly at sufficiently low temperature, for a weakly interacting system, it is appropriate to use a mean field approach. We decompose the field operator as

$$\hat{\Psi}(\mathbf{r}, t) = \psi(\mathbf{r}, t) + \delta\Psi'(\mathbf{r}, t) \quad (4.7)$$

Here $\psi(\mathbf{r}, t) \equiv \langle \hat{\Psi}(\mathbf{r}, t) \rangle$ is the classical field or the expectation value of $\hat{\Psi}(\mathbf{r}, t)$. The wave function of macroscopically occupied single particle state generally termed as macroscopic wavefunction, defines order parameter of the system. For a weakly interacting system, the order parameter can be thought of as the one particle wave function into which the particles Bose condense, multiplied by the number of condensed atoms. This picture is good for a non- or weakly interacting system. For a strongly interacting system a better definition for the order parameter is the *expectation value of the particle annihilation operator*.

The latter quantity $\delta\Psi'(\mathbf{r}, t)$ represents the fluctuations about this value and associated with the non-condensed atoms, induced by thermal and quantum effects.

In the limit of zero temperature, the thermal component of the system can be neglected. Moreover, due to the weakly-interacting nature ($a \ll \lambda_{dB}$) of the condensate, quantum depletion at zero temperature is negligible and hence as a first approximation one can neglect the non-condensed atoms component i.e. $\delta\Psi'(\mathbf{r}, t) \rightarrow 0$ and consider only the condensed atoms contribution i.e. $\hat{\Psi}(\mathbf{r}, t) \rightarrow \psi(\mathbf{r}, t)$. Here, a is the inter atomic separation and λ_{dB} is the de-Broglie wavelength defined in equation 1.3 in Chapter 1.

Also, when the gas is sufficiently dilute, the atomic interactions are dominated by low energy, two-body s-wave collisions, characterised by a single parameter a which is the s-wave scattering length. The effective two body potential is given by

$$U(\mathbf{r} - \mathbf{r}') = g\delta(\mathbf{r} - \mathbf{r}') \quad (4.8)$$

and is characterised by a single parameter a which is the s wave scattering length. The parameter g is given by

$$g = \frac{4\pi\hbar^2 a}{2m} \quad (4.9)$$

where m is the atomic mass. It is to be noted that the interactions are attractive or repulsive depending on whether $g < 0$ or $g > 0$ respectively. Substituting equation (4.8) into (4.6) we get the equation for the macroscopic wave function

$$i\hbar \frac{\partial \psi(\mathbf{r}, t)}{\partial t} = \left(-\frac{\hbar^2}{2m} \nabla^2 + V_{ext}(\mathbf{r}, t) + g|\psi(\mathbf{r}, t)|^2 \right) \psi(\mathbf{r}, t) \quad (4.10)$$

This time-dependent equation is known as the Gross-Pitaevskii equation (GPE) [19, 174]. The GPE resembles the time-dependent Schrödinger equation apart from the $|\psi(\mathbf{r}, t)|^2$ nonlinear term, which arises due to the atomic interactions and has important effects on the properties of the system.

The time independent solutions of the GPE can be written in the form

$$\psi(\mathbf{r}, t) = \psi(\mathbf{r}) e^{-i\mu t/\hbar} \quad (4.11)$$

Here, μ is the chemical potential which is the energy associated with adding or removing a particle from the system and characterises the ground state energy of the condensate. Substituting equation (4.11) into (4.10), we get the following time independent GPE as

$$\left(-\frac{\hbar^2}{2m} \nabla^2 + V_{ext}(\mathbf{r}, t) + g|\psi(\mathbf{r})|^2 \right) \psi(\mathbf{r}) = \mu \psi(\mathbf{r}) \quad (4.12)$$

The GPE is used to study the macroscopic behavior of the BEC, at length scales larger than the interatomic separation distance. The validity of this equation depends on the macroscopic occupation of the ground state and small fluctuation around mean field which is necessary for making the Bogoliubov approximation [3]. Also, the interatomic distances should be much larger than the interaction range such that a contact potential can be employed.

Alternatively the GPE can be obtained by the variational formulation starting from the action principle

$$\delta \int_{t_1}^{t_2} \mathcal{L} dt = 0 \quad (4.13)$$

where the mean field Lagrangian \mathcal{L} is given by

$$\begin{aligned} \mathcal{L} &= \int d\mathbf{r} \left[\frac{i\hbar}{2} \left(\psi^* \frac{\partial \psi}{\partial t} - \psi \frac{\partial \psi^*}{\partial t} \right) \right] - E \\ &= \int d\mathbf{r} \left[\frac{i\hbar}{2} \left(\psi^* \frac{\partial \psi}{\partial t} - \psi \frac{\partial \psi^*}{\partial t} \right) - \mathcal{E} \right] \end{aligned} \quad (4.14)$$

Here, E is the energy and \mathcal{E} is the energy density given by

$$\mathcal{E} = \frac{\hbar^2}{2m} |\nabla \psi(\mathbf{r})|^2 + V_{ext}(\mathbf{r}, t) |\psi(\mathbf{r})|^2 + g |\psi(\mathbf{r})|^4 \quad (4.15)$$

In the variational principle the variations of ψ or ψ^* is arbitrary with the requirement of suitable boundary conditions. The variational principle can be used for the approximate solutions of dynamical problems with an appropriate choice of the trial function for ψ .

The GPE has proven to give an excellent qualitative and quantitative description of many static and dynamic properties in dilute BECs at temperature much less than the transition temperature. Examples include the condensate density profile, dynamics under expansion, interference effects, collective excitations and sound [174], vortices [175–177] and bright [178, 179] and dark solitary waves [180].

In this section, we use GPE to determine the dynamics of the condensate, and derive equations very similar to those of classical hydrodynamics. This is very useful in calculating the collective modes of the condensate. As will be explained in further sections, this is an extremely important property to study the dynamics of the condensate.

4.1.1 Hydrodynamic theory

The Gross Pitaevskii equation (4.6) may be conveniently represented in terms of classical fluid dynamics by employing the Madelung transformation [181]

$$\psi(\mathbf{r}, t) = \sqrt{\rho(\mathbf{r}, t)} e^{i\phi(\mathbf{r}, t)} \quad (4.16)$$

where $\rho(\mathbf{r}, t)$ can be identified as superfluid density and $\phi(\mathbf{r}, t)$ represents a macroscopic phase factor. The fluid velocity is defined by the gradient of the phase i.e

$$\mathbf{v}_s(\mathbf{r}, t) = \frac{\hbar}{m} \nabla \phi(\mathbf{r}, t) \quad (4.17)$$

Substituting equations (4.16) and (4.17) into GPE (4.6) and equating real and imaginary parts, we get

$$\frac{\partial \rho}{\partial t} + \nabla \cdot (\rho \mathbf{v}_s) = 0 \quad (4.18)$$

$$m \frac{\partial \mathbf{v}_s}{\partial t} + \nabla \left(\frac{1}{2} m v_s^2 + V_{ext} + g\rho - \frac{\hbar^2}{2m\sqrt{\rho}} \nabla^2 \sqrt{\rho} \right) = 0 \quad (4.19)$$

These equations resembles the classical continuity and Euler equation for an ideal fluid. The Euler equation (4.19) can also be written as

$$\frac{\partial \mathbf{v}_s}{\partial t} + \nabla \left(\frac{1}{2} v_s^2 \right) = -\nabla \left(\frac{V_{ext} + g\rho + T}{m} \right) = -\frac{\nabla \mu}{m} = -\frac{\nabla P}{m\rho} \quad (4.20)$$

where $\mu = (V_{ext} + g\rho + T)$ is the chemical potential, which is related to pressure as $dP = \rho d\mu$. T is the quantum pressure term given by

$$T = \frac{\hbar^2}{2m} \left[\frac{(\nabla\rho)^2}{4\rho^2} - \frac{1}{2\rho} \nabla^2\rho \right] \quad (4.21)$$

As we can see from the form of the quantum pressure term, it describes the forces due to spatial variations in the magnitude of the wavefunction of the condensate. This term becomes less important when the spatial variations in the density occur on length scale larger than the coherence length and hence can be neglected.

In the hydrodynamic formalism, we have specified the equation of motion of the condensate in terms of a local density $\rho(\mathbf{r}, t)$ and a local velocity $\mathbf{v}_s(\mathbf{r}, t)$, which are the degrees of freedom of the condensate wave function. For ordinary liquids and gases, generally one needs a microscopic description in terms of distribution function because there are many more degrees of freedom associated with their motion [19].

Such a hydrodynamic description can be employed for ordinary gases and liquids also, provided the collisions between particles are sufficiently frequent that thermodynamic equilibrium is established locally. In such situation, the motion of the fluid can be specified completely in terms of the local particle density, the local velocity, and the local temperature. At zero temperature, just as for condensate, the motion is completely described in terms of the local density and the local fluid velocity. The equations of motion for a perfect fluid and a condensate are similar under such conditions, as they are just the expressions of the particle number and momentum conservation law for the systems. However, the physical reasons behind such description are quite different for the two situations [19].

The hydrodynamic equations can be used to investigate the properties of elementary excitations by considering small deviations of the state of the gas from the equilibrium state. BEC exhibits completely different type of excitations termed as collective excitations. These excitations are associated with density fluctuations and involve the collective wave-like motion of all particles. A striking property of a BEC is that its elementary and collective excitations are identical. This is because of the fact that all atoms in a condensate are described by the same single-particle wave function. Thus, any excitation involving one particle automatically involves all others leading to a collective response, and hence it is termed as collective excitation of the condensate.

The calculations of the energy of the elementary excitations can be determined from the hydrodynamic formalism [19] and the results agree with the spectrum derived by Bogoliubov method [3] at low values of wave vector. The calculations provides sound waves for the BEC superfluid systems which are obvious elementary excitations in hydrodynamic

systems. For ultracold atomic BEC system, such elementary excitations give rise to appearance of additional sound mode termed as *second sound* which is the signature of the presence of superfluidity in the system. Moreover, in many experimental situations, the response of the system will be determined by its elementary excitations produced by application of small fluctuations to the equilibrium system and study the response of system after it.

Such hydrodynamic formalism and determination of collective excitations has been extended for rotating condensates, and there are a number of theoretical [104, 182–185] and experimental works [34] which describe the same. Collective excitations is one of the most useful tool to study the dynamics of rotating condensates with vortex lattice [34, 182, 184] and it is the topic of discussion of next section.

4.1.2 Hydrodynamic equations for a rotating superfluid

We consider a superfluid gas rotating in the xy plane with angular velocity $\mathbf{\Omega} = \Omega \hat{z}$, with \hat{z} as the unit vector along the z direction. To get a time dependent description of such system, we consider the Gross Pitaevskii equation in the rotating frame can be written as

$$i\hbar \frac{\partial \psi}{\partial t} = -\frac{\hbar^2}{2m} \nabla^2 \psi + V_{ext} \psi + g|\psi|^2 \psi - \Omega \hat{L}_z \psi \quad (4.22)$$

Substitute $\psi = \sqrt{\rho} e^{i\phi}$ in terms of density and phase in above equation (4.22) and equating the real and imaginary parts, we get

$$\frac{\partial \rho}{\partial t} + \nabla \cdot [\rho(\mathbf{v}_s - \mathbf{\Omega} \times \mathbf{r})] = 0 \quad (4.23)$$

and,

$$\frac{\partial \mathbf{v}_s}{\partial t} + \nabla \left(\frac{1}{2} \mathbf{v}_s^2 + \frac{V_{ext} + g\rho + T}{m} - \mathbf{v}_s \cdot (\mathbf{\Omega} \times \mathbf{r}) \right) = 0 \quad (4.24)$$

Equation (4.23) and (4.24) are the modified Continuity equation and Euler equation for a condensate rotating at an angular frequency $\mathbf{\Omega}$. Here, \mathbf{v}_s is the velocity in the laboratory (inertial) frame of reference. We briefly discuss the relation between the inertial and rotational frames of reference below [186].

Laboratory and Rotational frames of reference

We consider a frame of reference rotating at an angular velocity $\mathbf{\Omega}$ with respect to an inertial frame. If a position vector is at rest in rotating frame, it undergoes circular

motion with angular velocity $\mathbf{\Omega}$ as seen in the inertial frame, thus

$$\left(\frac{d\mathbf{r}}{dt}\right)_I = \mathbf{\Omega} \times \mathbf{r} \quad (4.25)$$

We use $(\cdot)_I$ and $(\cdot)_R$ to indicate quantities measured in the inertial and rotating frame respectively. Assuming now that, \mathbf{r} moves in the rotating frame, then

$$\left(\frac{d\mathbf{r}}{dt}\right)_I = \left(\frac{d\mathbf{r}}{dt}\right)_R + \mathbf{\Omega} \times \mathbf{r}$$

or,

$$\mathbf{v}_{sI} = \mathbf{v}_{sR} + \mathbf{\Omega} \times \mathbf{r} \quad (4.26)$$

Applying equation (4.25) to \mathbf{v}_I , we get

$$\begin{aligned} \left(\frac{d\mathbf{v}_{sI}}{dt}\right)_I &= \left(\frac{d\mathbf{v}_{sI}}{dt}\right)_R + \mathbf{\Omega} \times \mathbf{v}_{sI} \\ &= \left(\frac{d\mathbf{v}_{sR}}{dt}\right)_R + \mathbf{\Omega} \times \left(\frac{d\mathbf{r}}{dt}\right)_R + \mathbf{\Omega} \times (\mathbf{v}_{sR} + \mathbf{\Omega} \times \mathbf{r}) \\ &= \left(\frac{d\mathbf{v}_{sR}}{dt}\right)_R + 2\mathbf{\Omega} \times \mathbf{v}_{sR} + \mathbf{\Omega} \times (\mathbf{\Omega} \times \mathbf{r}) \end{aligned} \quad (4.27)$$

Thus, we hereby use above equations (4.26) and (4.27) to write the continuity and Euler equations in terms of velocity in rotating frame \mathbf{v}_{sR} .

$$\frac{\partial \rho}{\partial t} + \nabla \cdot (\rho \mathbf{v}_{sR}) = 0 \quad (4.28)$$

and,

$$\frac{\partial \mathbf{v}_{sR}}{\partial t} + 2\mathbf{\Omega} \times \mathbf{v}_{sR} - \nabla \left(\frac{1}{2} \Omega^2 r^2 \right) + \nabla \left(\frac{V_{ext} + g\rho + T}{m} \right) = 0 \quad (4.29)$$

We shall drop the subscript R with the understanding that from now on all quantities are measured in the rotating frame, thus equations (4.28) and (4.29) can be written as

$$\frac{\partial \rho}{\partial t} + \nabla \cdot (\rho \mathbf{v}_s) = 0 \quad (4.30)$$

$$m \left(\frac{\partial \mathbf{v}_s}{\partial t} + 2\mathbf{\Omega} \times \mathbf{v}_s \right) = -\frac{\nabla P'}{\rho} \quad (4.31)$$

where

$$P' = \rho \left(V_{ext} + g\rho + T - \frac{1}{2} m \Omega^2 r^2 \right) \quad (4.32)$$

Here, $\frac{1}{2} m \Omega^2 r^2$ is the centrifugal force which modifies the pressure term and $2\mathbf{\Omega} \times \mathbf{v}_s$ represents the Coriolis force. We mention here that we neglect the overall effect of the

trap potential, because in the limit of high rotation, $\Omega \sim \omega$ the term $V_{ext} - \frac{1}{2}m\Omega^2 r^2 = \frac{1}{2}m(\omega^2 - \Omega^2)r^2$ is zero and hence the trap is effectively cancelled by the centrifugal force.

Equation (4.31) can be written as

$$m \left(\frac{\partial \mathbf{v}_s}{\partial t} + (2\boldsymbol{\Omega} + \nabla \times \mathbf{v}_s) \times \mathbf{v}_s \right) = -\frac{\nabla P'}{\rho} \quad (4.33)$$

where $\nabla \times \mathbf{v}_s$ is zero except at the location of vortices. The transformation to the rotating frame changes the vorticity too, which means that the velocity field which was irrotational in the laboratory frame, possesses the vorticity $\nabla \times \mathbf{v}_s = -2\boldsymbol{\Omega}$ after the transformation. We always deal with absolute vorticity which is related to the superfluid velocity in the rotating frame by the relation

$$\tilde{\omega} = 2\boldsymbol{\Omega} + \nabla \times \mathbf{v}_s \quad (4.34)$$

Hence the above equation (4.33) is

$$m \left(\frac{\partial \mathbf{v}}{\partial t} + \tilde{\omega} \times \mathbf{v}_s \right) = -\frac{\nabla P'}{\rho} \quad (4.35)$$

It is to note that the continuity equation represents the law of conservation of mass and the Euler equation is momentum conservation equation, balancing the Coriolis and the Centrifugal force arising due to rotation.

It is known that when a quantum fluid is rotated at a frequency Ω , it attempts to distribute the vorticity as uniformly as possible. This is similar to a rigid body, for which the vorticity is constant $\nabla \times \mathbf{v}_s = 2\boldsymbol{\Omega}$. As mentioned in equation (4.17), the circulation of the superfluid velocity field \mathbf{v} is quantized in units of $\kappa = h/M$, with M as the atomic mass. These quantized vortex lines are distributed in the fluid with a uniform area density [143]

$$n_v = \frac{2\Omega}{\kappa} \quad (4.36)$$

Thus the quantum fluid achieves the same average vorticity as that of a rigidly rotating body, when *coarse-grained* over several vortex lines.

For rotating ultracold atomic superfluids, the vortices arrange themselves in highly ordered triangular lattices [187]. This has been both theoretically predicted in context of type-II superconductors by Abrikosov [83] and then experimentally verified in rotating ultracold atomic condensates [187]. The striking feature of the experimental observation was the extreme regularity of these lattices, free of any major distortions, even near the boundary. Such regular vortex lattices were first predicted for quantized magnetic flux

lines in type-II superconductors [83], and further Tkachenko showed that their lowest energy configuration structure should be triangular for an infinite system [185].

Thus, we average above equation (4.35) over a vortex lattice cell, the assumption is that any vortex line bears only one quantum of circulation $\kappa = h/m$, with m as the mass of the atom. The vorticity is given by

$$\tilde{\omega}(\mathbf{R}) = \sum_j \kappa_j \int d\mathbf{R}_j \delta(\mathbf{R} - \mathbf{R}_j) \quad (4.37)$$

Substituting in equation (4.35),

$$m \left(\frac{\partial \mathbf{v}_s}{\partial t} + \sum_j \kappa_j \int [d\mathbf{R}_j \times \mathbf{v}_s(\mathbf{R})] \delta(\mathbf{R} - \mathbf{R}_j) \right) = -\frac{\nabla P'}{\rho} \quad (4.38)$$

In above equation (4.38), the second term involves local velocity of the point on the vortex line, which is denoted by \mathbf{v}_L . Thus, when averaged over the vortex lattice cell, the hydrodynamic equation becomes

$$m \left(\frac{\partial \mathbf{v}_s}{\partial t} + \tilde{\omega} \times \mathbf{v}_L \right) = -\frac{\nabla P'}{\rho} \quad (4.39)$$

with \mathbf{v}_s as the averaged superfluid velocity and $\tilde{\omega}$ as the absolute vorticity. Here, due to the singular nature of the vorticity field, the velocity of the fluid in the vector product remains unaffected. It continues to be the local velocity of the point of vortex line and denoted by \mathbf{v}_L . Equation (4.39) is obtained by averaging equation (4.35) over the entire vortex lattice cell.

The velocity of the vortex is given by \mathbf{v}_L and it is equal to time derivative of the displacement vector of the vortex lattice $\mathbf{v}_L = \frac{d\mathbf{u}^v}{dt}$. Alternatively, for a set of parallel vortex lines [104], the velocity of the i th vortex line is given by

$$\frac{d\mathbf{u}_i^v}{dt} = \sum_{j \neq i} \frac{\kappa_j \times (\mathbf{u}_i^v - \mathbf{u}_j^v)}{2\pi |\mathbf{u}_i^v - \mathbf{u}_j^v|^2} \quad (4.40)$$

with \mathbf{u}_i^v is the position vector of the i th vortex line.

When there is an embedded vortex lattice in the superfluid, there can be small deformations due to the displacement of the vortex lattice [19]. It demands to take into account the elastic behavior of the vortex lattice under long wavelength description. Within this description, the vortex lattice may be treated by continuum elasticity theory, with the condition that the quantities are averaged over a volume containing many vortices, which has been explained above. This limits the validity of the hydrodynamic approach to wavelengths that are long compared to the inter vortex spacing. Thus, the next step

is to rewrite equation (4.39) as

$$m \left(\frac{\partial \mathbf{v}_s}{\partial t} + \tilde{\omega} \times \mathbf{v}_s + \tilde{\omega} \times (\mathbf{v}_L - \mathbf{v}_s) \right) = -\frac{\nabla P'}{\rho}$$

or,

$$m \left(\frac{\partial \mathbf{v}_s}{\partial t} + \tilde{\omega} \times \mathbf{v}_s \right) = -\frac{\nabla P'}{\rho} - \frac{\mathbf{f}}{\rho}$$

with

$$\mathbf{f} = -m\rho\tilde{\omega} \times (\mathbf{v}_L - \mathbf{v}_s) \quad (4.41)$$

Here, \mathbf{f} is the force acting per unit volume of the fluid moving with velocity \mathbf{v}_s , and it should be connected with a variation of energy due to vortex displacements.

To determine the complete set of hydrodynamic equations for a rotating superfluid, we write the total energy density in terms of the density ρ , phase ϕ and the displacement of the vortex lattice \mathbf{u}^v as below

$$\mathcal{E} = \mathcal{E}_{in}(\rho) + \mathcal{E}_{ph}(\phi) + \mathcal{E}_{el}(\nabla \mathbf{u}^v) \quad (4.42)$$

with

$$\mathcal{E}_{in} = \frac{\hbar^2}{2m} \left(\frac{1}{4\rho} (\nabla \rho)^2 \right) + \frac{g}{2} \rho^2 = \mu \rho \quad (4.43)$$

$$\mathcal{E}_{ph} = \frac{\hbar^2}{2m} \rho (\nabla \phi)^2 - m\rho \mathbf{v}_s \cdot (\Omega \times \mathbf{r}) \quad (4.44)$$

$$\mathcal{E}_{el} = \frac{1}{2} \lambda_{iklm}^v \epsilon_{ik}^v \epsilon_{lm}^v \quad (4.45)$$

Here, \mathcal{E}_{in} is the internal energy density which depends only on the fluid density ρ , and \mathcal{E}_{ph} is the energy density contribution due to the phase ϕ of the fluid, written in terms of the fluid velocity $\mathbf{v}_s = \frac{\hbar}{m} \nabla \phi$.

The last equation (4.45) is the general form of the free energy of the deformed crystal [188]. It is a functional of vortex line displacements \mathbf{u}^v . Here ϵ_{ik} is the strain tensor, given by

$$\epsilon_{ik} = \frac{1}{2} \left(\frac{\partial u_i}{\partial x_k} + \frac{\partial u_k}{\partial x_i} \right) \quad (4.46)$$

and λ_{iklm} is a tensor of rank four, called the *elastic modulus tensor*. The number of different components of a tensor of rank four is in general 21, and if the crystal possesses symmetry, relations exist between the various components of the tensor λ_{iklm} so that the number of independent components is less than 21. For a hexagonal system, the

modulii of elasticity components reduces to 5 in number due to symmetry properties [188]. We discuss this in detail in section 4.1.3.

From equation (4.45), we see that the elastic energy of the lattice, depends on the gradient of the displacement field \mathbf{u}^v , and not on the displacement vector itself. Now, we use coupled hydrodynamic-elastic formalism for further calculations and write the change in energy in terms of functional derivatives of the density, phase and gradient of the displacement vector.

$$d\mathcal{E} = \frac{\partial \mathcal{E}}{\partial \rho} d\rho + \frac{\partial \mathcal{E}}{\partial \phi} d\phi + \frac{\partial \mathcal{E}}{\partial \nabla \mathbf{u}^v} d\nabla \mathbf{u}^v \quad (4.47)$$

We calculate the last term in above equation (4.47) as follows. It is known that for the case of rotating superfluids the vortices arrange themselves in the form of triangular lattice with hexagonal symmetry [185]. It is known that triangular lattice is isotropic i.e the elastic properties are identical in all directions and hence the number of essential elastic constants which describe the system completely reduces to 2 [188]. Thus we can use the elastic energy density expression for an isotropic triangular vortex lattice to calculate the variation of elastic energy of the vortex lattice with respect to the displacement vector.

We consider the axis of rotation to be in the z direction. The elastic energy density \mathcal{E}_{el} for a triangular lattice with hexagonal symmetry [183, 188] is given by

$$\mathcal{E}_{el} = 2C_1(\nabla \cdot \mathbf{u}^v)^2 + C_2 \left[\left(\frac{\partial u_x^v}{\partial x} - \frac{\partial u_y^v}{\partial y} \right)^2 + \left(\frac{\partial u_x^v}{\partial y} + \frac{\partial u_y^v}{\partial x} \right)^2 \right] \quad (4.48)$$

where C_1 and C_2 are constants related to the compressional modulus and shear modulus of the vortex lattice. This implies

$$f_{el,i} = -\frac{\delta \mathcal{E}_{el}}{\delta u_i^v} = -\frac{\partial}{\partial x_k} \left(\frac{\delta \mathcal{E}_{el}}{\delta (\partial u_k^v / \partial x_i)} \right)$$

which gives

$$\mathbf{f}_{el} = -[4C_1 \nabla (\nabla \cdot \mathbf{u}^v) + 2C_2 \nabla^2 \mathbf{u}^v] \quad (4.49)$$

We can also alternatively write the expression in terms of Lamé coefficients as

$$\mathbf{f}_{el} = -[(\lambda^v + \mu_s^v) \nabla (\nabla \cdot \mathbf{u}^v) + \mu_s^v \nabla^2 \mathbf{u}^v] \quad (4.50)$$

where $\lambda^v = K^v - \frac{2}{3}\mu_s^v$ is the Lamé coefficient [188] with K^v and μ_s^v as the compressibility and shear modulus of the vortex lattice.

Thus, from equations (4.140), (4.48) and (4.49), we can write

$$2\Omega\rho[\hat{z} \times (\mathbf{v}_L - \mathbf{v}_s)] = \frac{[4C_1\nabla(\nabla \cdot \mathbf{u}^v) + 2C_2\nabla^2\mathbf{u}^v]}{m} \quad (4.51)$$

Equations (4.30), (4.39) and (4.51) constitute the equations of motion of a superfluid in a rotating co-ordinate frame and are written together as below

$$\frac{\partial\rho}{\partial t} + \nabla \cdot (\rho\mathbf{v}_s) = 0 \quad (4.52)$$

$$\frac{\partial\mathbf{v}_s}{\partial t} + 2\Omega \times \mathbf{v}_L = -\frac{\nabla P'}{\rho} \quad (4.53)$$

$$2\Omega\rho[\hat{z} \times (\mathbf{v}_L - \mathbf{v}_s)] = \frac{[4C_1\nabla(\nabla \cdot \mathbf{u}^v) + 2C_2\nabla^2\mathbf{u}^v]}{m} \quad (4.54)$$

Above set of equations (4.52-4.54) are the hydrodynamic equations of motion for a rotating superfluid and describes the long wavelength low frequency behavior of the system. Before going into the dispersion calculations for the hydrodynamic equations obtained above, we briefly describe the symmetry properties and the elastic constants for crystals in next section.

4.1.3 Components of the elastic modulus tensor

The elastic modulus tensor λ_{ijkl} used in equation (4.134) in above section, is a rank four tensor which relates the stress tensor to the strain tensor. This is because the stress and strain tensors are both 2nd order tensors and it implies that the most general relationship between them would involve a fourth order tensor. It is also termed as *stiffness tensor*. In the most general case, the stiffness tensor λ_{ijkl} has $3 \times 3 \times 3 \times 3 = 81$ components.

But, both the stress and strain tensors are symmetric so that the stiffness tensor must also have some symmetries, called *minor symmetries*

$$\lambda_{ijkl} = \lambda_{jikl} = \lambda_{ijlk}$$

In elasticity, there exists a strain energy density function W which is related to stress by

$$\sigma_{ij} = \frac{\partial W}{\partial e_{ij}}$$

which implies

$$\lambda_{ijkl} = \frac{\partial^2 W}{\partial e_{ij} \partial e_{kl}}$$

Here, since the order of differentiation is irrelevant, the stiffness tensor has the property

$$\lambda_{ijkl} = \lambda_{klij}$$

and termed as the *major symmetry* of the stiffness tensor. This reduces the number of elastic constants to 21, the most for a completely anisotropic solid.

For an isotropic medium, the stiffness tensor has no preferred direction which implies that an applied force will give the same displacements (relative to the direction of the force), no matter the direction in which the force is applied [113, 189]. Thus the material properties are independent of direction. Such materials have only 2 independent variables, in their stiffness matrix as opposed to 21 elastic constants in general anisotropic case. The Stiffness tensor for an isotropic material can be expressed as

$$\lambda_{ijkl} = \lambda \delta_{ij} \delta_{kl} + \mu (\delta_{ik} \delta_{jl} + \delta_{il} \delta_{jk})$$

where λ and μ are Lamé constants, with μ as the shear modulus and λ is related to Poisson's ratio ν as

$$\lambda = \frac{2\mu\nu}{1-2\nu}$$

After this brief description of the elastic modulus tensor and its properties for isotropic and anisotropic lattices, we carry on with the calculations for dispersion relations for rotating superfluid using the hydrodynamic equations of motion obtained in section 4.1.2.

4.1.4 Collective modes in a vortex lattice for rotating ultracold atomic superfluids

From the hydrodynamic equations of motion for a rotating superfluid, we can determine the excitation spectrum for the low energy long wavelength modes of the system. To characterize the dynamics of the system, we investigate the small perturbations around the equilibrium state and thus write the linearized version of above equations as

$$\frac{\partial \rho'}{\partial t} + \rho_0 \nabla \cdot \mathbf{v}_s = 0 \quad (4.55)$$

$$\rho_0 \left(\frac{\partial \mathbf{v}_s}{\partial t} + 2\Omega \times \mathbf{v}_L \right) = -c_s^2 \nabla \rho' \quad (4.56)$$

$$2\Omega\rho_0 \times (\mathbf{v}_L - \mathbf{v}_s) = \frac{[4C_1 \nabla(\nabla \cdot \mathbf{u}^v) + 2C_2 \nabla^2 \mathbf{u}^v]}{m} \quad (4.57)$$

As mentioned before, the trapping effectively gets cancelled by the centrifugal term in the limit $\Omega \sim \omega$ and the system is homogenous. Here $\rho'(\mathbf{r})$ is the oscillating component of the density $\rho(\mathbf{r}) = \rho_0(\mathbf{r}) + \rho'(\mathbf{r})$ around the equilibrium homogenous density, c_s is the sound velocity which is given by the expression

$$\nabla P' = mc_s^2 \nabla \rho' \quad (4.58)$$

The dispersion relation [104, 183, 184] is obtained by considering the spectrum of plane waves $\propto \exp(i\mathbf{q} \cdot \mathbf{r} - i\omega t)$

$$\omega^4 - \omega^2 \left[4\Omega^2 + \left(c_s^2 + \frac{4(C_1 + C_2)}{m\rho} \right) q^2 \right] + \frac{2c_s^2 C_2}{m\rho} q^4 = 0 \quad (4.59)$$

As is generally the case that the shear mode of the vortex lattice which depends on C_2 is very small, in the long wavelength limit the condition becomes

$$\frac{2c_s^2 C_2}{m\rho} q^4 \ll \{ 4\Omega^2 + \left(c_s^2 + \frac{4(C_1 + C_2)}{m\rho} \right) q^2 \}^2 \quad (4.60)$$

the modes frequencies are given by

$$\omega_I^2 = 4\Omega^2 + \left(c_s^2 + \frac{4(C_1 + C_2)}{m\rho} \right) q^2 \quad (4.61)$$

and,

$$\omega_T^2 = \frac{2C_2}{m\rho} \left[\frac{c_s^2 q^4}{4\Omega^2 + \left(c_s^2 + \frac{4(C_1 + C_2)}{m\rho} \right) q^2} \right] \quad (4.62)$$

The first mode given in equation (4.61) is the standard inertial mode of a rotating superfluid. In the limit $\Omega^2 \ll c_s^2 q^2$, we can see that it yields the sound wave with frequency varying linearly with q and given by

$$\omega_I^2 = \left(c_s^2 + \frac{4(C_1 + C_2)}{m\rho} \right) q^2 \quad (4.63)$$

whereas in the other limit, for $\Omega^2 \gg c_s^2 q^2$, the mode frequency begins at 2Ω

$$\omega_I^2 = 4\Omega^2 + \left(c_s^2 + \frac{4(C_1 + C_2)}{m\rho} \right) q^2 \quad (4.64)$$

which is the gapped sound mode. Further, in the limit $4(C_1 + C_2) \ll m\rho c_s^2$ it corresponds to the usual sound mode of the superfluid modified by rotation [104, 182]. This limit follows from the fact that the elastic constants of the vortex lattice are too small

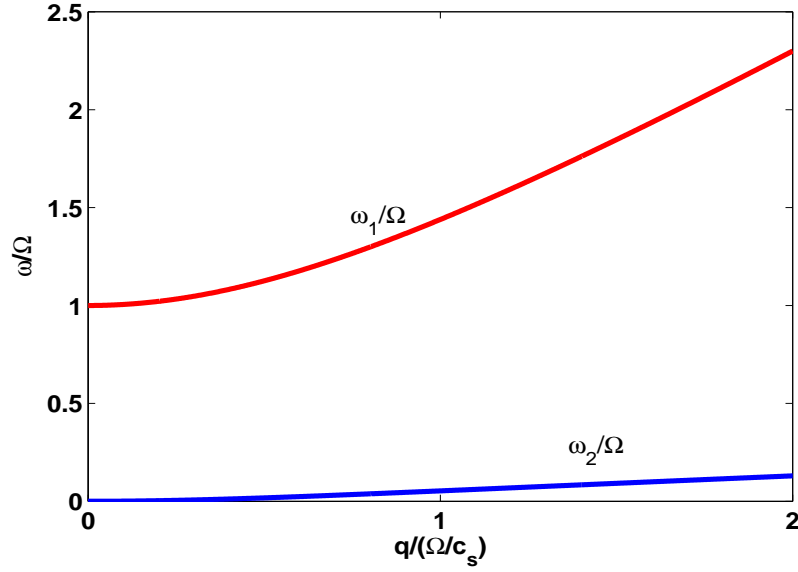


FIGURE 4.1: Inertial and Tkachenko mode frequencies vs wave vector, in units of Ω/c_s for a rotating superfluid system. Both the mode frequencies are in units of Ω .

to contribute and their speed contribution can be taken to be very small compared to the usual sound speed c_s .

These modes are termed as inertial waves which implies that the vortices rotate about the equilibrium position in the same sense as the underlying superfluid.

Essentially in the limit when there is no vortex lattice (vanishing elastic constants) in the system, equation (4.64) gives the inertial wave ($\omega_I = 2\Omega$) familiar for rotating fluids [104] in the $q = 0$ limit and equation (4.63) gives the usual linear spectrum of superfluids $\omega_I = c_s q$. It is interesting to point out that the rotation induced gap is $(2\Omega)^2$ because of the inherent 2Ω in the Coriolis force term (4.31). This is because the vorticity assumes a value $\nabla \times \mathbf{v}_s = -2\Omega$ in the rotating frame, whereas it was irrotational in the laboratory frame.

The second mode (4.62) is the elliptically polarized Tkachenko mode [182, 185] observed in [34]. The elliptical nature of polarization is described in detail in Appendix A. The Tkachenko modes are the lowest energy branch of the spectrum involving the oscillations of the vortex lines about their equilibrium position. Microscopically, the vortices are observed to perform elliptical oscillations with major axis perpendicular to the direction of wave propagation. On a macroscopic scale over length scale $\gg u^v$, the lattice undergoes shear distortions which causes the rotation of the array to alternatively slow down and speed up. This ability of the fluid to support transverse Tkachenko waves is remarkable and can be seen as arising from a non-trivial shear modulus due to the intervortex force.

The components of velocity \mathbf{v}_s and \mathbf{v}_L are introduced as follows: the component v_{sq} and v_{Lq} along the wave vector \mathbf{q} and the component v_{st} and v_{Lt} along the axis normal to both \mathbf{q} and the rotation axis. The oscillatory motion of the fluid with no vortex lattice is circularly polarized. As the Tkachenko wave velocity increases from zero, the oscillatory motion of the fluid transforms from the circularly polarized motion into the motion with transverse linear polarization corresponding to the Tkachenko wave. For vortices, they move in the xy plane on elliptical paths with their major axes perpendicular to \mathbf{q} . The ratio of the axes of the ellipse is small at $\omega \ll \Omega$ and hence the small longitudinal components of the velocities v_q and v_{Lq} can be neglected. This allows to consider the slow motion in the xy plane to be transverse with coinciding vortex and averaged fluid velocities $v_t = v_{Lt}$. Thus, the Tkachenko waves are the transverse sound modes in a vortex lattice [104, 183].

In the limit

$$4(C_1 + C_2) \ll m\rho c_s^2 \quad (4.65)$$

the dispersion relation (4.62) becomes

$$\omega_T^2 = \frac{2C_2 q^2}{m\rho} \frac{c_s^2 q^2}{4\Omega^2 + c_s^2 q^2} \quad (4.66)$$

where we can define the Tkachenko wave velocity [185]

$$c_T = \sqrt{\frac{2C_2 q^2}{m\rho}} \quad (4.67)$$

It is to note that large values of q , the frequency of Tkachenko mode (4.62) is linear in q and proportional to the square root of elastic constant C_2 similar to the shear wave in an isotropic solid, i.e

$$\omega_T = \sqrt{\frac{2C_2}{m\rho}} q$$

This is actually the limit where the Tkachenko wave frequency depends linearly on wave vector q and is related by the shear modulus C_2 of the isotropic vortex lattice, and hence it is the pure shear wave limit of the vortex lattice oscillations.

Whereas in the long wavelength limit $q \ll \Omega/c_s$ which we are studying, the Tkachenko mode wave with the sound spectrum $\omega_T = c_T q$ transforms to a mode of lower frequency with $\omega_T \propto q^2$, and is given by

$$\omega_T = \sqrt{\frac{C_2}{2m\rho}} \frac{c_s q^2}{\Omega}$$

These soft Tkachenko waves for oscillations of a vortex lattice have been observed experimentally [34] for rotating ultracold atomic superfluids and in the next subsection,

we describe in detail how the oscillations are measured experimentally for a rotating superfluid system.

4.1.5 Experimental measurement of Tkachenko waves

The first experimental measurement of Tkachenko waves in a rotating superfluid of ultracold atomic condensate was done by Coddington et.al [34]. It involved firstly the formation of vortex lattice in the condensate, followed by perturbing the vortex lattice and subsequently measuring the lattice oscillations in the system. The first step involves the generation of a lattice of vortices, which is done by rotating the trap potential and hence the condensate at high frequency which results in the formation of vortex lattice in the condensate. The next step is to give small perturbation to the system, which can be done experimentally by two ways.

The 1st mechanism involves the selective removal of atoms [34], which implies that some atoms are removed from the center of the condensate. This is done with the help of a focused laser beam sent through the condensate along the axis of rotation which removes a small fraction of atoms from the center of condensate. This selective removal results in the increase in average angular momentum per particle, and hence requires a corresponding increase in the condensate radius. Moreover, the atom removal also creates a density dip in the center of condensate, which results in the inward motion of fluid flow to fill the density dip.

Thus, there is an inward flow due to the density dip and an outward flow of the fluid due to the expansion of condensate to increase the radius. The Coriolis force due to rotation acts on these flows which causes the inward motion to be diverted in the lattice rotation direction and the outward flow to be diverted in the opposite direction. This produces a sheared fluid flow in the system, which drags the vortices from their equilibrium position and sets the initial conditions for the lattice oscillations.

The other mechanism to create lattice oscillations in vortex lattice is the inverse of the previous method. In this method [34], a beam is sent through the center of the condensate along the direction of rotation which creates a Gaussian dip in the trapping potential of the atoms. Thus, instead of removing the atoms, as done in previous method, here an optical potential is used to draw atoms into the middle of the condensate. The dip in the trapping potential creates an inward fluid flow similar to before.

These two methods are equivalent since one works by creating a dip in the interaction potential and the other creates a similar dip in the trapping potential. After inducing

small lattice oscillations in the system by either of the above mentioned methods, the next and most important step is to measure such lattice oscillations experimentally.

The data is extracted in experiments by destructively imaging the vortex lattice in expansion and then fitting the lattice oscillations [34]. It is performed by fitting a curvilinear row of vortices going through the center of the cloud, after which sinewave is fitted to the locations of the vortex centers, recording the sine amplitude. This is repeated for all the directions of lattice symmetry, with the amplitudes averaged to yield the net fit amplitude of the distortion. In this way, the amplitude of distortion is determined in experiments and the frequency of oscillation is determined by fitting it to the sinewave. The Tkachenko modes are confirmed to exist because of the characteristic s-bend shape and the low resonant frequency of these oscillations as predicted by theory [104, 182–185]

Motivated by theoretical [104, 183, 184] and experimental [34] success in prediction and observation of collective oscillation modes of a vortex lattice in rotating ultracold superfluid system, we study the properties of collective modes of a rotating supersolid within the hydrodynamic approach. In the next section, we develop a hydrodynamic theory for rotating supersolid starting from Gross-Pitaevskii like model for supersolid and calculate the oscillation frequencies for small perturbations around the non-deformed state [110].

4.2 The Gross Pitaevskii like model of Supersolid

Our model is based upon the original form of the GPE for wavefunction of a weakly interacting BEC, as explained in section 4.1.

$$i\hbar \frac{\partial \psi}{\partial t} = -\frac{\hbar^2}{2m} \nabla^2 \psi + V_{ext} \psi + \psi(\mathbf{r}) \int U(|\mathbf{r} - \mathbf{r}'|) |\psi(\mathbf{r}')|^2 d\mathbf{r}' \quad (4.68)$$

The difference with the most commonly used GPE equation (4.10) is that the potential of interaction between atoms includes a non-trivial dependence on the distance although usually for alkali gases this interaction is taken as a delta function in such a way that the cubic term in equation (1) becomes simply $g\psi(\mathbf{r})|\psi(\mathbf{r})|^2$. It was shown in [69] that such non-local GPE can be used to model a supersolid phase with a suitable two body interaction potential $U(|\mathbf{r} - \mathbf{r}'|)$.

The existence of supersolid phase which is periodic pattern in the superfluid density, has been regarded as a manifestation of an instability as the roton minum in the energy momentum spectrum touches the zero energy line [69, 190]. The *roton* minimum can be

interpreted with the help of Feynman's formula for the dispersion relation for excitations of energy E and momentum $\hbar k$ of a Bose liquid [143] given by

$$E(k) = \frac{\hbar^2 k^2}{2mS(k)} \quad (4.69)$$

with m as the atomic mass. We can see that this formula relates the excitation spectrum to the static structure factor $S(k)$. The static structure factor gives the correlation properties and is the Fourier transform of the pair correlation function as explained in chapter 2. Relation (4.69) shows that a peak in the structure factor indicates a minimum in the energy spectrum of the system. A distinguished example of a roton minimum is *He* II, where a roton minimum occurs and is regarded as an indication that the superfluid is very close to crystallization [191, 192]. This is because ordering of atoms in a periodic lattice pattern will give rise to peak in structure factor and hence, a minimum in the the energy spectrum.

In context of mean field GPE with non-local potential, it was proposed by Pomeau et. al [69, 190] that a roton minimum in the dispersion relation could be a signature of first order transition to a crystalline state. Since the inter atomic potentials in ultracold atomic condensates can be tailored, these systems are ideal to see signatures of roton minimum in the dispersion, and hence the possible formation of supersolid phase in the system. Motivated by this, we calculate the Bogoliubov [3] energy momentum dispersion relation in the next subsection and show that certain type of inter atomic potentials results in the roton minimum in the excitation spectrum and hence the instability towards the formation of supersolid phase.

4.2.1 Calculation of Bogoliubov dispersion relation

Our starting point is the uniform nonlinear, nonlocal GPE (4.68)

$$i\hbar \frac{\partial \psi}{\partial t} = -\frac{\hbar^2}{2m} \nabla^2 \psi + \psi(\mathbf{r}, t) \int d\mathbf{r}' U(|\mathbf{r} - \mathbf{r}'|) |\psi(\mathbf{r}', t)|^2 \quad (4.70)$$

where ψ is the condensate wave function, $U(|\mathbf{r} - \mathbf{r}'|)$ is the interparticle potential and $2\pi\hbar$ is the Planck's constant. This equation has a uniform solution $\psi_0 e^{iE_0 t/\hbar}$, and small perturbations around this uniform solution are dispersive waves:

$$\psi(\mathbf{r}, t) = \psi_g + \delta\psi$$

where $\psi_g = \psi_0 e^{-iE_0 t/\hbar}$ and

$$\delta\psi = e^{-iE_0 t/\hbar} [u(\mathbf{r})e^{-i\omega t} - v^*(\mathbf{r})e^{i\omega t}] \quad (4.71)$$

Since, the bose gas is uniform (no trap considered), due to translational invariance, the solutions could be plane waves, with

$$u(\mathbf{r}) = u_q e^{i\mathbf{q}\cdot\mathbf{r}} \quad (4.72)$$

and,

$$v(\mathbf{r}) = v_q e^{-i\mathbf{q}\cdot\mathbf{r}} \quad (4.73)$$

Using above plane wave solutions for $u(\mathbf{r})$ and $v(\mathbf{r})$, the momentum q and frequency ω are found to obey the following dispersion relation

$$\epsilon(\mathbf{q}) = \hbar\omega = \sqrt{\frac{\hbar^2 q^2}{2m} \left(\frac{\hbar^2 q^2}{2m} + 2n\hat{U}_q \right)} \quad (4.74)$$

Here, \hat{U}_q is the fourier transform of the interaction potential

$$\hat{U}_q = \int U(|\mathbf{r}|) e^{i\mathbf{q}\cdot\mathbf{r}} d\mathbf{r} \quad (4.75)$$

We assume that the potential scales as \hat{U}_0 and possesses a single length scale a , thus the spectrum depends on single dimensionless parameter,

$$\Lambda = \frac{ma^2}{\hbar^2} n\hat{U}_0$$

with the following dimensionless dispersion relation

$$\hbar\omega_q = \frac{\hbar^2}{ma^2} \omega_\Lambda(qa) = \sqrt{\frac{(qa)^4}{4} + \Lambda(qa)^2 u^D(qa)} \quad (4.76)$$

For getting some analytical results and for ease of numerics, we choose the interaction U to be positive and constant U_0 within a certain range a and zero elsewhere i.e.

$$\begin{aligned} U(|\mathbf{r} - \mathbf{r}'|) &= U_0 > 0, |\mathbf{r} - \mathbf{r}'| < a \\ &= 0, |\mathbf{r} - \mathbf{r}'| > a \end{aligned} \quad (4.77)$$

For this kind of interaction, the fourier transform of the interaction potential \hat{U}_k takes the following form [193] in one, two and three dimensions respectively.

$$\begin{aligned} u^{1D}(qa) &= \frac{\sin(qa)}{qa} \\ u^{2D}(qa) &= 2 \frac{J_1(qa)}{qa} \\ u^{3D}(qa) &= \frac{3}{(qa)^2} \left[\frac{\sin(qa)}{qa} - \cos(qa) \right] \end{aligned} \quad (4.78)$$

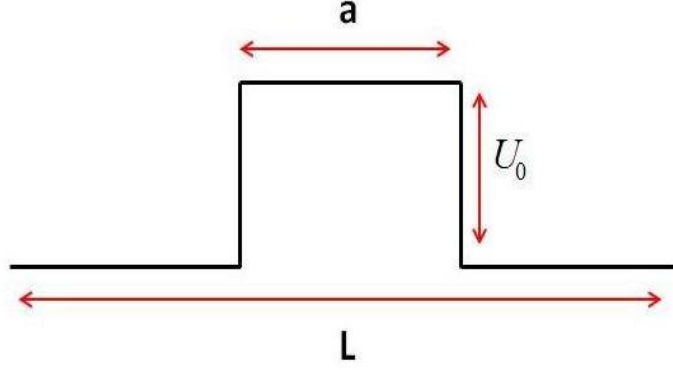


FIGURE 4.2: Model interaction potential (Step-like)

where $J_1(qa)$ is the Bessel function. We show the dispersion spectrum for three dimensional step like potential in Fig. 4.3. One can see that at small values of q , $\epsilon(q)$ has a phonon like character, while at sufficiently higher values of q , it has the free particle character. However, with \hat{U}_q having a negative minimum at finite momentum, $\epsilon(q)$ drops near that particular momentum and eventually becomes imaginary when increasing the strength Λ , which is proportional to the number density. Thus, from the dispersion spectrum, one can conclude that the assumed uniform superfluid state is unstable beyond a critical interaction strength of the long range interaction, and indicates the possible formation of non uniform (periodic) order.

After calculating the Bogoliubov dispersion relation, which indicates the formation of supersolid ground state in the system, we verify the same by solving the GPE with non-local potential given by equation (4.68). We perform numerical simulations in one and two dimensions for the GPE (equation (4.68)) using imaginary time propagation technique for a model step like interparticle interaction potential shown in Fig. 4.2 with periodic boundary conditions. We numerically obtained the ground state density profile of the system, which indeed shows that the system shows a crystalline modulation in superfluid density above a certain value of interaction strength, both in one and two dimensions. As shown in Fig. 4.4, the system minimizes its energy by transforming to a state with density modulations. The two dimensional superfluid density profile shows formation of a periodic hexagonal lattice as shown in Fig. 4.4.

As already explained in section 1.3, due to the tunability of the interaction potentials between atoms under well defined and highly controllable conditions, ultracold atomic condensates have emerged as prominent candidates to study the supersolid phase. Several theoretical works have shown that specific type of long range interaction potentials [24, 48, 70] stabilize the supersolid phase in BEC. Recent experiments with cavity mediated long-range interaction in ultra cold atomic BEC demonstrates the roton like mode

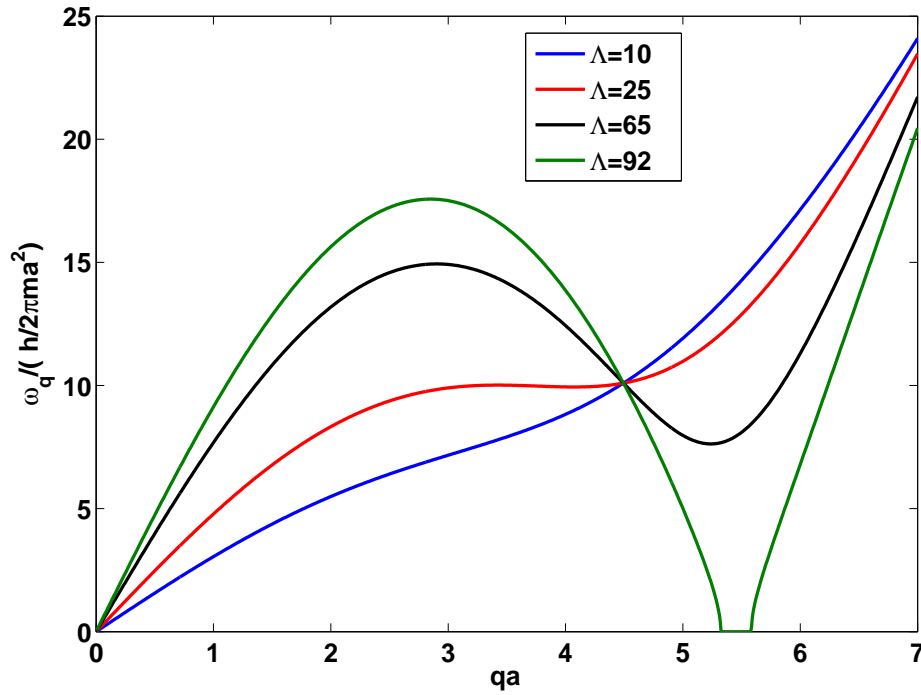


FIGURE 4.3: Plot of dispersion relation $\epsilon(q)$ in three dimensions for increasing values of interaction strength, $\Lambda = 10, 25, 65, 92$. Roton instability where the minima in the energy spectrum touches the q axis, is seen to occur after a critical value of the interaction strength, indicating the possible formation of a periodic ground state

softening [81], which indicates the instability towards the formation of uniform superfluid. Hence, ultracold atomic condensates with specific type of long range interactions are excellent systems to study supersolidity and its properties.

Supersolid phase possesses the superfluid and solid like properties simultaneously. In analogy with rotating superfluids where collective behavior is well understood both theoretically [104, 182–184] and experimentally [34], we develop hydrodynamic theory for rotating supersolid and determine the collective oscillations in the system. The collective oscillations in the rotating supersolid system might carry additional signatures due to presence of modulation in superfluid density and hence could be one of the efficient ways to detect the supersolidity in ultracold atomic condensates. Thus to explore such properties, we develop hydrodynamic theory for rotating supersolids in the next section and calculate the collective modes which carry signatures of co-existing superfluid and crystalline behavior in such systems.

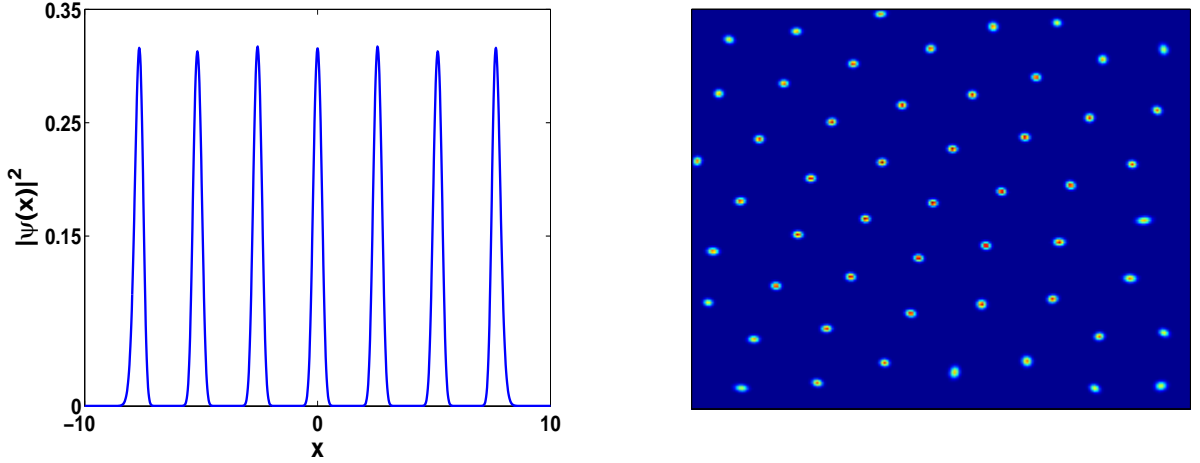


FIGURE 4.4: Ground state of the GPE obtained numerically for one and two dimensions, using imaginary time propagation technique. The ground state shows a periodic modulation in density after critical value of interaction strengths. It is to note that the system favors the formation of a hexagonal lattice in two dimensions.

4.3 Hydrodynamic theory for rotating supersolids

In this section we present the derivation of the equations of motion for a rotating supersolid by developing a hydrodynamic theory for the system [110]. By hydrodynamic formalism, we mean that we will be concerned with phenomenon whose characteristic length is much larger than the lattice parameters of the vortex as well as supersolid lattice.

To do this we begin with the mean field Gross Piteavskii description of an ultra cold atomic condensate at zero temperature with non-local interaction. Such condensate is characterized by a complex superfluid order parameter $\psi(\mathbf{r})$ and the mean field Lagrangian, which is the space integral of Lagrangian density \mathcal{L} , can be written as

$$L = \int d\mathbf{r} \mathcal{L} = \int d\mathbf{r} \left[i\frac{\hbar}{2}(\psi^* \frac{\partial \psi}{\partial t} - \psi \frac{\partial \psi^*}{\partial t}) - \mathcal{E}(\psi, \psi^*) \right] \quad (4.79)$$

\mathcal{E} can be identified as the usual Gross-Pitaevskii energy functional and is given by

$$\mathcal{E}(\psi, \psi^*) = \frac{\hbar^2}{2m} |\nabla \psi|^2 + V(\mathbf{r}) |\psi|^2 + \int d\mathbf{r}' |\psi(\mathbf{r})|^2 U(|\mathbf{r} - \mathbf{r}'|) |\psi(\mathbf{r}')|^2 \quad (4.80)$$

Upon writing the superfluid order parameter as $\psi(\mathbf{r}, t) = \sqrt{n(\mathbf{r}, t)} e^{i\Phi(\mathbf{r}, t)}$ in terms of the density n and phase Φ the above Lagrangian density \mathcal{L} takes the form

$$\mathcal{L} = - \left[\hbar n \frac{\partial \Phi}{\partial t} + \frac{\hbar^2}{2m} \left(n(\nabla \Phi)^2 + \frac{1}{4n} (\nabla n)^2 \right) \right] d\mathbf{r} + \frac{1}{2} \int U(|\mathbf{r} - \mathbf{r}'|) n(\mathbf{r}) n(\mathbf{r}') d\mathbf{r}' \quad (4.81)$$

For the theory of supersolids, we denote the density of particles by n unlike ρ as in the case for superfluids. We denote ρ to represent the average density of particles shown further in this section. It is shown in [69] that a model of supersolid is found by considering the non-local GP equation with energy functional given by equation (4.80). The possible experimental system can be an ultracold atomic BEC with cavity mediated long range interactions, which already indicates the instability towards formation of uniform superfluid phase [81], and the ultracold atomic Rydberg dressed atoms [78].

The action $S = \int dt \int dr \mathcal{L} = \int dt L$ defined through the above Lagrangian density can be extremized to obtain the Euler Lagrangian equation for superfluid density $n(\mathbf{r}, t) = |\psi(\mathbf{r}, t)|^2$ the velocity field

$$\mathbf{v}_s(\mathbf{r}, t) = \frac{\psi^*(\mathbf{r}, t) \nabla \psi(\mathbf{r}, t) - \psi(\mathbf{r}, t) \nabla \psi^*(\mathbf{r}, t)}{2imn(\mathbf{r}, t)} \quad (4.82)$$

These equations provide a hydrodynamic description of such ultra cold atomic superfluid.

It is well known that for certain type of effective interaction potential $U(|\mathbf{r} - \mathbf{r}'|)$ the condensate shows a supersolid ground state as the critical strength of the non-local interaction strength exceeds a critical value [24, 69]. The supersolid ground state behaves simultaneously as superfluid as well as a solid and a low energy long wavelength hydrodynamic theory can be constructed for such a supersolid condensate following Landau two fluid model [194, 195]. Here superfluid component of this two fluid model will be the superfluid order itself, the density modulation of the superfluid which is treated as a lattice structure embedded in the superfluid will be treated as the normal component. Given that the normal component is now no more a fluid, but a solid like lattice configuration, the contribution from this part to the energy functional is also needed to be handled accordingly.

We are interested in studying the effect of the artificial gauge field on such superfluid created either by rotating such ultra cold atomic condensate or by any other technique that will induce vortices in such supersolid due to presence of the superfluid component. These *supersolid vortices* are topological defects in the superfluid density with a $\pm 2\pi$ jump around the vortex core. At high enough rotational frequency, such vortices are expected to form an Abrikosov lattice [83] like structure. Assuming this condition is satisfied, within this two-fluid approximation, we develop a hydrodynamic theory for a rotating supersolid, where the vortex lattice co-exists with the density modulations or the crystal lattice of superfluid component.

To extend the usual hydrodynamics description of a ultra cold atomic superfluid to a rotating supersolid we first introduce the lattice vector $\mathbf{u}^{ss}(\mathbf{r}, t)$ to denote the co-ordinates of the supersolid lattice and the vector $\mathbf{u}^v(\mathbf{r}, t)$. In the absence of any normal crystal like component, for a prototype ultra cold atomic superfluid the average number density of the particles ρ is defined through the normalisation condition

$$\rho = \frac{1}{V} \int_V n(\mathbf{r}) d\mathbf{r} \quad (4.83)$$

and does not vary as function of (\mathbf{r}, t) . Thus for a ultra cold atomic superfluid ρ cannot be changed without changing the number of ultra cold atoms in a given volume. On the other hand in a classical crystalline solid ρ represents fixed number of atoms per unit cell for a given set of lattice vectors and given number of atoms in the solid. So for a fixed number of atoms, the lattice vectors and the number density of atoms are constrained to depend on each other. The following equation takes into account the change in number density due to elastic deformations of the classical lattice

$$\frac{\delta\rho}{\rho} = -\nabla \cdot \mathbf{u}^{ss}$$

The above condition needs to be relaxed in the case of an ultra cold atomic supersolid. For such a system the crystalline solid component of the supersolid is superfluid density modulation which can be identified with a crystalline structure. In a more naive language this corresponds to set of position vectors that gives us the location of the local maxima and minima's of the superfluid density. Thus number density is liable to get change due to the compression/dilation effects of the lattice (which is basically the change in displacement vector $\mathbf{u}^{ss}(\mathbf{r}, t)$) or equivalently by changing the density of superfluid component. In a quantum supersolid, the equation is

$$\frac{\delta\rho}{\rho} + \nabla \cdot \mathbf{u}^{ss} = O(\rho^{ss})$$

with ρ as the average number density of the system.

Same is also true for the vortex lattice which can also be characterized as a patterned modulation in the superfluid density and phase. Thus the lattice vectors $\mathbf{u}^{ss}(\mathbf{r}, t)$ and $\mathbf{u}^v(\mathbf{r}, t)$ as well as the average density ρ can be varied independently and the phase and density of the mean field order parameter $\psi(\mathbf{r}, t)$ is now a functional of three field variables, namely $\rho(\mathbf{r}, t)$, $\mathbf{u}^{ss}(\mathbf{r}, t)$, $\mathbf{u}^v(\mathbf{r}, t)$

$$n(\mathbf{r}, t) = n(\rho(\mathbf{r}, t), \mathbf{u}^s(\mathbf{r}, t) \mathbf{u}^v(\mathbf{r}, t)) \quad (4.84)$$

To entail a time independent description of such a rotating supersolid again one goes to

the energy functional in the co-rotating frame is related with the non rotating energy functional as shown in section 4.1.2

$$\mathcal{E}_R = \mathcal{E} - \Omega \cdot (\mathbf{r} \times \mathbf{p})$$

In the following section we provide a systematic derivation of the Lagrangian density for the rotating supersolid, where supersolid lattice co-exist with the vortex lattice. We also provide the limiting cases of the non-rotating supersolid and rotating superfluid from the effective Lagrangian for rotating supersolid.

4.3.1 Homogenization technique for long wave effective Lagrangian

Here, we derive the coupled equations for the three fields $\rho(\mathbf{r}, t)$, $\mathbf{u}(\mathbf{r}, t) = \mathbf{u}^{ss}(\mathbf{r}, t) + \mathbf{u}^v(\mathbf{r}, t)$ and $\phi(\mathbf{r}, t)$, following the method called Homogenization [196]. This technique splits the long wave behavior of various parameters and the short range periodic dependence on the lattice parameters.

Following the work by Josserand et. al [69, 194] to perform the long wavelength analysis of the system, we use the ansatz for density and phase as

$$n(\mathbf{r}, t) = \rho_0(\mathbf{r} - \mathbf{u}^{ss}(\mathbf{r}, t) - \mathbf{u}^v(\mathbf{r}, t)|\rho(\mathbf{r}, t)) + \tilde{\rho}(\mathbf{r} - \mathbf{u}^{ss} - \mathbf{u}^v, \rho, t) + \dots \quad (4.85)$$

$$\Phi(\mathbf{r}, t) = \phi(\mathbf{r}, t) + \tilde{\phi}(\mathbf{r} - \mathbf{u}^{ss} - \mathbf{u}^v, \rho(\mathbf{r}, t), t) + \dots \quad (4.86)$$

Here, the displacement of the vortex lattice and the supersolid lattice enters the modulated density as $\rho_0(\mathbf{r} - \mathbf{u}^{ss}(\mathbf{r}, t) - \mathbf{u}^v(\mathbf{r}, t)|\rho(\mathbf{r}, t))$. Also, ϕ , $\mathbf{u} = \mathbf{u}^{ss} + \mathbf{u}^v$ and ρ are slowly varying fields and $\tilde{\phi}$ and $\tilde{\rho}$ are small and fast varying periodic functions.

Now we calculate the gradients and time derivatives of various expressions which will be further used in the calculations.

$$\begin{aligned} (\nabla n)_i &= \frac{\partial \rho_0}{\partial x_i} - \frac{\partial \rho_0}{\partial u_k^{ss}} \frac{\partial u_k^{ss}}{\partial x_i} - \frac{\partial \rho_0}{\partial u_k^v} \frac{\partial u_k^v}{\partial x_i} + \frac{\partial \rho_0}{\partial \rho} \frac{\partial \rho}{\partial x_i} + \frac{\partial \tilde{\rho}}{\partial x_i} - \frac{\partial \tilde{\rho}}{\partial u_k^{ss}} \frac{\partial u_k^{ss}}{\partial x_i} - \frac{\partial \tilde{\rho}}{\partial u_k^v} \frac{\partial u_k^v}{\partial x_i} + \frac{\partial \tilde{\rho}}{\partial \rho} \frac{\partial \rho}{\partial x_i} \\ &= (\delta_{ik} - \partial_i u_k^{ss} - \partial_i u_k^v) \partial_k \rho_0 + \frac{\partial \rho_0}{\partial \rho} \frac{\partial \rho}{\partial x_i} + (\delta_{ik} - \partial_i u_k^{ss} - \partial_i u_k^v) \partial_k \tilde{\rho} + \frac{\partial \tilde{\rho}}{\partial \rho} \frac{\partial \rho}{\partial x_i} \end{aligned}$$

Next,

$$\begin{aligned} \partial_t \Phi &= \frac{\partial \phi}{\partial t} - \frac{\partial \tilde{\phi}}{\partial u_k^{ss}} \frac{\partial u_k^{ss}}{\partial t} - \frac{\partial \tilde{\phi}}{\partial u_k^v} \frac{\partial u_k^v}{\partial t} + \frac{\partial \tilde{\phi}}{\partial t} + \frac{\partial \tilde{\phi}}{\partial \rho} \frac{\partial \rho}{\partial t} \\ &= \partial_t \phi - \partial_t u_k^{ss} \partial_k \tilde{\phi} - \partial_t u_k^v \partial_k \tilde{\phi} + \partial_t \tilde{\phi} + \frac{\partial \tilde{\phi}}{\partial \rho} \partial_t \rho \end{aligned}$$

$$\begin{aligned}
(\nabla\Phi)_i &= \frac{\partial\phi}{\partial x_i} + \frac{\partial\tilde{\phi}}{\partial x_i} - \frac{\partial\tilde{\phi}}{\partial u_k^{ss}} \frac{\partial u_k^{ss}}{\partial x_i} - \frac{\partial\tilde{\phi}}{\partial u_k^v} \frac{\partial u_k^v}{\partial x_i} + \frac{\partial\tilde{\phi}}{\partial\rho} \frac{\partial\rho}{\partial x_i} \\
&= (\nabla\phi)_i + (\delta_{ik} - \partial_i u_k^{ss} - \partial_i u_k^v) \partial_k \tilde{\phi} + \frac{\partial\tilde{\phi}}{\partial\rho} (\nabla\rho)_i
\end{aligned}$$

Now keeping the relevant contributions for the long-wave description and calculating

$$\begin{aligned}
n\partial_t\Phi &= (\rho_0 + \tilde{\rho}) \left(\partial_t\phi - \partial_t u_k^{ss} \partial_k \tilde{\phi} - \partial_t u_k^v \partial_k \tilde{\phi} + \partial_t \tilde{\phi} + \frac{\partial\tilde{\phi}}{\partial\rho} \partial_t \rho \right) \\
&= \rho_0 \partial_t\phi - \rho_0 \partial_t u_k^{ss} \partial_k \tilde{\phi} - \rho_0 \partial_t u_k^v \partial_k \tilde{\phi} + \partial_t \phi \tilde{\rho} + h.o.t, \tag{4.87}
\end{aligned}$$

Here and throughout the chapter *h.o.t* are the higher order terms. In above equation (4.87), the fast varying terms in $\tilde{\phi}$ multiplied by other fast varying term such as $\tilde{\rho} \partial_t u_k^{ss} \partial_k \tilde{\phi}$ and $\tilde{\rho} \partial_t \tilde{\phi}$ are ignored and not taken into account.

$$\begin{aligned}
(\nabla n)^2 &= \left((\delta_{ik} - \partial_i u_k^{ss} - \partial_i u_k^v) \partial_k \rho_0 + \frac{\partial\rho_0}{\partial\rho} \frac{\partial\rho}{\partial x_i} + (\delta_{ik} - \partial_i u_k^{ss} - \partial_i u_k^v) \partial_k \tilde{\rho} + \frac{\partial\tilde{\rho}}{\partial\rho} \frac{\partial\rho}{\partial x_i} \right)^2 \\
&= \left((\delta_{ik} - \partial_i u_k^{ss} - \partial_i u_k^v) \partial_k \rho_0 + \frac{\partial\rho_0}{\partial\rho} \frac{\partial\rho}{\partial x_i} \right)^2 + \left((\delta_{ik} - \partial_i u_k^{ss} - \partial_i u_k^v) \partial_k \tilde{\rho} + \frac{\partial\tilde{\rho}}{\partial\rho} \frac{\partial\rho}{\partial x_i} \right)^2 \\
&\quad + 2 \left((\delta_{ik} - \partial_i u_k^{ss} - \partial_i u_k^v) \partial_k \rho_0 + \frac{\partial\rho_0}{\partial\rho} \frac{\partial\rho}{\partial x_i} \right) \left((\delta_{ik} - \partial_i u_k^{ss} - \partial_i u_k^v) \partial_k \tilde{\rho} + \frac{\partial\tilde{\rho}}{\partial\rho} \frac{\partial\rho}{\partial x_i} \right) \tag{4.88}
\end{aligned}$$

We calculate this quantity (4.88) term by term as follows :

Term 1:

$$\begin{aligned}
\left((\delta_{ik} - \partial_i(u_k^{ss} + u_k^v)) \partial_k \rho_0 + \frac{\partial\rho_0}{\partial\rho} \frac{\partial\rho}{\partial x_i} \right)^2 &= [(\delta_{ik} + (\partial_i(u_k^{ss} + u_k^v)))^2 - 2\delta_{ik} \partial_i(u_k^{ss} + u_k^v)] \left(\frac{\partial\rho_0}{\partial x_k} \right)^2 \\
&\quad + \left(\frac{\partial\rho_0}{\partial\rho} \frac{\partial\rho}{\partial x_i} \right)^2 + 2(\delta_{ik} + \partial_i(u_k^{ss} + u_k^v)) \frac{\partial\rho_0}{\partial x_k} \frac{\partial\rho_0}{\partial\rho} \frac{\partial\rho}{\partial x_i} \\
&= \delta_{ik} \frac{\partial\rho_0}{\partial x_i} \frac{\partial\rho_0}{\partial x_k} + (\partial_l u_i^{ss} + \partial_l u_i^v)(\partial_l u_k^{ss} + \partial_l u_k^v) \frac{\partial\rho_0}{\partial x_i} \frac{\partial\rho_0}{\partial x_k} \\
&\quad - 2(\partial_i u_k^{ss} + \partial_l u_k^v) \frac{\partial\rho_0}{\partial x_i} \frac{\partial\rho_0}{\partial x_k} \\
&= (\delta_{ik} - 2(\partial_i u_k^{ss} + \partial_l u_k^v) + (\partial_l u_i^{ss} + \partial_l u_i^v)(\partial_l u_k^{ss} + \partial_l u_k^v)) \\
&\quad \times \frac{\partial\rho_0}{\partial x_i} \frac{\partial\rho_0}{\partial x_k} \\
&= (\delta_{ik} - 2\partial_i u_k^{ss} - 2\partial_i u_k^v + \partial_l u_i^v \partial_l u_k^v + \partial_l u_i^{ss} \partial_l u_k^{ss}) \frac{\partial\rho_0}{\partial x_i} \frac{\partial\rho_0}{\partial x_k} \\
&= (\delta_{ik} + 2\epsilon_{ik}^s + 2\epsilon_{ik}^v) \frac{\partial\rho_0}{\partial x_i} \frac{\partial\rho_0}{\partial x_k} + h.o.t \tag{4.89}
\end{aligned}$$

where

$$\epsilon_{ik}^s = \frac{1}{2}(\partial_i u_k^{ss} + \partial_k u_i^{ss}) + \frac{1}{2}\partial_l u_i^{ss} \partial_l u_k^{ss} \tag{4.90}$$

is the strain tensor [188] for supersolid lattice and,

$$\epsilon_{ik}^v = \frac{1}{2}(\partial_i u_k^v + \partial_k u_i^v) + \frac{1}{2}\partial_l u_i^v \partial_l u_k^v \quad (4.91)$$

is the strain tensor [188] for vortex lattice.

Term 2

$$\begin{aligned} & (\delta_{ik} - (\partial_i u_k^{ss} + \partial_i u_k^v))^2 \left(\frac{\partial \tilde{\rho}}{\partial x_k} \right)^2 + \left(\frac{\partial \tilde{\rho}}{\partial \rho} \frac{\partial \rho}{\partial x_i} \right) + 2(\delta_{ik} - (\partial_i u_k^{ss} + \partial_i u_k^v)) \frac{\partial \tilde{\rho}}{\partial x_k} \frac{\partial \tilde{\rho}}{\partial \rho} \frac{\partial \rho}{\partial x_i} \\ &= \delta_{ik} \left(\frac{\partial \tilde{\rho}}{\partial x_k} \right)^2 + h.o.t \\ &= (\partial_i \tilde{\rho})^2 + h.o.t \end{aligned} \quad (4.92)$$

Here, again to keep the relevant terms for long wavelength description, terms which are quadratic in fast varying variable $\tilde{\rho}$ multiplied by other derivatives are ignored.

Term 3

$$\begin{aligned} & 2 \left((\delta_{ik} - \partial_i u_k^{ss} - \partial_i u_k^v) \partial_k \rho_0 + \frac{\partial \rho_0}{\partial \rho} \frac{\partial \rho}{\partial x_i} \right) \left((\delta_{ik} - \partial_i u_k^{ss} - \partial_i u_k^v) \partial_k \tilde{\rho} + \frac{\partial \tilde{\rho}}{\partial \rho} \frac{\partial \rho}{\partial x_i} \right) \\ &= 2(\delta_{ik} - \partial_i u_k^{ss} - \partial_i u_k^v)^2 \frac{\partial \rho_0}{\partial x_k} \frac{\partial \tilde{\rho}}{\partial x_k} + h.o.t \simeq 2(\delta_{ik} + 2\epsilon_{ik}^s + 2\epsilon_{ik}^v) \partial_k \rho_0 \partial_k \tilde{\rho} \end{aligned} \quad (4.93)$$

Substituting equations (4.89),(4.92),(4.93) into equation (4.88), we get

$$(\nabla n)^2 = (\delta_{ik} + 2\epsilon_{ik}^s + 2\epsilon_{ik}^v) \partial_i \rho_0 \partial_k \rho_0 + 2(\delta_{ik} + 2\epsilon_{ik}^s + 2\epsilon_{ik}^v) \partial_k \rho_0 \partial_k \tilde{\rho} + (\partial_i \tilde{\rho})^2 + h.o.t \quad (4.94)$$

Next we calculate

$$\begin{aligned} (\nabla \Phi)^2 &= \left[(\nabla \phi)^2 + (\delta_{ik} - (\partial_i u_k^{ss} + \partial_i u_k^v)) \frac{\partial \tilde{\phi}}{\partial x_k} + \frac{\partial \tilde{\phi}}{\partial \rho} (\nabla \rho) \right]^2 \\ &= (\partial_i \phi)^2 + [\delta_{ik} + (\partial_i u_k^{ss} + \partial_i u_k^v)^2 - 2\delta_{ik}(\partial_i u_k^{ss} + \partial_i u_k^v)] \left(\frac{\partial \tilde{\phi}}{\partial x_k} \right)^2 \\ &\quad + 2(\delta_{ik} - (\partial_i u_k^{ss} + \partial_i u_k^v)) \frac{\partial \phi}{\partial x_i} \frac{\partial \tilde{\phi}}{\partial x_k} + h.o.t \\ &= (\partial_i \phi)^2 + (\nabla \tilde{\phi})^2 + 2(\delta_{ik} - (\partial_i u_k^{ss} + \partial_i u_k^v)) \partial_i \phi \partial_k \tilde{\phi} + h.o.t \end{aligned} \quad (4.95)$$

The higher order terms are the terms quadratic in fast varying variable $\tilde{\phi}$ multiplied by other derivatives, which we again neglect in the long wavelength description. The next

term is

$$\begin{aligned}
 n\nabla\Phi &= (\rho_0 + \tilde{\rho}) \left((\nabla\phi) + (\delta_{ik} - \partial_i u_k^{ss} - \partial_i u_k^v) \partial_k \tilde{\phi} + \frac{\partial \tilde{\phi}}{\partial \rho} (\nabla\rho) \right) \\
 &= \rho_0 \nabla\phi + \rho_0 (\delta_{ik} - \partial_i u_k^{ss} - \partial_i u_k^v) \frac{\partial \tilde{\phi}}{\partial x_k} + \rho_0 \frac{\partial \tilde{\phi}}{\partial \rho} (\nabla\rho) + h.o.t
 \end{aligned}$$

Before going into the calculation for the non-local interaction term, we calculate the 1st and 2nd term of Lagrangian (4.79) and label their contribution to the corresponding energy part of the Lagrangian, which will be explained later.

In the 1st term L_1 we use equation (4.87) and get the following expression

$$\begin{aligned}
 L_1 &= - \int \hbar n \frac{\partial \Phi}{\partial t} d\mathbf{r} \\
 &= \underbrace{- \int \hbar \partial_t \phi \rho_0 d\mathbf{r}}_{L_\phi} + \underbrace{\int \hbar \rho_0 \partial_t u_k^{ss} \partial_k \tilde{\phi} d\mathbf{r}}_{L_{\tilde{\phi}}} \\
 &\quad + \underbrace{\int \hbar \rho_0 \partial_t u_k^v \partial_k \tilde{\phi} d\mathbf{r}}_{L_{\tilde{\phi}}} - \underbrace{\int \hbar \partial_t \Phi \tilde{\rho} d\mathbf{r}}_{neglected}
 \end{aligned} \tag{4.96}$$

2nd term of Lagrangian (4.79) is calculated using (4.95) as

$$\begin{aligned}
 L_2 &= - \int \frac{\hbar^2}{2m} n (\nabla\Phi)^2 d\mathbf{r} \\
 &= - \int \frac{\hbar^2}{2m} [\rho_0 (\partial_i \phi)^2 + \rho_0 (\nabla\tilde{\phi})^2 + 2\rho_0 (\delta_{ik} - \partial_i u_k^{ss} - \partial_i u_k^v) \partial_i \phi \partial_k \tilde{\phi} \\
 &\quad + \tilde{\rho} (\partial_i \phi)^2 + \tilde{\rho} (\nabla\tilde{\phi})^2 + 2\tilde{\rho} (\delta_{ik} - \partial_i u_k^{ss} - \partial_i u_k^v) \partial_i \phi \partial_k \tilde{\phi}] d\mathbf{r} \\
 &= \underbrace{- \frac{\hbar^2}{2m} \int (\nabla\phi)^2 \rho_0(\mathbf{r}) d\mathbf{r}}_{L_\phi} + \underbrace{\frac{\hbar^2}{m} \int (\partial_i u_k^{ss} + \partial_i u_k^v) \partial_i \phi \partial_k \tilde{\phi} \rho_0(\mathbf{r}) d\mathbf{r}}_{L_{\tilde{\phi}}} \\
 &\quad - \underbrace{\frac{\hbar^2}{m} \int \nabla\phi \cdot \nabla\tilde{\phi} \rho_0(\mathbf{r}) d\mathbf{r}}_{L_{\tilde{\phi}}} - \underbrace{\frac{\hbar^2}{2m} \int (\nabla\tilde{\phi})^2 \rho_0(\mathbf{r}) d\mathbf{r}}_{L_{\tilde{\phi}}}
 \end{aligned} \tag{4.97}$$

Considering the non-local term now, given by

$$N(\rho(\mathbf{r}), \rho(\mathbf{r}')) = \frac{1}{2} \int U(|\mathbf{r} - \mathbf{r}'|) \rho(\mathbf{r} - \mathbf{u}^{ss}(\mathbf{r}) - \mathbf{u}^v(\mathbf{r})) \rho(\mathbf{r}' - \mathbf{u}^{ss}(\mathbf{r}') - \mathbf{u}^v(\mathbf{r}')) d\mathbf{r} d\mathbf{r}' \tag{4.98}$$

STEPS

1) Using the change of variables, $\mathbf{R} = \mathbf{r} - \mathbf{u}(\mathbf{r})$ and, $\mathbf{R}' = \mathbf{r}' - \mathbf{u}(\mathbf{r}')$, we can determine

$$d\mathbf{R} = d(\mathbf{r} - (u^{ss}(\mathbf{r}) + u^v(\mathbf{r})))$$

with

$$(d\mathbf{R})_i = d(\mathbf{r} - (u^{ss}(\mathbf{r}) + u^v(\mathbf{r})))_i = \left(dx_i - \frac{\partial(u_i^{ss} + u_i^v)}{\partial x_k} dx_k \right)$$

which implies

$$\begin{aligned} |d\mathbf{R}|^2 &= (d\mathbf{R})_i \cdot (d\mathbf{R})_i \\ &= \left(dx_i - \frac{\partial(u_i^{ss} + u_i^v)}{\partial x_k} dx_k \right)^2 \\ &= dx_i dx_k \delta_{ik} - 2 dx_i \frac{\partial(u_i^{ss} + u_i^v)}{\partial x_k} dx_k + \left(\frac{\partial(u_i^{ss} + u_i^v)}{\partial x_k} \right)^2 (dx_k)^2 \\ &= (\delta_{ik} - 2(\partial_k u_i^{ss} + \partial_k u_i^v) + (\partial_k u_i^{ss} + \partial_k u_i^v)(\partial_k u_i^{ss} + \partial_k u_i^v)) dx_i dx_k \\ &= (\delta_{ik} + 2\epsilon_{ik}^s + 2\epsilon_{ik}^v) dx_i dx_k \end{aligned} \quad (4.99)$$

with strain tensors ϵ_{ik}^s and ϵ_{ik}^v defined in equations (4.90) and (4.91). Similarly,

$$|d\mathbf{R}'|^2 = (\delta_{ik} + 2\epsilon_{ik'}^s + 2\epsilon_{ik'}^v) dx'_i dx'_k$$

2) Any integral with argument $\mathbf{r} - \mathbf{u}(\mathbf{r})$ may be transformed to

$$\begin{aligned} \int Q(\mathbf{r} - \mathbf{u}(\mathbf{r})) d\mathbf{r} &= \int Q(\mathbf{R}) d\mathbf{r} \\ &= \int Q(\mathbf{R}) \frac{d\mathbf{R}}{\sqrt{\det(\delta_{ik} + 2\epsilon_{ik}^s + 2\epsilon_{ik}^v)}} \end{aligned} \quad (4.100)$$

$$\begin{aligned} &= \int Q(\mathbf{r}) \frac{d\mathbf{r}}{\sqrt{\det(\delta_{ik} + 2\epsilon_{ik}^s + 2\epsilon_{ik}^v)}} \\ &= \int Q(\mathbf{r}) (\delta_{ik} + 2\epsilon_{ik}^s + 2\epsilon_{ik}^v)^{-1/2} d\mathbf{r} \\ &\simeq \int Q(\mathbf{r}) (1 - \epsilon_{kk}^s - \epsilon_{kk}^v) d\mathbf{r} \end{aligned} \quad (4.101)$$

The step (4.100) in equation (4.101) is obtained by using equation (4.99).

3) Relative distance

$$\begin{aligned} \Delta\mathbf{R} &= \mathbf{R} - \mathbf{R}' \\ &= \Delta\mathbf{r} - (\mathbf{u}^{ss}(\mathbf{r}) - \mathbf{u}^{ss'}(\mathbf{r}')) - (\mathbf{u}^v(\mathbf{r}) - \mathbf{u}^{v'}(\mathbf{r}')) \\ &= \Delta\mathbf{r} - \Delta(\mathbf{u}^v(\mathbf{r}) + \mathbf{u}^{ss}(\mathbf{r})) \end{aligned} \quad (4.102)$$

where $\Delta\mathbf{r} = \mathbf{r} - \mathbf{r}'$. Above equation (4.102) implies

$$\begin{aligned} |\Delta\mathbf{R}|^2 &\simeq |\Delta\mathbf{r}|^2 + |\Delta\mathbf{u}(\mathbf{r})|^2 - 2\Delta\mathbf{r} \cdot \Delta\mathbf{u}(\mathbf{r}) \\ &= |\Delta\mathbf{r}|^2 + \frac{\partial u_l}{\partial x_i} \frac{\partial u_l}{\partial x_k} \Delta x_i \Delta x_k + \Delta\mathbf{r} \cdot (-\partial_i u_k - \partial_k u_i) \Delta x \\ &= |\Delta\mathbf{r}|^2 + 2\epsilon_{ik}^s \Delta x_i \Delta x_k + 2\epsilon_{ik}^v \Delta x_i \Delta x_k \end{aligned}$$

Thus,

$$|\Delta \mathbf{r}| \simeq \Delta \mathbf{R} - \frac{(\epsilon_{ik}^s + \epsilon_{ik}^v) \Delta x_i \Delta x_k}{\Delta \mathbf{R}} \quad (4.103)$$

The final result of non-local term given by (4.98) thus can be calculated as

$$\begin{aligned} N(\rho(\mathbf{r}), \rho(\mathbf{r}')) &= \frac{1}{2} \int U \left(|\Delta \mathbf{R}| - (\epsilon_{ik}^s + \epsilon_{ik}^v) \frac{\Delta x_i \Delta x_k}{|\Delta \mathbf{R}|} + \dots \right) \frac{\rho(\mathbf{R}) d\mathbf{R}}{\sqrt{\det(\delta_{ik} + 2\epsilon_{ik}^s + 2\epsilon_{ik}^v)}} \\ &\quad \times \frac{\rho(\mathbf{R}') d\mathbf{R}'}{\sqrt{\det(\delta_{ik'} + 2\epsilon_{ik'}^s + 2\epsilon_{ik'}^v)}} \\ &= \frac{1}{2} \int (1 - (\epsilon_{ll}^s + \epsilon_{ll}^{s'} + \epsilon_{ll}^v + \epsilon_{ll}^{v'})) (U(|\mathbf{r} - \mathbf{r}'|) \\ &\quad - (\epsilon_{ik}^s + \epsilon_{ik}^v) ((x_i - x_{i'}) (x_k - x_{k'})) \frac{U(\mathbf{r} - \mathbf{r}')}{|\mathbf{r} - \mathbf{r}'|} + \dots) \rho(\mathbf{r}) \rho(\mathbf{r}') d\mathbf{r} d\mathbf{r}' \\ &= \frac{1}{2} \int (1 - (\epsilon_{ll}^s + \epsilon_{ll}^{s'}) - (\epsilon_{ll}^v + \epsilon_{ll}^{v'})) (U(|\mathbf{r} - \mathbf{r}'|) - (\epsilon_{ik}^s + \epsilon_{ik}^v) f_{ik}(\mathbf{r} - \mathbf{r}') + \dots) \\ &\quad \rho(\mathbf{r}) \rho(\mathbf{r}') d\mathbf{r} d\mathbf{r}' \end{aligned} \quad (4.104)$$

Here, in the last expression the variables \mathbf{R} and \mathbf{R}' have been renamed as \mathbf{r} and \mathbf{r}' , and $f_{ik}(\mathbf{r} - \mathbf{r}') = (x_i - x_{i'}) (x_k - x_{k'}) \frac{U(\mathbf{r} - \mathbf{r}')}{|\mathbf{r} - \mathbf{r}'|}$.

The 1st and 2nd term of the Lagrangian (4.79) are already calculated. Here we determine the 3rd and 4th terms by substituting the ansatz in equations (4.85) and (4.86) in the Lagrangian (4.79). 3rd term of the Lagrangian (4.79) is calculated using (4.94) and (4.101) as

$$\begin{aligned} L_3 &= -\frac{\hbar^2}{2m} \int \frac{1}{4n} (\nabla n)^2 d\mathbf{r} \\ &= -\frac{\hbar^2}{2m} \int \frac{(\nabla n)^2}{4} \frac{1}{(\rho_0(\mathbf{r} - u) + \tilde{\rho}(\mathbf{r} - u))} d\mathbf{r} \\ &\simeq -\frac{\hbar^2}{2m} \int \frac{(\nabla n)^2}{4} \frac{1}{\rho_0(\mathbf{r} - u)} \left(1 - \frac{\tilde{\rho}(\mathbf{r} - u)}{\rho_0(\mathbf{r} - u)} \right) d\mathbf{r} \\ &= -\frac{\hbar^2}{2m} \left[\int \frac{(\nabla n)^2}{4} \frac{1}{\rho_0(\mathbf{r} - u)} d\mathbf{r} - \int \frac{(\nabla n)^2}{4} \frac{\tilde{\rho}(\mathbf{r} - u)}{\rho_0(\mathbf{r} - u)} d\mathbf{r} \right] \\ &= -\frac{\hbar^2}{2m} \int [(\delta_{ik} + 2\epsilon_{ik}^s + 2\epsilon_{ik}^v) \partial_i \rho_0 \partial_k \rho_0 + 2(\delta_{ik} + 2\epsilon_{ik}^s + 2\epsilon_{ik}^v) \partial_i \rho_0 \partial_k \tilde{\rho} + (\partial_i \tilde{\rho})^2 + h.o.t] \\ &\quad \cdot \left(\frac{1}{4\rho_0(\mathbf{r})} + \frac{\tilde{\rho}(\mathbf{r})}{4\rho_0^2(\mathbf{r})} \right) (1 - \epsilon_{kk}^s - \epsilon_{kk}^v) d\mathbf{r} \end{aligned}$$

$$\begin{aligned}
= & - \underbrace{\frac{\hbar^2}{8m} \int \frac{(\nabla \rho_0)^2}{\rho_0} d\mathbf{r}}_{L_\rho} + \underbrace{\frac{\hbar^2}{8m} \int \frac{(\nabla \rho_0)^2}{\rho_0} (\epsilon_{kk}^s + \epsilon_{kk}^v) d\mathbf{r}}_{L_u} \\
& - \underbrace{\frac{\hbar^2}{4m} \int (\epsilon_{ik}^s + \epsilon_{ik}^v) \frac{\partial_i \rho_0 \partial_k \rho_0}{\rho_0} (1 - \epsilon_{ll}^s - \epsilon_{ll}^v) d\mathbf{r}}_{L_u} - \underbrace{\frac{\hbar^2}{4m} \int \frac{\partial_i \rho_0 \partial_i \tilde{\rho}}{\rho_0} d\mathbf{r}}_{L_{\tilde{\rho}}} \\
& - \underbrace{\frac{\hbar^2}{2m} \int (\epsilon_{ik}^s + \epsilon_{ik}^v) \frac{\partial_i \rho_0 \partial_i \tilde{\rho}}{\rho_0} d\mathbf{r}}_{L_{\tilde{\rho}}} - \underbrace{\frac{\hbar^2}{8m} \int \frac{(\nabla \tilde{\rho})^2}{\rho_0} d\mathbf{r}}_{L_{\tilde{\rho}}} + \underbrace{\frac{\hbar^2}{8m} \int \frac{(\nabla \rho_0)^2}{\rho_0^2} \tilde{\rho} d\mathbf{r}}_{L_{\tilde{\rho}}} + \dots
\end{aligned} \tag{4.105}$$

Now, the 4th term of the Lagrangian (4.79) is calculated using (4.104) as

$$\begin{aligned}
L_4 &= -\frac{1}{2} \int U(|\mathbf{r} - \mathbf{r}'|) n(\mathbf{r}) n(\mathbf{r}') d\mathbf{r} d\mathbf{r}' \\
&= -\frac{1}{2} \int (1 - (\epsilon_{ll}^s + \epsilon_{ll}^{s'}) - (\epsilon_{ll}^v + \epsilon_{ll}^{v'})) (U(|\mathbf{r} - \mathbf{r}'|) - (\epsilon_{ik}^s + \epsilon_{ik}^v) f_{ik}(\mathbf{r} - \mathbf{r}') + \dots) \\
&\quad \cdot (\rho_0(\mathbf{r}) \rho_0(\mathbf{r}') + \rho_0(\mathbf{r}) \tilde{\rho}(\mathbf{r}') + \tilde{\rho}(\mathbf{r}) \rho_0(\mathbf{r}') + \tilde{\rho}(\mathbf{r}) \tilde{\rho}(\mathbf{r}')) d\mathbf{r} d\mathbf{r}' \\
&= -\underbrace{\frac{1}{2} \int U(|\mathbf{r} - \mathbf{r}'|) \rho_0(\mathbf{r}) \rho_0(\mathbf{r}') d\mathbf{r} d\mathbf{r}'}_{L_\rho} - \underbrace{\frac{1}{2} \int U(|\mathbf{r} - \mathbf{r}'|) (\rho_0(\mathbf{r}) \tilde{\rho}(\mathbf{r}') + \tilde{\rho}(\mathbf{r}) \rho_0(\mathbf{r}')) d\mathbf{r} d\mathbf{r}'}_{L_{\tilde{\rho}}} \\
&\quad - \underbrace{\frac{1}{2} \int U(|\mathbf{r} - \mathbf{r}'|) \tilde{\rho}(\mathbf{r}) \tilde{\rho}(\mathbf{r}') d\mathbf{r} d\mathbf{r}'}_{L_{\tilde{\rho}}} \\
&\quad - \underbrace{\frac{1}{2} \int [(\epsilon_{ik}^s + \epsilon_{ik}^v) f_{ik}(\mathbf{r} - \mathbf{r}')] (\rho_0(\mathbf{r}) \tilde{\rho}(\mathbf{r}') + \tilde{\rho}(\mathbf{r}) \rho_0(\mathbf{r}')) d\mathbf{r} d\mathbf{r}'}_{L_{\tilde{\rho}}} \\
&\quad - \underbrace{\frac{1}{2} \int [((\epsilon_{ll}^s + \epsilon_{ll}^{s'}) + (\epsilon_{ll}^v + \epsilon_{ll}^{v'})) f_{ik}(\mathbf{r} - \mathbf{r}')] (\rho_0(\mathbf{r}) \tilde{\rho}(\mathbf{r}') + \tilde{\rho}(\mathbf{r}) \rho_0(\mathbf{r}')) d\mathbf{r} d\mathbf{r}'}_{L_{\tilde{\rho}}} \tag{4.106}
\end{aligned}$$

So, adding and collecting all the terms, we get following five kind of terms

$$L = L_\rho + L_\phi + L_u + L_{\tilde{\phi}} + L_{\tilde{\rho}} \tag{4.107}$$

L_ρ : Internal energy part which includes only the slowly varying variable $\rho_0(\mathbf{r})$.

L_ϕ : This part arises from the mixing of slowly varying phase and slowly varying density, hence the name Hydrodynamical part I.

L_u : This is the Elastic energy I part involving strain tensor terms mixed with the slowly varying density.

$L_{\tilde{\phi}}$: Hydrodynamical part II, involving the fast varying terms in density and phase.

$L_{\tilde{\rho}}$: Labelled as Elastic energy II, this part involves the strain tensor terms mixed with

fast varying components of density.

Below we simplify these terms separately.

(1) L_ρ is the **internal energy part**, which only depends on $\rho_0(\mathbf{r})$ which is slowly varying, and is given by

$$L_\rho = -\frac{\hbar^2}{8m} \int \frac{(\nabla \rho_0)^2}{\rho_0} d\mathbf{r} - \frac{1}{2} \int U(|\mathbf{r} - \mathbf{r}'|) \rho_0(\mathbf{r}) \rho_0(\mathbf{r}') d\mathbf{r} d\mathbf{r}' \quad (4.108)$$

(2) L_ϕ is the **hydrodynamical part I**, which mixes the slowly varying phase $\phi(\mathbf{r}, t)$ and slowly varying density $\rho_0(\mathbf{r})$, and is given below

$$L_\phi = - \int \left(\hbar \partial_t \phi + \frac{\hbar^2}{2m} (\nabla \phi)^2 \right) \rho_0(\mathbf{r}) d\mathbf{r} \quad (4.109)$$

The term in the integral (4.109) is the Lagrangian density. This quantity when integrated over a unit cell of the lattice gives an average energy density for the system that depends on parameter ϕ only. Thus, we shall write the term as

$$\begin{aligned} E(\phi) &= \frac{1}{V} \int_V \left(\hbar \partial_t \phi + \frac{\hbar^2}{2m} (\nabla \phi)^2 \right) \rho_0(\mathbf{r}) d\mathbf{r} \\ &= \left(\hbar \partial_t \phi + \frac{\hbar^2}{2m} (\nabla \phi)^2 \right) \frac{1}{V} \int_V \rho_0(\mathbf{r}) d\mathbf{r} - \frac{1}{V} \int_V \left(\nabla \left(\hbar \partial_t \phi + \frac{\hbar^2}{2m} (\nabla \phi)^2 \right) \int_V \rho_0(\mathbf{r}) d\mathbf{r} \right) d\mathbf{r} \\ &\simeq \left(\hbar \partial_t \phi + \frac{\hbar^2}{2m} (\nabla \phi)^2 \right) \rho \end{aligned} \quad (4.110)$$

Here, we performed integration by parts and ignored the terms with higher order derivatives.

(3) L_u is the **elastic part I**, given by

$$\begin{aligned} L_u &= -\frac{\hbar^2}{4m} \int (\epsilon_{ik}^s + \epsilon_{ik}^v) \frac{\partial_i \rho_0 \partial_k \rho_0}{\rho_0} (1 - \epsilon_{ll}^s - \epsilon_{ll}^v) d\mathbf{r} + \frac{\hbar^2}{8m} \int \frac{(\nabla \rho_0)^2}{\rho_0} (\epsilon_{kk}^s + \epsilon_{kk}^v) d\mathbf{r} \\ &\quad + \frac{1}{2} \int ((\epsilon_{ik}^s + \epsilon_{ik}^v) f_{ik}(\mathbf{r}' - \mathbf{r}) + (\epsilon_{ll}^s + \epsilon_{ll}^{s'} + \epsilon_{ll}^v + \epsilon_{ll}^{v'}) U(|\mathbf{r} - \mathbf{r}'|) \rho_0(\mathbf{r}) \rho_0(\mathbf{r}') d\mathbf{r} d\mathbf{r}' \end{aligned} \quad (4.111)$$

It can be averaged directly. However it involves both quadratic and linear terms, they can be grouped and simplified and hence, the elastic part I of the Lagrangian reduces to,

$$L_u = \int \left(\frac{1}{2} c_{ik}^{(2)} \epsilon_{ik}^s \epsilon_{ll}^s - \mu \rho \epsilon_{ll}^s \right) d\mathbf{r} + \int \left(\frac{1}{2} c_{ik}^{(2)} \epsilon_{ik}^v \epsilon_{ll}^v - \mu \rho \epsilon_{ll}^v \right) d\mathbf{r} \quad (4.112)$$

where $c_{ik}^{(2)}$ is the elastic constant entering through the quadratic term, and is given by

$$c_{ik}^{(2)} = \frac{1}{V} \int_V \frac{\hbar^2}{2m} \frac{\partial_i \rho_0 \partial_k \rho_0}{\rho_0} d\mathbf{r}$$

and

$$\mu = \frac{\hbar^2}{4m} \left(\frac{(\nabla \rho_0)^2}{2\rho_0^2} - \frac{\nabla^2 \rho_0}{\rho_0} \right) + \int U(|\mathbf{r} - \mathbf{r}'|) \rho_0(\mathbf{r}') d\mathbf{r}' \quad (4.113)$$

(4) $L_{\tilde{\phi}}$ is the **hydrodynamical part II**, given as

$$\begin{aligned} L_{\tilde{\phi}} = & \hbar \int \rho_0(\mathbf{r}) (\partial_t u_k^{ss} \partial_k \tilde{\phi} + \partial_t u_k^v \partial_k \tilde{\phi} + \frac{\hbar}{m} \partial_i u_k^{ss} \partial_i \Phi \partial_k \tilde{\phi} + \frac{\hbar}{m} \partial_i u_k^v \partial_i \Phi \partial_k \tilde{\phi} \\ & - \frac{\hbar}{m} \nabla \phi \cdot \nabla \tilde{\phi} - \frac{\hbar}{2m} (\nabla \tilde{\phi})^2) d\mathbf{r} \end{aligned} \quad (4.114)$$

Now, above equation (4.114) can be re-written as

$$L_{\tilde{\phi}} = -\frac{\hbar^2}{2m} \int (2\rho_0 \mathbf{A}^s \cdot \nabla \tilde{\phi} + 2\rho_0 \mathbf{A}^v \cdot \nabla \tilde{\phi} + \rho_0 (\nabla \tilde{\phi})^2) d\mathbf{r}$$

with

$$\mathbf{A}^s = \left(\nabla \phi - (\nabla \phi \cdot \nabla) \mathbf{u}^{ss} - \frac{m}{\hbar} \partial_t \mathbf{u}^{ss} \right) \quad (4.115)$$

and,

$$\mathbf{A}^v = \left(-(\nabla \phi \cdot \nabla) \mathbf{u}^v - \frac{m}{\hbar} \partial_t \mathbf{u}^v \right) \quad (4.116)$$

The Euler-Lagrange condition for this part of Lagrangian $L_{\tilde{\phi}}$ is

$$\mathbf{A}^s \cdot \nabla \rho_0 + \mathbf{A}^v \cdot \nabla \rho_0 + \nabla \cdot (\rho_0 \nabla \tilde{\phi}) = 0$$

Solving this equation for $\tilde{\phi}$ we get $\tilde{\phi} = K_i(A_i^s + A_i^v)$ with $\mathbf{K}(\mathbf{r})$ is a periodic function [194] which satisfies

$$\nabla_i \rho_0 + \nabla \cdot (\rho_0 \nabla K_i) = 0 \quad (4.117)$$

Above equation is to be solved within the unit cell of the lattice i.e. for a function $\tilde{\phi}$ which is periodic with the same period as ρ_0 . It can be written as $\tilde{\phi} = K_i(A_i^v + A_i^s)$, which is a periodic function of \mathbf{r} and linear in \mathbf{A} .

Substituting this expression into the condition (4.117), we see that the function $\mathbf{K}(\mathbf{r})$ satisfies

$$\nabla_i \rho_0 + \nabla \cdot (\rho_0 \nabla K_i) = 0 \quad (4.118)$$

and Lagrangian (4.114) for the phase part is

$$L_{\tilde{\phi}} = \frac{\hbar^2}{2m} \int \rho_{ij}^c A_i^s A_j^s + \rho_{ij}^v A_i^v A_j^v d\mathbf{r} \quad (4.119)$$

with ρ_{ij}^c is the tensor which for symmetric crystal structures is $\rho_{ij}^c = \rho \delta_{ij} - \rho_{ij}^{ss}$, defined as

$$\rho_{ij}^c = \frac{1}{V} \int_V \rho_0(\mathbf{r}) \nabla K_i \cdot \nabla K_j d\mathbf{r}$$

The quantity $\rho^{ss} = \rho$ if the crystal modulation is absent. It is to note that we neglected the last term in equation (4.119) because we donot want to take into account the vortex crystal effective mass. We only consider the mass density of the supersolid lattice and the superfluid component in the system. However when this term is included it will probably give rise to terms with interaction between the two lattices. In present set of calculations, we assume both the lattices to be independent of each other with no interaction among them.

(5) $L_{\tilde{\rho}}$ is the **elastic part II**, given by

$$L_{\tilde{\rho}} = \frac{\hbar^2}{4m} \int \left(\frac{(\nabla \rho_0)^2}{2\rho_0^2} \tilde{\rho} - \frac{\partial_i \rho_0}{\rho_0} \partial_i \tilde{\rho} \right) d\mathbf{r} - \frac{1}{2} \int U(|\mathbf{r} - \mathbf{r}'|) (\rho_0(\mathbf{r}) \tilde{\rho}(\mathbf{r}') + \tilde{\rho}(\mathbf{r}) \rho_0(\mathbf{r}')) d\mathbf{r} d\mathbf{r}' \quad (4.120)$$

$$\begin{aligned} & - \frac{\hbar^2}{8m} \int \left(-2(\epsilon_{ik}^s + \epsilon_{ik}^v) \frac{\partial_i \rho_0 \partial_k \rho_0}{\rho_0^2} \tilde{\rho} + 4(\epsilon_{ik}^s + \epsilon_{ik}^v) \frac{\partial_i \rho_0}{\rho_0} \partial_k \tilde{\rho} + \frac{1}{\rho_0} (\nabla \tilde{\rho})^2 \right) d\mathbf{r} \\ & - \frac{1}{2} \int U(|\mathbf{r} - \mathbf{r}'|) \tilde{\rho}(\mathbf{r}) \tilde{\rho}(\mathbf{r}') d\mathbf{r} d\mathbf{r}' \\ & - \frac{1}{2} \int ((\epsilon_{ik}^s + \epsilon_{ik}^v) f_{ik}(\mathbf{r} - \mathbf{r}')) + ((\epsilon_{il}^s + \epsilon_{il}^v) + (\epsilon_{il}^v + \epsilon_{il}^v)) U(|\mathbf{r} - \mathbf{r}'|) \\ & (\rho_0(\mathbf{r}) \tilde{\rho}(\mathbf{r}') + \tilde{\rho}(\mathbf{r}) \rho_0(\mathbf{r}')) d\mathbf{r} d\mathbf{r}' \end{aligned} \quad (4.121)$$

The terms which are quadratic in the gradients of $\tilde{\rho}$ are the relevant terms because the terms linear in $\tilde{\rho}$ disappears, as the action is at minimum when $n = \rho_0(\mathbf{r})$. Also, the line (4.120) in above equation is equal to $-\mu \int \tilde{\rho}(\mathbf{r}) d\mathbf{r}$. Thus, keeping only relevant terms as below:

$$\begin{aligned} \frac{\hbar^2}{4m} \nabla \cdot \left(\frac{\nabla \tilde{\rho}}{\rho_0} \right) - \int U(|\mathbf{r} - \mathbf{r}'|) \tilde{\rho}(\mathbf{r}') d\mathbf{r}' &= \mu(\epsilon_{kk}^s + \epsilon_{kk}^v) \\ &+ \frac{\hbar^2}{4m} (\epsilon_{ik}^s + \epsilon_{ik}^v) \left(\frac{\partial_i \rho_0 \partial_k \rho_0}{\rho_0^2} - 2 \frac{\partial_{ik} \rho_0}{\rho_0} \right) \\ &+ \epsilon_{ik} \int (f_{ik}(\mathbf{r} - \mathbf{r}') + 2\delta_{ik} U(|\mathbf{r} - \mathbf{r}'|)) \rho_0(\mathbf{r}') d\mathbf{r}' \end{aligned} \quad (4.122)$$

The solution of above equation is periodic function $E_{ik}(\mathbf{r})$ (following ref. [194, 196]) and of the form $\tilde{\rho} = \epsilon_{ik} E_{ik}(\mathbf{r})$. Putting in expression (4.122) and adding the expression (4.112) we get

$$L_u + L_{\tilde{\rho}} = -\frac{1}{2} \int (\lambda_{iklm}^s \epsilon_{ik}^s \epsilon_{lm}^s + \lambda_{iklm}^v \epsilon_{ik}^v \epsilon_{lm}^v) d\mathbf{r} \quad (4.123)$$

This particular form comes from the two elastic energy contributions given in equations (4.111) and (4.121) originating from the third and fourth terms of the original Lagrangian

density (4.81). Here λ_{iklm} is given by

$$\begin{aligned} \lambda_{iklm}^s = & -\frac{1}{V} \int_V \frac{\hbar^2}{2m} \frac{\partial_i \rho_0 \partial_k \rho_0}{\rho_0} \delta_{lm} d\mathbf{r} - \frac{1}{V} \int_V \mu (\delta_{ik} E_{lm}^s(\mathbf{r}) + \delta_{lm} E_{ik}^s(\mathbf{r})) d\mathbf{r} \\ & - \frac{1}{V} \int_V d\mathbf{r} \left(\frac{\hbar^2}{4m} \frac{1}{\rho_0} (\nabla E_{ik}^s) \cdot (\nabla E_{lm}^s) + \int U(|\mathbf{r} - \mathbf{r}'|) E_{ik}^s(\mathbf{r}) E_{lm}^s(\mathbf{r}') d\mathbf{r}' \right) \end{aligned} \quad (4.124)$$

and,

$$\begin{aligned} \lambda_{iklm}^v = & -\frac{1}{V} \int_V \frac{\hbar^2}{2m} \frac{\partial_i \rho_0 \partial_k \rho_0}{\rho_0} \delta_{lm} d\mathbf{r} - \frac{1}{V} \int_V \mu (\delta_{ik} E_{lm}^v(\mathbf{r}) + \delta_{lm} E_{ik}^v(\mathbf{r})) d\mathbf{r} \\ & - \frac{1}{V} \int_V d\mathbf{r} \left(\frac{\hbar^2}{4m} \frac{1}{\rho_0} (\nabla E_{ik}^v) \cdot (\nabla E_{lm}^v) + \int U(|\mathbf{r} - \mathbf{r}'|) E_{ik}^v(\mathbf{r}) E_{lm}^v(\mathbf{r}') d\mathbf{r}' \right) \end{aligned} \quad (4.125)$$

The expression $\frac{1}{2} \lambda_{iklm} \epsilon_{ik} \epsilon_{lm}$ is the expression for the elastic energy density of a solid, and λ_{iklm} is the elastic modulus tensor.

Hence, we can write the effective Lagrangian for the long wave perturbations of displacement of both lattices, of average density and of the phase as the sum of various contribution mentioned above.

$$\begin{aligned} L_{eff} = & -\hbar \rho \frac{\partial \phi}{\partial t} - \frac{\hbar^2}{2m} \left[\rho (\nabla \phi)^2 - (\rho \delta_{ik} - \rho_{ik}^{ss}) \left(\nabla \phi - \frac{m}{\hbar} \frac{D\mathbf{u}^{ss}}{Dt} \right)_i \left(\nabla \phi - \frac{m}{\hbar} \frac{D\mathbf{u}^{ss}}{Dt} \right)_k \right] \\ & - \mathcal{E}(\rho) - \frac{1}{2} \lambda_{iklm}^s \epsilon_{ik}^s \epsilon_{lm}^s - \frac{1}{2} \lambda_{iklm}^v \epsilon_{ik}^v \epsilon_{lm}^v - m \rho \mathbf{v}_s \cdot (\Omega \times \mathbf{r}) \end{aligned} \quad (4.126)$$

where

$$\frac{D\mathbf{u}^{ss}}{Dt} = \frac{\partial \mathbf{u}^{ss}}{\partial t} + \frac{\hbar}{m} \nabla \phi \cdot \nabla \mathbf{u}^{ss} \quad (4.127)$$

It can be clearly seen from the above equation (4.126) that the crystal lattice may have a different velocity than the superfluid component, with the velocity difference proportional to $(\nabla \phi - \frac{\hbar}{m} \frac{D\mathbf{u}^{ss}}{Dt})$, with \mathbf{u}^{ss} as the displacement vector of crystal lattice due to density modulations in superfluid. Hence the third term in equation (4.126) gives the product of the mass density of the supersolid lattice and the square of the supersolid lattice velocity.

One should expect a similar term arising from the relative motion of vortex with respect to the local superfluid, given by product of mass density of vortex lattice and square of vortex lattice velocity. But for sake of simplicity, we have assumed effective mass of the vortex to be negligible, valid for all practical purposes and hence no such term appears in the calculations. For the case of rotating superfluids, it has been taken into account in [183] where one can see the vortex effective mass contribution. In our case, we assume

it to be negligible and consider only the effective mass of supersolid crystal lattice for the system.

Here ρ_{ik}^{ss} is the superfluid density tensor, which is in general a symmetric matrix. The reason is that we consider the supersolid as consisting of a crystal lattice and a superfluid, using Landau two fluid model, with crystal lattice as the normal component of the fluid. In free space, the superfluid density is just the density of the superfluid component, whereas the situation is different in presence of lattice. In the lattice, the superfluid density is a tensor and not just a scalar quantity, because the hopping and hence the effective masses can depend on the direction [197]. In our further calculations, we express that the superfluid density is a function of local number density ρ and for isotropic symmetry of lattice, it is given by $\rho_{ik}^{ss} = \rho^{ss}(\rho)\delta_{ik}$.

We mention here again that we consider a very shallow trap so that the system is effectively flattened in the bulk. Moreover, at high rotational frequencies $\Omega \sim \omega$ the centrifugal force cancels the trapping potential, so that the system is translationally invariant.

It may be noted from the structure of the proposed Lagrangian that we do not take into account coupling of the two lattices with displacement vectors $\mathbf{u}^{ss}, \mathbf{u}^v$ in the lowest order expansion and thus the elastic deformations of the two lattices do not interact with each other directly.

Before obtaining the equations of motion for the rotating supersolid case, we show below that the above Lagrangian (4.126) reduces to that of non-rotating supersolid and rotating superfluid in the respective limits. We show the limiting cases below.

(a) Non-rotating Supersolid

For the case of non-rotating supersolid, the field variables are the density ρ , phase ϕ and the displacement vector of the supersolid lattice \mathbf{u}^{ss} . There is no vortex lattice in the system, and hence the elastic energy contribution from the vortex lattice is kept zero. Also, the rotational term is zero ($\Omega = 0$). Thus, the effective Lagrangian for the non-rotating supersolid is

$$L_{eff} = -\hbar\rho\frac{\partial\phi}{\partial t} - \frac{\hbar^2}{2m} \left[\rho(\nabla\phi)^2 - (\rho\delta_{ik} - \rho_{ik}^{ss}) \left(\nabla\phi - \frac{m}{\hbar} \frac{D\mathbf{u}^{ss}}{Dt} \right)_i \left(\nabla\phi - \frac{m}{\hbar} \frac{D\mathbf{u}^{ss}}{Dt} \right)_k \right] - \mathcal{E}(\rho) - \frac{1}{2} \lambda_{iklm}^s \epsilon_{ik}^s \epsilon_{lm}^s \quad (4.128)$$

This agrees with the results obtained in [69, 194] for the effective Lagrangian for the supersolid phase.

(b) Rotating superfluid

From equation (4.126), we can recover the Lagrangian for rotating superfluid by switching off the supersolid crystalline component in the equation. The contribution of elastic energy due to the supersolid lattice is zero, and only the elastic energy of vortex lattice is taken into account. Also, the third term in equation (4.126) is zero for rotating superfluid case since it gives the product of mass density of the supersolid crystal lattice multiplied by difference in the superfluid velocity and the crystal lattice velocity. This is because no crystal lattice is present in the system which implies $\rho = \rho_{ik}^{ss}$ thus making $(\rho\delta_{ik} - \rho_{ik}^{ss}) = 0$ in the third term of equation (4.126). In addition to this the crystal lattice velocity given by Du/Dt also vanishes for same reason. Thus, the Lagrangian for the limiting case of rotating superfluid is

$$L_{eff} = -\hbar\rho\frac{\partial\phi}{\partial t} - \frac{\hbar^2}{2m}\rho(\nabla\phi)^2 - \mathcal{E}(\rho) - \frac{1}{2}\lambda_{iklm}^v\epsilon_{ik}^v\epsilon_{lm}^v + m\rho\mathbf{v}_s \cdot (\boldsymbol{\Omega} \times \mathbf{r}) \quad (4.129)$$

where ρ is the smoothened density [183] of the rotating superfluid system and $\mathcal{E}(\rho)$ is the internal energy of the rotating fluid depending on the chemical potential as shown in equation (4.43)

$$\mathcal{E}(\rho) = \mu\rho = \frac{\hbar^2}{2m}\frac{(\nabla\rho)^2}{4\rho} + \frac{g}{2}\rho^2 \quad (4.130)$$

It is to note that ρ is not identified with n here, which is the density of the superfluid defined from the mean field order parameter. ρ is the average density and related to n by the relation (4.83). It differs from the supersolid case as there is no superfluid density tensor, hence $\rho = \rho_{ik}^{ss}$, removing all the supersolid crystal lattice terms. Else it can be derived using the homogenization technique in the same manner.

After verification of the existing cases, we derive the hydrodynamic equations of motion for the rotating supersolid system.

4.4 Hydrodynamic equations of motion for rotating supersolid

The dynamical equations are derived by variation of action S taken as a functional of ρ , ϕ , \mathbf{u}^{ss} and \mathbf{u}^v . This yields a set of coupled of partial differential equations for those fields. The action to be extremised is $S = \int L_{eff}dt$, gives the condition

$$\delta \int Ldt = 0$$

where, $L_{eff} = L_{eff}(\rho, \phi, \nabla\mathbf{u}^{ss}, \nabla\mathbf{u}^v)$, which implies

$$\frac{\partial L_{eff}}{\partial\rho}d\rho + \frac{\partial L_{eff}}{\partial\phi}d\phi + \frac{\partial L_{eff}}{\partial(\nabla\mathbf{u}^{ss})}d(\nabla\mathbf{u}^{ss}) + \frac{\partial L_{eff}}{\partial(\nabla\mathbf{u}^v)}d(\nabla\mathbf{u}^v) = 0 \quad (4.131)$$

The above Lagrangian can also be written as

$$L_{eff} = \int d\mathbf{r} \left[-\hbar\rho \frac{\partial\phi}{\partial t} - \mathcal{E} \right]$$

where

$$\mathcal{E} = \mathcal{E}_{in}(\rho) + \mathcal{E}_{ph}(\phi) + \mathcal{E}_{el}^{ss}(\nabla\mathbf{u}^{ss}) + \mathcal{E}_{el}^v(\nabla\mathbf{u}^v) \quad (4.132)$$

with

$$\begin{aligned} \mathcal{E}_{in}(\rho) &= \frac{\hbar^2}{2m} \frac{(\nabla\rho)^2}{4\rho} + \rho \int U(|\mathbf{r} - \mathbf{r}'|) \rho(\mathbf{r}') d\mathbf{r}' = \mu\rho \\ \mathcal{E}_{ph}(\phi) &= \frac{\hbar^2}{2m} \left[\rho(\nabla\phi)^2 - (\rho\delta_{ik} - \rho_{ik}^{ss}) \left(\nabla\phi - \frac{m}{\hbar} \frac{D\mathbf{u}^{ss}}{Dt} \right)_i \left(\nabla\phi - \frac{m}{\hbar} \frac{D\mathbf{u}^{ss}}{Dt} \right)_k \right] \\ &\quad + m\rho\mathbf{v}_s \cdot (\boldsymbol{\Omega} \times \mathbf{r}) \\ \mathcal{E}_{el}^{ss}(\nabla\mathbf{u}^{ss}) &= \frac{1}{2} \lambda_{iklm}^s \epsilon_{ik}^s \epsilon_{lm}^s \\ \mathcal{E}_{el}^v(\nabla\mathbf{u}^v) &= \frac{1}{2} \lambda_{iklm}^v \epsilon_{ik}^v \epsilon_{lm}^v \end{aligned} \quad (4.133)$$

The elastic energy density has a general form [188] given by

$$\mathcal{E}_{el} = \frac{1}{2} \lambda_{iklm} \epsilon_{ik} \epsilon_{lm} \quad (4.134)$$

The equation (4.134) is the general form of the free energy of the deformed crystal. Here ϵ_{ik} is the strain tensor, given by

$$\epsilon_{ik} = \frac{1}{2} \left(\frac{\partial u_i}{\partial x_k} + \frac{\partial u_k}{\partial x_i} \right) \quad (4.135)$$

and λ_{iklm} is a tensor of rank four which relates the strains to the stresses and called as the *elastic modulus tensor*. The elastic modulus tensor and its symmetry properties have already been explained in detail in section 4.1.3.

From extremisation condition, we get the following equations of motion for the density and phase of the rotating supersolid system, in the rotating reference frame along with the equations of elastic response of the system due to the supersolid lattice and the vortex lattice. The equations of motion for the density and phase are given as

$$\frac{\partial\rho}{\partial t} + \nabla \cdot \left(\rho \frac{\hbar}{m} \nabla\phi \right) + \frac{\partial}{\partial x_k} \left[(\rho - \rho^{ss})(\delta_{ik} - \partial_k u_i^{ss}) \left(\dot{u}_i^{ss} - \frac{\hbar}{m} \partial_i \phi \right) \right] = 0 \quad (4.136)$$

and,

$$m \left(\frac{\partial \mathbf{v}_s}{\partial t} + 2\boldsymbol{\Omega} \times \mathbf{v}_s \right) = - \frac{\nabla P'}{\rho} \quad (4.137)$$

Here, ρ_{ik}^{ss} is the superfluid density tensor which assumes the form $\rho_{ik}^{ss} = \rho^{ss} \delta_{ik}$ for isotropic symmetry of the system and,

$$P' = \rho \left(T + \int U(|\mathbf{r} - \mathbf{r}'|) \rho(\mathbf{r}') d\mathbf{r}' \right) \quad (4.138)$$

In the equation (4.137), we have kept only the linearized terms and the nonlinear terms with higher orders of derivatives have been dropped. The neglected terms in equation (4.137) are given below.

$$\begin{aligned} \frac{\partial}{\partial \rho} (\rho - \rho_{ss}) \left(\nabla \phi - \frac{m}{\hbar} \frac{D\mathbf{u}^{ss}}{Dt} \right)^2 &= \left(\frac{(\rho^2 - 1)\delta\rho}{\rho} - \nabla \cdot \mathbf{u}^{ss} \right) \left(\nabla \phi - \frac{m}{\hbar} \frac{D\mathbf{u}^{ss}}{Dt} \right)^2 \\ &= \left(\frac{(\rho^2 - 1)\delta\rho}{\rho} - \nabla \cdot \mathbf{u}^{ss} \right) ((\nabla \phi)^2 + \left(\frac{m}{\hbar} \right)^2 \left(\frac{D\mathbf{u}^{ss}}{Dt} \right)^2 \\ &\quad - 2 \frac{m}{\hbar} \nabla \phi \cdot \frac{D\mathbf{u}^{ss}}{Dt}) \end{aligned}$$

These terms contain the product of the derivatives of different terms, for example, $\frac{(\rho^2 - 1)\delta\rho}{\rho} (\nabla \phi)^2$, $\nabla \cdot \mathbf{u}^{ss} \left(\frac{m}{\hbar} \right)^2 \left(\frac{D\mathbf{u}^{ss}}{Dt} \right)^2$, and hence are neglected and not taken into account. As pointed out earlier, when averaged over a vortex lattice cell, equation (4.137) can be written as

$$m \left(\frac{\partial \mathbf{v}_s}{\partial t} + \tilde{\omega} \times \mathbf{v}_L \right) = - \frac{\nabla P'}{\rho} \quad (4.139)$$

with \mathbf{v}_s as the averaged velocity and $\tilde{\omega} = 2\mathbf{\Omega} + \nabla \times \mathbf{v}_s$ as the averaged vorticity. The velocity of the vortex is given by \mathbf{v}_L and it is equal to time derivative of the displacement vector of the vortex lattice $\dot{\mathbf{u}}^v$.

As already mentioned, the continuity equation (4.136) represents the law of conservation of mass and the Euler equation (4.139) is momentum conservation equation, balancing the various force terms arising due to rotation, the Coriolis and the Centrifugal force. As already mentioned in section 4.1.2, for the case of rotating superfluid with an embedded vortex lattice, the small deformations due to displacement of the vortex lattice are taken into account using the classical theory of elasticity. The force \mathbf{f} acting per unit volume of the fluid moving with velocity \mathbf{v}_s is

$$\mathbf{f}_{el}^v = -\rho \tilde{\omega} \times (\mathbf{v}_L - \mathbf{v}_s) \quad (4.140)$$

and it should be connected with a variation of energy due to vortex displacements. Thus,

$$\begin{aligned} f_{el,i}^v &= - \frac{\delta \mathcal{E}_{el}^v}{\delta u_i^v} = - \frac{\partial}{\partial x_k} \left(\frac{\delta \mathcal{E}_{el}^v}{\delta (\partial u_k^v / \partial x_i)} \right) \\ &= - [(\lambda^v + \mu_s^v) \nabla (\nabla \cdot \mathbf{u}^v) + \mu_s^v \nabla^2 \mathbf{u}^v] \end{aligned} \quad (4.141)$$

Here the general expression for elastic energy density equation (4.134) is used and when the lattice is isotropic (section 4.1.3) i.e it has the same properties in all directions.

Hence using equations (4.140) and (4.141) we get

$$\rho 2\Omega[\hat{z} \times (\mathbf{v}_L - \mathbf{v}_s)] = \frac{(\lambda^v + \mu_s^v)\nabla(\nabla \cdot \mathbf{u}^v) + \mu_s^v \nabla^2 \mathbf{u}^v}{m} \quad (4.142)$$

where $\lambda^v = K^v - \frac{2}{3}\mu_s^v$ is the Lamé coefficient [188], and K^v and μ_s^v are the compressibility and shear modulus of the vortex lattice. Equation (4.142) is the equation of motion of the system due to the elastic response of the vortex lattice.

Next we determine the equation of motion due to the elastic response of the supersolid crystal lattice by considering the 3rd term in equation (4.131) and is thus given by

$$m \frac{\partial}{\partial t} \left[(\rho - \rho^{ss}) \left(\dot{u}_i^{ss} - \frac{\hbar}{m} \partial_i \phi \right) \right] + \hbar \frac{\partial}{\partial x_k} \left[(\rho - \rho^{ss}) \left(\dot{u}_i^{ss} - \frac{\hbar}{m} \partial_i \phi \right) \partial_k \phi \right] + \frac{\partial}{\partial x_k} (\lambda_{iklm}^s \epsilon_{lm}^s) = 0 \quad (4.143)$$

Here also when the lattice is assumed to be isotropic then above equation (4.143) can be written as

$$m \frac{\partial}{\partial t} \left[(\rho - \rho^{ss}) \left(\dot{u}_i^{ss} - \frac{\hbar}{m} \partial_i \phi \right) \right] + \hbar \frac{\partial}{\partial x_k} \left[(\rho - \rho^{ss}) \left(\dot{u}_i^{ss} - \frac{\hbar}{m} \partial_i \phi \right) \partial_k \phi \right] + (\lambda^{ss} + \mu_s^{ss}) \partial_{ik} u_k^{ss} + \mu_s^{ss} \nabla^2 u_i^{ss} = 0 \quad (4.144)$$

where $\lambda^{ss} = K^{ss} - \frac{2}{3}\mu_s^{ss}$ is the second Lamé coefficient [188], and K^{ss} and μ_s^{ss} are the compressibility and shear modulus of the solid [188].

Thus, equations (4.136), (4.139), (4.142) and (4.144) are the equations of motion for a rotating supersolid with elastic properties of both vortex lattice and supersolid crystal lattice taken into account [110].

$$\frac{\partial \rho}{\partial t} + \nabla \cdot \left(\rho \frac{\hbar}{m} \nabla \phi \right) + \frac{\partial}{\partial x_k} \left[(\rho - \rho^{ss}) (\delta_{ik} - \partial_k u_i^{ss}) \left(\dot{u}_i^{ss} - \frac{\hbar}{m} \partial_i \phi \right) \right] = 0 \quad (4.145)$$

$$m \left(\frac{\partial \mathbf{v}_s}{\partial t} + 2\Omega \times \mathbf{v}_L \right) = -\frac{\nabla P'}{\rho} \quad (4.146)$$

$$\rho 2\Omega[\hat{z} \times (\mathbf{v}_L - \mathbf{v}_s)] = \frac{(\lambda^v + \mu_s^v)\nabla(\nabla \cdot \mathbf{u}^v) + \mu_s^v \nabla^2 \mathbf{u}^v}{m} \quad (4.147)$$

$$m \frac{\partial}{\partial t} \left[(\rho - \rho^{ss}) \left(\dot{u}_i^{ss} - \frac{\hbar}{m} \partial_i \phi \right) \right] + \hbar \frac{\partial}{\partial x_k} \left[(\rho - \rho^{ss}) \left(\dot{u}_i^{ss} - \frac{\hbar}{m} \partial_i \phi \right) \partial_k \phi \right] - (\lambda^{ss} + \mu_s^{ss}) \partial_{ik} u_k^{ss} + \mu_s^{ss} \nabla^2 u_i^{ss} = 0 \quad (4.148)$$

These set of four equations form the hydrodynamic equations of motion for a rotating supersolid system [110]. For consistency, we write all the equations in tensorial notation as given below

$$\frac{\partial \rho}{\partial t} + \rho \frac{\hbar}{m} \nabla^2 \phi + \frac{\partial}{\partial x_k} \left[(\rho - \rho^{ss}) (\delta_{ik} - \partial_k u_i^{ss}) \left(\dot{u}_i^{ss} - \frac{\hbar}{m} \partial_i \phi \right) \right] = 0 \quad (4.149)$$

$$m \left(\frac{\partial v_s^i}{\partial t} + 2 \epsilon_{ijk} \Omega^j v_L^k \right) = - \frac{\partial_i P'}{\rho} \quad (4.150)$$

$$2 \rho \epsilon_{ijk} \Omega^j (v_L - v_s)^k = \frac{(\lambda^v + \mu_s^v) \partial_{ik}^2 u_k^v + \mu_s^v \nabla^2 u_i^v}{m} \quad (4.151)$$

$$m \frac{\partial}{\partial t} \left[(\rho - \rho^{ss}) \left(\dot{u}_i^{ss} - \frac{\hbar}{m} \partial_i \phi \right) \right] + \hbar \frac{\partial}{\partial x_k} \left[(\rho - \rho^{ss}) \left(\dot{u}_i^{ss} - \frac{\hbar}{m} \partial_i \phi \right) \partial_k \phi \right] - (\lambda^{ss} + \mu_s^{ss}) \partial_{ik}^2 u_k^{ss} + \mu_s^{ss} \nabla^2 u_i^{ss} = 0 \quad (4.152)$$

where ϵ_{ijk} is the Levi Civita symbol.

In the next section, we investigate the small perturbations around a non-deformed steady state of system to characterize the dynamics of the system [110].

4.5 Dispersion calculations

Using the set of hydrodynamic equations obtained in previous section, we investigate the small perturbations around a non-deformed ($\mathbf{u}^{ss} = 0$, $\mathbf{u}^v = 0$) state of average density $\bar{\rho}$ to characterize the dynamics of the rotating supersolid system. So, we write the linearized version of the four equations derived in previous section in terms of small perturbations for $\delta \rho$, $\delta \phi$, $\nabla \cdot \mathbf{u}^{ss} = \delta J^{ss}$ and \mathbf{u}^v .

Here, $\delta J^{ss} = \nabla \cdot \mathbf{u}^{ss}$ is the elastic compressibility of the supersolid lattice.

Since an ordinary compression in a solid changes the number density of particle, because of the small deformation itself we take

$$\rho = \bar{\rho} + \bar{\rho} \nabla \cdot \mathbf{u}^{ss} + \delta\rho \quad (4.153)$$

Here, ρ is the total average density which is related to the superfluid density n by equation (4.83). The above equation (4.153) implies the oscillations around the equilibrium state $\bar{\rho}$. $\bar{\rho}$ is the average density of the non-deformed state over which small perturbations are taken into account. Here the perturbation around the uniform state $\bar{\rho}$ is unusual because it takes into account two types of density variations : one is the usual change in the density of solids which is because of strain in the solid $\nabla \cdot \mathbf{u}_{ss}$ and the second change comes from the long range superfluid behavior $\delta\rho$. Due to negligible vortex effective mass, there is no such term due to the compression effects of vortex lattice in the expansion for average density ρ in equation (4.153). This first hydrodynamic equation is given by

$$\frac{\partial \rho}{\partial t} + \nabla \cdot \left(\rho \frac{\hbar}{m} \nabla \phi \right) + \frac{\partial}{\partial x_k} \left[(\rho - \rho^{ss})(\delta_{ik} - \partial_k u_i^{ss}) \left(\dot{u}_i^{ss} - \frac{\hbar}{m} \partial_i \phi \right) \right] = 0 \quad (4.154)$$

Linearization around the steady state solution $\rho = \bar{\rho}$, gives

$$\begin{aligned} & \left. \frac{\partial \rho}{\partial t} \right|_{\rho=\bar{\rho}} + \left. \frac{\partial}{\partial \rho} \left(\frac{\partial \rho}{\partial t} \right) \right|_{\rho=\bar{\rho}} \cdot (\rho - \bar{\rho}) + \left. \nabla \cdot (\rho \mathbf{v}_s) \right|_{\rho=\bar{\rho}} + \left. \frac{\partial}{\partial \rho} [\nabla \cdot (\rho \mathbf{v}_s)] \right|_{\rho=\bar{\rho}} \cdot (\rho - \bar{\rho}) \\ & + \left. \frac{\partial}{\partial x_k} \left[(\rho - \rho^{ss})(\delta_{ik} - \partial_k u_i^{ss}) \left(\dot{u}_i^{ss} - \frac{\hbar}{m} \partial_i \phi \right) \right] \right|_{\rho=\bar{\rho}} \\ & + \left. \frac{\partial}{\partial \rho} \left[\frac{\partial}{\partial x_k} \left[(\rho - \rho^{ss})(\delta_{ik} - \partial_k u_i^{ss}) \left(\dot{u}_i^{ss} - \frac{\hbar}{m} \partial_i \phi \right) \right] \right] \right|_{\rho=\bar{\rho}} \cdot (\rho - \bar{\rho}) = 0 \end{aligned} \quad (4.155)$$

The steady state solution (4.136), sets the combination 1st, 3rd and 5th terms in above equation to zero leaving us with,

$$\begin{aligned} & \left. \frac{\partial}{\partial t} (\bar{\rho} \nabla \cdot \mathbf{u}_{ss} + \delta\rho) + \frac{\partial}{\partial \rho} [\nabla \cdot (\rho \mathbf{v}_s)] \right|_{\rho=\bar{\rho}} \cdot (\bar{\rho} \nabla \cdot \mathbf{u}_{ss} + \delta\rho) \\ & + \left. \frac{\partial}{\partial \rho} \left[\frac{\partial}{\partial x_k} \left[(\rho - \rho^{ss})(\delta_{ik} - \partial_k u_i^{ss}) \left(\dot{u}_i^{ss} - \frac{\hbar}{m} \partial_i \phi \right) \right] \right] \right|_{\rho=\bar{\rho}} \cdot (\rho - \bar{\rho}) = 0 \end{aligned} \quad (4.156)$$

Starting from equation (4.156), further derivation is provided below

$$\begin{aligned}
& \frac{\partial}{\partial t}(\bar{\rho} \nabla \cdot \mathbf{u}_{ss} + \delta\rho) + \frac{\partial}{\partial \rho} [\nabla \cdot (\rho \mathbf{v}_s)] \Big|_{\rho=\bar{\rho}} \cdot (\bar{\rho} \nabla \cdot \mathbf{u}_{ss} + \delta\rho) \\
& + \frac{\partial}{\partial \rho} \left[\frac{\partial}{\partial x_k} \left[(\rho - \rho^{ss})(\delta_{ik} - \partial_k u_i^{ss}) \left(\dot{u}_i^{ss} - \frac{\hbar}{m} \partial_i \phi \right) \right] \right] \Big|_{\rho=\bar{\rho}} \cdot (\rho - \bar{\rho}) = 0 \\
\Rightarrow & \frac{\partial}{\partial t}(\bar{\rho} \nabla \cdot \mathbf{u}_{ss}) + \frac{\partial}{\partial t} \delta\rho + h.o.t \\
& + \frac{\partial}{\partial \rho} \left[\frac{\partial}{\partial x_k} [(\rho - \rho^{ss})(\delta_{ik} - \partial_k u_i^{ss})(\dot{u}_i^{ss} - (\mathbf{v}_s)_i)] \right] \Big|_{\rho=\bar{\rho}} \cdot (\bar{\rho} \nabla \cdot \mathbf{u}_{ss} + \delta\rho) = 0 \\
\Rightarrow & \frac{\partial}{\partial t} \delta\rho + \frac{\partial}{\partial \rho} \left[\frac{\partial}{\partial x_k} [(\rho - \rho^{ss})(\dot{u}_k^{ss} - (\mathbf{v}_s)_k - \partial_k u_i^{ss}(\dot{u}_i^{ss} - (\mathbf{v}_s)_i))] \right] \Big|_{\rho=\bar{\rho}} \cdot (\bar{\rho} \nabla \cdot \mathbf{u}_{ss} + \delta\rho) = 0 \\
\Rightarrow & \frac{\partial}{\partial t} \delta\rho + \frac{\partial}{\partial \rho} \left\{ (\rho_{ss} - \rho) \left(\nabla \cdot \mathbf{v}_s - \frac{\partial}{\partial t} \delta J_{ss} \right) \right\} \Big|_{\rho=\bar{\rho}} \cdot (\bar{\rho} \nabla \cdot \mathbf{u}_{ss} + \delta\rho) + h.o.t = 0 \quad (4.157)
\end{aligned}$$

We now focus on the last term separately as shown below

$$\begin{aligned}
& \frac{\partial}{\partial \rho} \left\{ (\rho_{ss} - \rho) \left(\nabla \cdot \mathbf{v}_s - \frac{\partial}{\partial t} \delta J_{ss} \right) \right\} \Big|_{\rho=\bar{\rho}} \cdot (\bar{\rho} \nabla \cdot \mathbf{u}_{ss} + \delta\rho) \\
& = \frac{\partial}{\partial \rho} \left\{ \rho_{ss} \left(\nabla \cdot \mathbf{v}_s - \frac{\partial}{\partial t} \delta J_{ss} \right) \right\} \Big|_{\rho=\bar{\rho}} \cdot (\bar{\rho} \nabla \cdot \mathbf{u}_{ss} + \delta\rho) \\
& - \frac{\partial}{\partial \rho} \left\{ \rho \left(\nabla \cdot \mathbf{v}_s - \frac{\partial}{\partial t} \delta J_{ss} \right) \right\} \Big|_{\rho=\bar{\rho}} \cdot (\bar{\rho} \nabla \cdot \mathbf{u}_{ss} + \delta\rho) \\
& = \left(\nabla \cdot \mathbf{v}_s - \frac{\partial}{\partial t} \delta J_{ss} \right) \frac{\partial \rho_{ss}}{\partial \rho} \cdot (\bar{\rho} \nabla \cdot \mathbf{u}_{ss} + \delta\rho) \\
& + \rho_{ss} \frac{\partial}{\partial \rho} \left(\nabla \cdot \mathbf{v}_s - \frac{\partial}{\partial t} \delta J_{ss} \right) \Big|_{\rho=\bar{\rho}} \cdot (\bar{\rho} \nabla \cdot \mathbf{u}_{ss} + \delta\rho) \\
& - \frac{\partial \rho}{\partial \rho} \Big|_{\rho=\bar{\rho}} \left(\nabla \cdot \mathbf{v}_s - \frac{\partial}{\partial t} \delta J_{ss} \right) \cdot (\bar{\rho} \nabla \cdot \mathbf{u}_{ss} + \delta\rho) \\
& - \bar{\rho} \frac{\partial}{\partial \rho} \left(\nabla \cdot \mathbf{v}_s - \frac{\partial}{\partial t} \delta J_{ss} \right) \Big|_{\rho=\bar{\rho}} \cdot (\bar{\rho} \nabla \cdot \mathbf{u}_{ss} + \delta\rho) \\
& = \left(\nabla \cdot \mathbf{v}_s - \frac{\partial}{\partial t} \delta J_{ss} \right) \frac{\partial}{\partial \rho} [\rho_{ss} \cdot (\bar{\rho} \nabla \cdot \mathbf{u}_{ss} + \delta\rho)] - \rho_{ss} \frac{\partial}{\partial \rho} (\bar{\rho} \nabla \cdot \mathbf{u}_{ss} + \delta\rho) \\
& + \text{zero} - h.o.t - \text{zero} \\
& = \left(\nabla \cdot \mathbf{v}_s - \frac{\partial}{\partial t} \delta J_{ss} \right) \rho_{ss} \cdot 1 \quad (4.158)
\end{aligned}$$

So from equation (4.157) and (4.158) we get

$$\frac{\partial \delta\rho}{\partial t} + \rho_{ss} \left(\nabla \cdot \mathbf{v}_s - \frac{\partial}{\partial t} \delta J_{ss} \right) = 0 \quad (4.159)$$

Here, we have ignored the higher order terms. This gives us the first linearized hydrodynamic equation.

We next linearize the second hydrodynamic equation which is given by

$$m \left(\frac{\partial \mathbf{v}_s}{\partial t} + 2\Omega \times \mathbf{v}_L \right) = -\frac{\nabla P'}{\rho} \quad (4.160)$$

Now, it is known that the change in pressure is related to density change by

$$\nabla P' = mc_s^2 \nabla \rho \quad (4.161)$$

Thus, the equation (4.160) can be written as

$$\rho \left(\frac{\partial \mathbf{v}_s}{\partial t} + 2\Omega \times \mathbf{v}_L \right) = -c_s^2 \nabla \rho$$

Linearizing,

$$\begin{aligned} \rho \left(\frac{\partial \mathbf{v}_s}{\partial t} + 2\Omega \times \mathbf{v}_L \right) \Big|_{\rho=\bar{\rho}} + \frac{\partial}{\partial \rho} \left\{ \rho \left(\frac{\partial \mathbf{v}_s}{\partial t} + 2\Omega \times \mathbf{v}_L \right) \right\} \Big|_{\rho=\bar{\rho}} \cdot (\rho - \bar{\rho}) \\ = -c_s^2 \nabla \rho \Big|_{\rho=\bar{\rho}} - \frac{\partial}{\partial \rho} (c_s^2 \nabla \rho) \Big|_{\rho=\bar{\rho}} \cdot (\rho - \bar{\rho}) \end{aligned} \quad (4.162)$$

which implies

$$\bar{\rho} \left(\frac{\partial \mathbf{v}_s}{\partial t} + 2\Omega \times \mathbf{v}_L \right) = -c_s^2 \nabla \delta \rho \quad (4.163)$$

and can be written as

$$\rho^{ss} \left(\frac{\partial \mathbf{v}_s}{\partial t} + 2\Omega \times \mathbf{v}_L \right) = -c_{sm}^2 \nabla \delta \rho \quad (4.164)$$

where

$$c_{sm}^2 = c_s^2 (\rho^{ss} / \bar{\rho}) \quad (4.165)$$

is the modified sound wave velocity. Thus, equation (4.164) is the linearized second hydrodynamic. The third hydrodynamic equation of motion in linearized form is very straightforward to obtain and is given below

$$\bar{\rho} 2\Omega [\hat{z} \times (\mathbf{v}_L - \mathbf{v}_s)] = \frac{(\lambda^v + \mu_s^v) \nabla (\nabla \cdot \mathbf{u}^v) + \mu_s^v \nabla^2 \mathbf{u}^v}{m} \quad (4.166)$$

Now the fourth hydrodynamic equation of motion

$$m(\bar{\rho} - \rho^{ss}) \frac{\partial}{\partial t} \left(\frac{\partial}{\partial t} \delta J_{ss} - \frac{\hbar}{m} \nabla^2 \delta \phi \right) - (\lambda^{ss} + 2\mu_s^{ss}) \nabla^2 \delta J_{ss} = 0 \quad (4.167)$$

Equation (4.167) has been obtained after taking divergence of the equation for the elastic response of the supersolid lattice and linearized in terms of small perturbations

in the elastic compressibility δJ_{ss} [110] . This is done as follows, starting from the 4th hydrodynamic equation

$$m \frac{\partial}{\partial t} \left[(\rho - \rho^{ss}) \left(\dot{u}_i^{ss} - \frac{\hbar}{m} \partial_i \phi \right) \right] + \hbar \frac{\partial}{\partial x_k} \left[(\rho - \rho^{ss}) \left(\dot{u}_i^{ss} - \frac{\hbar}{m} \partial_i \phi \right) \partial_k \phi \right] - [(\lambda^{ss} + \mu_s^{ss}) \partial_{ik} u_k^{ss} + \mu_s^{ss} \nabla^2 u_i^{ss}] = 0 \quad (4.168)$$

Take divergence,

$$m \frac{\partial}{\partial t} \left[(\rho - \rho^{ss}) \left(\frac{\partial}{\partial t} \delta J_{ss} - \nabla \cdot \mathbf{v}_s \right) \right] + \hbar \nabla^2 \left[(\rho - \rho^{ss}) \left(\dot{u}_i^{ss} - \frac{\hbar}{m} \partial_i \phi \right) \partial_k \phi \right] - [(\lambda^{ss} + \mu_s^{ss}) \nabla^2 \delta J_{ss} + \mu_s^{ss} \nabla^2 \delta J_{ss}] = 0 \quad (4.169)$$

which implies

$$m \frac{\partial}{\partial t} \left[(\rho - \rho^{ss}) \left(\frac{\partial}{\partial t} \delta J_{ss} - \nabla \cdot \mathbf{v}_s \right) \right] - (\lambda^{ss} + 2\mu_s^{ss}) \nabla^2 \delta J_{ss} = 0$$

Here we have ignored the second term which is of higher order in equation (4.169). Now we move ahead to linearize above equation

$$\begin{aligned} & m \frac{\partial}{\partial t} \left[(\rho - \rho^{ss}) \left(\frac{\partial}{\partial t} \delta J_{ss} - \nabla \cdot \mathbf{v}_s \right) \right] \Big|_{\rho=\bar{\rho}} \\ & + \frac{\partial}{\partial \rho} \left\{ m \frac{\partial}{\partial t} \left[(\rho - \rho^{ss}) \left(\frac{\partial}{\partial t} \delta J_{ss} - \nabla \cdot \mathbf{v}_s \right) \right] \right\} \Big|_{\rho=\bar{\rho}} \cdot (\bar{\rho} \nabla \cdot \mathbf{u}_{ss} + \delta \rho) - (\lambda^{ss} + 2\mu_s^{ss}) \nabla^2 \delta J_{ss} = 0 \end{aligned} \quad (4.170)$$

implying the following equation,

$$m \frac{\partial}{\partial t} \left[(\bar{\rho} - \rho^{ss}) \left(\frac{\partial}{\partial t} \delta J_{ss} - \nabla \cdot \mathbf{v}_s \right) \right] - (\lambda^{ss} + 2\mu_s^{ss}) \nabla^2 \delta J_{ss} = 0 \quad (4.171)$$

We ignored the second term in above equation being of higher order and hence not taken into account in the linearization process. It is to note that we ignore the effect of an overall trap potential, which gets cancelled due to the centrifugal force at high rotation frequency.

The set of linearized hydrodynamic equations for rotating supersolid is given below

$$\frac{\partial \delta \rho}{\partial t} + \rho^{ss} \frac{\hbar}{m} \nabla^2 \delta \phi + (\bar{\rho} - \rho^{ss}) \frac{\partial}{\partial t} \delta J^{ss} = 0 \quad (4.172)$$

$$\rho^{ss} \left(\frac{\partial \mathbf{v}_s}{\partial t} + 2\mathbf{\Omega} \times \mathbf{v}_L \right) = -c_{sm}^2 \nabla \delta \rho \quad (4.173)$$

$$\bar{\rho}2\Omega[\hat{z} \times (\mathbf{v}_L - \mathbf{v}_s)] = \frac{(\lambda^v + \mu_s^v)\nabla(\nabla \cdot \mathbf{u}^v) + \mu_s^v \nabla^2 \mathbf{u}^v}{m} \quad (4.174)$$

$$m(\bar{\rho} - \rho^{ss})\frac{\partial}{\partial t} \left(\frac{\partial}{\partial t} \delta J^{ss} - \frac{\hbar}{m} \nabla^2 \delta \phi \right) - (\lambda^{ss} + 2\mu_s^{ss}) \nabla^2 \delta J^{ss} = 0 \quad (4.175)$$

Also, in equation (4.173) c_{sm} is the modified sound velocity which is related to usual sound velocity and as shown in equation (4.165) given by

$$c_{sm}^2 = c_s^2(\rho^{ss}/\bar{\rho}) \quad (4.176)$$

The superfluid sound velocity c_s connects the deviations of the pressure and density by

$$\delta P' = mc_s^2 \delta \rho \quad (4.177)$$

where P' is given by expression (4.138).

As mentioned earlier, we ignore the effect of an overall trap potential which gets cancelled due to the centrifugal force at high rotation frequency. Thus to calculate the dispersion relation and the sound modes for the rotating supersolid system. we can write the solutions in terms of plane waves, as given below

$$\delta \rho = \delta \rho(\mathbf{q}) \exp(i\mathbf{q} \cdot \mathbf{r} - i\omega t)$$

$$\mathbf{v}_s = \mathbf{v}_s(\mathbf{q}) \exp(i\mathbf{q} \cdot \mathbf{r} - i\omega t)$$

$$\delta J^{ss} = \delta J^{ss}(\mathbf{q}) \exp(i\mathbf{q} \cdot \mathbf{r} - i\omega t)$$

Here, \mathbf{r} is the two dimensional position vector, in the xy plane normal to the rotation axis. Two components of velocity \mathbf{v}_s are introduced as follows: the component v_{sq} along the wave vector \mathbf{q} and the component v_{st} along the axis normal to both \mathbf{q} and the rotation axis.

We begin by transforming the continuity equation (4.172) and the Euler equation (4.173) in fourier space. This is done as follows.

$$-i\omega \delta \rho + i\rho^{ss} \mathbf{q} \cdot \mathbf{v}_s - i\omega(\bar{\rho} - \rho^{ss}) \delta J^{ss} = 0 \quad (4.178)$$

$$-i\omega \mathbf{v}_s + 2\Omega \times \mathbf{v}_L + \frac{c_{sm}^2}{\rho^{ss}} i\mathbf{q} \delta \rho = 0 \quad (4.179)$$

From equation (4.178), we write

$$\delta \rho = \frac{\rho^{ss} q v_{sq} - \omega(\bar{\rho} - \rho^{ss}) \delta J^{ss}}{\omega} \quad (4.180)$$

Eliminating $\delta\rho$ from equations for v_q and v_t given by equation (4.179) yields two equations,

$$iv_{sq} + 2\Omega \frac{\omega}{(\omega^2 - c_{sm}^2 q^2)} v_{Lt} - \frac{i\omega c_{sm}^2 q(1 - \bar{\rho}/\rho^{ss})}{(\omega^2 - c_{sm}^2 q^2)} \delta J^{ss} = 0 \quad (4.181)$$

$$-i\omega v_{st} + 2\Omega v_{Lq} = 0 \quad (4.182)$$

Now, for further simplification we write the q and t components of equation (4.174),

$$i\omega(v_{Lt} - v_{st}) = \frac{(\lambda^v + 2\mu_s^v)q^2}{2\Omega m\bar{\rho}} v_{Lq} \quad (4.183)$$

$$-i\omega(v_{Lq} - v_{sq}) = \frac{\mu_s^v q^2}{2\Omega m\bar{\rho}} v_{Lt} \quad (4.184)$$

From equations (4.181) and (4.182),

$$v_{st} = -i \frac{2\Omega}{\omega} v_{Lq} \quad (4.185)$$

$$v_{sq} = i \frac{2\Omega\omega}{(\omega^2 - c_{sm}^2 q^2)} v_{Lt} + \frac{c_{sm}^2 q\omega(1 - \bar{\rho}/\rho^{ss})}{(\omega^2 - c_{sm}^2 q^2)} \delta J^{ss} \quad (4.186)$$

Substituting values from equations (4.185) and (4.186) into equations (4.183)-(4.184), we get the following equations for determining the dispersion relation :

$$i\omega v_{Lt} - v_{Lq} \left(\frac{c_{vt}^2 q^2}{2\Omega} + 2\Omega \right) = 0 \quad (4.187)$$

$$i\omega v_{Lq} + v_{Lt} \left[\frac{c_{vs}^2 q^2}{2\Omega} + 2\Omega \frac{\omega^2}{(\omega^2 - c_{sm}^2 q^2)} \right] - i \frac{c_{sm}^2 q\omega^2(1 - \bar{\rho}/\rho^{ss})}{(\omega^2 - c_{sm}^2 q^2)} \delta J^{ss} = 0 \quad (4.188)$$

$$\left[m\omega^2(\bar{\rho} - \rho^{ss}) \frac{\omega^2 - c_s^2 q^2}{\omega^2 - c_{sm}^2 q^2} - q^2(\lambda^{ss} + 2\mu_s^{ss}) \right] \delta J^{ss} + im(\bar{\rho} - \rho^{ss}) 2\Omega \frac{\omega^2}{\omega^2 - c_{sm}^2 q^2} q v_{Lt} = 0 \quad (4.189)$$

where we have labelled the longitudinal and shear parts of vortex lattice velocities by

$$c_{vt}^2 = \frac{\lambda^v + 2\mu_s^v}{m\bar{\rho}}; c_{vs}^2 = \frac{\mu_s^v}{m\bar{\rho}}$$

We write these equations in matrix form as below :

$$\begin{bmatrix} i\omega & -\left(\frac{c_{vt}^2 q^2}{2\Omega} + 2\Omega\right) & 0 \\ \left[\frac{c_{vs}^2 q^2}{2\Omega} + 2\Omega \frac{\omega^2}{(\omega^2 - c_{sm}^2 q^2)}\right] & i\omega & -i \frac{(c_{sm}^2 - c_s^2)q\omega^2}{(\omega^2 - c_{sm}^2 q^2)} \\ \frac{2im\Omega\omega^2(\bar{\rho} - \rho^{ss})}{\omega^2 - c_{sm}^2 q^2} q & 0 & \left[m\omega^2(\bar{\rho} - \rho^{ss}) \frac{\omega^2 - c_s^2 q^2}{\omega^2 - c_{sm}^2 q^2} - q^2(\lambda^{ss} + 2\mu_s^{ss})\right] \end{bmatrix} \begin{bmatrix} v_{Lt} \\ v_{Lq} \\ \delta J^{ss} \end{bmatrix} = 0 \quad (4.190)$$

Before solving these set of coupled equations to determine the various modes for this system, we determine the decoupled shear waves for the rotating supersolid system. It is

obtained by taking curl of equation (4.148) after expanding in terms of small fluctuations, as below

$$\nabla \times \left(m(\bar{\rho} - \rho^{ss}) \frac{\partial}{\partial t} \left(\frac{\partial \mathbf{u}^{ss}}{\partial t} - \frac{\hbar}{m} \nabla \delta \phi \right) - (\lambda^{ss} + 2\mu_s^{ss}) \nabla (\nabla \cdot \mathbf{u}^{ss}) - \mu_s^{ss} \nabla^2 \mathbf{u}^{ss} \right) = 0 \quad (4.191)$$

$$\Rightarrow m(\bar{\rho} - \rho^{ss}) \frac{\partial}{\partial t} \left(\frac{\partial}{\partial t} (\nabla \times \mathbf{u}^{ss}) - 0 \right) - 0 - \mu_s \nabla^2 (\nabla \times \mathbf{u}^{ss}) = 0 \quad (4.192)$$

which gives

$$m(\bar{\rho} - \rho^{ss}) \frac{\partial^2}{\partial t^2} \varpi - \mu_s^{ss} \nabla^2 \varpi = 0 \quad (4.193)$$

where

$$\varpi = \nabla \times \mathbf{u}^{ss} \quad (4.194)$$

This equation (4.193) gives the shear mode velocity which depends on the supersolid density, namely

$$v_{shear}^{ss} = \sqrt{\frac{\mu_s^{ss}}{m(\bar{\rho} - \rho^{ss})}} \quad (4.195)$$

We note that the shear mode for the supersolid is obtained by taking curl of the equation (4.148) for elastic response of the supersolid lattice, and the divergence of the same equation is used to calculate the longitudinal modes of the supersolid lattice. Solving this linear system of equations (4.187-4.189) provides the following algebraic equation for the dispersion equation given by

$$\begin{aligned} & \omega^6 - \omega^4 (c_{km}^2 q^2 + c_s^2 q^2 + (b_1 q^2 + 2\Omega)(b_2 q^2 + 2\Omega)) \\ & + \omega^2 [(c_{sm}^2 q^2 + (b_1 q^2 + 2\Omega)(b_2 q^2 + 2\Omega)) c_{km}^2 q^2 + (b_1 q^2 + 2\Omega)(b_2 q^2)(c_s^2 q^2)] \\ & - (b_1 q^2 + 2\Omega)(b_2 q^2)(c_{sm}^2 q^2)(c_{km}^2 q^2) = 0 \end{aligned} \quad (4.196)$$

where

$$b_1 = \frac{c_{vl}^2}{2\Omega} = \frac{1}{2\Omega} \left[\frac{\lambda^v + 2\mu_s^v}{m\bar{\rho}} \right] \quad (4.197)$$

$$b_2 = \frac{c_{vs}^2}{2\Omega} = \frac{1}{2\Omega} \left[\frac{\mu_s^v}{m\bar{\rho}} \right] \quad (4.198)$$

$$c_{km} = \sqrt{\frac{\lambda^{ss} + 2\mu_s^{ss}}{m(\bar{\rho} - \rho^{ss})}} \quad (4.199)$$

is a quantity that can be written in terms of usual sound speed c_k as

$$c_{km} \approx c_k \left(1 + \frac{\rho^{ss}}{\bar{\rho}} \right)$$

To confirm the validity of our formalism, in the next section, we check the various existing limits from our obtained dispersion equation (4.196) for rotating supersolid.

4.5.1 Checking with various existing limits: Non rotating Supersolid, Rotating superfluid and Non-rotating superfluid

a) Non-rotating Supersolid

We start to cross check the case for a two dimensional non-rotating supersolid. Dispersion relation of a non-rotating supersolid is obtained by setting the condition that for $\Omega = 0$, there is no vortex lattice. Hence equation (4.196) reduces to

$$\omega^4 - \omega^2(c_{km}^2 q^2 + c_s^2 q^2) + (c_{sm}^2 q^2)(c_{km}^2 q^2) = 0 \quad (4.200)$$

Solution of above equation gives us the following dispersion modes

$$\omega^2 = \frac{1}{2}(c_{km}^2 + c_s^2)q^2 \left[1 \pm \left(1 - \frac{4c_{sm}^2 c_{km}^2}{(c_{km}^2 + c_s^2)^2} \right)^{1/2} \right] \quad (4.201)$$

The roots obtained in equation (4.201) confirms with the modes for a non-rotating supersolid as calculated in [69, 194].

It can be easily seen that the dispersion is linear, $\omega = vq$, where v gives the speed of the sound modes which in the limit of small superfluid fraction $\rho^{ss} \rightarrow 0$ are given by

$$v_1^{ss} = \sqrt{c_s^2 + c_k^2} \quad (4.202)$$

$$v_2^{ss} = \sqrt{\frac{c_k^2 c_s^2}{c_k^2 + c_s^2}} \sqrt{\frac{\rho^{ss}}{\bar{\rho} - \rho^{ss}}} \quad (4.203)$$

In addition, a decoupled shear mode is also obtained as in equation (4.195) and is given by

$$v_{shear}^{ss} = \sqrt{\frac{\mu_s^{ss}}{m(\bar{\rho} - \rho^{ss})}} \quad (4.204)$$

This also comply with the results for dispersion modes for non rotating supersolid obtained in [69, 194]. We show the plots of these dispersion modes in Fig. 4.5. The analytical results [110] which show the appearance of two distinct longitudinal modes for a supersolid, are also verified by Saccani et. al [198]. The calculations in [198] are carried out using Quantum Monte Carlo technique and the excitation spectrum of the supersolid phase is obtained. The calculations showed that the spectral weight gets partitioned in two distinct branches. The higher energy mode is the longitudinal acoustic phonon mode, with a linear dispersion at small q and the lower branch of the supersolid

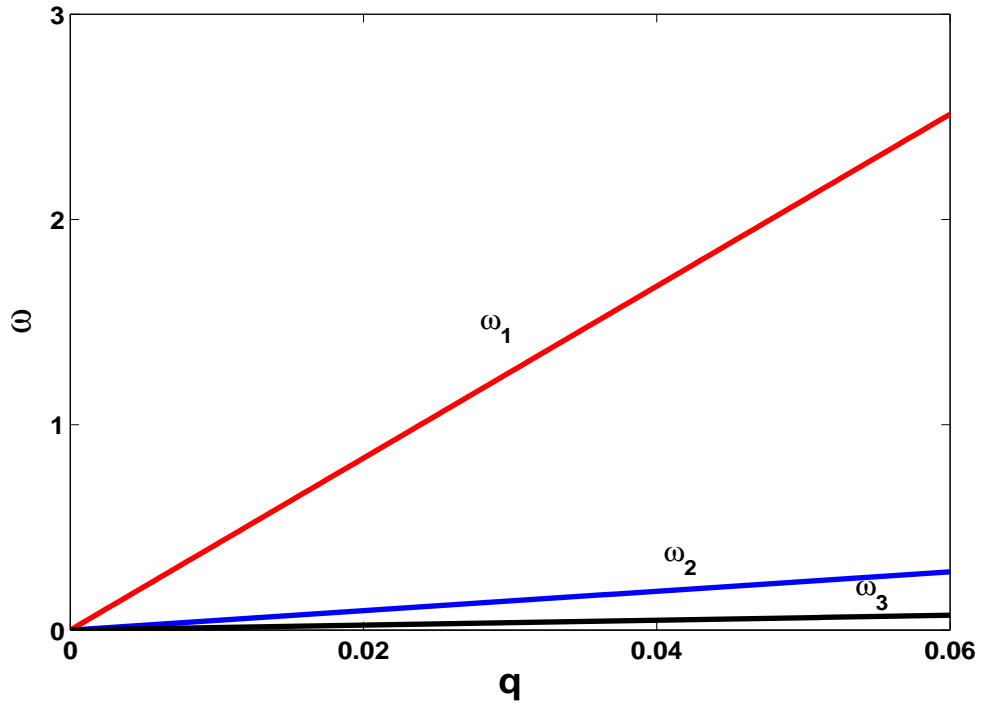


FIGURE 4.5: Dispersion roots for non-rotating supersolid, ω as a function of wave vector q . It is to note that the parameters for the the elastic wave c_k velocity, superfluid velocity c_s are taken from quantum monte carlo calculations done in [198] with superfluid fraction $f_{ss} = 0.3$.

spectrum appears due to the presence of a superfluid fraction co-existing along with the crystal lattice and the dispersion is again linear at small wave vectors.

Similar results are obtained using the hydrodynamic formalism which is valid in the long wavelength or small wave vectors limit. The equations (4.202) and (4.203) are the corresponding two distinct branches or modes as obtained in [198] and shown in Fig. refnrss. However, using the hydrodynamic approach, we also get additional shear mode which is transverse in nature. This mode is not reported in [198] as the calculations are performed only for the longitudinal modes and not the transverse modes for the system. The agreement of the distinct branches for the supersolid in small wave vector limit with the exact Quantum Monte Carlo results, proves the reliability of hydrodynamic theory in long wavelength limit and thus, one expects to see distinct behavior of the supersolid phase compared to superfluid within this theory.

b) Rotating Superfluid

Here we provide the results for the limiting case of a superfluid which is rotating at an angular frequency Ω . To verify this limit of rotating superfluids using the dispersion equation (4.196) for rotating supersolids, we proceed as below.

Since we have only the superfluid component present now with no co-existing lattice or crystal component, the entire contribution to the density is due to the superfluid. Hence, we have to substitute

$$\bar{\rho} = \rho^{ss} \quad (4.205)$$

since there is no crystalline order present. Under these circumstances the following things happen. First the modified elastic wave speed due to presence of the normal component drops out the description. Secondly the modified second sound velocity

$$c_{sm}^2 = c_s^2 \frac{\rho^{ss}}{\bar{\rho}}$$

becomes the second side velocity $c_{sm} = c_s$.

To see how this limit correctly reproduces the result for a rotating superfluid, we separate out in the equation the terms that depend on c_{km}^2 by writing it as

$$\begin{aligned} & [\omega^6 - \omega^4(4\Omega^2 + (c_{vl}^2 + c_{vs}^2)q^2 + c_s^2q^2) + \omega^2c_{vs}^2q^2c_s^2q^2] \\ & = c_{km}^2q^2[\omega^4 - \omega^2(4\Omega^2 + c_{sm}^2q^2 + (c_{vl}^2 + c_{vs}^2)q^2) + c_{vs}^2q^2c_{sm}^2q^2] \end{aligned}$$

We now multiply both side of the equation by $\bar{\rho} - \rho_{ss}$ and take the limit $\rho_{ss} \rightarrow \bar{\rho}$ We also set $c_{sm} = c_s$. This yields (since the left hand side becomes 0).

$$\omega^4 - \omega^2(4\Omega^2 + c_s^2q^2 + (c_{vl}^2 + c_{vs}^2)q^2) + c_{vs}^2q^2c_s^2q^2 = 0 \quad (4.206)$$

It is known that for rotating superfluids, the lattice of vortices arrange themselves in the form of triangular lattice with hexagonal symmetry [34, 185]. The constants b_1 and b_2 are thus written in terms of constants C_1 and C_2 of hexagonal isotropic lattice as

$$b_1 = \frac{1}{2\Omega} \frac{4C_1 + 2C_2}{m\bar{\rho}}; b_2 = \frac{1}{2\Omega} \frac{2C_2}{m\bar{\rho}} \quad (4.207)$$

Substituting relations (4.207) in above equation (4.206) we get

$$\omega^4 - \omega^2 \left[c_s^2q^2 + 4\Omega^2 + \frac{4(C_1 + C_2)}{m\bar{\rho}} \right] + \frac{2c_s^2C_2}{m\bar{\rho}}q^4 = 0 \quad (4.208)$$

For the general case, the shear mode is very small compared to the other modes of the rotating superfluid, hence

$$\frac{2c_s^2C_2}{m\bar{\rho}}q^4 \ll \left[c_s^2q^2 + 4\Omega^2 + \frac{4(C_1 + C_2)}{m\bar{\rho}} \right]^2 \quad (4.209)$$

the mode frequencies are given by

$$\omega_I^2 = \left[c_s^2 q^2 + 4\Omega^2 + \frac{4(C_1 + C_2)}{m\bar{\rho}} \right] \quad (4.210)$$

and,

$$\omega_T^2 = \frac{2C_2}{m\bar{\rho}} \frac{c_s^2 q^4}{\left[c_s^2 q^2 + 4\Omega^2 + \frac{4(C_1 + C_2)}{m\bar{\rho}} \right]} \quad (4.211)$$

The explanation of the roots obtained and the experimental observation of the modes

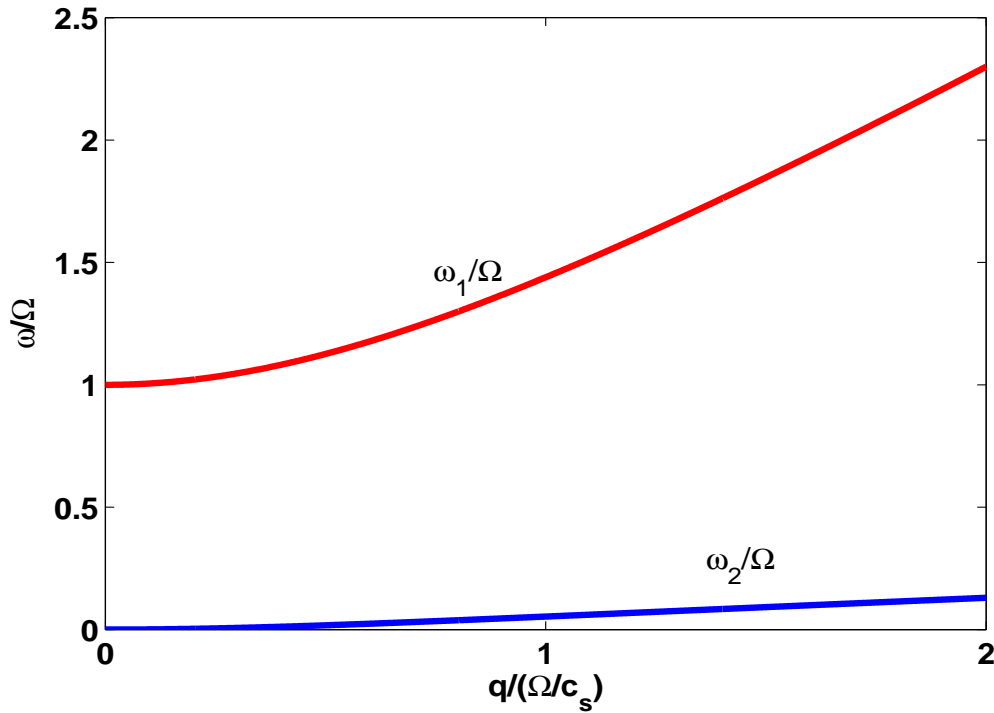


FIGURE 4.6: Dispersion roots for a rotating superfluid, ω in units of Ω as a function of wave vector q in units of Ω/c_s

for a rotating superfluid has already been done in detail in section 4.1.4. Fig. 4.1 shows the plot of the dispersion roots for rotating superfluid system.

Thus, we show that the dispersion equation for rotating supersolid (4.196) reproduces the known results for rotating superfluid [104, 182–184] in the correct limit.

c) Non-rotating Superfluid

Last we consider the limit when we have the case of non-rotating superfluid, for which the parameters reduces as

$$\Omega = 0; \bar{\rho} = \rho^{ss}$$

Substituting the values in equation (4.196), we recover the following mode relation for non-rotating superfluid

$$\omega^2 = c_s^2 q^2$$

where c_s is the usual Bogoliubov sound speed for the superfluid, also termed as *second sound*. We point out that the density ρ in non-rotating superfluid case is the usual density of the superfluid whereas for rotating superfluid with a vortex lattice, it is the smoothened density [182] averaged over the entire lattice cell.

Hence, we have verified the obtained dispersion relation with the case of a) non-rotating supersolid, b) rotating superfluid, c) non-rotating superfluid. In the next section, we calculate the sound modes for rotating supersolid by solving the third order equation (4.196)

4.6 Roots of the Dispersion Relation for Rotating Supersolid

In this section, we determine the roots of the dispersion equation (4.196) for a rotating supersolid. In the low energy long wavelength limit the frequency of the modes is given by solution of the following equation

$$\begin{aligned} & \omega^6 - \omega^4(4\Omega^2 + c_{km}^2 q^2 + c_s^2 q^2 + (c_{vl}^2 + c_{vs}^2)q^2) \\ & + \omega^2[(4\Omega^2 + c_{sm}^2 q^2 + (c_{vl}^2 + c_{vs}^2)q^2)c_{km}^2 q^2 + (c_{vs}^2 q^2)(c_s^2 q^2)] - (c_{vs}^2 q^2)(c_{sm}^2 q^2)(c_{km}^2 q^2) = 0 \end{aligned} \quad (4.212)$$

Even though the general nature of solutions of such cubic (in terms of ω^2) equations are quite involved, the above dispersion relation gets simplified when the velocity associated with the shear mode of the vortex lattice is smaller compared to the other mode velocities. This criteria is generally met for the rotating ultra cold atomic superfluid [182, 183] and therefore it is reasonable to assume a similar condition for ultra cold atomic supersolid as well. Such a condition reads as

$$(c_{vs}^2 q^2)(c_{sm}^2 q^2) << \left(4\Omega^2 + c_{sm}^2 q^2 + (c_{vl}^2 + c_{vs}^2)q^2 + c_{vs}^2 q^2 \frac{c_s^2}{c_{km}^2} \right)^2 \quad (4.213)$$

which is generally the case for long wavelengths in both the incompressible and quantum Hall limits [199]. This approximation is valid since the shear mode of the vortex lattice with velocity given by c_{vs} is too small compared to the other velocities in the system.

Using approximation (4.213) in (4.212) reduces it to a quadratic equation in ω^2 which effectively implies that one of the roots of above equation is very small and can be neglected to zero. The equation reduces to

$$\begin{aligned} & \omega^4 - \omega^2(4\Omega^2 + c_{km}^2 q^2 + c_s^2 q^2 + (c_{vl}^2 + c_{vs}^2)q^2) \\ & + [(4\Omega^2 + c_{sm}^2 q^2 + (c_{vl}^2 + c_{vs}^2)q^2)c_{km}^2 q^2 + (c_{vs}^2 q^2)(c_s^2 q^2)] = 0 \end{aligned} \quad (4.214)$$

Under the condition of very high rotation frequencies and low q

$$[(4\Omega^2 + c_{sm}^2 q^2 + (c_{vl}^2 + c_{vs}^2)q^2)c_{km}^2 q^2 + (c_{vs}^2 q^2)(c_s^2 q^2)] < (4\Omega^2 + c_{km}^2 q^2 + c_s^2 q^2 + (c_{vl}^2 + c_{vs}^2)q^2)^2 \quad (4.215)$$

Consequently the two mode frequencies are

$$\omega_1^2 \simeq 4\Omega^2 + c_{km}^2 q^2 + c_s^2 q^2 + (c_{vl}^2 + c_{vs}^2)q^2 \quad (4.216)$$

and,

$$\omega_2^2 \simeq \frac{[(4\Omega^2 + c_{sm}^2 q^2 + (c_{vl}^2 + c_{vs}^2)q^2)c_{km}^2 q^2 + (c_{vs}^2 q^2)(c_s^2 q^2)]}{(4\Omega^2 + c_{km}^2 q^2 + c_s^2 q^2 + (c_{vl}^2 + c_{vs}^2)q^2)} \quad (4.217)$$

In addition to this, as obtained in equation (4.195) there exists a supersolid shear mode which is decoupled from other modes and is given by

$$\omega_3^2 = \frac{\mu_s^{ss}}{m(\bar{\rho} - \rho^{ss})} q^2 \quad (4.218)$$

Within the approximation (4.215), the first mode (4.216) is the inertial mode of the rotating supersolid. For $\Omega^2 \ll c_{km}^2 q^2$ it is a sound wave while for $\Omega^2 \gg c_{km}^2 q^2$ the mode frequency begins essentially at 2Ω .

The second mode (4.217) is the coupled mode where all the three velocities, the supersolid lattice velocity, the superfluid velocity and the vortex lattice velocity gets coupled. The last mode (4.218) is the decoupled shear mode of the supersolid lattice which depends on the supersolid density [110]. Thus, the dispersion equation provides us the bulk excitation spectrum of the rotating supersolid within this hydrodynamic approximation.

All three modes have been plotted in the figure (4.7), where the wave vector is scaled in units of $2\Omega/c_{km}$ and the mode frequencies are scaled in units of 2Ω .

To understand the significance of the mode frequencies, we can rewrite the first collective mode frequency (4.216) $\omega_1^2 = \omega_{vl}^2 + \omega_{ss}^2$ where $\omega_{vl}^2 = [4\Omega^2 + (c_{vl}^2 + c_{vs}^2)q^2]$, $\omega_{ss}^2 = (c_{km}^2 q^2 + c_s^2 q^2)$. This is a symmetric combination of the modes corresponding to the vortex lattice and the supersolid lattice. In the limit of first rotation and small wave

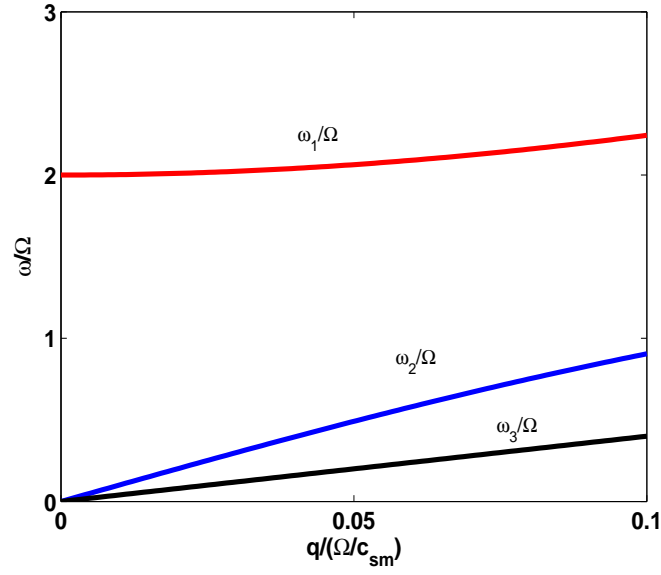


FIGURE 4.7: Dispersion roots for rotating supersolid. Inertial(ω_1), coupled mode(ω_2) and shear mode (ω_3) frequencies as a function of wave vector q . The wave vector is in units of Ω/c_{sm} and the mode frequencies are in units of Ω . The value of vortex lattice velocity c_{vl} and c_{vs} have been taken from [182] and the elastic wave c_k velocity, superfluid velocity c_s are taken from quantum monte carlo calculations done in [198] with superfluid fraction $f_{ss} = 0.3$.

vector, the second mode (4.217) can be approximately written as

$$\omega_2^2 \approx \frac{\omega_{ss}^2}{\omega_{vl}^2} \left(\omega_{vl}^2 - \omega_{ss}^2 + c_{sm}^2 q^2 + c_{vs}^2 q^2 \frac{c_s^2}{c_{km}^2} \right) \quad (4.219)$$

To understand this mode, we set the simplifying assumption $\omega_{vl} = \omega_{ss}$, and also takes $c_{sm}^2 q^2 \ll 4\Omega^2$ and $c_{vs}^2 q^2 (c_s^2/c_{km}^2) \ll 4\Omega^2$ due to fast rotation and small q . This yields

$$\omega_2^2 = \omega_{vl}^2 - \omega_{ss}^2$$

Thus this mode represents the antisymmetric coupling between the vortex and the supersolid lattice. For a more realistic situation one can readily calculate the modification of this mode frequency due to the difference between ω_{vl} and ω_{ss} as well as finite c_{sm} . Thus the normal modes frequencies ω_1 and ω_2 indicates symmetric and antisymmetric combination of modes corresponding to vortex lattice and supersolid lattice and indicates in and out of phase oscillation of two coupled harmonic lattices. Even though hydrodynamic Lagrangian is derived retaining only the lowest order terms and there is no direct coupling between supersolid lattice displacement \mathbf{u}^{ss} and the vortex lattice displacement and the vortex lattice displacement \mathbf{u}^v , the symmetric and antisymmetric modes indicates the in and out of phase oscillations of these lattices.

We depict this in and out of phase oscillation of these two lattices with the help of a schematic diagram in Fig. 4.8. The general nature of our results suggests its applicability well beyond the hydrodynamic approximations and other simplifying assumptions made and may shed light on supersolidity in other systems also

This is one of the main results of this chapter, where we can explicitly observe the coupling between the two lattices in the dispersion and hence the sound modes of the system [110]. It is thus possible to detect the co-existing superfluid and crystalline behavior in the form of coupled sound modes for rotating supersolid system as compared to the rotating superfluid system. We explain the possibilities to observe such coupled modes in experiments in the next section.

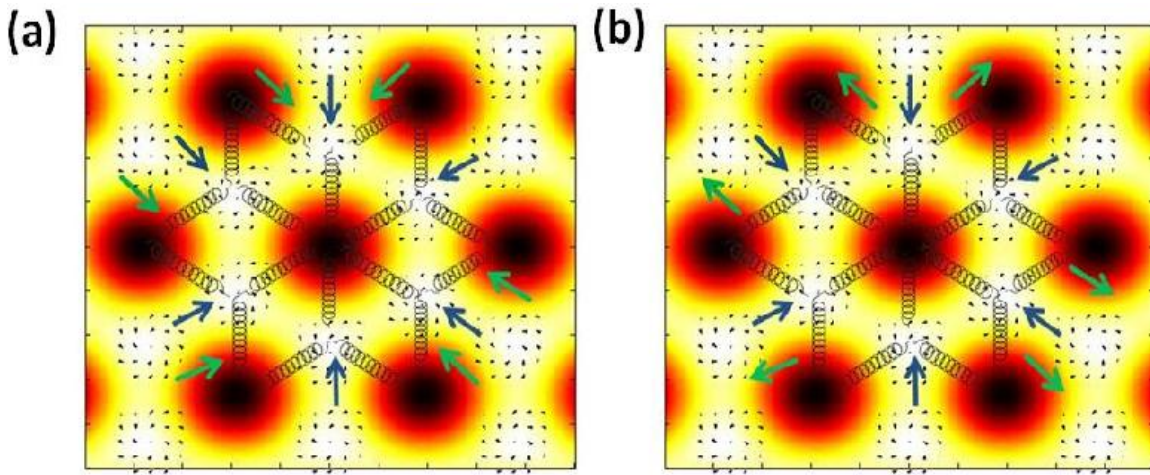


FIGURE 4.8: Schematic diagram to show the symmetric (in phase) and antisymmetric (out of phase) oscillations of the two coupled lattices. The direction of the arrows shows the in-phase or out of phase oscillations of the lattices.

4.6.1 Possibility of experimental verification

As already explained in detail in section 4.1.5, the collective oscillations for the case of rotating superfluids have been successfully observed experimentally [34]. Motivated by this, one can apply the same techniques used for rotating superfluids to perturb the system slightly and hence induce a deformation in the co-existing supersolid and vortex lattice for the case of rotating supersolids. The oscillations of these lattices can be observed using the TOF expansion technique and the data for the frequency of the oscillations can be extracted by fitting the lattice oscillations [34] as done for rotating superfluids.

In the limit of long wavelength low frequency limit, the rotating supersolid system shows symmetric and anti-symmetric coupled modes of the two lattices and hence detection of such coupled modes could be a convincing proof of the existence of two lattices in the rotating supersolid system. The rotating supersolid system shows a normal mode splitting in the oscillation modes, which is a novel proof of the supersolidity, since it indicates the existence of a supersolid lattice alongwith the vortex lattice in the superfluid. In addition to these modes, there could be other complicated oscillation modes which may be present in the system due to the interaction of the two lattices. This has not been considered in the current thesis and will be a subject matter of research in future work.

4.7 Summary of the work done in this Chapter

To summarize, in this chapter we study the rotation of supersolids in continuum systems. Following the Gross-Pitaevskii theory for rotating superfluids, we developed the hydrodynamic theory for rotating supersolid in such continuum systems [110]. We obtain an effective Lagrangian for the system by Homogenization technique where the vortex lattice co-exists with the supersolid lattice. We describe the lattice part of the supersolid as the normal component within the well known two fluid component. The resulting hydrodynamic equations of motion are obtained which enables us to calculate the dispersion relations and hence collective oscillations for the system with embedded vortex lattice and the supersolid lattice. We showed that the oscillation modes of the rotating supersolid system carry signatures of superfluid, the supersolid lattice and the vortex lattice in the system and are comparatively different from rotating superfluids. It is also shown that the system exhibits coupled harmonic lattice oscillation modes corresponding to a normal mode splitting in the system [110]. This is the most important result of this work. We also suggest the experimental ways by which such oscillations can be induced and observed in the system. As mentioned earlier in this chapter, there are quite a number of candidates to realise these specific type of long range interaction potentials which stabilize the supersolid phase in BEC. A promising candidate are the experiments with cavity mediated long-range interaction in ultra cold atomic BEC which can possibly demonstrate the formation of supersolid phase and study the effect of rotation on such system.

Experiments with rotating ultracold condensates with non-local long range interactions opens new avenue to look into the physics of the interior of the neutron stars [200]. It is established that the superfluids form vortices when they are rotated. In context of neutron stars, astronomers believe that the superfluid in neutron stars contain giant vortices or in other words, superfluid tornadoes. This is because the many neutron stars

are pulsar stars, which emits radio waves, light regularly while spinning at extremely high rotational speeds. It is observed that some times these pulsars start running very fast or very slow, and the belief is that this is because of the decay and formation of vortices in the rotating superfluid neutron star system.

Moreover, the hydrodynamic equations for neutron star systems [201] have similar structure as that of rotating superfluid and rotating supersolid systems. The neutron star systems can have coexisting superfluid and elastic component [202] which provides an additional dynamical degree of freedom to the system. The understanding of rotating superfluid and rotating supersolid systems using hydrodynamic equations can find applications to study the behavior of analogous spinning neutron star systems, which is an important field of study in astrophysics.

Chapter 5

Conclusions

5.1 Summary

In this thesis we have discussed the quantum simulation of the supersolid phase using ultracold atomic condensates in the presence of artificial gauge potentials. For ultracold BEC with certain type of long range interactions, our theory provides results for the exotic supersolid phase in such gauge potentials, in both lattice and continuum systems. The main proposition of this thesis is that behavior of the supersolid phase under such artificial gauge fields could be a convincing proof of supersolidity whose occurrence is otherwise debated in context of other systems such as solid ^4He [51, 56–59, 67, 68]. We particularly show how the signatures for solid like behavior coexisting with superfluidity can be demonstrated in the presence of such gauge fields and is the major content of the work done in this thesis.

We begin our study of supersolid phase in the context of ultracold atoms with general long range interactions in the presence of optical lattice potentials. Depending on the strength of long range interactions, it can lead to appearance of states with different types of long range order like various types of Density Wave (DW) phases and supersolid (SS) phases, in addition to the Mott Insulator (MI) and superfluid (SF) phase. In deep optical lattice potential, under tight binding approximation, this system is described by the extended Bose Hubbard model where the long range interactions splits up into onsite, nearest neighbor interactions, next nearest neighbor interactions and so on. We have studied the minimal extended Bose Hubbard model where the system shows DW phase with n_0 and $n_0 - 1$ particles on alternating sites and the SS phase along with MI and SF phase.

In chapter 2 we report the calculations for the effect of artificial gauge field on the DW-SS and MI-SF transition boundaries. We perform the calculations analytically using

the mean field Gutzwiller variational formalism in the framework of extended Bose Hubbard model under the effect of such gauge fields. The minimization of the energy functional very near to the transition boundaries, shows that both the DW-SS and MI-SF phase boundaries extends with increasing values of the gauge fields. It shows that in a supersolid phase, superfluid order parameter very near the transition boundaries satisfies the spinorial Harper equation, and the such boundaries can be analytically determined from the edge of the eigen value of the corresponding Hofstadter Butterfly spectrum [105].

Further, the spatial vortex profile of the superfluid density in the supersolid phase shows a checkerboard-like two sublattice modulation with the vortex like relative phase winding of the superfluid order parameter defined on each of these sublattices. We analytically determined such vortex profiles and demonstrated the co-existence of superfluid and crystal order in the system near the transition boundary, which provides a distinct signature of supersolidity. We have shown structural difference in vortex in a supersolid compared to vortex in a superfluid [105], can be used to identify the supersolid phase in cold-atom experiments. In chapter 2, we also discussed the possible ways to experimentally detect such vortices. One can use the Time of Flight (TOF) imaging technique to get the sublattice modulation of the superfluid density in the form of extra peaks in momentum distribution. Moreover, for getting the detailed vortex structure, one can use the Bragg scattering technique, which is sensitive to the spatial phase distribution of the initial state and the direction of rotation.

All the research results in chapter 2 have been published in **Physical Review A** **82**, **063617 (2010)** [105].

Chapter 3 of the thesis continues to explore properties of supersolid phase within the strongly interacting regime, but with a more accurate and reliable technique, called as the strong coupling perturbation theory. We use this approach to calculate the effect of artificial gauge field on the transition boundaries of DW-SS and MI-SF phase and also calculate the experimental signatures of the vortex structures in a supersolid phase. Due to the involved nature of calculations, we divide this chapter into two parts and study the effect of an artificial magnetic (gauge) field on the supersolid phase within this strong coupling perturbation formalism.

In part 3A of the chapter, we calculate the modification of the DW-SS and MI-SF phase boundaries as a function of increasing magnetic field using strong coupling perturbation approach. As compared to the mean field theory, which is linear in t and has limited accuracy in lower dimensions, the strong coupling perturbation theory which is a many body perturbation expansion in terms of the scaled hopping parameter t/U , includes higher order corrections in t/U , and hence provides more accuracy and gives

us a quantitative insight of the critical points. We found that the shapes of the insulating lobes depend on the dimensionality of the system and, also on the application of artificial gauge field. Mean-field theory always gives a concave shape to the MI and DW lobes because the dimensionality only enters as a prefactor in the expressions, while the strong-coupling expansion easily distinguishes the shape of insulating lobes in different dimensions, both in the absence and presence of the artificial magnetic field. The determination of DW-SS and MI-SF transition boundaries as a function of artificial gauge field, using strong-coupling perturbation theory, is one of the important results of this work [109].

To further go beyond the finite order strong coupling perturbation expansion, we also carried out an extrapolation of phase boundaries using chemical potential exploration technique based on the scaling hypothesis and compared with the results obtained from mean field in chapter 2. The effect of increasing artificial gauge field again shows the increasing stability of the insulating phase (i.e. the Density Wave and Mott Insulator phases grow in size as the strength of the magnetic field is increased from zero to finite values). This is again explained due to the localization effect of magnetic field on the moving bosons, hence favoring the insulating phases to occupy a larger area in the phase diagram [109].

Further, in the other part 3B of the chapter, we calculate the possible experimental signatures for effect of gauge field on the supersolid phase, within the framework of strong coupling perturbation theory. We calculated the momentum distribution profile at the Density Wave - supersolid and Mott Insulator - superfluid phase boundary in presence of artificial gauge field for both type of gauge potentials, the Landau gauge and the symmetric gauge potential. The results for the momentum distribution shows the dependence of this physically observable quantity on the type of artificial gauge potential used to generate the artificial gauge field. We explain this apparent gauge dependence of momentum distribution as a direct result of the realization of a specific vector potential and not the field, in the typical experimental setups. The momentum distribution profiles show the reduction in the Brillouin zone depending on the type of gauge potential used. Another very important conclusion of these calculations is that the momentum distribution profiles at the DW-SS phase boundary shows small extra peaks in addition to the peaks observed at the MI-SF transition [109]. The extra peaks in addition to peaks for rotating superfluid for symmetric gauge potential reflects that the system possesses co-existing crystalline and superfluid behavior will help to identify supersolidity experimentally.

In the presence of a symmetric gauge potential in optical lattice, the system will have conserved quasi angular momentum. This quasi-angular momentum is analogous to the

Bloch momentum for a rotationally invariant system in presence of lattice. Thus, we re-evaluate the momentum distribution, but for a given fixed quasi-angular momentum and found that the results at the DW-SS phase boundary can be distinguished from the MI-SF phase boundary by noting the appearance of small extra peaks in the former. The fact that a zero quasi-angular momentum state can be distinguished from a nonzero one by looking at the corresponding momentum distribution allows the experimentalists to verify that vorticity has entered the system through the TOF measurement.

All the research results in chapter 3 have been published in **Physical Review A** **85**, **013624 (2012)** [109].

To complete our study of the supersolid phase, we also did calculations for the same in the weakly interacting regime for a continuum system. As we decrease the depth of the lattice potential, we move away from the strongly interacting regime to the weakly interacting regime, where the Hubbard model description is replaced by the mean field Gross-Pitaevskii formalism. In the absence of optical lattice, the continuum limit of studying supersolid phase and its signatures in an artificial gauge field are much more convincing as compared to the lattice counterparts. As we explained in chapter 4, the reason is that the induced periodicity of the underlying lattice is partly responsible for the occurrence of supersolidity. In the continuum limit, the supersolidity in ultracold atomic condensates is entirely intrinsic or in other words interaction driven and not an artifact of the applied optical lattice potential.

An important method of investigation of such continuum supersolids is to study the collective modes of the system and detect the various sound modes which are the reflection of system's elastic properties. The study of vortex dynamics in rotating superfluids is quite remarkable both theoretically and experimentally and served as an important test for ultracold atomic superfluidity. The theoretical approach based on macroscopic Gross-Pitaevskii based hydrodynamics was found capable of describing the oscillation modes of a regular vortex lattice in ultracold atomic superfluids, which was also subsequently verified experimentally. They were able to detect the Tkachenko modes, which are transverse sound modes in the vortex lattice.

Chapter 4 of the thesis focuses in construction of a Gross-Pitaevskii hydrodynamic theory for rotating supersolid in the weakly interacting regime, where a vortex lattice co-exist with supersolid lattice. The purpose of our study is to understand the nature of the collective excitations of such vortex lattice as much as possible within an analytical framework and point out its difference with the corresponding situation in a superfluid. Rotating supersolids when subjected to small perturbations reveal interesting features that result due to the interplay of two embedded lattice structures, the supersolid lattice

and the vortex lattice, and provide signatures in the sound modes to detect it in comparison to rotating superfluids. We find the nature of collective oscillations of a rotating supersolid is quite different from the rotating superfluids and non-rotating supersolids.

The lattice part of the supersolid is described as the normal component within the well known two-fluid approximation. Within this framework, we derive the set of hydrodynamic equations for rotating supersolid. This is valid under the general conditions of applicability of hydrodynamic theory, in particular the perturbations under consideration are long wave (practically much longer than the lattice size). We also point out typical cold atomic systems where such theory may be applicable. Using these equations, we calculate and analyze the dispersion relations for such collective excitations of vortex lattice in a supersolid [110] within this hydrodynamic approach and compare them against the results for a fast rotating superfluid that was studied theoretically and experimentally. We also showed that our theory [110] can reproduce known solutions of such hydrodynamic equations under various limits, like for a rotating superfluid and for non-rotating supersolid. We also briefly discussed how such hydrodynamic equations gets modified where mutual friction between the supersolid lattice and the vortex lattice is taken into account. We calculate the excitations for the vortex lattice in supersolid and found that it distinctly depends on the quantized nature of circulation in a supersolid and provide unambiguous signature of the existence of macroscopic quantum order.

The most important result of this work is the coupled modes which form as a result of normal mode splitting of the harmonic oscillations of the supersolid and the vortex lattice. The appearance of such novel modes can indeed be a clear signature for supersolid behavior in the system. This may provide a convincing way of verifying supersolidity in continuum systems.

These results will be submitted for publication [110].

To conclude, we study the quantum simulation of the supersolid phase using ultracold atomic condensates with long range interactions in presence of artificial gauge field. We performed the study covering both the strongly interacting and weakly interacting regime of the system and hence, this concludes the work done in the thesis.

5.2 Future scope

The work done in this thesis can lead to exploration of interesting future prospects. This includes the generalization of the mean field calculations done for the minimal extended Bose Hubbard model. The effect of artificial gauge fields on other variants of the eBHM can be studied such as one that includes next nearest neighbor interaction, which shows

other types of Density Wave and supersolid phases. Moreover, with recent progress in manipulating the interactions, these studies will possibly lead to the detection of interesting phases, particularly the supersolid phase and the study of many associated interesting phenomena which are yet to be explored. Thus, our calculations will hopefully stimulate further study in the behavior of different types of supersolid phase in the presence of an artificial gauge field.

The calculations done using the strong coupling perturbation for the eBHM in presence of gauge field can be generalized to higher dimensions. This requires the solution of the Hofstadter Butterfly (HB) problem for the corresponding dimension, which is a highly non-trivial problem. Subsequently the momentum distribution in higher dimensions can also be determined using the minimum eigen value of the HB problem. Moreover, the strong coupling perturbation expansion can also be extended to ultracold atomic systems in optical lattices in presence of non-abelian gauge fields.

The calculations done within the continuum Gross-Pitaevskii hydrodynamic theory could be extended by taking into account higher order terms and including the effect of interaction between the vortex lattice and the supersolid lattice explicitly in the calculations. This might lead to a kind of *mutual friction* between the two lattices, that result in modification of the collective oscillations in the system. Moreover, new modes in addition to the already obtained modes are expected to occur due to mutual friction between the two components. One can also go beyond the hydrodynamic theory whose validity is limited to long wavelength or low frequency and solve the full Bogoliubov dispersion equations for getting all the oscillation modes of the rotating supersolid system. The calculations can also be extended for case of trapped systems, where the small perturbations will no longer be plane waves and hence, should be expanded for finite systems with different geometry.

The hydrodynamic study of the rotating superfluid and rotating supersolid phases may find applications to study the analogous spinning neutron star system. A similar hydrodynamic study of co-existing superfluid and elastic components [202] for spinning neutron stars is an active field study and the study of ultracold atomic condensates can provide some interesting clue for further understanding of these astrophysical systems.

Appendix A

Elliptical Polarization of Tkachenko waves

As mentioned in section 4.1.4, Tkachenko waves are elliptically polarized in nature. We calculate and show below the polrization of these waves from the dispersion equations. The linearized continuity equation for rotating superfluid is given by

$$\frac{\partial \delta \rho}{\partial t} + \rho \nabla \cdot \mathbf{v}_s = 0 \quad (\text{A.1})$$

Writing the x component of above equation in fourier space gives

$$-i\Omega \delta \rho + \rho i q v_{sx} = 0 \quad (\text{A.2})$$

We next write the equation for momentum conservation as derived in section 4.1.2 as

$$\frac{\partial \mathbf{v}_s}{\partial t} + 2\Omega \times \mathbf{v}_s = -\frac{c_s^2 \nabla \delta \rho}{\rho} - \frac{\mathbf{f}}{m\rho} \quad (\text{A.3})$$

We write the x and y components of the above equation for momentum conservation. It is given below as

$$\frac{\partial v_{sx}}{\partial t} - 2\Omega v_{sy} = -\frac{c_s^2 \nabla \delta \rho}{\rho} - \frac{f_x}{m\rho} \quad (\text{A.4})$$

and,

$$\frac{\partial v_{sy}}{\partial t} + 2\Omega v_{sx} = -\frac{f_y}{m\rho} \quad (\text{A.5})$$

where $f_x = (4C_1 + 2C_2) \frac{\partial^2 u_x^v}{\partial x^2}$ and $f_y = 2C_2 \frac{\partial^2 u_y^v}{\partial x^2}$.

In addition to these equations, we also write the x and y components of the acceleration equation given by equation (4.39) as

$$\frac{\partial v_{sx}}{\partial t} - 2\Omega \frac{\partial u_y^v}{\partial t} = -\frac{c_s^2 \nabla \delta \rho}{\rho} \quad (\text{A.6})$$

and,

$$\frac{\partial}{\partial t}(v_{sy} + 2\Omega u_x^v) = 0 \quad (\text{A.7})$$

We now use equation (A.7) and write equations (A.4) and (A.5) in fourier space as

$$-i\omega v_{sx} + (2\Omega)^2 u_x^v - \frac{(4C_1 + 2C_2)}{m\rho} q^2 u_x^v + \frac{c_s^2}{\rho} i q \delta \rho = 0 \quad (\text{A.8})$$

and,

$$2\Omega i\omega u_x^v + 2\Omega v_{sx} - \frac{2C_2}{m\rho} q^2 u_y^v = 0 \quad (\text{A.9})$$

Also, we have the fourier space form of the x component of acceleration equation (A.6) as

$$-i\omega v_{sx} + 2\Omega i\omega u_y^v + \frac{c_s^2}{\rho} i q \delta \rho = 0 \quad (\text{A.10})$$

Thus, we proceed with equations (A.2), (A.8), (A.9) and (A.10) and get the following two equations relating the x and y components of the lattice displacement vector \mathbf{u}^v as

$$\begin{aligned} -2\Omega i\omega u_y^v + \left[(2\Omega)^2 - \frac{(4C_1 + 2C_2)}{m\rho} q^2 \right] u_x^v &= 0 \\ 2\Omega i\omega u_x^v + \left[(2\Omega)^2 \frac{\omega^2}{\omega^2 - c_s^2 q^2} - \frac{2C_2}{m\rho} q^2 \right] u_y^v &= 0 \end{aligned} \quad (\text{A.11})$$

It is evident from the above derived two equations for x and y components of the displacement field of the vortex lattice vector that the Tkachenko waves are elliptically polarized. The x and y components differ in amplitude and phase by 90° , which defines elliptical motion of the waves.

References

- [1] S.N. Bose, Zeitschrift für Physik **26**, 178 (1924)
- [2] A. Einstein, Zweite Abhandlung, Sitzungsber. Preuss. Akad. Wiss **1925**, **3** (1925)
- [3] N. N. Bogoliubov, J. Phys. (USSR), **11:23**, 1947.
- [4] O. Penrose and L. Onsager, Phys. Rev. **104**, 576 (1956)
- [5] C. N. Yang, Rev. Mod. Phys. **34**, 694 (1962)
- [6] M.H. Anderson, J. R. Ensher, M. R. Matthews, C. E. Wieman, E. A. Cornell, Science **269**, 198 (1995);
- [7] K.B. Davis, M. O. Mewes, M. R. Andrews, N. J. van Druten, D. S. Durfee, D. M. Kurn, and W. Ketterle, Phys. Rev. Lett. **75**, 3969 (1995)
- [8] F. London, Nature **141**, 643 (1938)
- [9] E. P. Gross, Nuovo Cimento **20**, 454 (1961); L. P. Pitaevskii, Sov. Phys. JETP **13**, 451 (1961).
- [10] 2001 Nobel prize in Physics, <http://www.nobel.se/physics/laureates/2001/illpres>.
- [11] 1997 Nobel prize in Physics, <http://www.nobel.se/physics/laureates/1997/illpres>.
- [12] C. C. Bradley, C. A. Sackett, J. J. Tollett, and R. G. Hulet, Phys. Rev. Lett. **75**, 1687 (1995).
- [13] S. L. Cornish, N. R. Claussen, J. L. Roberts, E. A. Cornell, and C. E. Wieman, Phys. Rev. Lett. **85**, 1795 (2000).
- [14] G. Modugno, G. Ferrari, G. Roati, R. J. Brecha, A. Simoni, and M. Inguscio, Science **294**, 1320 (2001).
- [15] T. Weber, J. Herbig, M. Mark, H. C. Nägerl, and R. Grimm, Science **299**, 232 (2003).

- [16] D. G. Fried, T. C. Killian, L. Willmann, D. Landhuis, S. C. Moss, D. Kleppner, and T. J. Greytak, Phys. Rev. Lett. **81**, 3811 (1998).
- [17] A. Robert, O. Sirjean, A. Browaeys, J. Poupard, S. Nowak, D. Boiron, C. I. Westbrook, and A. Aspect, Science **292**, 461 (2001).
- [18] F. P. D. Santos, J. Léonard, J. Wang, C. J. Barrelet, F. Perales, E. Rasel, C. S. Unnikrishnan, M. Leduc, and C. Cohen-Tannoudji, Phys. Rev. Lett. **86**, 3459 (2001).
- [19] C. J. Pethick and H. Smith, *Bose-Einstein condensation in dilute gases* (Cambridge, UK, 2002).
- [20] A. Griesmaier, J. Werner, S. Hensler, J. Stuhler, and T. Pfau, Phys. Rev. Lett. **94**, 160401 (2005)
- [21] K. Aikawa, A. Frisch, M. Mark, S. Baier, A. Rietzler, R. Grimm, and F. Ferlaino, Phys. Rev. Lett. **108**, 210401 (2012)
- [22] M. Lu, N. Q. Burdick and B. L. Lev, Phys. Rev. Lett. **108**, 215301 (2012)
- [23] K. K. Ni, S. Ospelkaus, M. H. G. de Miranda, A. Pe'er, B. Neyenhuis, J. J. Zirbel, S. Kotochigova, P. S. Julienne, D. S. Jin, and J. Ye, Science **322**, 231 (2008).
- [24] N. Henkel, R. Nath and T. Pohl, Phys. Rev. Lett **104** , 195302 (2010).
- [25] F. Cinti, P. Jain, M. Boninsegni, A. Micheli, P. Zoller, and G. Pupillo, Phys. Rev. Lett. **105**, 135301 (2010).
- [26] X. Li, W. V. Liu and C. Lin, Phys. Rev. A **83**, 021602(R) (2011)
- [27] R. Heidemann, U. Raitzsch, V. Bendkowsky, B. Butscher, R. Löw, and T. Pfau, Phys. Rev. Lett. **100**, 033601 (2008).
- [28] D. Comparat and P. Pillet, J. Opt. Soc. Am. B: Opt. Phys. **27**, A208 (2010).
- [29] C. Chin, R. Grimm, P. Julienne and E. Tiesinga, Rev. Mod. Phys., **82**, 1225 (2010)
- [30] A. J. Moerdijk, B. J. Verhaar, and A. Axelsson, Phys. Rev. A **51**, 4852 (1995)
- [31] P. O. Fedichev, Y. Kagan, G. V. Shlyapnikov, and J. T. M. Walraven, Phys. Rev. Lett. **77**, 2913 (1996)
- [32] I. Bloch, Physics World **17**, 25 (2004).
- [33] M. Greiner, O. Mandel, T. Esslinger, T. W. Hänsch and I. Bloch, Nature **415**, 39 (2002)

- [34] I. Coddington, P. Engels, V. Schweikhard, and E. A. Cornell, Phys. Rev. Lett. **91**, 100402 (2003)
- [35] R. P. Feynmann, Int. J. Theor. Phys. **21**, 467-488 (1982)
- [36] M. P. A. Fisher, P. B. Weichman, G. Grinstein and D. S. Fisher, Phys. Rev. B **40**, 546 (1989)
- [37] D. Jaksch, C. Bruder, J. I. Cirac, C. W. Gardiner and P. Zoller, Phys. Rev. Lett. **81**, 3108 (1998)
- [38] J. Bardeen, L. N. Cooper, and J. R. Schrieffer, Phys. Rev. **106**, 162 (1957)
- [39] K. M. O'Hara, S. L. Hemmer, M. E. Gehm, S. R. Granade and J. E. Thomas, Science **298**, 2179 (2002)
- [40] S. Giorgini, L. P. Pitaevskii, and S. Stringari, Rev. Mod. Phys. **80**, 1215 (2008).
- [41] A. J. Leggett, *Modern Trends in the Theory of Condensed Matter*, edited by A. Pekalski and R. Przystawa (Springer-Verlag, Berlin, 1980).
- [42] R. Nozières and S. Schmitt-Rink, J. Low Temp. Phys. **59**, 195 (1985).
- [43] D. Porras and J. I. Cirac, Phys. Rev. Lett. **92**, 207901 (2004); A. Friedenauer, H. Schmitz, J. T. Glueckert, D. Porras, and T. Schätz, Nature Phys. **4**, 757 (2008); K. Kim, M.-S. Chang, S. Korenblit, R. Islam, E. E. Edwards, J. K. Freericks, G. D. Lin, L. M. Duan, and C. Monroe, Nature (London) **465**, 590 (2010).
- [44] H. Weimer, M. Müller, I. Lesanovsky, P. Zoller, and H. P. Büchler, Nature Phys. **6**, 382 (2010).
- [45] H. Moritz, T. Stöferle, M. Köhl, and T. Esslinger, Phys. Rev. Lett. **91**, 250402 (2003); B. L. Tolra, K. M. O'Hara, J. H. Huckans, W. D. Phillips, S. L. Rolston, and J. V. Porto Phys. Rev. Lett. **92**, 190401 (2004); T. Kinoshita, T. R. Wenger, and D. S. Weiss, Science **305**, 1125 (2004); B. Paredes, A. Widera, V. Murg, O. Mandel, S. Fölling, I. Cirac, G. V. Shlyapnikov, T. W. Hänsch, and I. Bloch, Nature (London) **429**, 277 (2004)
- [46] L. Sanchez-Palencia, D. Clément, P. Lugan, P. Bouyer, G. V. Shlyapnikov, and A. Aspect, Phys. Rev. Lett. **98**, 210401 (2007)
- [47] P. Nozières, *Bose Einstein Condensation*, edited by A. Griffin, D. W. Snoke and S. Stringari (Cambridge University Press, Cambridge)
- [48] E. P. Gross, Phys. Rev. **106**, 161 (1957)

- [49] E. P. Gross, *Ann. Phys. (N. Y.)* **4**, 57 (1958)
- [50] A. J. Leggett, *Phys. Rev. Lett.* **25**, 1543 (1970)
- [51] A. F. Andreev and I. M. Lifshitz, *Sov. Phys. JETP*, **29**, 1107 (1969).
- [52] G. V. Chester, *Phys. Rev. A* **2**, 256 (1970).
- [53] M. Prokof'ev and B. Svistunov, *Phys. Rev. Lett.* **94**, 155302 (2005).
- [54] P. L. Kapitza, *Nature* **141**, 74 (1938)
- [55] W. H. Keesom, "Helium", Amsterdam, Elsevier, 1st edition 1942
- [56] E. Kim and M. H. W. Chan, *Nature (London)* **427**, 225 (2004)
- [57] E. Kim and M. H. W. Chan, *Science* **305**, 1941 (2004)
- [58] J. Day and J. Beamish, *Nature* **450**, 853 (2007)
- [59] J. Day, O. Syshchenko and J. Beamish, *Phys. Rev. B* **79**, 214524 (2009)
- [60] X. Rojas, A. Haziot, V. Bapst, S. Balibar and H. J. Maris, *Phys. Rev. Lett.* **105**, 145302 (2010)
- [61] J. Day, T. Herman and J. Beamish, *Phys. Rev. Lett.* **95**, 035301 (2005)
- [62] J. Day and J. Beamish, *Phys. Rev. Lett.* **96**, 105304 (2006)
- [63] A. S. C. Rittner, W. Choi, E. J. Mueller and J. D. Reppy, *Phys. Rev. B* **80**, 224516 (2009)
- [64] N. Prokof'ev, *Adv. Phys.* **56**, 381 (2007); D. M. Ceperley and B. Bernu, *Phys. Rev. Lett.* **93**, 155303 (2004)
- [65] S. Balibar, *Nature* **464**, 176 (2010)
- [66] P. W. Anderson, W. F. Brinkman, and D. A. Huse, *Science* **310**, 1164 (2005).
- [67] P. W. Anderson, *Nature Phys.* **3**, 160 (2007); P.W. Anderson, *Phys. Rev. Lett.* **100**, 215301 (2008)
- [68] D. Y. Kim and M. H. W. Chan, *Phys. Rev. Lett.* **109**, 155301 (2012)
- [69] Y. Pomeau, S. Rica, *Phys. Rev. Lett.* **72**, 2426 (1994)
- [70] C. Josserand, Y. Pomeau and S. Rica, *Phys. Rev. Lett.* **98**, 195301 (2007)
- [71] T. Lahaye, C. Menotti, L. Santos, M. Lewenstein and T. Pfau, *Rep. Prog. Phys.* **72**, 126401 (2009).

- [72] M. Baranov, L. Dobrek, K. Góral, L. Santos, and M. Lewenstein, *Physica Scripta*, **102** 74, (2002)
- [73] C. Bruder, R. Fazio and G. Schon, *Phys. Rev.* **47**, 342 (1997); A. van Otterlo and K. H. Wagenblast, *Phys. Rev. Lett.* **72**, 3598 (1994); G. G. Batrouni, R. T. Scalettar, G. T. Zimanyi and A. P. Kampf, *Phys. Rev. Lett.* **74**, 2527 (1995)
- [74] H. P. Buchler, E. Demler, M. Lukin, A. Micheli, N. Prokof'ev, G. Pupillo, and P. Zoller, *Phys. Rev. Lett.* **98**, 060404 (2007); G. E. Astrakharchik, J. Boronat, I. L. Kurbakov, and Y. E. Lozovik, *Phys. Rev. Lett.* **98**, 060405 (2007); C. Mora, O. Parcollet, and X. Waintal, *Phys. Rev. B* **76**, 064511 (2007)
- [75] L. He and W. Hofstetter, *Phys. Rev. A* **83**, 053629 (2011); P. Jain, F. Cinti and M. Boninsegni, *Phys. Rev. B* **84**, 014534 (2011)
- [76] M. Lukin, M. Fleischhauer, R. Cote, L. Duan, D. Jaksch, J. I. Cirac, and P. Zoller, *Phys. Rev. Lett.* **87**, 037901 (2001).
- [77] D. Jaksch, J. I. Cirac, P. Zoller, S. L. Rolston, R. Côté and M. D. Lukin , *Phys. Rev. Lett.* **85** 2208 (2000).
- [78] E. Urban, T. A. Johnson, T. Henage, L. Isenhower, D. D. Yavuz, T. G. Walker and M. Saffman, *Nat. Phys.* **5**, 110 (2009); A. Gaëtan, Y. Miroshnychenko, T. Wilk, A. Chotia, M. Viteau, D. Comparat, P. Pillet, A. Browaeys and P. Grangier, *Nat. Phys.* **5**, 115 (2009).
- [79] M. Müller, I. Lesanovsky, H. Weimer, H. P. Büchler and P. Zoller, *Phys. Rev. Lett.* **102**, 170502 (2009); H. Weimer, M. Müller, I. Lesanovsky, P. Zoller and H. P. Büchler, *Nat. Phys.* **6**, 382 (2010)
- [80] T. Pohl, E. Demler and M. D. Lukin, *Phys. Rev. Lett.* **104**, 043002 (2010); J. Schachenmayer, I. Lesanovsky, A. Micheli and A. J. Daley *New J. Phys.* **12**, 103044 (2010); H. Weimer and H. P. Büchler, *Phys. Rev. Lett.* **105**, 230403 (2010).
- [81] R. Mottl, F. Brennecke, K. Baumann, R. Landig, T. Donner, T. Esslinger *Science* **336**, 1570 (2012).
- [82] N. Henkel, F. Cinti, P. Jain, G. Pupillo, and T. Pohl, *Phys. Rev. Lett.* **108**, 265301 (2012).
- [83] A. A. Abrikosov, *Sov. Phys. JETP* **5**, 1174 (1957).
- [84] G. Juzeliūnas and P. Öhberg, *Phys. Rev. Lett.* **93**, 033602 (2004); M. Lewenstein, A. Sanpera, V. Ahufinger, B. Damski, A. Sen(De), and U. Sen, *Adv. Phys.* **56**, 243 (2007); K. J. Günter, M. Cheneau, T. Yefsah, S. P. Rath, and J. Dalibard, *Phys. Rev. A* **79**, 011604 (2009); I. B. Spielman, *Phys. Rev. A* **79**, 063613 (2009).

- [85] Y. J. Lin, R. L. Compton, A. R. Perry, W. D. Phillips, J. V. Porto, and I. B. Spielman, Phys. Rev. Lett. **102**, 130401 (2009).
- [86] Y.-J. Lin, R. L. Compton, K. J. García, J. V. Porto and I. B. Spielman, Nature **462**, 628, (2009)
- [87] D.C. Tsui, H.L. Stormer, A.C. Gossard, Phys. Rev. Lett. **48**, 1559 (1982)
- [88] S. M. Girvin. The quantum Hall effect: Novel excitations and broken symmetries. In A. Comtet, T. Jolicoeur, S. Ouvry, and F. David, editors, *Topological Aspects of Low Dimensional Systems* EDP Sciences and Springer-Verlag (1999); arXiv:cond-mat/9907002.
- [89] A. Stern, Annals of Physics **323**, 204 (2008.)
- [90] R. de Picciotto, M. Reznikov, M. Heiblum, V. Umansky, G. Bunin, and D. Mahalu, Nature (London) **389**, 162 (1997).
- [91] F. E. Camino, W. Zhou, and V. J. Goldman, Phys. Rev. Lett. **98**, 076805 (2007); I. P. Radu, J. B. Miller, C. M. Marcus, M. A. Kastner, L. N. Pfeiffer, and K. W. West, Science **320**, 899 (2008)
- [92] D. R. Hofstadter, Phys. Rev. B, **14**, 2239 (1976).
- [93] K.W. Madison, F. Chevy, W. Wohlleben, and J. Dalibard, Phys. Rev. Lett. **84**, 806 (2000); J. R. Abo-Sheer, C. Raman, J. M. Vogels and W. Ketterle, Science **292**, 476 (2001); P. Engels, I. Coddington, P. C. Haljan, and E. A. Cornell, Phys Rev. Lett. **89**, 100403 (2002).
- [94] M. W. Zwierlein, J. R. Abo-Shaeer, A. Schirotzek, C. H. Schunck and W. Ketterle, Nature **435**, 1047-1051 (2005); V. Schweikhard, I. Coddington, P. Engels, V. P. Mogendorff and E. A. Cornell, Phys. Rev. Lett. **92**, 040404 (2004).
- [95] S. Tung, V. Schweikhard, and E. A. Cornell, Phys. Rev. Lett. **97**, 240402 (2006)
- [96] R. A. Williams, S. Al Assam, and C. J. Foot, Phys. Rev. Lett. **104**, 050404 (2010).
- [97] J. Dalibard, F. Gerbier, G. Juzeliunas and P. Öhberg, Rev. Mod. Phys. **83**, 1523 (2011)
- [98] A. L. Fetter, Rev. Mod. Phys. **81**, 647 (2009)
- [99] I. Bloch, J. Dalibard and W. Zwerger, Rev. Mod. Phys. **80**, 885 (2008)
- [100] S. Sachdev, *Quantum Phase Transitions*, Second Edition, Cambridge University Press, Cambridge (2011)

- [101] K. Goral, L. Santos, and M. Lewenstein, Phys. Rev. Lett. **88**, 170406 (2002)
- [102] B. Damski, L. Santos, E. Tiemann, M. Lewenstein, S. Kotochigova, P. Julienne, and P. Zoller, Phys. Rev. Lett. **90**, 110401 (2003)
- [103] D. L. Kovrizhin, G. V. Pai and S. Sinha, Europhys. Lett. **72**, 162 (2005).
- [104] E. B. Sonin, Rev. Mod. Phys. **59** 87 (1987).
- [105] R. Sachdeva, S. Johri and S. Ghosh, Phys. Rev. A **82**, 063617 (2010)
- [106] R. O. Umucalilar and M. O. Oktel, Phys. Rev. A **76**, 055601 (2007); M. O. Oktel, M. Nita and B. Tanatar, Phys. Rev. B **75**, 045133 (2007).
- [107] D. S. Goldbaum and E. J. Mueller, Phys. Rev. A. **77**, 033629 (2008); D. S. Goldbaum, Ph.D Thesis (*unpublished*), Cornell University.
- [108] J. K. Freericks and H. Monien, Europhys. Lett. **26**, 545 (1994)
- [109] R. Sachdeva and S. Ghosh, Phys. Rev. A **85**, 013624 (2012)
- [110] R. Sachdeva and S. Ghosh, arXiv:1308.1592
- [111] T. D. Kuhner, S. R. White and H. Monien, Phys. Rev. B **61**, 12474 (2000)
- [112] L. Santos, G. V. Shlyapnikov and M. Lewenstein, Phys. Rev. Lett. **90**, 250403, (2003)
- [113] C. Kittel, 1962, *Elementary Solid State Physics: A Short Course*, Wiley, New York
- [114] W. Kohn, Phys. Rev. **115**, 809 (1959).
- [115] Jean Dalibard (*private communication*)
- [116] F. Chevy, Ph.D Thesis (*unpublished*) Laboratoire Kastler Brossel, Departement de Physique de l'Ecole Normale Superieure (2001)
- [117] L. D. Landau and S. M. Lifshitz, Mechanics, Volume 1 of Course of Theoretical Physics, Butterworth-Heinemann, 1976.
- [118] D. Jaksch and P. Zoller, New J. Phys. **5**, 56 (2003); A. S. Sorensen, E. Demler, and M. D. Lukin, Phys. Rev. Lett. **94**, 086803 (2005); M. Hafezi, A. S. Sorensen, E. Demler and M. D. Lukin, Phys. Rev. A **76**, 023613 (2007)
- [119] G. Juzeliunas and P. Ohberg, Phys. Rev. Lett. **93**, 033602 (2004); G. Juzeliunas, J. Ruseckas, P. Ohberg, and M. Fleischhauer, Phys. Rev. A **73**, 025602 (2006).

- [120] Shi-Liang Zhu, Hao Fu, C.J. Wu, S.C. Zhang, and L.M. Duan, Phys. Rev. Lett. **97**, 240401 (2006).
- [121] J. Higbie and D. M. Stamper-Kurn, Phys. Rev. Lett. **88**, 090401 (2002); F. Papoff, F. Mauri, and E. Arimondo, J. Opt. Soc. Am. B **9**, 321 (1992).
- [122] R. Bhat, B. M. Peden, B. T. Seaman, M. Kramer, L. D. Carr and M. J. Holland, Phys. Rev. A **74**, 063606 (2006)
- [123] D. J. Thouless, M. Kohmoto, M. P. Nightingale, and M. den Nijs, Phys. Rev. Lett. **49**, 405 (1982); J. E. Avron, R. Seiler and B. Simon Phys. Rev. Lett. **51**, 51 (1983).
- [124] J. Zak, Phys. Rev. **134**, A1602 (1964).
- [125] S. Bergkvist, P. Henelius, and A. Rosengren, Phys. Rev. A **70**, 053601 (2004); G. G. Batrouni, H. R. Krishnamurthy, K. W. Mahmud, V. G. Rousseau, and R. T. Scalettar, Phys. Rev. A **78**, 023627 (2008)
- [126] G. G. Batrouni, F. Hebert, and R. T. Scalettar, Phys. Rev. Lett. **97**, 087209 (2006)
- [127] R. V. Pai and R. Pandit, Phys. Rev. B **71**, 104508 (2005).
- [128] P. G. Harper, Proc. Phys. A **68**, 874 (1955)
- [129] M. C. Gutzwiller, Phys. Rev. Lett. **10**, 159 (1963); M. C. Gutzwiller, Phys. Rev. **137**, A1726 (1965).
- [130] D.S. Rokhsar and B. G. Kotliar, Phys. Rev. B **44**, 10328 (1991); W. Krauth, M. Caffarel and J. P. Bouchaud Phys. Rev. B, **45**, 3137 (1992)
- [131] K. Sheshadri, H. R. Krishnamurthy, R. Pandit and T. V. Ramakrishnan, Europhys. Lett. **22**, 257(1993).
- [132] D. V. Oosten, P. V. D. Straten and H. T. C. Stoof, Phys. Rev. A **63**, 053601(2001).
- [133] L.P. Pitaevskii and S. Stringari , *Bose Einstein Condensation*,(Clarendon Press, Oxford, 2003)
- [134] E. Altman and A. Auerbach, Phys. Rev. Lett. **89**, 250404 (2002).
- [135] R. Peierls, Z. Phys. **80**, 763 (1993).
- [136] M. Kohmoto, Phys. Rev. B **39**, 11943 (1989); J. Bellisard, Ch. Kreft and R. Seiler, J. Phys. A **24**, 2239 (1990); Y. Hasegawa, P. Lederer, T. M. Rice and P. B. Wiegmann, Phys. Rev. Lett. **63**, 907 (1989).
- [137] D. M. Stamper Kurn , A. P. Chikkatur, A. Grlitz , S. Inouye, S. Gupta, D. E. Pritchard, and W. Ketterle Phys. Rev. Lett. **83**, 2876 (1999).

- [138] J. Stenger, S. Inouye, A. P. Chikkatur, D. M. Stamper Kurn, D. E. Pritchard, and W. Ketterle, Phys. Rev. Lett. **82**, 4569 (1999).
- [139] J. Steinhauer, R. Ozeri, N. Katz, and N. Davidson, Phys. Rev. Lett. **88**, 120407 (2002).
- [140] J. E. Simsarian, J. Denschlag, M. Edwards, C. W. Clark, L. Deng, E. W. Hagley, K. Helmerson, S. L. Rolston, and W. D. Phillips, Phys. Rev. Lett. **85**, 2040 (2000);
- [141] P. B. Blakie and R. J. Ballagh, Phys. Rev. Lett. **86**, 3930 (2001).
- [142] Peter J. Martin, Bruce G. Oldaker, A. H. Miklich, and David E. Pritchard, Phys. Rev. Lett. **60**, 515 (1987).
- [143] P. Nozières and D. Pines, *The Thoery of Quantum Liquids*, Addison Wesley, Redwood City, CA (1990).
- [144] S. R. Muniz, D. S. Naik, and C. Raman, Phys. Rev. A, **73**, 041605(R) (2006).
- [145] J. W. Reijnders and R. A. Duine, Phys. Rev. Lett. **93**, 060401 (2004)
- [146] C. Wu, H. D. Chen, J. P. Hu, and S. C. Zhang, Phys. Rev. A **69**, 043609 (2004)
- [147] E. Lundh, Europhys. Lett. **84**, 10007 (2008)
- [148] V. W. Scarola and S. Das Sarma, Phys. Rev. Lett. **98**, 210403 (2007)
- [149] M. Niemeyer, J. K. Freericks and H. Monien, Phys. Rev. B **60**, 2357 (1999)
- [150] S. Powell, R. Barnett, R. Sensarma, and S. DasSarma, Phys. Rev. Lett. **104**, 255303 (2010)
- [151] S. Powell, R. Barnett, R. Sensarma and S. D. Sarma, Phys. Rev. A **83**, 013612 (2011)
- [152] S. Sinha and K. Sengupta, Europhys. Lett. **93**, 30005 (2011).
- [153] O. Tieleman, A. Lazarides and C. Morais Smith, Phys. Rev. A **83**, 013627 (2011)
- [154] N. V. Prokof'ev, B. V. Svistunov, and I. S. Tupitsyn, Phys. Lett. A **238**, 253 (1998); Sov. Phys. JETP **87**, 310 (1998).
- [155] U. Schollwöck, Rev. Mod. Phys. **77**, 259 (2005)
- [156] J. K. Freericks and H. Monien, Phys. Rev. B **53**, 2691 (1996).
- [157] M. Iskin and J. K. Freericks, Phys. Rev. A **79**, 053634 (2009)

-
- [158] C. Cohen-Tannoudji, B. Diu, and F. Laloë, *Quantum Mechanics* (Hermann, Paris, 1977).
- [159] N. Elstner and H. Monien, Phys. Rev. B **59**, 12184 (1999)
- [160] L. P. Kadanoff, W. Götze, D. Hamblen, R. Hecht, E. A. S. Lewis, V. V. Palciauskas, M. Rayl, J. Swift, D. Aspnes and J. Kane, Rev. Mod. Phys. **39**, 395 (1967)
- [161] E. Müller-Hartmann, Int. J. Mod. Phys. B **3**, 2169 (1989)
- [162] A. Georges and G. Kotliar, Phys. Rev. B **45**, 6479 (1992)
- [163] M. Iskin, Eur. Phys. J. B **85**, 76 (2012)
- [164] E. Toth, A. M. Rey, and P. B. Blaike, Phys. Rev. A **78**, 013627 (2008).
- [165] S. Powell, R. Barnett, R. Sensarma and S. D. Sarma, Phys. Rev. A **83**, 013612 (2011)
- [166] M. Iskin and J. K. Freericks, Phys. Rev. A **80**, 063610 (2009)
- [167] G. Möller and N. R. Cooper, Phys. Rev. A **82**, 063625 (2010)
- [168] P. Buonsante, R. Franco, and V. Penna, J. Phys. A, **38**, 8393 (2005); P. Buonsante, V. Penna, and A. Vezzani, Phys. Rev. A., **72** 043620 (2005)
- [169] M. Ueda and A. J. Leggett, Phys. Rev. Lett. **83**, 1489 (1999)
- [170] B.M. Peden, R. Bhat, M. Kramer and M. J. Holland, J. Phys. B: At. Mol. Opt. Phys. **40**, 3725 (2007).
- [171] M. Vengalattore, J. Guzman, S. R. Leslie, F. Serwane, and D. M. Stamper-Kurn, Phys. Rev. A **81**, 053612 (2010).
- [172] K. Baumann, C. Guerlin, F. Brennecke, and T. Esslinger, Nature (London) **464**, 1301 (2010).
- [173] S. Gopalakrishnan, B. L. Lev, and P. M. Goldbart, Phys. Rev. A **82**, 043612 (2010)
- [174] F. Dalfovo, S. Giorgini, L. P. Pitaevskii, and S. Stringari, Rev. Mod. Phys. **71**, 463 (1999).
- [175] A. L. Fetter and A. A. Svidzinsky, J. Phys. **13**, R135 (2001).
- [176] C. Lobo, A. Sinatra, and Y. Castin, Phys. Rev. Lett. **92**, 020403 (2004).
- [177] B. P. Anderson, P. C. Haljan, C. E. Wieman, and E. A. Cornell, Phys. Rev. Lett. **85**, 2857 (2000).

- [178] K. E. Strecker, G. B. Partridge, A. G. Truscott, and R. G. Hulet, *Nature* **417**, 150 (2002); L. Khaykovich et al., *Phys. Rev. Lett.* **296**, 1290 (2002).
- [179] U. A. Khawaja et al., *Phys. Rev. Lett.* **89**, 200404 (2002); L. Salasnich, A. Parola, and L. Reatto, *Phys. Rev. A* **66**, 043603 (2002); L. Salasnich, A. Parola, and L. Reatto, *Phys. Rev. Lett.* **91**, 080405 (2003); L. D. Carr and J. Brand, *Phys. Rev. Lett.* **92**, 040401 (2004).
- [180] S. Burger et al., *Phys. Rev. Lett.* **83**, 5198 (1999); J. Denschlag et al., *Science* **287**, 97 (2000); B. P. Anderson et al., *Phys. Rev. Lett.* **86**, 2926 (2001); Z. Dutton, M. Budde, C. Slowe, and L. V. Hau, *Science* **293**, 663 (2001).
- [181] E. Madelung, *Zeit. fur Phys.* **40**, 322 (1926).
- [182] G. Baym, *Phys. Rev. Lett.* **91**, 110402 (2003)
- [183] G. Baym, E. Chandler, *J. of Low Temp. Physics* **50**, 57 (1983).
- [184] E. B. Sonin, *Phys. Rev. A*, **71**, 011603(R), (2005).
- [185] V. K. Tkachenko, *Zh. Eksp. Teor. Fiz.* **49**, 1875 (1965) [*Sov. Phys. JETP* **22**, **1282** (1966)]; *Zh. Eksp. Teor. Fiz.* **50**, 1573 (1966) [*Sov. Phys. JETP* **23**, 1049 (1966)]; *Zh. Eksp. Teor. Fiz.* **56**, 1763 (1969) [*Sov. Phys. JETP* **29**, 245 (1969)]
- [186] James A. Fay, *Introduction to fluid mechanics* (MIT Press, 1994).
- [187] J. R. Abo-Shaeer, C. Raman, J. M. Vogels, W. Ketterle, *Science* **292**, 476 (2001)
- [188] L. D. Landau and E. M. Lifshitz, 1965, *Theory of Elasticity*
- [189] M. Born and K. Huang, 1954, *Dynamical Theory of Crystal Lattices* (Oxford: Oxford University Press)
- [190] Y. Pomeau and S. Rica, *Phys. Rev. Lett.* **71**, 247 (1993)
- [191] T. Schneider, C.P. Enz, *Phys. Rev. Lett.* **27**, 1186 (1971)
- [192] D. A. Kirzhnits and Yu. A. Nepomnyashchii, *ZETF* **59**, 2203 (1970) [*Sov. Phys. JETP* **32**, 1191 (1971)]; Yu. A. Nepomnyashchii, *Theor. Math. Phys.* **8**, 928 (1971); Yu. A. Nepomnyashchii and A. A. Nepomnyashchii, *Theor. Math. Phys.* **9**, 1033 (1971).
- [193] G. B. Arfken, H. J. Weber, F. E. Harris, *Mathematical Methods for Physicists, Sixth Edition: A Comprehensive Guide*, Elsevier Science (2005)
- [194] C. Josserand, Y. Pomeau and S. Rica, *Euro. Phys. J. Special Topics* **146**, 47 (2007)

- [195] G. During, C. Josserand, Y. Pomeau and S. Rica, *Lecture Notes of the 4th Warsaw school on statistical physics*, cond-mat/arXiv:1110.1323
- [196] A. Bensoussan, J.L. Lions, G. Papanicolaou, *Asymptotic Analysis in Periodic Structures* (North- Holland, Amsterdam, 1978); E. Sánchez-Palencia, *Non-Homogeneous Media and Vibration Theory*, Lecture Notes Phys. **127** (Springer-Verlag, Berlin, 1980)
- [197] T. Paananen, J. Phys. B: At. Mol. Opt. Phys. **42**, 165304 (2009)
- [198] S. Saccani, S. Moroni, and M. Boninsegni, Phys. Rev. Lett. **108**, 175301 (2012)
- [199] J. Sinova, C. B. Hanna, and A. H. MacDonald, Phys. Rev. Lett. **89**, 030403 (2002)
- [200] K. Hebeler, J. M. Lattimer, C. J. Pethick and A. Schwenk, Phys. Rev. Lett. **105**, 161102 (2010); A. Cetoli and C.J. Pethick, Phys. Rev. D **85**, 064036 (2012)
- [201] K. Glampedakis, N. Andersson and L. Samuelsson, Mon. Not. R. Astron. Soc. **410**, 805 (2011)
- [202] A. Passamonti and N. Andersson, Mon. Not. R. Astron. Soc. **419**, 638 (2012)

List of Publications

1. **Rashi Sachdeva**, Sonika Johri and Sankalpa Ghosh, *Cold atoms in rotating optical lattice with nearest neighbor interaction*, **Phys. Rev. A** **82**, 063617 (2010)
2. **Rashi Sachdeva** and Sankalpa Ghosh, *Density Wave Supersolid and Mott Insulator - Superfluid transition in the presence of an artificial gauge field: a strong Coupling perturbation approach*, **Phys. Rev. A** **85**, 013624 (2012)
3. **Rashi Sachdeva** and Sankalpa Ghosh, *Hydrodynamic theory for rotating ultracold supersolids* arXiv:1308.1592

Brief Bio data of the author

Rashi Sachdeva

Date of Birth : 14 April, 1985

EDUCATION

M.Sc Physics

Percentage: **83%**

First Division with Distinction (**Gold Medalist**)

B.Sc. (Physics, Mathematics)

Percentage: **80.5%**

First Division with Distinction (**Gold Medalist**)

Physics Department, Bareilly College

MJP Rohilkhand University, Bareilly, UP, India

SCHOLARSHIPS AND AWARDS

1. Gold Medalist in Graduation (B.Sc) and Post Graduation (M.Sc) for excellent performance and outstanding merit
2. CSIR-NET qualified (Dec 2007) and with an SPM call, for being among the top 5 in the country in the Physics examination. Awarded the Junior Research Fellowship from 2008-2010 and Senior Research Fellowship from 2010-present

INTERNATIONAL/NATIONAL CONFERENCES

1. ICTS Condensed Matter Programme (ICMP 2009), school and conference organized by International Center for Theoretical Sciences (ICTS),TIFR from 10-23 December 2009 in Mahabaleshwar, India.

2. International School and Conference on Cold Atoms and Ions (ICCIA 2010), Winter school and conference organized by Tata Institute of Fundamental Research (TIFR) and International Center of Theoretical Physics (ICTP), from 6-21 January 2010 in Kolkata, India.
3. Workshop on Physics of Strong Correlations organized by Harish Chandra Research Institute(HRI), Allahabad, from 12-14 November 2010 in HRI, Allahabad, India.
4. ICTS Condensed Matter Programme (ICMP 2010), school and conference organized by International Center for Theoretical Sciences (ICTS) from 12-22 December 2010 in Mysore, India
5. Conference on Research Frontiers in Ultra Cold Atomic and Molecular gases, organized by International Center of Theoretical Physics (ICTP), Italy from 10-14 January 2011, in Goa, India.
6. Workshop on Non-Standard Superfluids and Insulators, organized by International Center of Theoretical Physics (ICTP), Italy from 18 July -22 July 2011, at ICTP, Trieste, Italy.
7. ICTS Condensed Matter Programme (ICMP 2011) organized by International Center for Theoretical Sciences (ICTS), TIFR from 19-22 December 2011 in Bangalore, India.
8. International Conference on Frontiers of Cold Atoms and Related Topics organized by The Chinese University of Hong Kong and The Hong Kong University for Science and Technology from 14-17 May 2012, in Hong Kong.
9. Summer School on Quantum Many Body physics of ultra cold atoms and molecules organized by International Center of Theoretical Physics (ICTP), Italy, from 2-13 July 2012, at ICTP, Trieste, Italy.
10. Workshop on Quantum Simulations with cold atoms organized by International Center of Theoretical Physics (ICTP), Italy, from 16-20 July 2012, at ICTP, Trieste, Italy.

ACADEMIC VISITS

1. Visiting fellow at the Max Planck Institute for the Physics of Complex Systems (MPIPKS) , Dresden, Germany, from May 2011- August 2011 in the 'Finite Systems group' under the Condensed Matter Division.

2. Visiting fellow at the Tata Institute of Fundamental Research (TIFR), Mumbai, India, from May 2009 - June 2009

TECHNICAL SKILLS

1. **Operating Systems:** Windows, Linux
2. **Programming:** Fortran 77/90
3. **Packages:** MATLAB, Mathematica, LaTeX